NTIA Report 84-148

Microwave Terrestrial Link Rain Attenuation Prediction Parameter Analysis

E. J. Dutton

U.S. DEPARTMENT OF COMMERCE
Malcolm Baldrige, Secretary
David J. Markey, Assistant Secretary
for Communications and Information

April 1984

PREFACE

This report and the associated project work have been part of an effort sponsored by the Propagation Engineering Branch of the United States Army Communications Electronics Engineering-Installation Agency (USACEEIA). Their contributions and guidance are gratefully acknowledged.

Appreciation is also expressed to R. Hassler, C. E. Lewis, J. Spiegel, and C. Timmons--employees and students at the University of Colorado in Boulder, Colorado, who have contributed to the results in this report, as well as to F. K. Steele of the Institute for Telecommunication Sciences, NTIA. The drafting work of C. M. Miller and consultation efforts of Dr. H. T. Dougherty, both private contractors, are also acknowledged.

TABLE OF CONTENTS

	PAGE
LIST OF FIGURES	iv
LIST OF TABLES	xiv
PREFACE	xv
ABSTRACT	1
1. RAIN RATE DISTRIBUTION MODEL-DATA COMPARISONS	2
1.1 Thunderstorm Ratios	2
1.2 Methods of Comparison and Data Summary	3
1.3 Results	11
2. PREDICTION OF MICROWAVE TERRESTRIAL LINK RAIN ATTENUATION	14
2.1 Rain Attenuation Distribution Prediction Models	15
2.1.1 Older Models	15
2.1.2 Moderately New Models	16
2.1.3 Very Recent Models	17
2.1.4 A Proposed New Model	18
2.1.5 Modeling Year-to-Year Variability	21
2.2 Comparison of Models with Data	22
2.3 Conclusions from the Comparisons	37
3. WORLDWIDE RAINFALL CONTOUR MAPS	37
3.1 The Federal Republic of Germany and Vicinity	40
3.2 Okinawa	60
3.3 Republic of Korea and Vicinity	60
3.4 Southwest Asia	76
3.5 Central America	76
3.6 The United States of America	110
3.7 Southeast Asia	110
4. SYNOPSIS	147
5. REFERENCES	147
APPENDIX: IDENTIFICATION OF SITES USED IN THE PREPARATION OF CONTOUR MAPS in SECTION 3	149

LIST OF FIGURES

FIGURE		PAGE
1	Rice-Holmberg rain rate distribution model predictions using thunderstorm ratio, β, at Miami, FL, compared with one year's distribution of observed data.	4
2	Rice-Holmberg rain rate distribution model predictions using the thunderstorm ratio, $U'/D'_{.01}$, at Miami, FL, compared with one year's distribution of observed data.	5
3	Comparison of observed data distributions at Wallops Island, VA, with the Rice-Holmberg rain rate distribution prediction model using the β and $U'/D'_{.01}$ thunderstorm ratios. The first column shows three data-regression summary techniques. The resultant regression and the 5 and 95 percent confidence limits are compared with β and $U'/D'_{.01}$ modeling results in the second and third columns, respectively.	8
4	Comparison of observed data and predicted distributions at Miami, FL, in the format of Figure 3.	9
5	Comparison of observed data and predicted distributions at Rio de Janeiro, Brazil, in the format of Figure 3.	10
6	Map of the world showing 13 worldwide locations with usable rain rate distribution data.	12
7	Illustration of ray-path geometry used in the PROMOD terrestrial-link attenuation distribution prediction model.	20
8	Comparison of the PROMOD attenuation distribution prediction model with data over a 5.1 km, 17.7 GHz link between Rico and Palmetto, GA.	24
9	Comparison of the Barsis et al. (1973) attenuation distribution model with data over a 5.1 km, 17.7 GHz link between Rico and Palmetto, GA.	25
10	Comparison of the Battesti et al. (1971) attenuation distribution prediction model with data over a 5.1 km, 17.7 GHz link between Rico and Palmetto, GA.	26
11	Comparison of the GLOBAL (Crane, 1980) attenuation distribution prediction model with data over a 5.1 km, 17.7 GHz link between Rico and Palmetto, GA.	27
12	Comparison of the TWO-COMPONENT (Crane, 1982) attenuation distribution prediction model with data over a 5.1 km, 17.7 GHz link between Rico and Palmetto, GA.	28

FIGURE		PAGE
13	Comparison of the Lin (1977) attenuation distribution prediction model with data over a 5.1 km, 17.7 GHz link between Rico and Palmetto, GA.	29
14	Comparison of the Morita and Higuti (1976) attenuation distribution prediction model with data over a 5.1 km, 17.7 GHz link between Rico and Palmetto, GA.	30
15	Comparison of the Misme and Fimbel (1975) attenuation distribution prediction model with data over a 5.1 km, 17.7 GHz link between Rico and Palmetto, GA.	31
16	Comparison of the modified Lin (Kanellopoulos, 1983) attenuation distribution prediction model with data over a 5.1 km, 17.7 GHz link between Rico and Palmetto, GA.	32
17	Comparison of the CCIR (1982) attenuation distribution prediction model with data over a 5.1 km, 17.7 GHz link between Rico and Palmetto, GA.	33
18	Map of data locations in the Federal Republic of Germany and vicinity.	41
19	Contour map of the average annual precipitation, M, in millimeters for the Federal Republic of Germany and vicinity.	42
20	Contour map of the average annual number of days, $D_{.01}$, with precipitation greater than .01 in. for the Federal Republic of Germany and vicinity.	43
21	Contour map of the average annual number of days, U, with thunderstorms for the Federal Republic of Germany and vicinity.	44
22	Contour map of the greatest monthly precipitation, M_m, in 30 consecutive years, in millimeters, for the Federal Republic of Germany and vicinity.	45
23	Contour map of the thunderstorm ratio, β, for the Federal Republic of Germany and vicinity.	46
24	Contour map of the thunderstorm ratio, $U/D_{.01}$, for the Federal Republic of Germany and vicinity.	47
25	Contour map of the year-to-year standard deviation, s_M, in millimeters, of total annual precipitation for the Federal Republic of Germany and vicinity.	48

FIGURE		PAGE
26	Contour map of the year-to-year standard deviation, s_C, of the annual number of days with precipitation greater than .01 in. for the Federal Republic of Germany and vicinity.	49
27	Contour map of the year-to-year standard deviation, s_U, of the annual number of days with thunderstorms for the Federal Republic of Germany and vicinity.	50
28	Contour map of the rain rate, $R_1(\beta)$, in millimeters per hour, expected to be exceeded 1 percent of an average year and derived using the thunderstorm ratio, β, for the Federal Republic of Germany and vicinity.	51
29	Contour map of the rain rate, $R_{.1}(\beta)$, in millimeters per hour, expected to be exceeded 0.1 percent of an average year and derived using the thunderstorm ratio, β, for the Federal Republic of Germany and vicinity.	52
30	Contour map of the rain rate, $R_{.01}(\beta)$, in millimeters per hour, expected to be exceeded 0.01 percent of an average year and derived using the thunderstorm ratio, β, for the Federal Republic of Germany and vicinity.	53
31	Contour map of the rain rate, $R_1(U/D)$, in millimeters per hour, expected to be exceeded 1 percent of an average year and derived using the thunderstorm ratio, $U/D_{.01}$, for the Federal Republic of Germany and vicinity.	54
32	Contour map of the rain rate, $R_{.1}(U/D)$, in millimeters per hour, expected to be exceeded 0.1 percent of an average year and derived using the thunderstorm ratio, $U/D_{.01}$, for the Federal Republic of Germany and vicinity.	55
33	Contour map of the rain rate, $R_{.01}(U/D)$, in millimeters per hour, expected to be exceeded 0.01 percent of an average year and derived using the thunderstorm ratio, $U/D_{.01}$, for the Federal Republic of Germany and vicinity.	56
34	Contour map of the estimated year-to-year standard deviation, s_{R_1}, in millimeters per hour, of rain rate expected at the 1 percent exceedance level for the Federal Republic of Germany and vicinity.	57
35	Contour map of the estimated year-to-year standard deviation, $s_{R_{.1}}$, in millimeters per hour, of rain rate expected at the 0.1 percent exceedance level for the Federal Republic of Germany and vicinity.	58

FIGURE		PAGE
36	Contour map of the estimated year-to-year standard deviation, $s_{R_{.01}}$, in millimeters per hour, of rain rate expected at the 0.01 percent exceedance level for the Federal Republic of Germany and vicinity.	59
37	Map of data locations in the Republic of Korea and vicinity.	62
38	Contour map of the average annual precipitation, M, in millimeters, for the Republic of Korea and vicinity.	63
39	Contour map of the average annual number of days, $D_{.01}$, with precipitation greater than .01 in., for the Republic of Korea and vicinity.	64
40	Contour map of the average annual number of days, U, with thunderstorms for the Republic of Korea and vicinity.	65
41	Contour map of the thunderstorm ratio, $U/D_{.01}$, for the Republic of Korea and vicinity.	66
42	Contour map of the year-to-year standard deviation, s_M, in millimeters, of total annual precipitation for the Republic of Korea and vicinity.	67
43	Contour map of the year-to-year standard deviation, s_D, of the annual number of days with precipitation greater than .01 in., for the Republic of Korea and vicinity.	68
44	Contour map of the year-to-year standard deviation, s_U, of the annual number of days with thunderstorms for the Republic of Korea and vicinity.	69
45	Contour map of the rain rate, $R_1(U/D)$, in millimeters per hour, expected to be exceeded 1 percent of an average year and derived using the thunderstorm ratio, $U/D_{.01}$, for the Republic of Korea and vicinity.	70
46	Contour map of the rain rate, $R_{.1}(U/D)$, in millimeters per hour, expected to be exceeded 0.1 percent of an average year and derived using the thunderstorm ratio, $U/D_{.01}$, of the Republic of Korea and vicinity.	71
47	Contour map of the rain rate, $R_{.01}(U/D)$, in millimeters per hour, expected to be exceeded 0.01 percent of an average year and derived using the thunderstorm ratio, $U/D_{.01}$, for the Republic of Korea and vicinity.	72

FIGURE PAGE

48 Contour map of the estimated year-to-year standard deviation, s_{R_1}, in millimeters per hour, of rain rate expected at the 1 percent exceedance level for the Republic of Korea and vicinity. 73

49 Contour map of the estimated year-to-year standard deviation, $s_{R_{.1}}$, in millimeters per hour, of rain rate expected at the 0.1 exceedance level for the Republic of Korea and vicinity. 74

50 Contour map of the estimated year-to-year standard deviation, $s_{R_{.01}}$, in millimeters per hour, of rain rate expected at the 0.01 percent exceedance level for the Republic of Korea and vicinity. 75

51 Map of data locations in Southwest Asia. 77

52 Contour map of the average annual precipitation, M, in millimeters, for Southwest Asia. 78

53 Contour map of the average annual number of days, $D_{.01}$, with precipitation greater than .01 in., for Southwest Asia. 79

54 Contour map of the average annual number of days, U, with thunderstorms for Southwest Asia. 80

55 Contour map of the greatest monthly precipitation, M_m, in 30 consecutive years, in millimeters, for Southwest Asia. 81

56 Contour map of the thunderstorm ratio, β, for Southwest Asia. 82

57 Contour map of the thunderstorm ratio, $U/D_{.01}$, for Southwest Asia. 83

58 Contour map of the year-to-year standard deviation, s_M, in millimeters, of total annual precipitation for Southwest Asia. 84

59 Contour map of the year-to-year standard deviation, s_D, of the annual number of days with precipitation greater than .01 in., for Southwest Asia. 85

60 Contour map of the year-to-year standard deviation, s_U, of the annual number of days with thunderstorms for Southwest Asia. 86

61 Contour map of the rain rate, $R_1(\beta)$, in millimeters per hour, expected to be exceeded 1 percent of an average year and derived using the thunderstorm ratio, β, for Southwest Asia. 87

62 Contour map of the rain rate, $R_{.1}(\beta)$, in millimeters per hour, expected to be exceeded 0.1 percent of an average year and derived using the thunderstorm ratio, β, for Southwest Asia. 88

FIGURE		PAGE
63	Contour map of the rain rate, $R_{.01}(\beta)$, in millimeters per hour, expected to be exceeded 0.01 percent of an average year and derived using the thunderstorm ratio, β, for Southwest Asia.	89
64	Contour map of the rain rate, $R_1(U/D)$, in millimeters per hour, expected to be exceeded 1 percent of an average year and derived using the thunderstorm ratio, $U/D_{.01}$, for Southwest Asia.	90
65	Contour map of the rain rate, $R_{.1}(U/D)$, in millimeters per hour, expected to be exceeded 0.1 percent of an average year and derived using the thunderstorm ratio, $U/D_{.01}$, for Southwest Asia.	91
66	Contour map of the rain rate, $R_{.01}(U/D)$, in millimeters per hour, expected to be exceeded 0.01 percent of an average year and derived using the thunderstorm ratio, $U/D_{.01}$, for Southwest Asia.	92
67	Contour map of the estimated year-to-year standard deviation, s_{R_1}, in millimeters per hour, of rain rate expected at the 1 percent exceedance level for Southwest Asia.	93
68	Contour map of the estimated year-to-year standard deviation, $s_{R_{.1}}$, in millimeters per hour, of the rain rate expected at the 0.1 percent exceedance level for Southwest Asia.	94
69	Contour map of the estimated year-to-year standard deviation, $s_{R_{.01}}$, in millimeters per hour, of rain rate expected at the 0.01 percent exceedance level for Southwest Asia.	95
70	Map of data locations in Central America.	96
71	Contour map of the average annual precipitation, M, in millimeters, for Central America.	97
72	Contour map of the average annual number of days, $D_{.01}$, with precipitation greater than .01 in., for Central America.	98
73	Contour map of the average annual number of days, U, with thunderstorms for Central America.	99
74	Contour map of the thunderstorm ratio, $U/D_{.01}$, for Central America.	100
75	Contour map of the year-to-year standard deviation, s_M, in millimeters, of total annual precipitation for Central America.	101
76	Contour map of the year-to-year standard deviation, s_D, of the annual number of days with precipitation greater than .01 inch, for Central America.	102

FIGURE		PAGE
77	Contour map of the year-to-year standard deviation, s_U, of the annual number of days with thunderstorms for Central America.	103
78	Contour map of the rain rate, $R_1(U/D)$, in millimeters per hour, expected to be exceeded 1 percent of an average year and derived using the thunderstorm ratio, $U/D_{.01}$, for Central America.	104
79	Contour map of the rain rate, $R_{.1}(U/D)$, in millimeters per hour, expected to be exceeded 0.1 percent of an average year and derived using the thunderstorm ratio, $U/D_{.01}$, for Central America.	105
80	Contour map of the rain rate, $R_{.01}(U/D)$, in millimeters per hour, expected to be exceeded 0.01 percent of an average year and derived using the thunderstorm ratio, $U/D_{.01}$, for Central America.	106
81	Contour map of the estimated year-to-year standard deviation, s_{R_1}, in millimeters per hour, of rain rate expected at the 1 percent exceedance level for Central America.	107
82	Contour map of the estimated year-to-year standard deviation, $s_{R_{.1}}$, in millimeters per hour, of rain rate expected at the 0.1 percent exceedance level for Central America.	108
83	Contour map of the estimated year-to-year standard deviation, $s_{R_{.01}}$, in millimeters per hour, of rain rate expected at the 0.01 percent exceedance level for Central America.	109
84	Map of data locations in the United States of America.	111
85	Contour map of the average annual precipitation, M, in millimeters, for the United States of America.	112
86	Contour map of the average annual number of days, $D_{.01}$, with precipitation greater than .01 in., for the United States of America.	113
87	Contour map of the average annual number of days, U, with thunderstorms for the United States of America.	114
88	Contour map of the greatest monthly precipitation, M_m, in 30 consecutive years, in millimeters, for the United States of America.	115
89	Contour map of the thunderstorm ratio, β, for the United States of America.	116
90	Contour map of the thunderstorm ratio, $U/D_{.01}$, for the United States of America.	117

FIGURE		PAGE
91	Contour map of the year-to-year standard deviation, s_M, in millimeters, of total annual precipitation for the United States of America.	118
92	Contour map of the year-to-year standard deviation, s_D, of the annual number of days with precipitation greater than .01 in., for the United States of America.	119
93	Contour map of the year-to-year standard deviation, s_U, of the annual number of days with thunderstorms for the United States of America.	120
94	Contour map of the rain rate, $R_1(\beta)$, in millimeters per hour, expected to be exceeded 1 percent of an average year and derived from the thunderstorm ratio, β, for the United States of America.	121
95	Contour map of the rain rate, $R_{.1}(\beta)$, in millimeters per hour, expected to be exceeded 0.1 percent of an average year and derived from the thunderstorm ratio, β, for the United States of America.	122
96	Contour map of the rain rate, $R_{.01}(\beta)$, in millimeters per hour, expected to be exceeded 0.01 percent of an average year and derived from the thunderstorm ratio, β, for the United States of America.	123
97	Contour map of the rain rate, $R_1(U/D)$, in millimeters per hour, expected to be exceeded 1 percent of an average year and derived from the thunderstorm ratio, $U/D_{.01}$, for the United States of America.	124
98	Contour map of the rain rate, $R_{.1}(U/D)$, in millimeters per hour, expected to be exceeded 0.1 percent of an average year and derived from the thunderstorm ratio, $U/D_{.01}$, for the United States of America.	125
99	Contour map of the rain rate, $R_{.01}(U/D)$, in millimeters per hour, expected to be exceeded 0.01 percent of an average year and derived from the thunderstorm ratio, $U/D_{.01}$, for the United States of America.	126
100	Contour map of the estimated year-to-year standard deviation, $s_{R_1}(\beta)$, in millimeters per hour, of rain rate expected at the 1 percent exceedance level, derived from the thunderstorm ratio, β, for the United States of America.	127

FIGURE		PAGE
101	Contour map of the estimated year-to-year standard deviation, $s_{R_{.1}}(\beta)$, in millimeters per hour, of rain rate expected at the 0.1 percent exceedance level, derived from the thunderstorm ratio, β, for the United States of America.	128
102	Contour map of the estimated year-to-year standard deviation, $s_{R_{.01}}(\beta)$, in millimeters per hour, of rain rate expected at the 0.01 percent exceedance level, derived from the thunderstorm ratio, β, for the United States of America.	129
103	Contour map of the estimated year-to-year standard deviation, $s_{R_1}(U/D)$, in millimeters per hour, of rain rate expected at the 1 percent exceedance level, derived from the thunderstorm ratio, $U/D_{.01}$, for the United States of America.	130
104	Contour map of the estimated year-to-year standard deviation, $s_{R_{.1}}(U/D)$, in millimeters per hour, of rain rate expected at the 0.1 percent exceedance level, derived from the thunderstorm ratio, $U/D_{.01}$, for the United States of America.	131
105	Contour map of the estimated year-to-year standard deviation, $s_{R_{.01}}(U/D)$, in millimeters per hour, of rain rate expected at the 0.01 percent exceedance level, derived from the thunderstorm ratio, $U/D_{.01}$, for the United States of America.	132
106	Map of data locations in Southeast Asia.	133
107	Contour map of the average annual precipitation, M, in millimeters, for Southeast Asia.	134
108	Contour map of the average annual number of days, $D_{.01}$, with precipitation greater than .01 in., for Southeast Asia.	135
109	Contour map of the average annual number of days, U, with thunderstorms for Southeast Asia.	136
110	Contour map of the thunderstorm ratio, $U/D_{.01}$, for Southeast Asia.	137
111	Contour map of the year-to-year standard deviation, s_M, in millimeters, of total annual precipitation for Southeast Asia.	138
112	Contour map of the year-to-year standard deviation, s_D, of the annual number of days with precipitation greater than .01 in., for Southeast Asia.	139

FIGURE		PAGE
113	Contour map of the year-to-year standard deviation, s_U, of the annual number of days with thunderstorms for Southeast Asia.	140
114	Contour map of the rain rate, $R_1(U/D)$, in millimeters per hour, expected to be exceeded 1 percent of an average year and derived from the thunderstorm ratio, $U/D_{.01}$, for Southeast Asia.	141
115	Contour map of the rain rate, $R_{.1}(U/D)$, in millimeters per hour, expected to be exceeded 0.1 percent of an average year and derived from the thunderstorm ratio, $U/D_{.01}$, for Southeast Asia.	142
116	Contour map of the rain rate, $R_{.01}(U/D)$, in millimeters per hour, expected to be exceeded 0.01 percent of an average year and derived from the thunderstorm ratio, $U/D_{.01}$, for Southeast Asia.	143
117	Contour map of the estimated year-to-year standard deviation, s_{R_1}, in millimeters per hour, of rain rate expected at the 1 percent exceedance level for Southeast Asia.	144
118	Contour map of the estimated year-to-year standard deviation, $s_{R_{.1}}$, in millimeters per hour, of rain rate expected at the 0.1 exceedance level for Southeast Asia.	145
119	Contour map of the estimated year-to-year standard deviation, $s_{R_{.01}}$, in millimeters per hour, of rain rate expected at the 0.01 exceedance level for Southeast Asia.	146

LIST OF TABLES

TABLE		PAGE
1	Absolute Value of Observed Rain Rate Deviation, ΔR, Outside Predicted 0.5 and 99.5 Percent Confidence Limits Using the Two Thunderstorm Ratio Estimation Procedures in the RH Model	13
2	Summary of Departures of Yearly Microwave Attenuation Data Distributions Above the Modeled 99.5 Percent Confidence Limit at the 0.01 Percentile Exceedance Level for 10 Prediction Models	35
3	Summary of Absolute Values of Departures of Yearly Microwave Attenuation Data Outside the 99 Percent Confidence Interval at the 0.01 Percentile Exceedance Level for 10 Prediction Models	36
4	Rain Rate and Rain Attenuation Prediction Parameters for Okinawa	61

Microwave Terrestrial Link
Rain Attenuation Prediction Parameter Analysis

E. J. Dutton*

Because rain attenuation continues to be a problem for the operation of microwave links worldwide, this report examines the behavior and the prediction of rain rate and rain attenuation distributions on a worldwide basis. Particular emphasis is placed on seven areas of the world of special interest to the U. S. Army Communications Electronics and Engineering-Installation Agency (USACEEIA).

The first part of the report discusses the need for, and provides, an alternative thunderstorm ratio in the Rice-Holmberg rain rate distribution prediction model. This new thunderstorm ratio is more readily obtained in regions of the world with sparse, and less historical, meteorological data. Comparisons of rain rate distributions predicted from the Rice-Holmberg model with observed distributions are then presented.

The second part of the report discusses rain attenuation prediction on terrestrial microwave links. Ten models, including a newly-derived model for this report, are presented for this purpose. Of these 10 models, however, only 3 contain a year-to-year variability prediction feature--a feature usually necessary to the annual distribution prediction process. An "ad hoc" annual variability is attached to the remaining 7 models. All 10 models are then intercompared with observed rain attenuation distribution data.

The third, and largest, part of the report presents contour maps of the parameters necessary for annual rain rate distribution predictions. Also presented are contour maps of rain rate distribution prediction results at the 1, 0.1, and 0.01 percentile exceedance levels, for use to the reader in predicting annual rain attenuation distributions at those levels. Seven specific regions of the world have been contoured in this report:

1. the Federal Republic of Germany and vicinity,
2. Okinawa,
3. the Republic of Korea and vicinity,
4. Southwest Asia,
5. Central America,
6. the United States of America,
7. Southeast Asia.

Key Words: attenuation distributions; contour maps; microwave links; model-data comparisons; rain attenuation

*The author is with the Institute for Telecommunication Sciences, National Telecommunications and Information Administration, U. S. Department of Commerce, Boulder, Colorado 80303.

1. RAIN RATE DISTRIBUTION MODEL-DATA COMPARISONS

The rain rate distribution prediction model used throughout this report is the Rice-Holmberg (RH) model developed by Rice and Holmberg (1973) and modified by Dutton (1977a). The modification consists of year-to-year variability "wings" around the median prediction originally given by the RH model. Most of the details of the development of the RH model are given in Dutton (1977a), so that in this report it suffices to indicate the inputs to and outputs from the RH model. The inputs are:

1. M, the average annual precipitation in millimeters, and its year-to-year standard deviation, s_M,
2. $D_{.01}$, the average annual number of days with precipitation greater than 0.01 inches (0.25 mm), and its year-to-year standard deviation, s_D,
3. U, the average annual number of days with thunderstorms, and its year-to-year standard deviation, s_U, and
4. M_m, the maximum monthly precipitation of 30 consecutive years of record, in millimeters.

The outputs are the rainrates, R, in millimeters per hour, at given percentile levels, P(R), at which R is expected to be exceeded, and the year-to-year standard deviations, s_R, at P(R).

1.1. Thunderstorm Ratios

The RH model as developed in the references above makes use of an intermediate parameter known as the "thunderstorm ratio," β. The basic purpose of this parameter is distinction between convective and stratiform types of rainfall. The thunderstorm ratio was originally defined as

$$\beta = \beta_o \left\{ 0.25 + 2 \exp \left[\frac{-0.35(1 + 0.125\ M)}{U} \right] \right\} \quad , \tag{1}$$

where

$$\beta_o = 0.03 + 0.97 \exp \left[-5 \exp(-0.004\ M_m) \right] \quad . \tag{2}$$

The exact origin of these formulations is not known, but they are most likely the result of curve-fitting to data in the original RH model of Rice and Holmberg (1973). Formulas (1) and (2) have two unfortunate aspects, however. First, they are cumbersome to use, except on a computer. Second, and more important, they require the only

use of M_m in the RH model calculations. The value M_m is very difficult to obtain on a worldwide data basis because so many years of data are required to obtain it. This often greatly reduces (sometimes to none) the number of RH model results that can be calculated in a given part of the world. This fact would have severely hampered the production of worldwide rain rate results were it not for an alternative "thunderstorm ratio" development.

This alternative is a straightforward one, defining the thunderstorm ratio as the ratio of U', the annual number of days with the thunderstorms to $D'_{.01}$, the annual number of days with precipitation >.01 inches. The statistical measures of U' are U and s_U, while the statistical measures of $D'_{.01}$, are $D_{.01}$ and $s_{D_{.01}}$. In order to obtain statistical variation of β, it is necessary to redefine β in (1) as β' with U' and an M', the annual precipitation in millimeters, measured by M and s_M, so that we now have

$$\beta' = \beta_o \left\{ 0.25 + 2 \exp \left[\frac{-0.35(1 + 0.125\ M')}{U'} \right] \right\} \quad , \tag{3}$$

where β_o, a quantity without much annual variability, is still given by (2). As a consequence, not only will rain rate predictions made with the thunderstorm ratio $U'/D'_{.01}$ have a different average annual value than predictions made with β', but they will have different confidence bands as well. This will be illustrated in the next subsection of this report, where comparisons of the two thunderstorm ratio definitions are made.

1.2 Methods of Comparison and Data Summary

The simplest method of comparison of rain rate data distributions and rain rate prediction distributions is exemplified in Figures 1 and 2. There, an observed yearly distribution of rain rate at Miami, Florida, is compared first (in Figure 1) with the prediction procedure using the β thunderstorm ratio, and then (in Figure 2) with the $U'/D'_{.01}$ thunderstorm ratio prediction procedure. In these figures, the five prediction (dotted) curves represent, from left to right, the 0.5, 5, 50 (median), 95, and 99.5 percent prediction confidence limits. About all that can be said regarding the success or failure of a given prediction method is that if the data curve tends to be bounded by the prediction curves, it is a more reasonable prediction than if the curve lies outside the bounds. For example, the 0.5 and 99.5 percent curves bound a region in which all but one extreme year out of 100 should

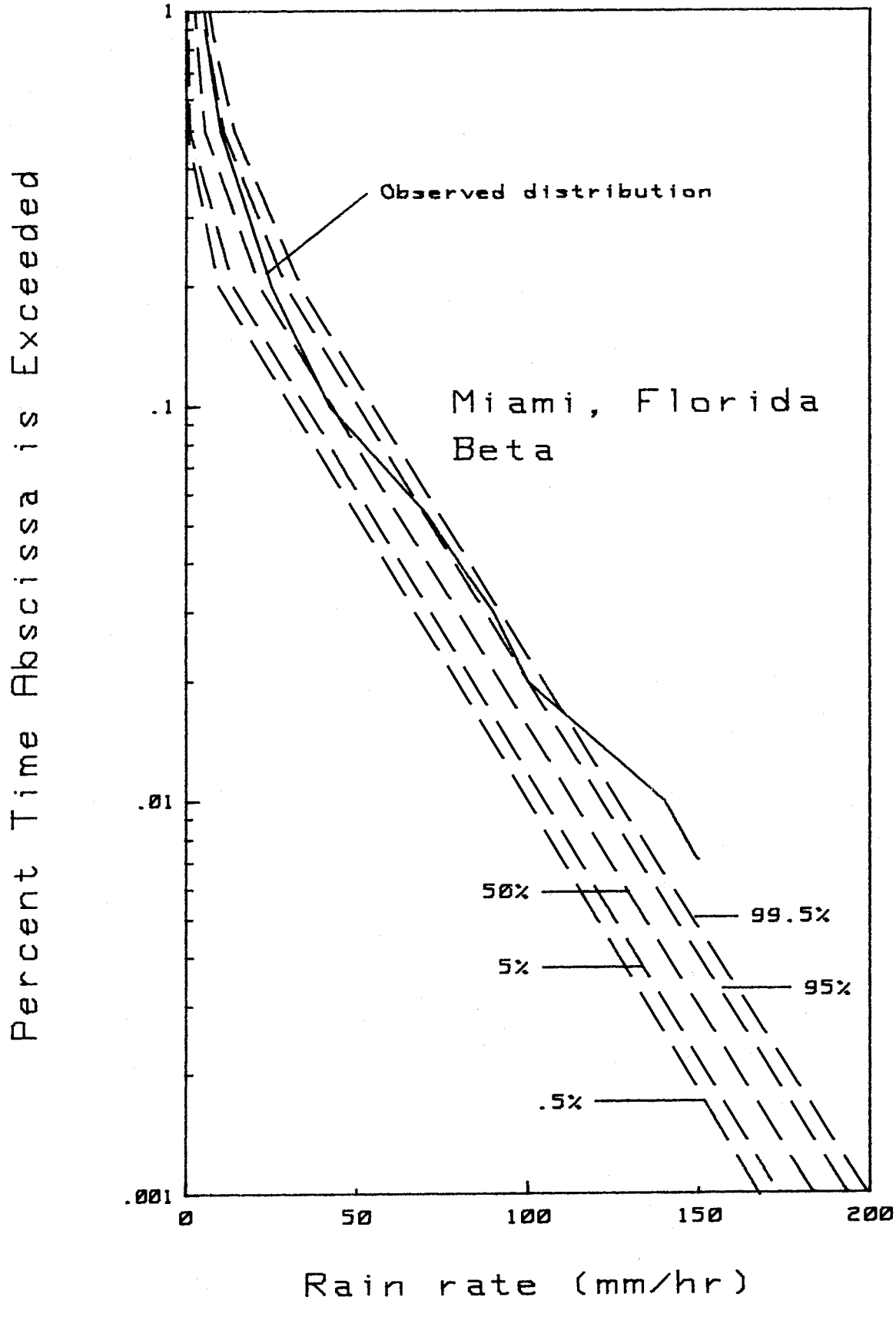

Figure 1. Rice-Holmberg rain rate distribution model predictions using the thunderstorm ratio, β, at Miami, FL, compared with one year's distribution of observed data.

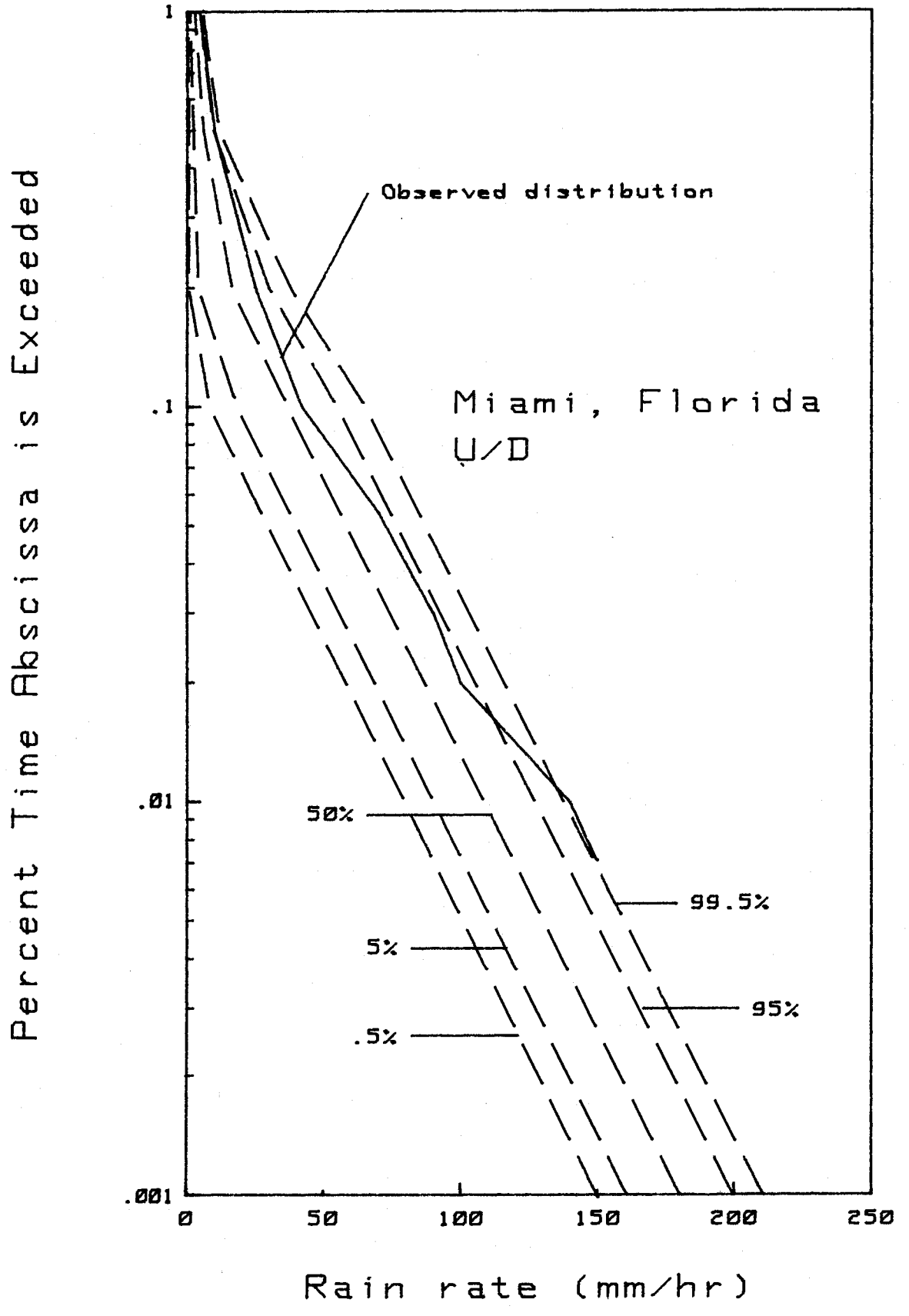

Figure 2. Rice-Holmberg rain rate distribution model predictions using the thunderstorm ratio, $U'/D'_{.01}$, at Miami, FL, compared with one year's distribution of observed data.

lie. It cannot be determined, a priori, what kind of year the data represent; hence; proximity to any one prediction curve has no inherent significance.

The difficulty with this simple method of comparison is that as more and more data-years become available, comparison graphs such as Figure 1 and 2 tend to become so replete with curves that confusion can result. To avoid this difficulty, a data summary procedure, resulting in fewer distribution curves, is highly desirable. However, there are more data summary procedures than one, and we shall now investigate the use of three of them.

All three of the data-summary procedures involve statistical regression. It should be noted that statistical regression using the method of least squares is not strictly applicable to distribution data, but should be a reasonable approximation (Crow et al., 1960, p. 150). The most reasonable starting point in the use of statistical regression is the use of the canonical, two-variable least-squares regression procedure. Although linear regression would normally be the first procedure investigated, because of the curvilinear shape of most rain rate distribution data, parabolic regression was used instead. This procedure will be referred to as "unweighted data-distribution summary," for reasons that we shall explain shortly. At this point it should be noted that the authors intend to avoid as much of the sometimes-formidable detail of the statistical mathematics and discussion as possible herein. A report by Dougherty and Dutton (1984) contains much of the necessary detail of applying regression techniques to data distributions.

Because rain rate data distributions tend to have greater year-to-year variability at lower percentiles of time than at higher percentiles, a procedure that we have termed "weighted data-distribution summary" has also been developed. The weighting refers to the mathematical weighting of the variances at each percentile used in a parabolic regression procedure (Dougherty and Dutton, 1984).

The third procedure has been termed "mean-scaled, data-distribution summary." This procedure is accomplished by taking data at any given (j^{th}) percentile level, p_j and obtaining the average rain rate, $\overline{R}(p_j)$ at that level. Then each individual rain rate, $R(p_j)$, at that level is normalized by dividing it by $\overline{R}(p_j)$. This process is repeated at all percentile levels of interest. Since rain rate at larger exceedance percentiles is ipso facto smaller than rain rate at smaller exceedance percentiles, the rain rate variability at the larger percentiles also will be correspondingly less than at the smaller percentiles. Therefore, the normalized data distribution should show more even variability (homoscedasticity) across all percentiles, and thus be amenable to an unweighted linear regression analysis. Such a regression

is performed, and the rain rate distribution is then recovered by multiplying regressed results by the appropriate $\overline{R}(p_j)$.

Figures 3, 4, and 5 are examples of the three distribution data-summarizing procedures applied to three different geographical locations that show some of the advantages and disadvantages of the three procedures. Figure 3 is an analysis for Wallops Island, Virginia, a location with five observed annual distributions of rain rate (Goldhirsh, 1982), shown as dashed curves in the left-hand three panels of Figure 3. The left-hand panels (top to bottom) of Figure 3 show the weighted-regression, unweighted-regression, and mean-scaled summaries, respectively, of these distributions as solid lines, representing the regression line itself (50 percent) and its 5 and 95 percent prediction limits. The middle (top to bottom) three panels of Figure 3 show the comparison of the data-summary curves with the rainfall prediction curves for Wallops Island (dash-dotted) from the RH model using the thunderstorm ratio, β. The right-hand three panels of Figure 3 show the comparison of the data-summary curves with the rainfall prediction curves for Wallops Island (dash-dotted) from the RH model using the thunderstorm ratio $U'/D'_{.01}$. In all cases, the prediction curves from the RH model are the median (50 percent) distribution prediction and the 5 and 95 percent confidence limit curves, as indicated in the upper middle and upper right-hand panels of Figure 3. Figures 4 and 5 are identical in format to Figure 3 except that they represent Miami, Florida, with two observed annual distributions of rain rate (Jones and Sims, 1971), and Rio de Janeiro, Brazil, with three observed annual distributions of rain rate (CCIR, 1981).

It is apparent from Figures 3, 4, and 5 that they tell more about the data-summarization procedures than they do about comparison of the two rain rate prediction methods. In Figure 3 all three data-summary procedures work fairly well, giving reasonably smooth results. In Figure 4, however, weighted regression summary looks almost comical. In Figure 5, no summary procedure is attractive. Weighted regression looks nearly as bad as in Figure 4, unweighted regression doesn't enclose all the data points it is supposed to summarize, and mean-scaling has a ridiculously large 95 percent confidence limit. One requirement for the use of weighted regression seems to be that at least 4 or 5 distributions are needed before it can be reasonably used. Otherwise, when you have, say, only two distributions, as for Miami in Figure 4, the data distributions can intersect, resulting in percentile levels with <u>zero</u> variability. Thus, the summary prediction limits can oscillate about the median, with a very nondistribution-like behavior.

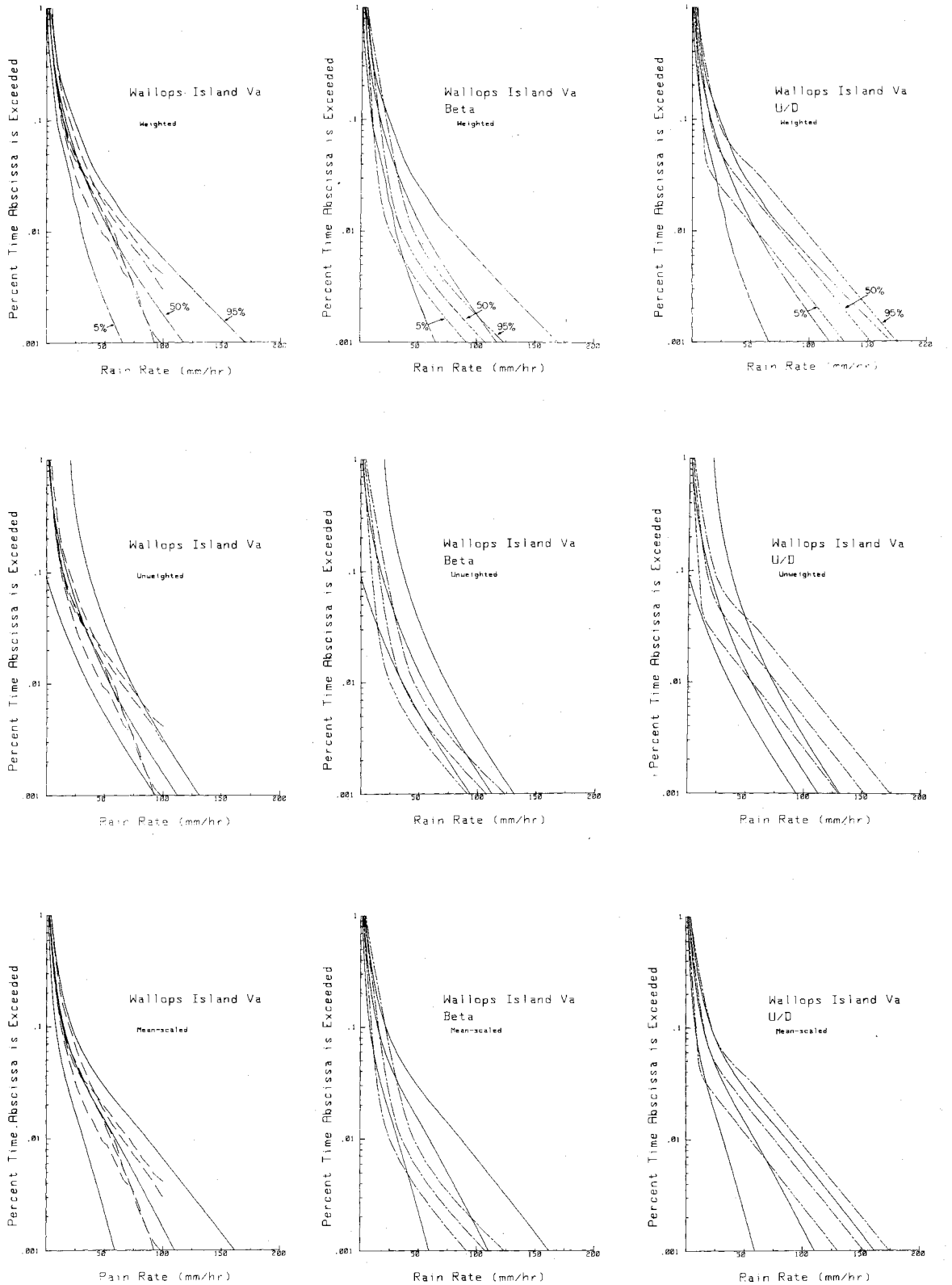

Figure 3. Comparison of observed data distributions at Wallops Island, VA, with the Rice-Holmberg rain rate distribution prediction model using the β and $U'/D'_{.01}$ thunderstorm ratios. The first column shows three data-regression summary techniques. The resultant regression and the 5 and 95 percent confidence limits are compared with the β and $U'/D'_{.01}$ modeling results in the second and third columns, respectively.

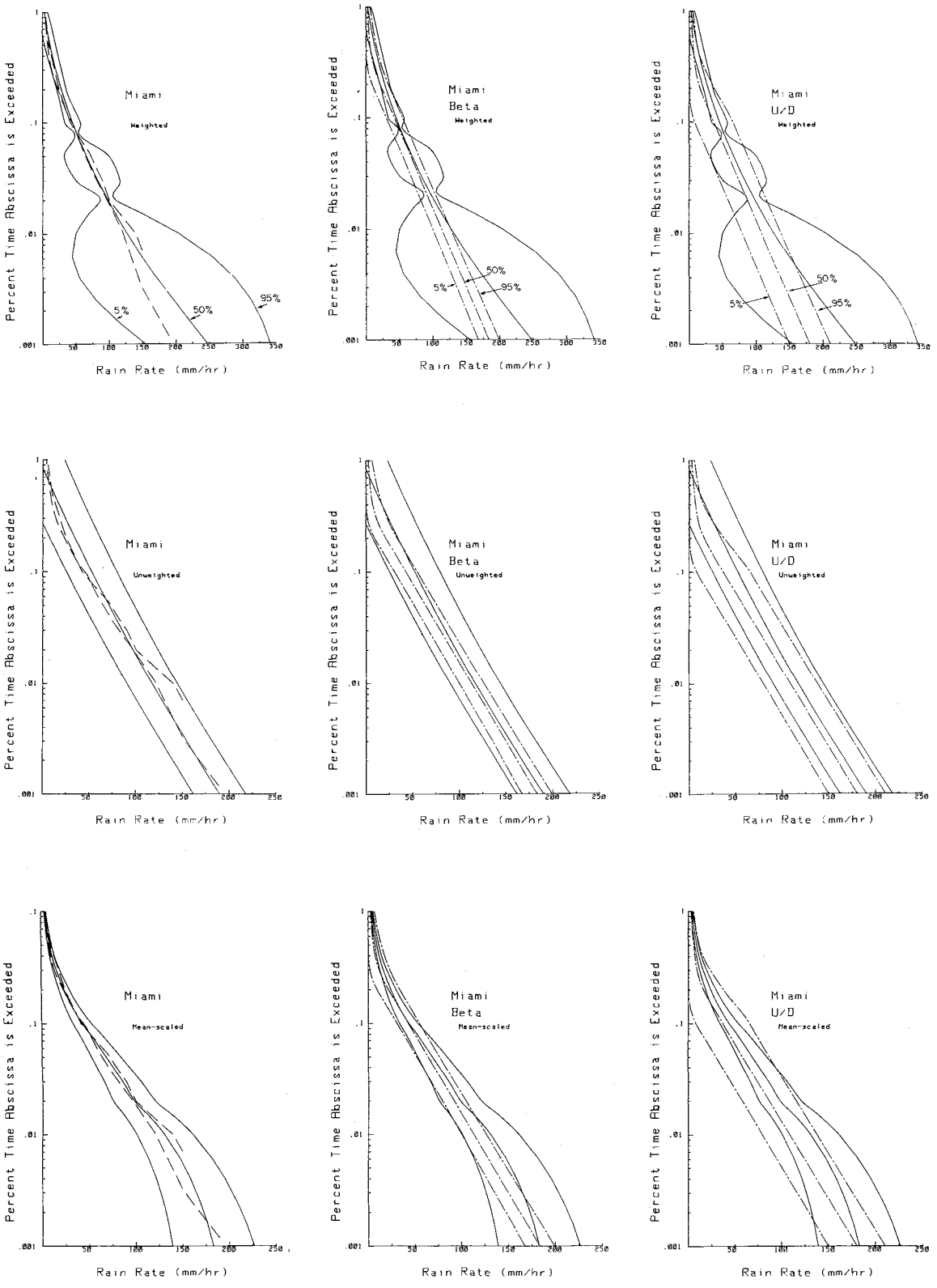

Figure 4. Comparison of observed data and predicted distributions at Miami, FL, in the format of Figure 3.

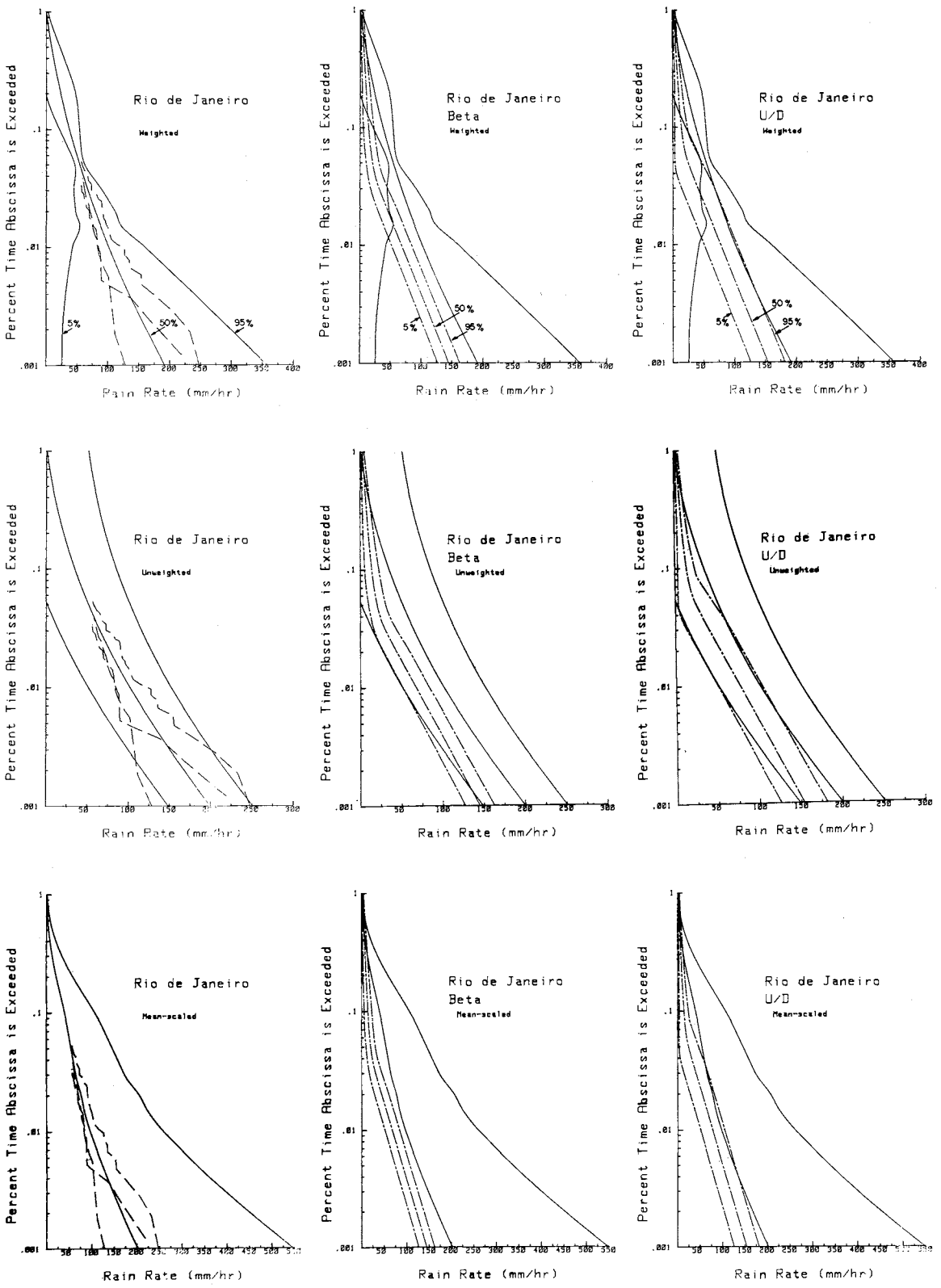

Figure 5. Comparison of observed data and predicted distributions at Rio de Janeiro, Brazil, in the format of Figure 3.

In general, the performance of the various data-summarization techniques should be such that when numerous years of annual distributions become available, weighted regression should perform rather well. At this point, however, rain rate distributions, at the locations for which we have them, are available for no more than five years and usually only for a single year (or less). Thus, we shall use the simple method of comparison of data and predicted distributions, discussed earlier, to further analyze the two RH model prediction methods.

1.3 Results

On the map of the world, given as Figure 6, 13 worldwide locations from which usable rain rate distribution data are available are shown. There are some rain rate distribution data from other locations around the world, but these data are generally not sufficiently extensive, are discontinuous, or are taken from measuring instruments with overly large integration times. In order to be used in the analysis given in this subsection, data were required to be taken continuously over at least a year in time, and the rain gauge integration time was required to be five minutes or less. This, in turn, contains the implicit requirement that the rain-measuring instrument had to be a recording rain gauge.

There are actually 20 locations worldwide that satisfied these requirements, but some of them were practically coincident geographically with others, resulting in only 13 locations that are distinct on the map of Figure 6. In the process of satisfying the stated location requirements, all available German data were eliminated. Because, however, Germany is an important location in the context of this report, the best example of German data--10 continuous months from Darmstadt--was retained and used in the analysis. Data from the other important locations, considered in the contour mapping in Section 3 of this report, were, with the exception of the U. S. A. (United States of America), unavailable to our knowledge. This is evident from the map of Figure 6, as well. In a few cases, mostly in Japan, integration times were unknown, but since the data were measured by recording rain gauges, it is most likely that the integration time is $\leq$5 minutes in all these cases. Hence, these data were included.

Table 1 shows an analysis and summary of the comparison of observed rain rate distributions from the 20 data locations versus predicted results from the RH model using the standard β and the $U'/D'_{.01}$ thunderstorm ratios. As noted earlier, the only likely significant comparison of data distributions with the prediction distributions is based upon whether the data distribution lies inside or outside the 0.5 and 99.5 percent prediction levels. This is the type of comparison made in Table 1.

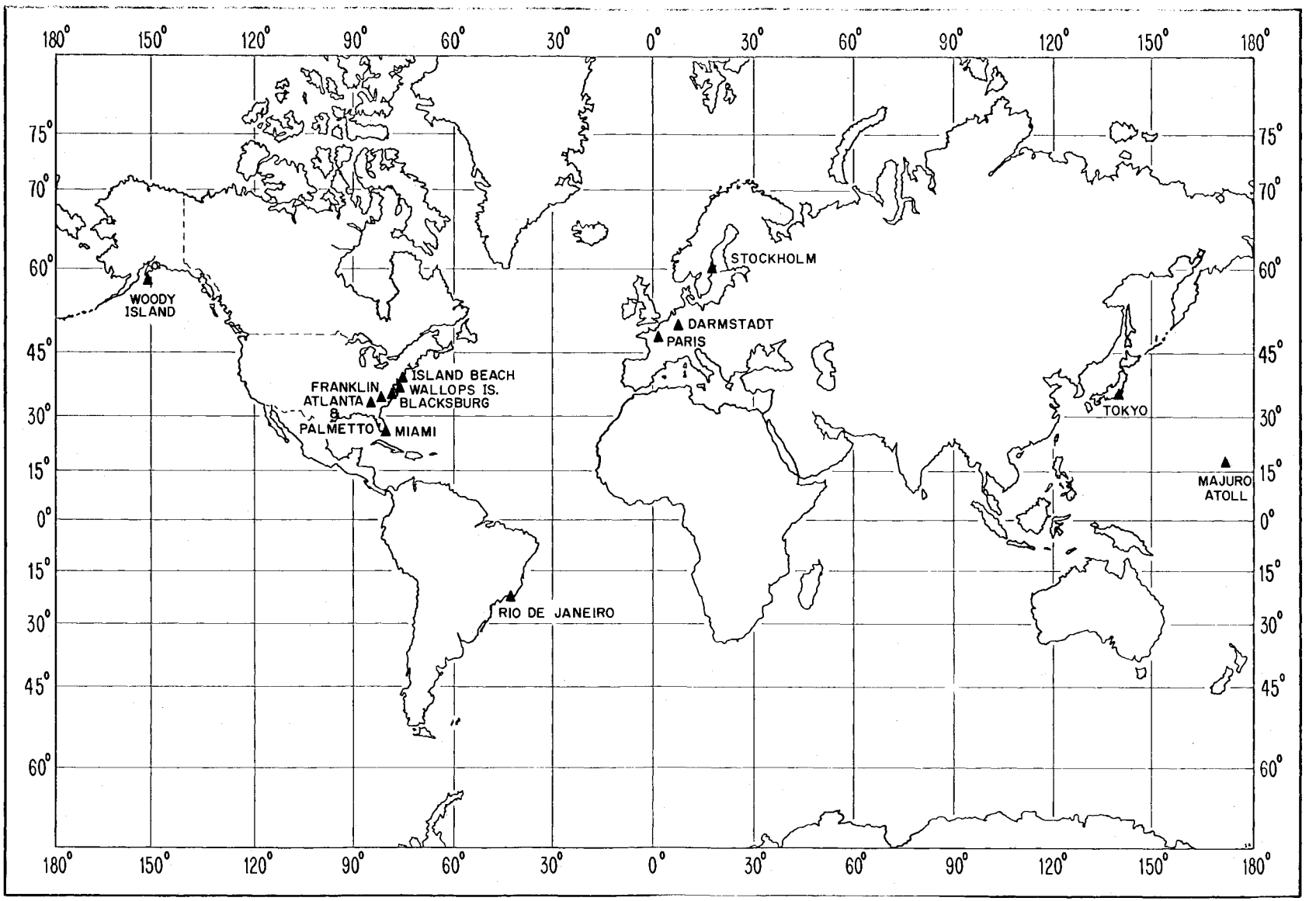

Figure 6. Map of the world showing 13 worldwide locations with usable rain rate distribution data.

Table 1

Absolute Value of Observed Rain Rate Deviation, ΔR, Outside 0.5 and 99.5 Percent Confidence limits Using the Two Thunderstorm Ratio Estimation Procedures in the RH Model

Observing Station i	Data Period (years)	Gauge Integration Time (min.)	$\lvert\Delta R_i\rvert$ at 1% Exceedance Level (mm/hr)		$\lvert\Delta R_i\rvert$ at 0.1% Exceedance Level (mm/hr)		$\lvert\Delta R_i\rvert$ at 0.01% Exceedance Level (mm/hr)		$\lvert\Delta R_i\rvert$ at 0.001% Exceedance Level (mm/hr)		Assigned Weight, w_i
			β	$U'/D'_{.01}$	β	$U'/D'_{.01}$	β	$U'/D'_{.01}$	β	$U'/D'_{.01}$	
Miami, FL	1	1	0	0	0	0	0	0	0	0	1
Island Beach, NJ	1	1	0	0	0	0	0	0	0	2	1
Franklin, NC	1.25	1	0	0	0	0	0	20	-	-	1.25
Wallops Island, VA	4	0.03	0	0	0	0	13	0	-	-	4
Stockholm, Sweden	2	1	0	0	0	0	14	7	1	3	2
Stockholm, Sweden	2	1	0	0	0	0	0	0	19	21	2
Atlanta, GA	20	5	0	0	0	0	0	0	1	0	20
Majuro Atoll, Marshall Islands	1	1	0	0	2	9	0	15	0	0	1
Palmetto, GA (near Atlanta)	2	5	-	-	3	0	0	0	15	12	2
Paris, France	13	1	-	-	-	-	0	0	0	4	13
Tokyo (Takematsu), Japan	1	?	0	0	0	0	0	9	-	-	1
Tokyo (Kashima), Japan	1	?	0	0	0	0	14	0	-	-	1
Woody Is., Alaska	2.83	1	0	0	0	0	0	0	32	0	2.83
Paris(Montsouris), France	10	1	-	-	-	-	0	0	0	4	10
Paris(Gometz), France	1	1	-	-	0	0	0	0	49	56	1
Rio de Janeiro, Brazil	3	1	-	-	-	-	8	0	59	37	3
Blacksburg, VA	3.67	?	2	1	0	0	0	0	4	21	3.67
Tokyo(Shakujii), Japan	1	?	-	-	0	0	0	24	0	43	1
Tokyo(Sakai), Japan	1	?	-	-	1	3	0	33	3	30	1
Darmstadt,FRG	0.83	5	0	0	0	0	0	0	13	21	0.83
Average departure, $\overline{\lvert\Delta R\rvert}$			0.10	0.05	0.13	0.17	1.62	1.65	6.02	6.94	

In order to put these comparisons on a quantitative basis, the absolute value of the departure, ΔR_i, outside either the 0.5 or 99.5 percent prediction value (largest of the two used, if both outside), for a given observing station, i, was assessed. Zero departures were assigned if the observed distribution lies inside the predicted confidence limits. Four exceedance percentiles, 1, 0.1, 0.01, and 0.001 percent, were checked in the analysis, as shown in Table 1.

Because some of the 20 locations observed annual rain rate distributions for a longer period of time than others, it was necessary to assign a weight, w_i, to each location. Nonunity weights represent situations where the data were "lumped" into a single distribution, longer (or shorter in the case of Darmstadt) than an annual distribution. The average departure $|\Delta R|$ is then given by

$$\overline{|\Delta R|} = \frac{\sum_{i=1}^{20} w_i |\Delta R_i|}{\sum_{i=1}^{20} w_i} \quad . \tag{4}$$

The results of the averaging process of Equation (4) are shown at the bottom of Table 1, which show a slight worsening of the deviation for the $U'/D'_{.01}$ thunderstorm ratio method as contrasted with the standard β method. The dashes in Table 1 indicate a lack of data that therefore could not be included in the average values at the bottom of Table 1.

The apparent slight increase in error by using the $U'/D'_{.01}$ method is, in the author's opinion, hardly sufficient to gainsay its use as an alternative to the standard β method. So much more data can be processed, with more meaningful contouring* as in Section 3, that $U'/D'_{.01}$ seems to be a significant and often desirable alternative to, and even replacement for, the standard β thunderstorm ratio usage in the RH model.

2. PREDICTION OF MICROWAVE TERRESTRIAL LINK RAIN ATTENUATION

The classical relationship between specific attenuation (attenuation per unit length), $\alpha(f)$, and rain rate, R, is

$$\alpha(f) = a(f)R^{b(f)} \quad , \tag{5}$$

*The $U'/D'_{.01}$ method appears to give a more reasonable estimate of low percentile rain rates in mountainous regions.

where f is frequency, and a(f) and b(f) are frequency-dependent coefficients, was developed nearly 40 years ago, and has been steadily refined since (Ryde, 1946; Medhurst, 1965; Olsen et al., 1978). This relationship can be regarded as reasonably well established for frequencies less than about 15 GHz. What is not so well established, however, is the behavior of total attenuation, $\tau(f)$, along a path of length L, versus a given point rain rate, R. We can establish a relationship,

$$\tau(f) = a(f)\overline{R}^{b(f)}L \quad , \tag{6}$$

from (5) without difficulty, where $\overline{R}$ is now a "path-average rain rate." We can also establish a relationship equivalent to (6),

$$\tau(f) = a(f)R^{b(f)}D_e \quad , \tag{7}$$

where D_e is an "effective path length."

Determining $\overline{R}$, D_e, or whatever other parameter can be defined to explain rain inhomogeneity along a microwave path is the real impediment. Numerous models have been developed to account for path rain inhomogeneity in predicting the distribution of rain attenuation over a year's time. A number of these models will be discussed next.

2.1 Rain Attenuation Distribution Prediction Models

Rain attenuation distribution prediction models have been available for about 10 years. Some of the earlier ones were not initially presented in the distribution prediction format, but are easily adapted. Chronologically, these models can be subdivided into three categories: older models, moderately new models, and very recent models. This is the context in which they are presented in this report.

2.1.1 Older Models

Barsis et al. (1973) present a set of curves for conversion of R to $\overline{R}$. There is not a tabular presentation of $\overline{R}/R$ given with this model, but rather a graph to which we fit curves for computer interpolation and extrapolation. This model introduces an effective distance maximum of 22 km. The model uses (5) to evaluate specific attenuation, but with no suggested a(f) and b(f) values, we have chosen to use the values of Olsen et al. (1978) in connection with this model.

Battesti et al. (1971) have presented a procedure for the reduction of rain intensity, presumably analogous to $\overline{R}/R$. It is not entirely clear that the "reduction

factor" in their paper is directly applicable to attenuation or to probability, but we have assumed it applies to attenuation. Little information is given on how the reduction factor was obtained. Therefore, again, we have taken the liberty of incorporating it into computer software by means of curvefitting. Rain rate, R, can be chosen at some percentile, P, of a year, permitting evaluation of $\tau(f)$ at P, also.

2.1.2 Moderately New Models

Lin (1975) presented a formidable model for the assessment of $\overline{R}/R$. Then Lin (1977) developed a much simpler version, which is, because of its relative simplicity, in widespread use today. The model can be described by,

$$\tau(f) = a(f)R^{b(f)}L\ K_r(R,L) \quad , \tag{8}$$

where $K_r(R,L)$, the path reduction coefficient, is given by

$$K_r(R,L) = \frac{1}{1 + L\ \frac{R - 6.2}{2636}} \quad , \tag{9}$$

provided $R > 10$ mm/hr. In (9), L is in kilometers and R is in millimeters per hour. This model has been verified at locations referred by Lin (1977) as "city A," "city B," etc. The rain rate, R, then, as in the older models, can be obtained for some percentile, P, of a year, so that $\tau(f)$ also applies to that percentile. The constants in (9) were evaluated from 11 GHz data taken at Palmetto, Georgia.

Morita and Higuti (1976) introduce a gamma distribution for point rain rates, then develop a "spatial correlation function" to extend the concept (implicitly) to path rain rates and then (explicitly) to rain attenuation distributions, still using a gamma distribution. They use the specific attenuation relation (5) to derive these results. However, rain rate is not needed as an input to this model, since we solve the inverse gamma function to obtain $\tau(f)$, given the exceedance percentile, $P(A>\tau(f))$, where A is a random-variable attenuation. The gamma distribution for rain rate, R, can be written as

$$P(r>R) = \int_R^\infty \frac{c^\nu}{\Gamma(\nu)}\ x^{\nu-1}e^{-cx}dx \tag{10}$$

In (10), ν and c are parameters of the distribution, $\Gamma(\nu)$ is a gamma function, x is a dummy variable, and r is a random-variable attenuation. It is necessary to evaluate ν and c in order to use the Morita-Higuti model, and they do not provide a

procedure. However, regression can be used to relate ν and c to total annual precipitation, M, in millimeters and the thunderstorm ratio, β, (see Section 1). This yields

$$\mu = 2.90 \times 10^{-4}(\beta M)^{0.926} \quad \text{mm/hr} \tag{11a}$$

$$\sigma^2 = 5.41 \times 10^{-3}(\beta M)^{1.024}, \quad (\text{mm/hr})^2 \tag{11b}$$

where

$$\nu = \mu^2/\sigma^2 , \tag{11c}$$

and

$$c = \mu/\sigma^2 . \tag{11d}$$

Misme and Fimbel (1975) developed a terrestrial link rain attenuation distribution prediction model that was later expanded by Misme and Waldtenfel (1980) into an earth/space attenuation model. The latter paper is brought to the attention of the reader because it is a direct extension of the terrestrial link model, and it is written in English, whereas the 1975 paper is written in French. This is a somewhat abstract model, the greatest abstraction surrounding the definition of an "area of storm centers," S. From this parameter the authors developed a ratio of S to the area of a precipitation cell from which they conclude that "the probability for intensity R to be observed at any point of the link is, of course, greater than that of R being observed at a given point by a factor found equal to. . ." the ratio. A computer algorithm is included with the methodology that calculates $P(A>\tau(f))$. This algorithm has proven helpful, but has had to be somewhat rewritten for our purposes to obtain the inverse of $P(A>\tau(f))$.

Crane (1980) has developed a model that has become more commonly known as the "global model." It is a straightforward and readily usable model, the basis of which is a tri-exponential expression that accounts for point-to-path rain rate conversion. The model has some abrupt changes depending upon the path length used. The model requires input of a rain rate R, observed for a percentile P. These R's must be obtained on a zonal basis, with eight zones worldwide, and an expanded zonal version for the U. S. A.

2.1.3 Very Recent Models

Crane (1982) published another model that shall be referred to as the "two-component" model. This model divides rainfall into a core "cell" (heavier rain) surrounded by "debris" (lighter rain). Then a bi-exponential distribution is used to represent the rain rate distribution, with one exponential term representing the

cellular rain and the other exponential term representing the debris rain. This concept, and the appearance of the resultant rain rate distribution, is very similar to the Rice-Holmberg procedure (see Section 1). The bi-exponential concept is then extended to attenuation distributions. The parameters of the distributions are evaluated on a rain-zone basis, as in the global model, and are tabulated. As a consequence, the "two-component" model can only be evaluated on the zonal basis, whereas other approaches (e.g., contour maps) can be interfaced with the global model.

Kanellopoulos (1983) has presented an interesting modification to the Lin (1977) model, described earlier. The Lin model is based on the use of rain rates observed from gauges having 5-minute integration times. Since smaller integration times (e.g., 1-minute times) are considered more representative of instaneous rates, Kanellopoulos (1983) introduces a factor in (8) that permits use of rain rates observed at any integration time.

Considering the worldwide proliferation of microwave terrestrial link rain attenuation distribution prediction models, the CCIR (1982) has developed its own model. They assume that the attenuation $\tau_{0.01}(f)$, expected to be exceeded 0.01 percent of an average year is given by (8) for the corresponding R at the 0.01 percentile. The $\tau(f)$ at any percentile, P, is then given by

$$\tau_f(f) = \tau_{0.01}(f)(P/0.01)^{-c} \quad , \tag{12}$$

where

$$c = \begin{cases} 0.03, & 0.001 \leq P \leq 0.01\%, \\ 0.41, & 0.01 < P \leq 0.1\% \ . \end{cases}$$

The factor $K_r(R,L)$ in (8) is taken to be independent of R, and is given by

$$K_r(R,L) = \frac{90}{90 + 4L} \quad . \tag{13}$$

2.1.4 A Proposed New Model

Dutton et al. (1982) discuss the concept of a "probability modification factor" (PMF) as a procedure for correcting for finite storm sizes on satellite/ground communication links. The PMF multiplies the percent of time, P_o, during an average year that homogeneous rainfall-caused attenuation is expected at a given location. The resultant value represents the percent of time, P ($P \leq P_o$), that the

actual attenuation is expected to be exceeded along the path to the satellite. As such, it is not directly interpretable as the $K_r(R,L)$ in (8).

The idea behind this model is the establishment of a PMF for use on terrestrial links. The first consideration is that the PMF should likely be larger than the satellite/earth PMF. This is because the total effective path length through rain is likely to be much smaller; hence, it should encounter more homogeneous rainfall conditions, as illustrated in Figure 7. In Figure 7 the ground-projection length, L_{TOP}, of the satellite/earth path through all possible rain is given by

$$L_{TOP} \cong 130.33 \sqrt{h_{TOP}} \quad , \tag{14}$$

where h_{TOP} is the expected storm-top height. In (14), h_{TOP} and L_{TOP} are in kilometers, and h_{TOP} is obtainable from the surface rain rate R. Note that the "satellite/earth path" in Figure 7 is assumed to have an elevation angle of 0° at the earth station*. In this case, the PMF of Dutton et al. (1982) becomes, for frequency, f, in gigahertz,

$$PMF = 0.987 \frac{(f/15)^2}{\tau(f)} \quad . \tag{15}$$

If we now introduce a factor,

$$G(L) = \frac{L_{TOP}}{L} \quad , \tag{16}$$

to (usually) increase the PMF for terrestrial-link application, (15) becomes

$$PMF = 0.987 \frac{(f/15)^2}{\tau(f)} G(L) \quad . \tag{17}$$

Hence, the Dutton-Dougherty rain attenuation model for satellite/earth links (Dutton et al., 1982) can be adapted for use as a terrestrial link model, which we shall call PROMOD.

*It is recognized that not all terrestrial links have 0° elevation angles, but accounting for other angles has little impact on the modeling.

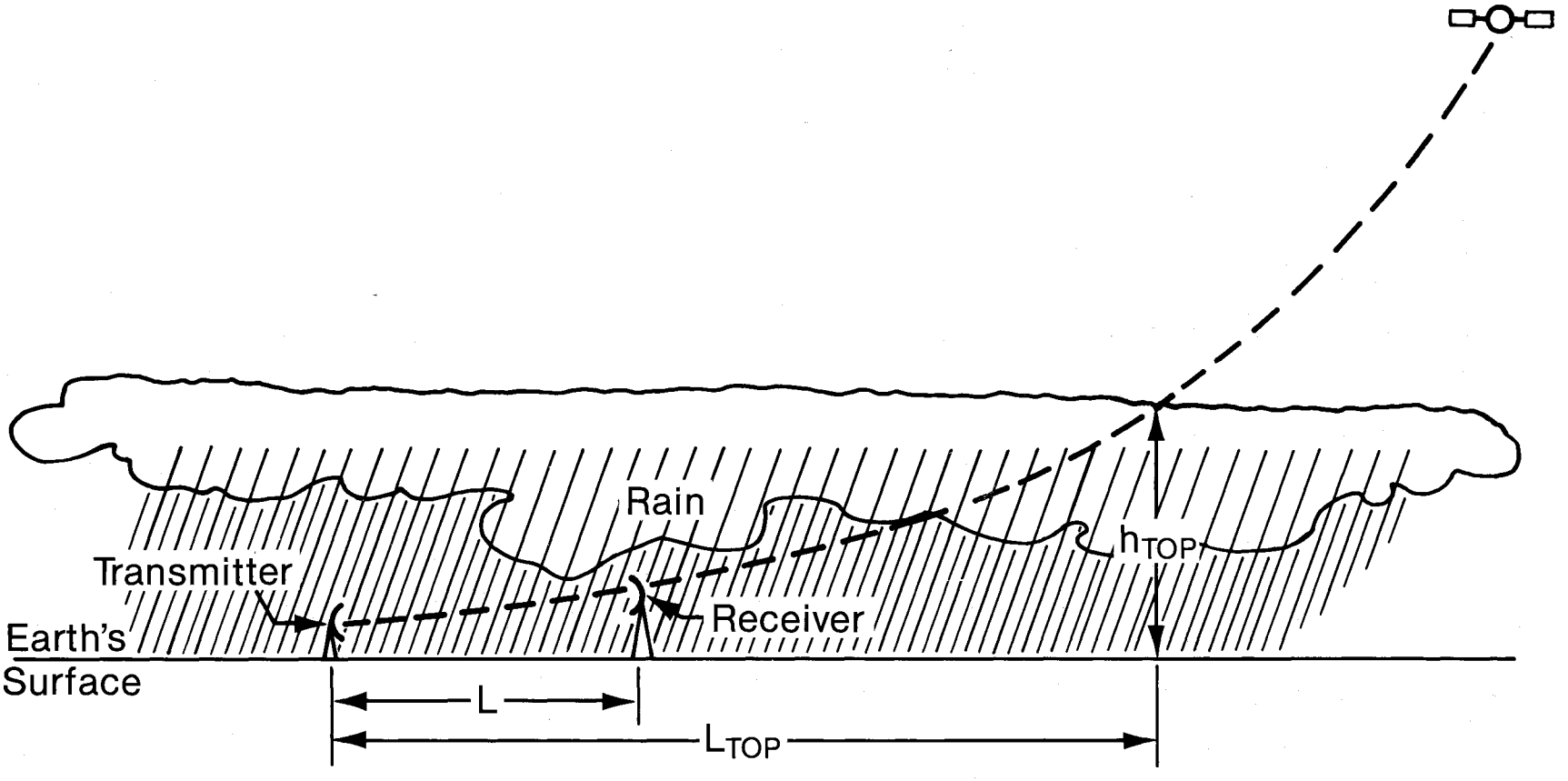

Figure 7. Illustration of ray-path geometry used in the PROMOD terrestrial-link attenuation distribution prediction model.

2.1.5 Modeling Year-to-Year Variability

The PROMOD model, since it is a direct modification of the Dutton et al. (1982) satellite/earth model, inherently contains an allowance for the often large year-to-year variability in the prediction of annual rain attenuation distributions. Most of the other models discussed in this section do not contain such a feature, being instead restricted to predicting an average or median annual distribution. More often, the modelers derive a single distribution, but do not indicate its statistical meaning; hence, we have chosen to interpret such models as median annual distributions.

It is necessary to accommodate year-to-year variability in these other models since it will be required for comparison of the various models, and the ultimate choice of one of them as "best" for a given area. The global model (Crane, 1980) and the two-component model (Crane, 1982) contain a recommendation that the year-to-year standard deviation be 36 percent of the expected (median) attenuation distribution at the 1 and 0.001 percentile levels, while at the 0.1 and 0.01 percentiles, it is 28 percent of the expected distribution. We have taken the liberty of fitting a quadratic to the four percentages (36, 28, 28, 36) to obtain percentage values for intermediate percentiles (e.g., we get 27.0 percent of the expected distribution at the 0.03 percentile). The remaining models do not consider year-to-year variability; therefore, we have chosen an ad hoc procedure to obtain year-to-year variability for each model. Whenever possible, we have tried to apply the Dutton et al. (1982) variability techniques to such models. This is because the variability can be based on local meteorological data rather than the universal percentage values of Crane (1980).

Thus, the Crane (1980) result is used with the CCIR (1982) and Misme and Fimbel (1975) methods. This is because the CCIR (1982) model is a zonal model, similar to the global model, and the Misme and Fimbel (1975) model is not amenable to the other variability technique. Otherwise, the Barsis (1973), Battesti et al. (1971), Lin (1977), Morita and Higuti (1976), and modified Lin (Kanellopoulas, 1983), models can be used in connection with the Dutton et al. (1982) year-to-year attenuation variability technique. Note, however, that the modifications (11a) and (11b) must be made in the Morita and Higuti (1976) model before the variability technique is usable.

It is not necessarily fair to many of these models to attach an arbitrary variability technique and then compare the models with data, as is done in the next section. Therefore, in addition to comparing all the models in the next section, a comparison is made limited to the PROMOD model, the global model, and the

two-component model (see Section 2.3. These are the three models that directly contain an allowance for year-to-year variability in the prediction of annual rain-rate attenuation distributions.

2.2 Comparison of Models with Data

The 10 models discussed in the last section must somehow be compared with one another using available data in a manner that has some physical meaning. An approach that has very little meaning is the comparison of a predicted median or average annual distribution of rain attenuation with one given yearly data distribution. Unless one knows where the observed annual distribution lies with respect to all other possible annual distributions in the historical sample space, one has no business comparing with the median, or any other such individual predicted distribution. This kind of comparison has been common in the past, but the conclusions to be drawn from such comparisons are generally nugatory.

Hence, another, more meaningful comparison approach must be sought. This approach undoubtedly must use the concept of predicted year-to-year variability in rain attenuation distributions, since this variability is usually significantly large for percentages below 0.1 percent of a year. The approach that seems best for the moment, although it is not as quantitative as might be desirable, determines whether a given yearly data distribution lies inside or outside a desired confidence interval about the median predicted rain attenuation distribution. This confidence interval is determined from the predicted year-to-year variability of the distribution.

We now must consider an appropriate confidence interval to use in this test. At first glance, a 90 percent confidence interval might seem sufficient, but then there is still a prediction of 1 chance in 10 that the inside/outside comparison test has no significance. If we extend to a 99 percent confidence interval, there is now a prediction of 1 chance in 100 that the test has no significance, and we shall deem that an appropriate risk to run.

As for the test itself, all we have discussed to this point is a very unquantitative binary (yes,no) test of simply whether or not a given annual data distribution lies inside or outside certain predicted confidence limits on a predicted median distribution. We can improve the quantitative aspect somewhat by determining the magnitude of the departure outside the confidence interval. This departure should tend to have more meaning the larger the confidence interval. Because system designers and users are often interested in the highest attenuation, the departure above the upper confidence limit only (99.5 percent) can be tabulated.

Since users are generally interested in a given availability requirement (percent of the time a given attenuation is exceeded--often 0.01 percent), the departure is probably more meaningful if tabulated in decibels at that level.

Figures 8 through 17 illustrate the comparison technique for a 17.7 GHz, 5.1 km link between Rico and Palmetto, Georgia. There is one figure for each of the 10 modeled distributions discussed earlier, as identified in the legend in the upper right-hand corner of each figure. On each of Figures 8 through 17 are five predicted distributions. The inner curve is the median (50 percent) year rain attenuation distribution, the region between the inner two curves surrounding the median-year curve is the 90 percent confidence interval of year-to-year variability (i.e., the two curves, from left to right are the 5 percent and 95 percent confidence limits). The region between the outer two curves surrounding the median-year distribution is the 99 percent confidence interval of year-to-year attenuation variability (i.e., the two curves, from left to right are the 0.5 percent and 99.5 percent confidence limits). We shall choose the 0.01 percent exceedance level as the ordinate value at which we shall make our inside/outside comparison for the 99 percent confidence interval. Furthermore, we shall use the same percentage values in the comparison of all data that follow, for reasons stated earlier. In Figures 8 through 17 there is no case where the data curve, represented by the dot-dashed line, is outside the 99 percent confidence interval. It is notable in Figures 8 through 17 that the confidence intervals range from very wide, as with the Battesti et al. (1971) model used in Figure 10, to very narrow, as with the Morita and Higuti (1976) model used in Figure 14. This inconsistency no doubt results from the amalgamation of different models in order to produce comparison results, and thereby to some unknown degree will prejudice the results. As will be seen, when all models are compared, the Battesti et al. (1971) modified model yields the best comparison with data, and the Morita and Higuti (1976) modified model yields the poorest comparison with data.

The 10 analyzed models generally use rain rate as an input, with the noted exception of the Morita and Higuti (1976) model. The Morita and Higuti (1976) modified model uses expressions (11a) and (11b) which require the thunderstorm ratio, β, and average annual precipitation, M, as inputs. Although the other nine models use rain rate as an input, no consistent choice of a value of rain rate at a specific location for a given percentage of time (e.g., 0.01 percent) exists among the models. Most of the models simply require rain rate, without specifying its choice, whereas the Crane (1980), the two-component (Crane, 1982), and the CCIR (1982) models require a tabulated zonal rain rate input. The PROMOD model

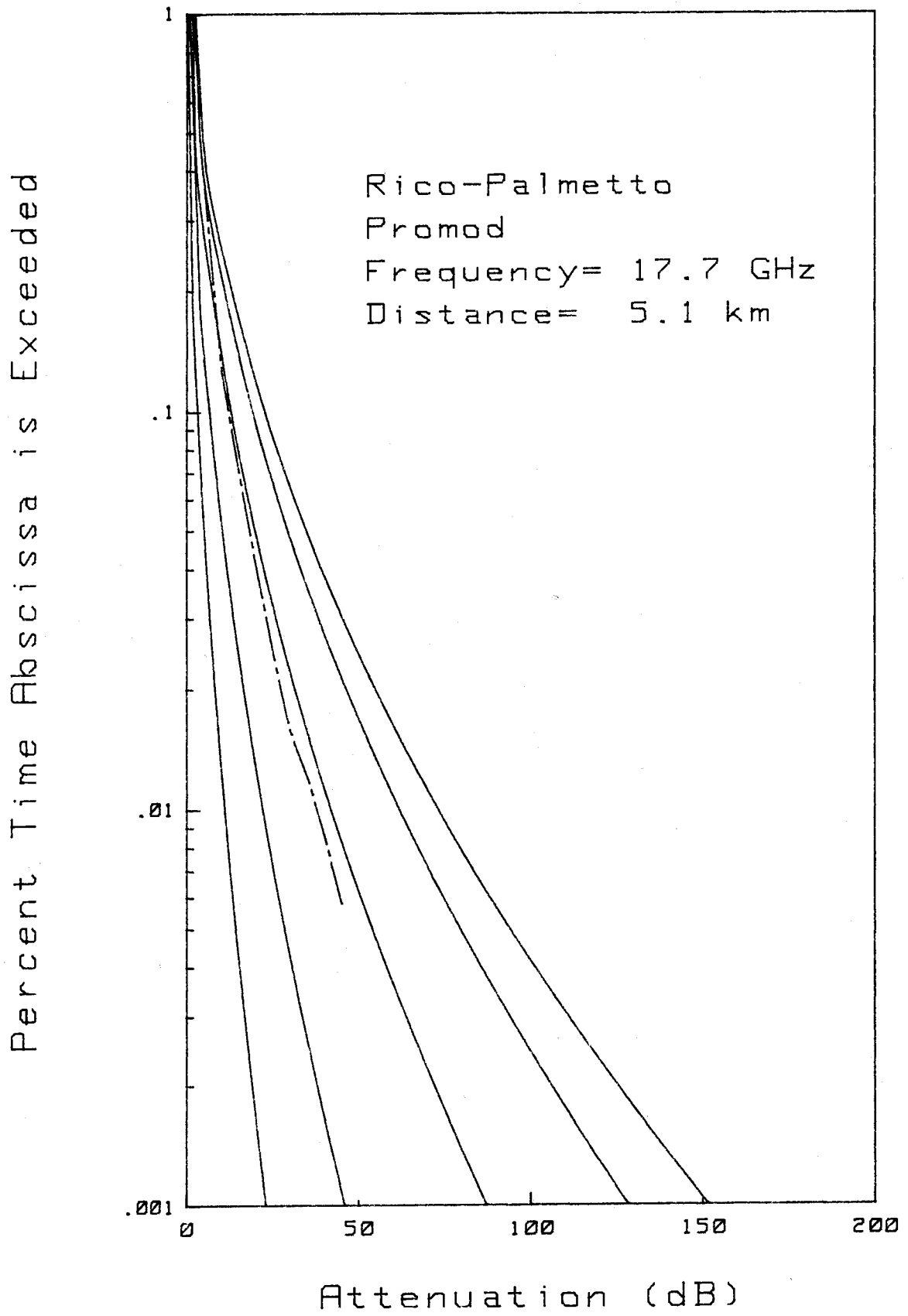

Figure 8. Comparison of the PROMOD attenuation distribution prediction model with data over a 5.1 km, 17.7 GHz link between Rico and Palmetto, GA.

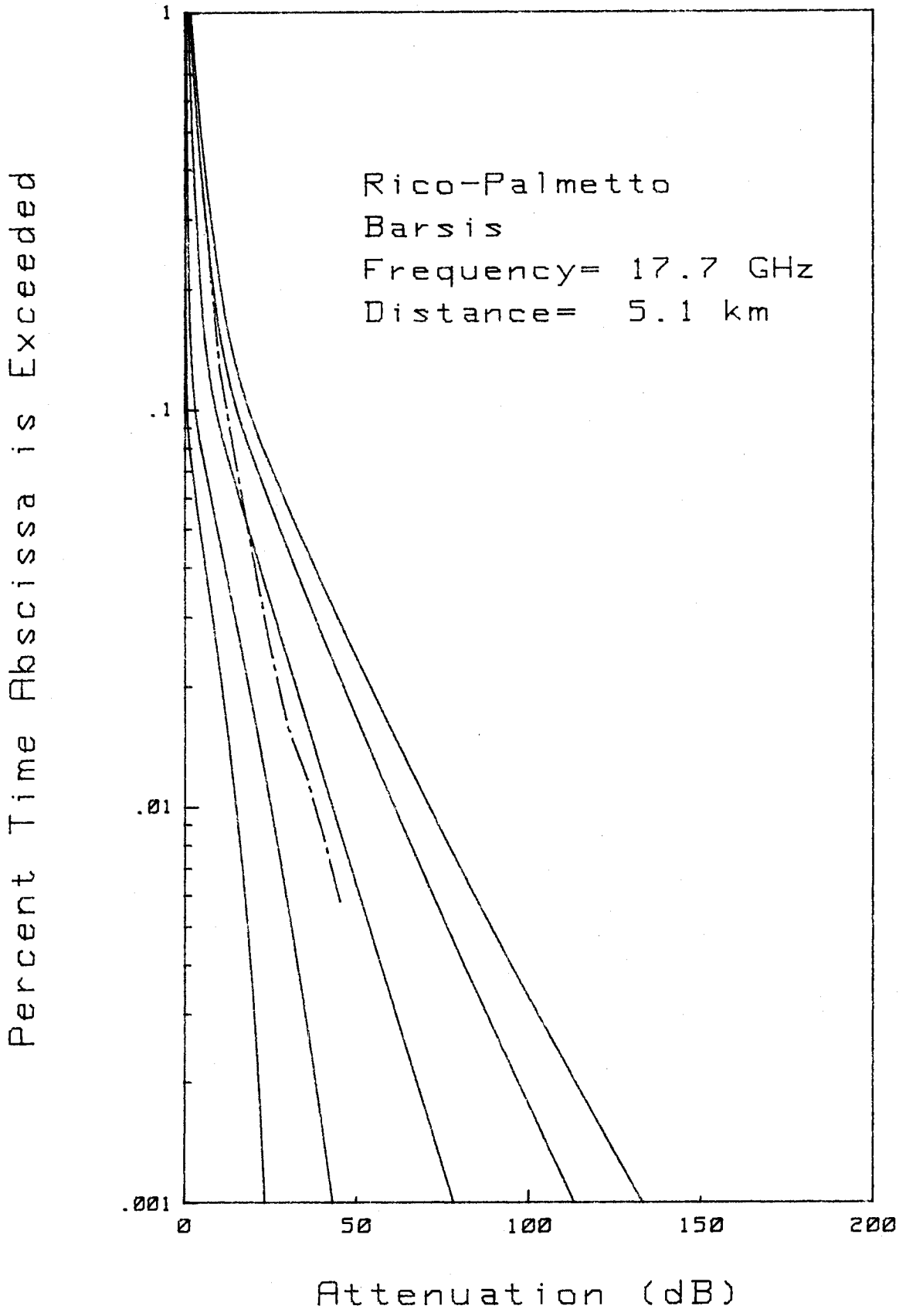

Figure 9. Comparison of the Barsis et al. (1973) attenuation distribution model with data over a 5.1 km, 17.7 GHz link between Rico and Palmetto, GA.

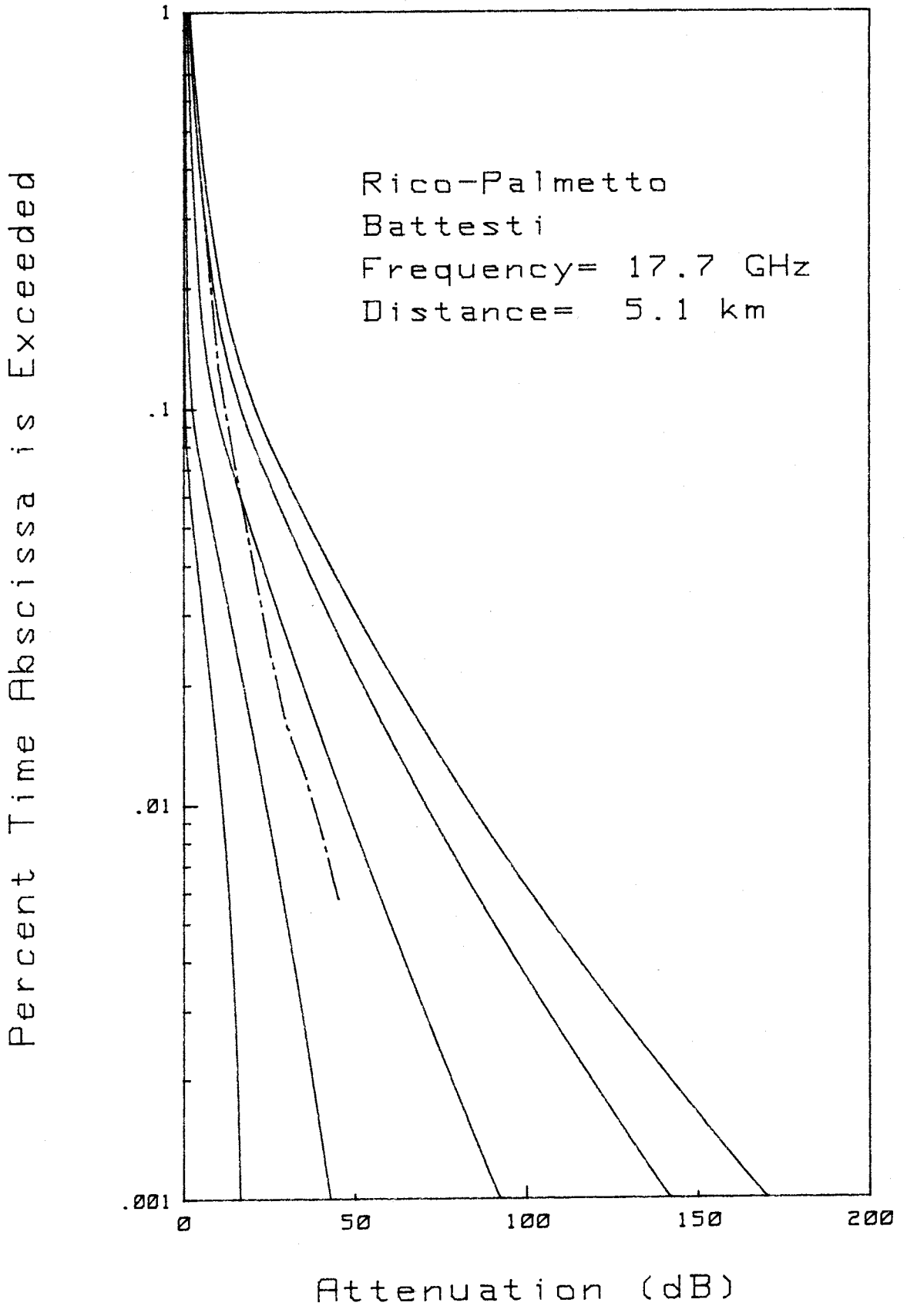

Figure 10. Comparison of the Battesti et al. (1971) attenuation distribution prediction model with data over a 5.1 km, 17.7 GHz link between Rico and Palmetto, GA.

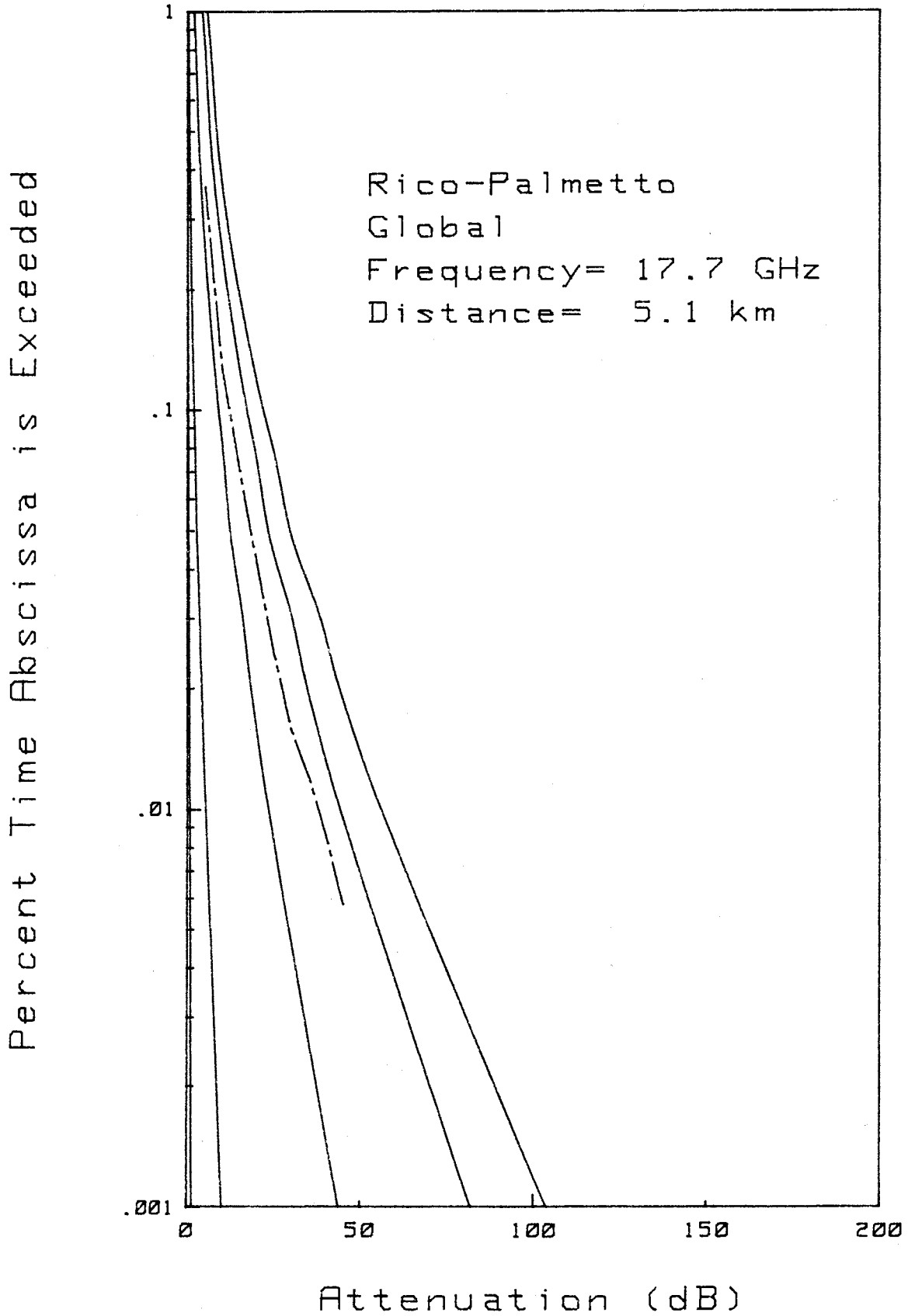

Figure 11. Comparison of the GLOBAL (Crane, 1980) attenuation distribution prediction model with data over a 5.1 km, 17.7 GHz link between Rico and Palmetto, GA.

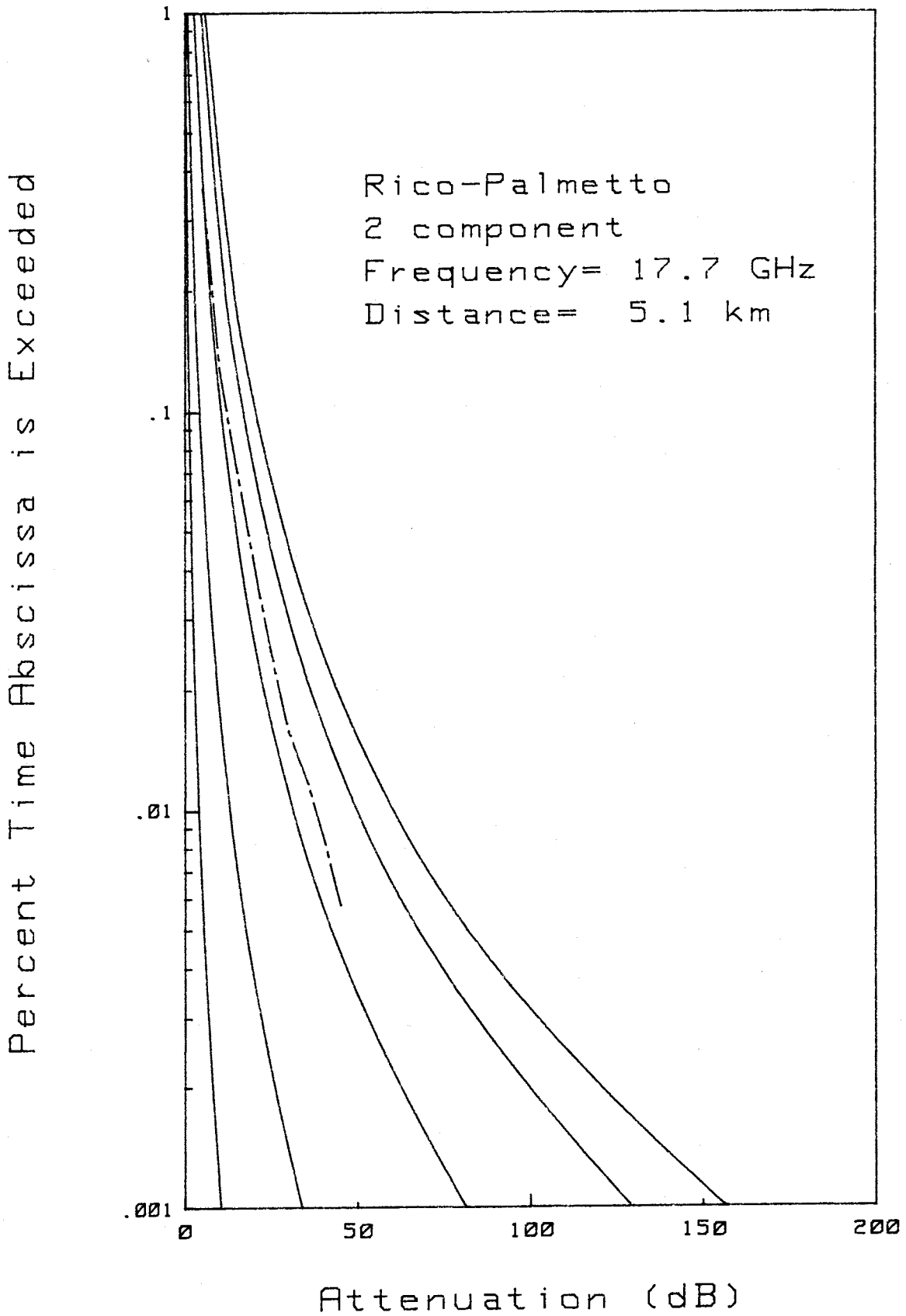

Figure 12. Comparison of the TWO-COMPONENT (Crane, 1982) attenuation distribution prediction model with data over a 5.1 km, 17.7 GHz link between Rico and Palmetto, GA.

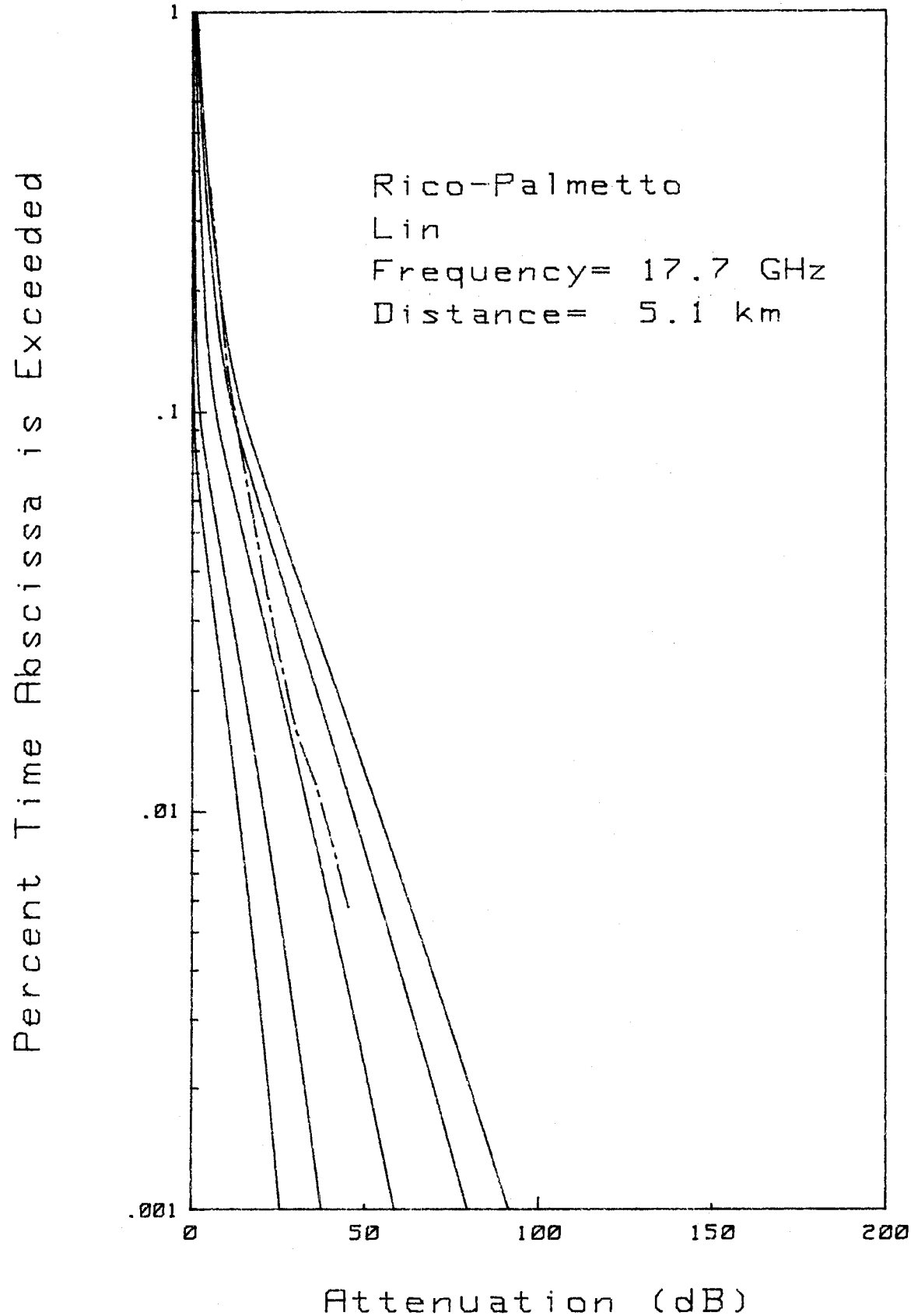

Figure 13. Comparison of the Lin (1977) attenuation distribution prediction model with data over a 5.1 km, 17.7 GHz link between Rico and Palmetto, GA.

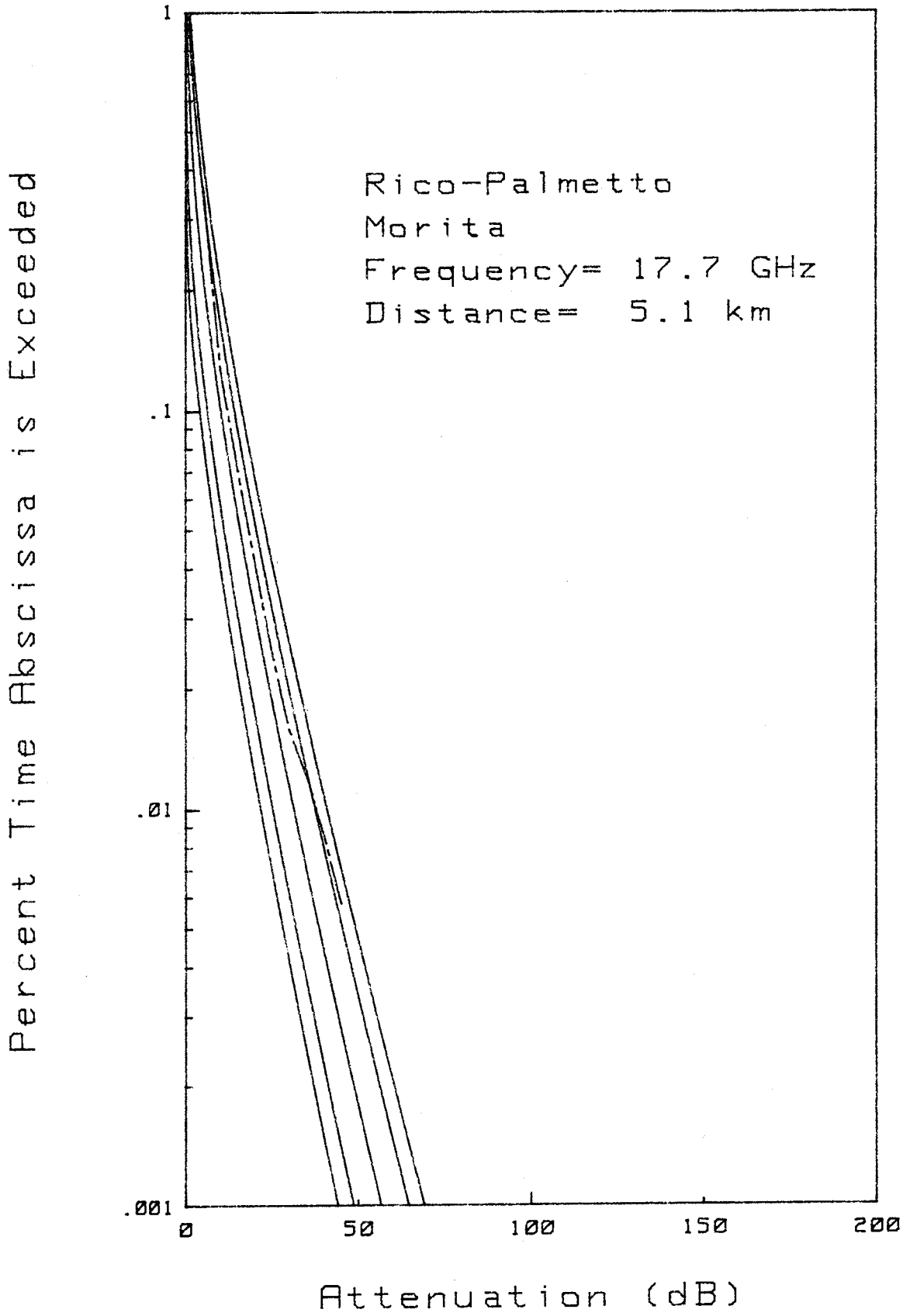

Figure 14. Comparison of the Morita and Higuti (1976) attenuation distribution prediction model with data over a 5.1 km, 17.7 GHz link between Rico and Palmetto, GA.

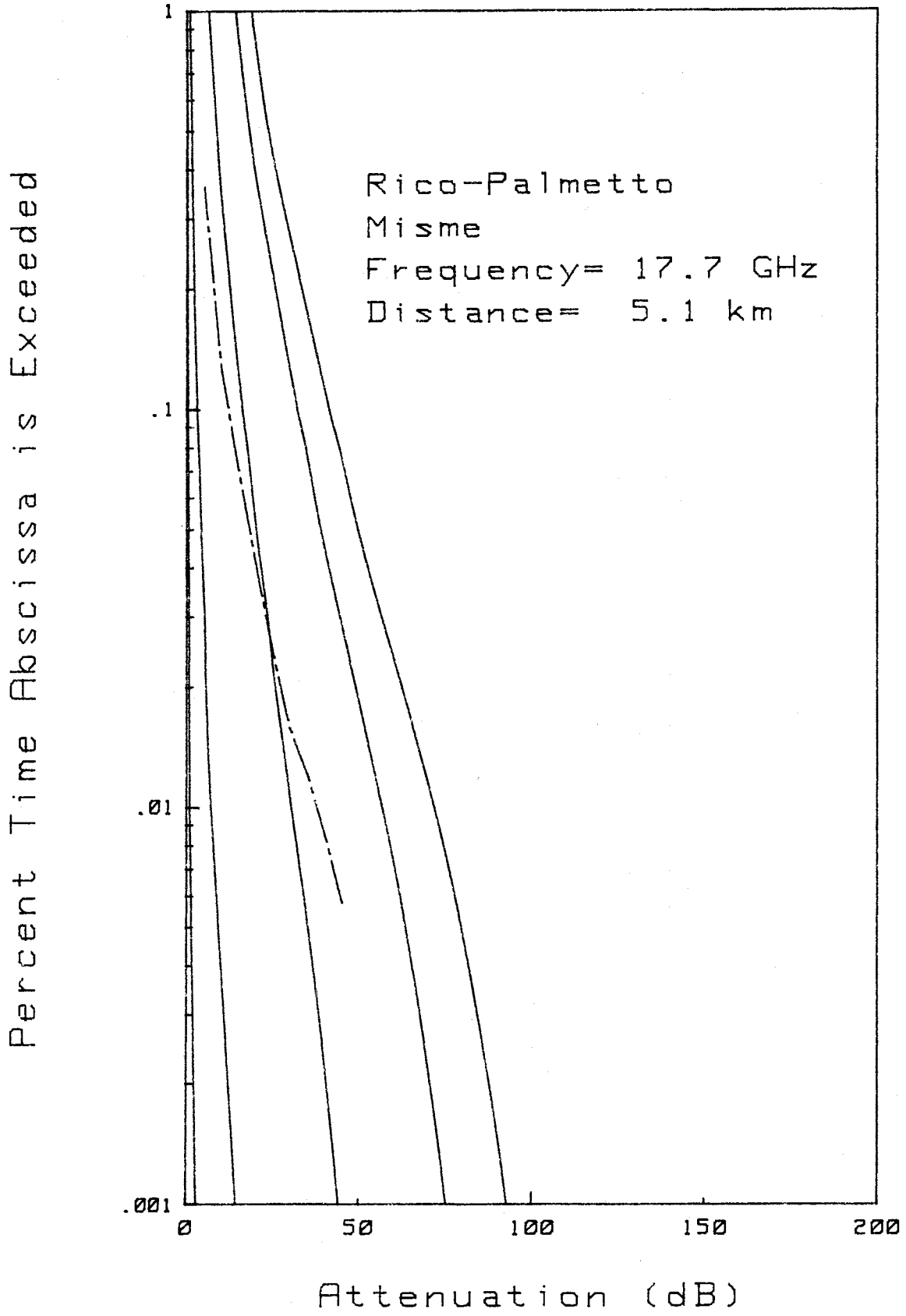

Figure 15. Comparison of the Misme and Fimbel (1975) attenuation distribution prediction model with data over a 5.1 km, 17.7 GHz link between Rico and Palmetto, GA.

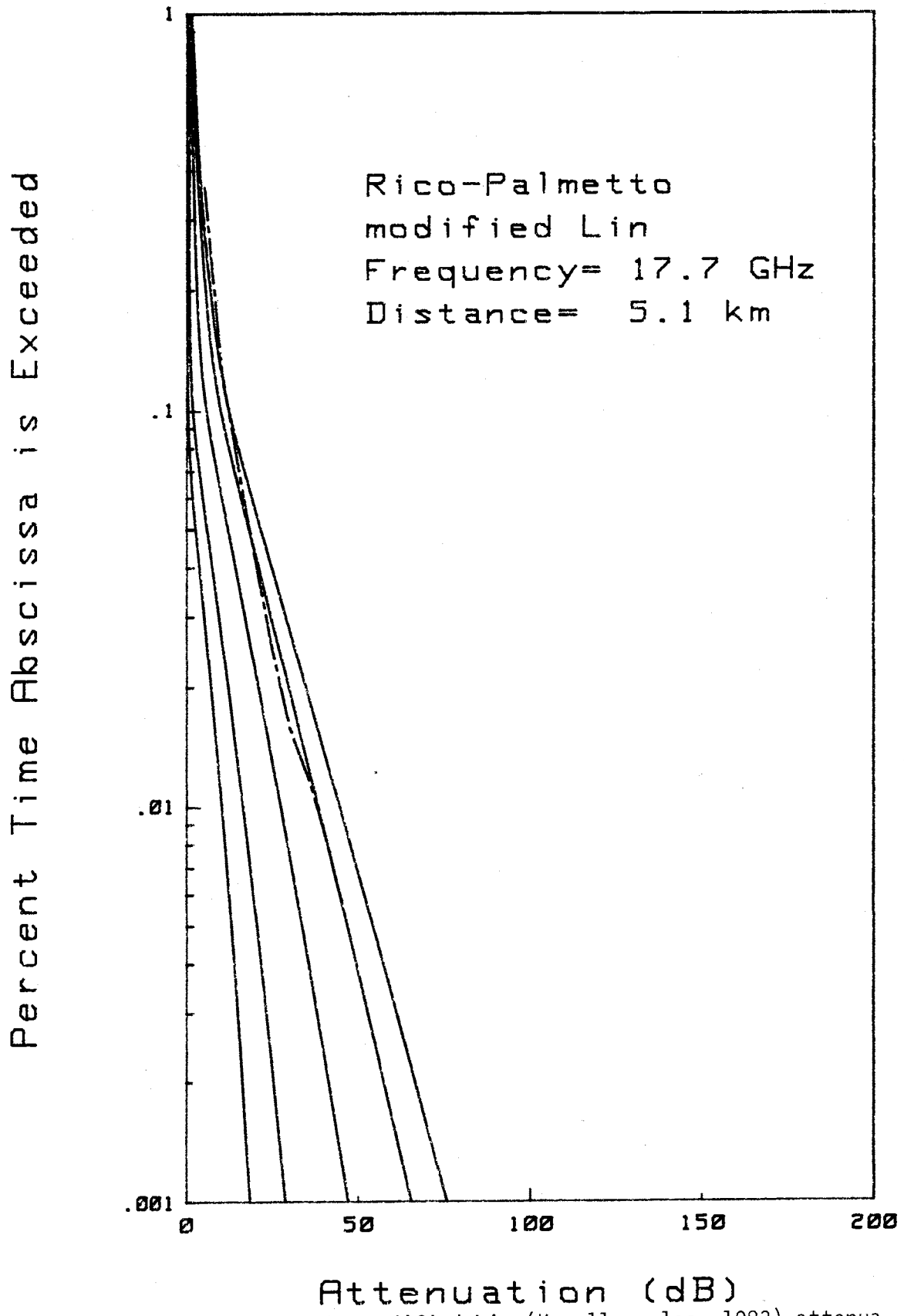

Figure 16. Comparison of the modified Lin (Kanellopoulos, 1983) attenuation distribution prediction model with data over a 5.1 km, 17.7 GHz link between Rico and Palmetto, GA.

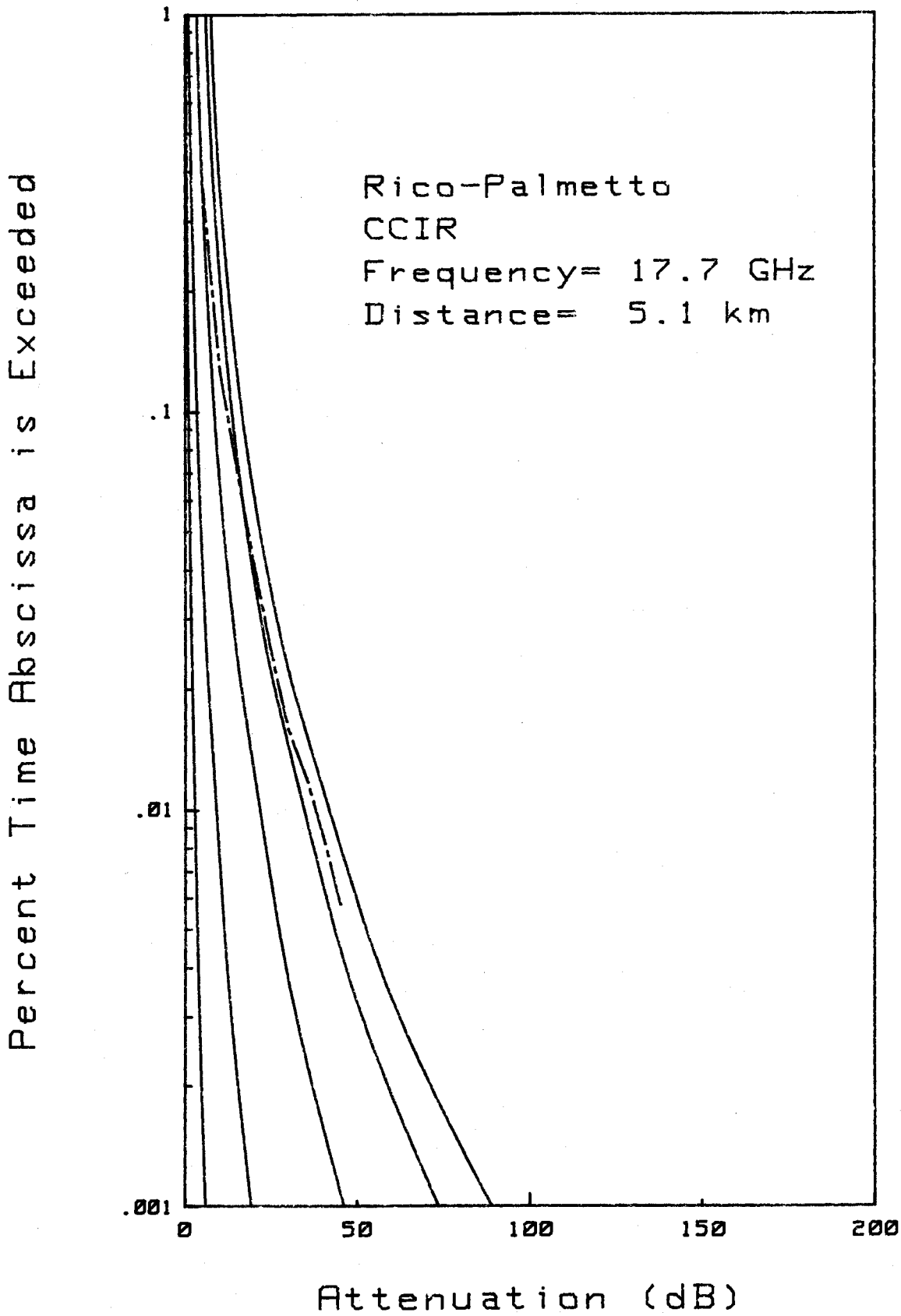

Figure 17. Comparison of the CCIR (1982) attenuation distribution prediction model with data over a 5.1 km, 17.7 GHz link between Rico and Palmetto, GA.

(see Section 2.1.4) prefers the use of a rain rate derived from the Rice-Holmberg (RH) model, using the $U'/D'_{.01}$ thunderstorm ratio (see Sections 1.0 and 1.1). For the other models that need rain rate input to predict the median annual attenuation distribution, we have arbitrarily chosen to use the $U'/D'_{.01}$ version of the RH model to obtain those rain rates. Year-to-year variability was discussed in Section 2.1.5, but it should be noted that the $U'/D'_{.01}$ thunderstorm ratio is also used in connection with obtaining year-to-year attenuation variability for the PROMOD model, and in those other models where the PROMOD-type year-to-year variability is also used.

Table 2 summarizes 56 individual attenuation comparisons made at the 0.01 percent level. Each of the 10 prediction models are compared with at least one year's worth of data distribution at several worldwide locations. There are not nearly as many locations as comparisons because each distribution represents results from a specific link, having a given path length and operating frequency, and there are often several links at one geographic location. Table 2 shows the average and maximum departures of the data above the 99.5 percent confidence limit at the 0.01 percent exceedance level for these 56 comparisons. In addition, Table 2 shows the "overall prediction efficiency," ε, in percent, where

$$\varepsilon = \frac{N - n_D}{N} \times 100 \quad . \tag{18}$$

In (18), n_D is the number of comparisons with departures and N(=56) is the total number of comparisons. An ε is also shown by climatic zone. Köppen (1918) subdivided the world into five major climatic zones, specified as zones A, B, C, D, E. Without going into further detail, zone A is a wet, tropical zone; zone B is a dry, arid zone; zone C is a warm, temperate zone; zone D is a cold, temperate zone; and zone E is a polar-region zone. Most major industrial nations are located in zone C; hence, therein occurred most of the data (50 out of 56 distributions) used in Table 2. Zones A and D accounted for three distributions apiece in Table 2, and zones B and E are not represented.

Table 3 is analogous to Table 2, except that it summarizes departures from the 99 percent confidence interval at the 0.01 percent exceedance level for the 56 comparisons. In other words, it summarizes departures (as absolute values) above the 99.5 percent confidence limit and below the 0.05 percent confidence limit. As mentioned earlier, there is more meaning for the system designer to Table 2 as

Table 2

Summary of Departures of Yearly Microwave Attenuation Data Distributions Above the Modeled 99.5 Percent Confidence Limit at the 0.01 Percentile Exceedance Level for 10 Prediction Models

	Promod	Barsis et al. (1973)	Battesti et al. (1971)	Global (Crane, 1980)	Two Component (Crane, 1982)	Lin (1977)	Morita and Higuti (1976)	Misme and Fimbel (1975)	Kanellopoulos (1983)	CCIR (1982)
Overall Prediction Efficiency, ε(percent)	100.0	94.6	100	98.2	98.2	92.9	82.1	92.9	89.3	78.6
Average outside departure (dB)	0	0.247	0	0.131	0.160	0.118	0.674	0.128	0.597	0.639
Maximum Outside Departure (dB)	0	12.50	0	7.36	8.94	3.34	7.33	5.89	9.26	9.48
Prediction Efficiency in Köppen Zone										
A	100.0	100.0	100.0	100.0	100.0	100.0	100.0	100.0	100.0	100.0
C	100.0	94.0	100.0	98.0	98.0	92.0	80.0	92.0	88.0	76.0
D	100.0	100.0	100.0	100.0	100.0	100.0	100.0	100.0	100.0	100.0

Table 3

Summary of Absolute Values of Departures of Yearly Microwave Attenuation Data Outside the 99 Percent Confidence Interval* at the 0.01 Percentile Exceedance Level for 10 Prediction Models

	Promod	Barsis et al. (1973)	Battesti et al. (1971)	Global (Crane, 1980)	Two Component (Crane, 1982)	Lin (1977)	Morita and Higuti (1976)	Misme and Fimbel (1975)	Kanellopoulos (1983)	CCIR (1982)
Overall Prediction Efficiency ε(percent)	98.2	94.6	100.0	98.2	92.9	91.1	66.1	92.9	87.5	80.4
Average Outside Departure (dB)	0.115	0.247	0	0.131	0.327	0.226	2.139	0.128	0.658	0.578
Maximum Outside Departure (dB)	6.46	12.50	0	7.36	8.94	6.02	19.66	5.89	9.26	9.48
Prediction Efficiency in Köppen Zone										
A	100.0	100.0	100.0	100.0	0	100.0	100.0	100.0	100.0	100.0
C	100.0	94.0	100.0	98.0	98.0	90.0	64.0	92.0	86.0	78.0
D	67.0	100.0	100.0	100.0	100.0	100.0	67.0	100.0	100.0	100.0

*i.e., outside either the 0.5% or 99.5% confidence limit

opposed to Table 3, but Table 3 represents the truer test of 99 percent significance (i.e., that there is only 1 chance in 100 that the data curve really should lie outside the 99 percent confidence interval).

2.3 Conclusions from the Comparisons

Tables 2 and 3 indicate that the poorest comparisons occur with those models for which a year-to-year variability estimate had to be arbitrarily added. This perhaps has biased the comparison against these models, but since, as we have also discussed, models without any year-to-year variability estimates are also not particularly valuable, we decided to make this type of comparison.

If we restrict comparison to the "complete" models (i.e., those with year-to-year variability estimates); namely, the PROMOD, global (Crane, 1980) and two-component (Crane, 1982) models, results from Tables 2 and 3 really indicate no clearly superior approach. It should be noted that the global model is the simplest approach of the three to apply, which, under some circumstances, might make it preferable to the others.

Of the five Köppen (1918) major worldwide climatic zones, only zone C contains enough data to convey any meaning from the results of Tables 2 and 3. At least as much data would have to be acquired in zones A, B, D, and E before much significance could be attached to conclusions about comparisons made for these climate types.

Hence, while these comparisons have been interesting and useful in delineating problem areas ranging from modeling inadequacies to the meaning of distribution data/model comparisons, they have not particularly shed any light on the question of which models work best in given regions of the world. Thus, we have not undertaken such a worldwide subdivision. It can be said that probably no more than 3 of the 10 models analyzed should be used under any circumstances. These are the three "complete" models just discussed.

3. WORLDWIDE RAINFALL CONTOUR MAPS

In this section, contour maps of specific areas of the world that are of especial interest to USACEEIA are presented. The data locations and their co-ordinates from which these maps were drawn are given in the Appendix. These maps contain (a) the rainfall parameters that are useful in predicting rain rates from the RH model, and (b) some of these selected predicted rain rates and their year-to-year variability that can be used in prediction of rainfall effects on microwave links. Generally, the maps present the following parameters (unless data are insufficient to represent them):

1. M, the average annual precipitation in millimeters,
2. $D_{.01}$, the average annual number of days with precipitation greater than 0.01 inches (0.25 mm),
3. U, the average annual number of days with thunderstorms,
4. M_m, the maximum monthly precipitation of 30 consecutive years (360 months) of record, in millimeters,
5. β, the thunderstorm ratio associated with the original RH model (see Section 1),
6. $U/D_{.01}$, an average annual thunderstorm ratio, generally obtained by dividing item 3 by item 2 at a given location* (see Section 1),
7. s_M, the year-to-year standard deviation of M, in millimeters,
8. s_D, the year-to-year standard deviation of $D_{.01}$, in days,
9. s_U, the year-to-year standard deviation of U, in days,
10. $R_1(\beta)$, the median annual rain rate expected to be exceeded 1 percent of a year, obtained using β, in millimeters per hour,
11. $R_{.1}(\beta)$, the median annual rain rate expected to be exceeded 0.1 percent of a year, obtained using β, in millimeters per hour,
12. $R_{.01}(\beta)$, the median annual rain rate expected to be exceeded 0.01 percent of a year, obtained using β, in millimeters per hour,
13. $R_1(U/D)$, the median annual rain rate expected to be exceeded 1 percent of a year, obtained using $U/D_{.01}$, in millimeters per hour,
14. $R_{.1}(U/D)$, the median annual rain rate expected to be exceeded 0.1 percent of a year, obtained using $U/D_{.01}$, in millimeters per hour,
15. $R_{.01}(U/D)$, the median annual rain rate expected to be exceeded 0.01 percent of a year, obtained using $U/D_{.01}$, in millimeters per hour,
16. s_{R_1}, the predicted year-to-year standard deviation of R_1, obtained from items 10 or 13, in millimeters per hour,
17. $s_{R_{.1}}$, the predicted year-to-year standard deviation of $R_{.1}$, obtained from items 11 or 14 above, in millimeters per hour,

and

18. $s_{R_{.01}}$, the predicted year-to-year standard deviation of $R_{.01}$, obtained from items 12 or 15 above, in millimeters per hour.

---

* Although this is not a strictly correct procedure for obtaining the average value, it is usually necessitated by lack of data.

Data from which to draw the contour maps contained herein were obtained from published compilations of summarized data. Usually the amount of data available for analysis of one parameter (e.g., M) was not equal to the amount of data available for analysis of another parameter in the same area (e.g., U). Some parameters in certain parts of the world were totally unavailable (e.g., β) forcing already-discussed alternative procedures to be developed for their estimation. The maps presented in this section appear to be about as thoroughly detailed as is possible from current data sources. Each global area discussed in this section contains a map showing the data locations used, but the reader should recognize that, often as not, some basic data were missing at these locations, and maps were often contoured on the basis of fewer locations. The following publications were the sources of the basic data used herein:

- Monthly Climatic Data for the World, 1950-1980, Volumes 3-33, Nos. 1-12, sponsored by the World Meteorological Organization (WMO), available through the National Oceanic and Atmospheric Administration, Environmental Data Center, Asheville, North Carolina 28801, U.S.A.
- Climatological Data, National Summary, Annual Summary, 1950-1980, Volumes 1-31, No. 13, available through the National Oceanic and Atmospheric Administration, Environmental Data Center, Asheville, North Carolina 28801, U.S.A.
- U. S. Naval Weather Service World-Wide Airfield Summaries, Volumes I-X, available through the National Technical Information Service, 5285 Port Royal Road, Springfield, VA 22161, U.S.A., May, 1970-April, 1971
- Climatological Normals (CLINO) for Climat and Climat Ship Stations for the Period 1931-1960, World Meteorological Organization Publication WMO/OMM No. 117, TP.52, 1971
- World Distribution of Thunderstorm Days, Parts I and II, World Meteorological Organization Publication WMO/OMM No. 21, TP.6
- Tables of Temperature, Relative Humidity, and Precipitation for the World, Parts I-VI, Publication M.O.617a-f, Air Ministry Meteorological Office, printed by Her Majesty's Stationery Office, London, U.K., 1961.

Now, let us consider the individual global areas that have been contour mapped.

3.1 The Federal Republic of Germany and Vicinity

Figure 18 shows the 131 data locations* used for contouring maps in the vicinity of the Federal Republic of Germany (FRG/"West Germany"). Data locations are also located in the German Democratic Republic ("East Germany"), The Netherlands, Belgium, France, Switzerland, Austria, and Czechoslovakia. Figures 19-36 show M, $D_{.01}$, U, M_m, β, $U/D_{.01}$, s_M, s_D, s_U, $R_1(\beta)$, $R_{.1}(\beta)$, $R_{.01}(\beta)$, $R_1(U/D)$, $R_{.1}(U/D)$, $R_{.01}(U/D)$, s_{R_1}, $s_{R_{.1}}$, and $s_{R_{.01}}$, in that order. The values of s_{R_1}, $s_{R_{.1}}$, and $s_{R_{.01}}$ were obtained using β. Values of these parameters were also available using $U/D_{.01}$, but are not presented since they are nearly identical. Some of the basic parameters--namely $D_{.01}$, s_D, and s_U--were estimated.

The only values of precipitation days that were available, to the author's knowledge, were values of $D_{.1}$, the number of days with precipitation greater than 0.1 inches. Therefore, simple linear extrapolation is used to obtain $D_{.01}$; viz,

$$D_{.01} = \overline{\left(\frac{D_{.01}}{D_{.1}}\right)}_{U.S.} D_{.1} \quad . \tag{19}$$

In (19), the ratio $(D_{.01}/D_{.1})_{U.S.}$ is obtained from data in the U.S.A. for 102 locations for which $D_{.1}$ and $D_{.01}$ are both available (Dutton et al., 1974). The average value of the ratio, denoted by the bar in (19), is then used on the Köppen (1918) zone climatic basis (see Section 2.2) to obtain a relational factor between $D_{.01}$ from $D_{.1}$ in the FRG vicinity, as well as in other global areas yet to be discussed. The FRG and vicinity are in zone C; hence, U.S.A. zone C data only were used to obtain the mean ratio in (19). This procedure for determining $D_{.01}$ from $D_{.1}$ is a departure from the regression procedures of Dutton et al. (1974) used in Europe, but it appears nearly as effective and is a good deal simpler.

As noted earlier, s_D and s_U were also estimated. Once again, the U.S.A. data sources provided 304 points from which we could establish the relations

$$s_D = \overline{\left(\frac{s_D}{D_{.01}}\right)}_{U.S.} D_{.01} \quad , \tag{20}$$

---

*Data were not always available from all locations for any given mapped parameter. Sometimes only one parameter (usually M) was available at a given data location.

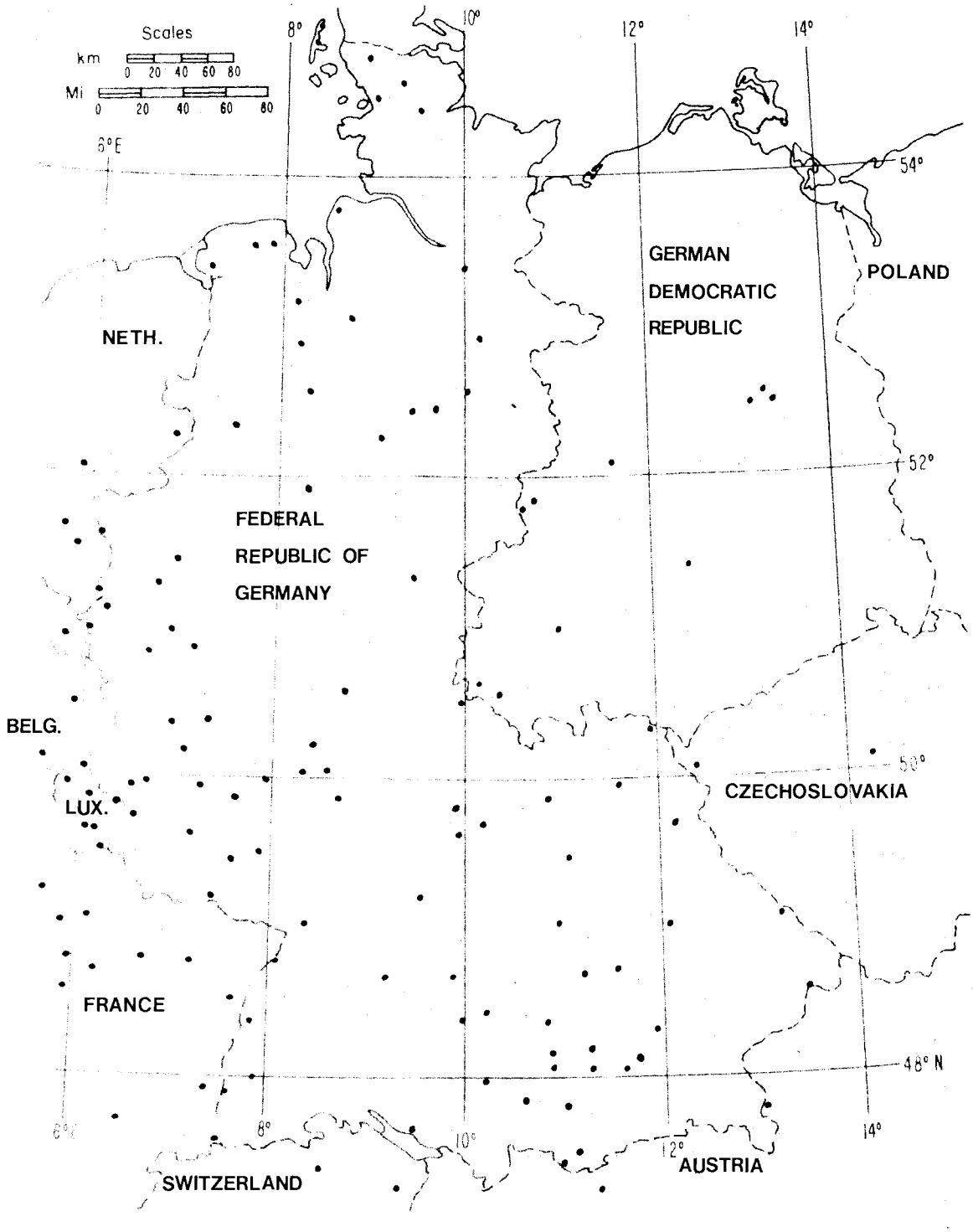

Figure 18. Map of data locations in the Federal Republic of Germany and vicinity.

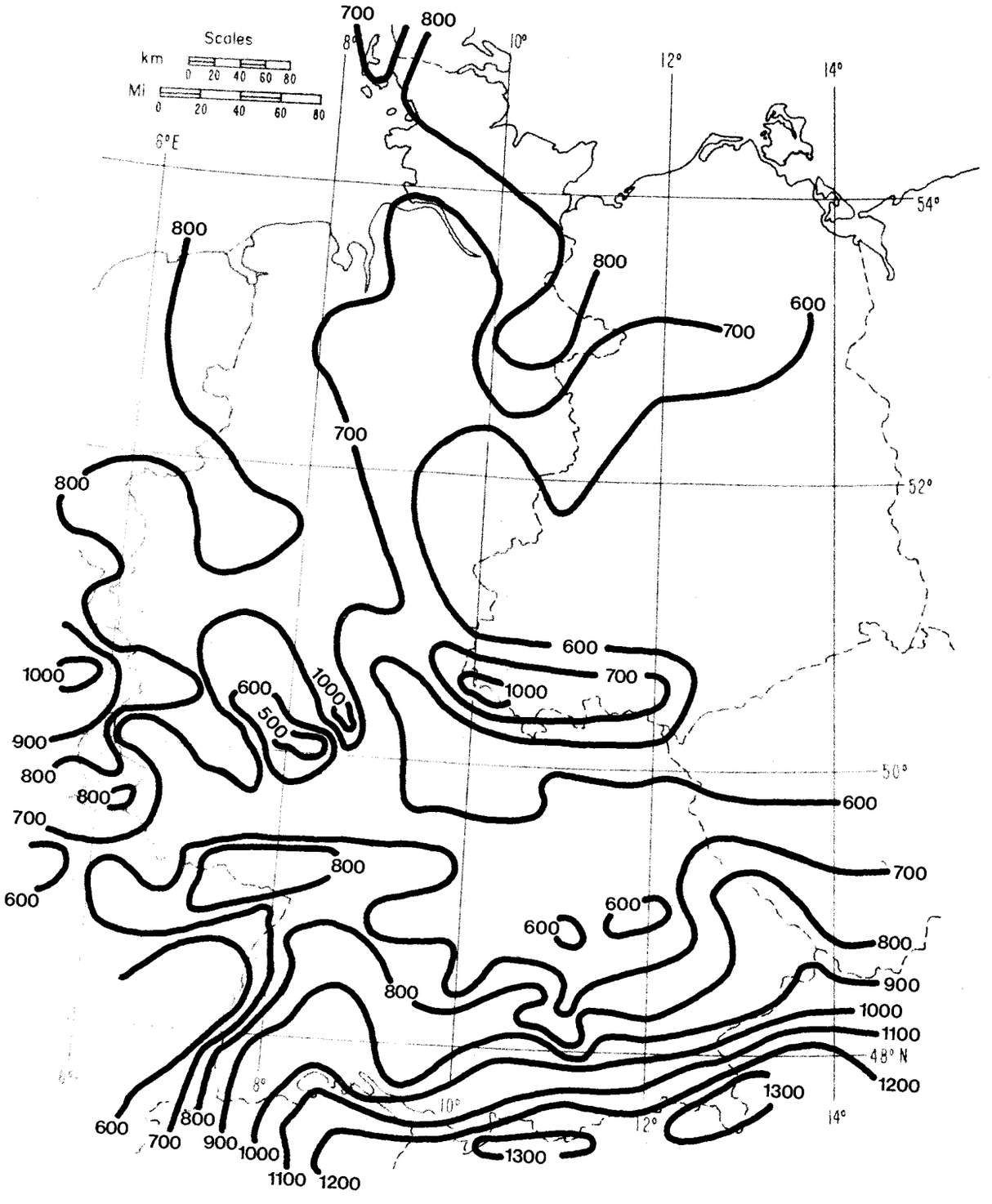

Figure 19. Contour map of the average annual precipitation, M, in millimeters for the Federal Republic of Germany and vicinity.

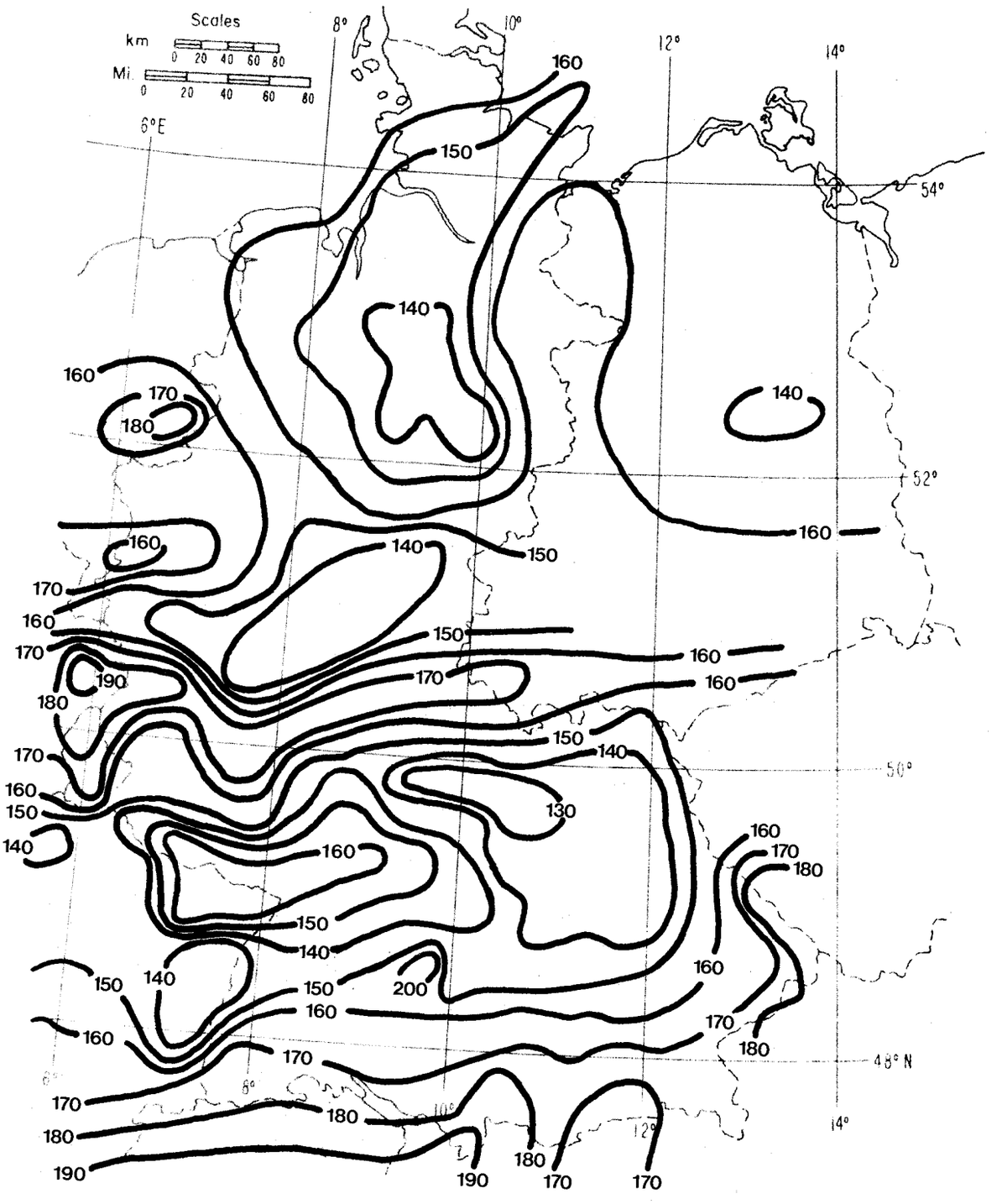

Figure 20. Contour map of the average annual number of days, $D_{.01}$, with precipitation greater than .01 in. for the Federal Republic of Germany and vicinity.

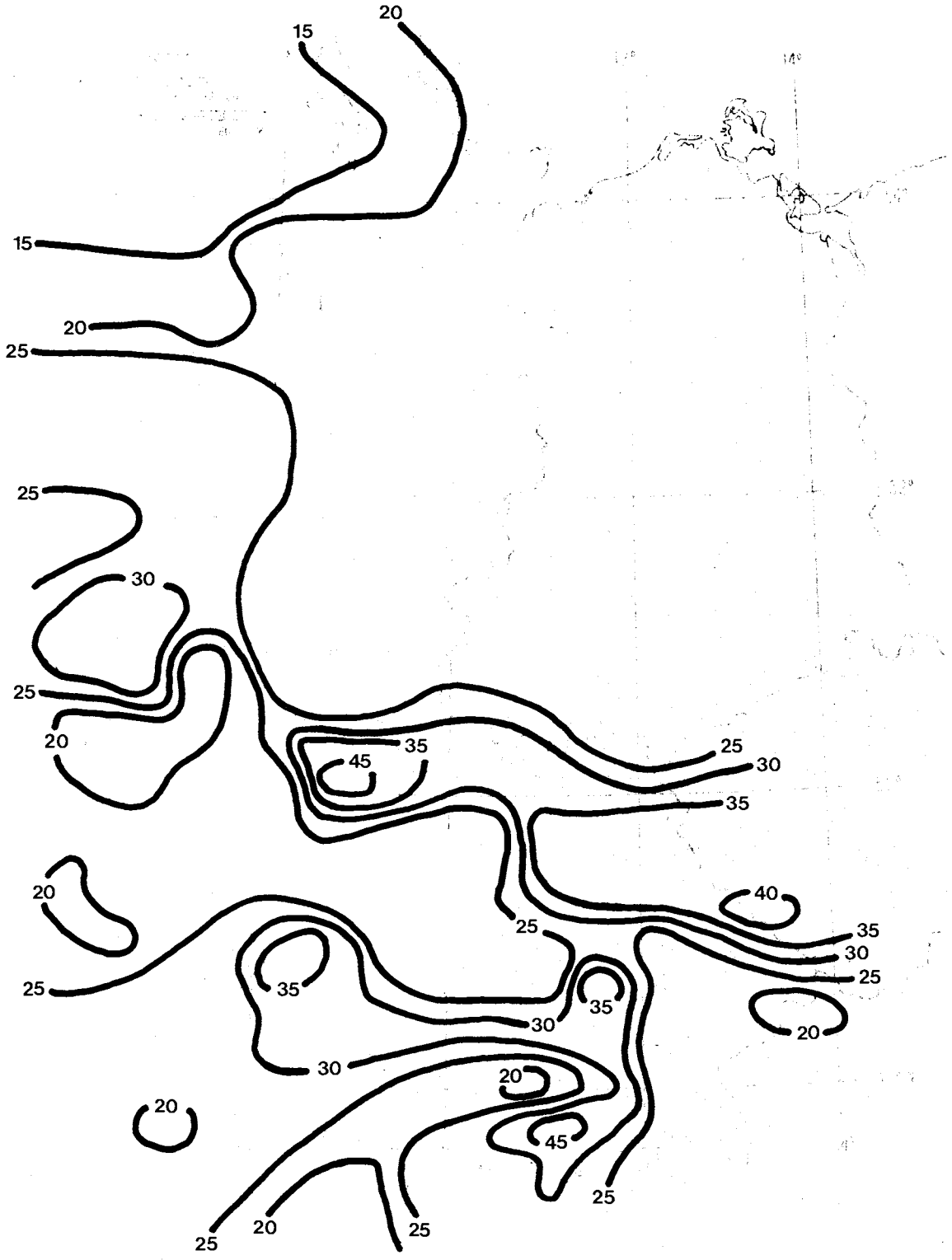

Figure 21. Contour map of the average annual number of days, U, with thunderstorms for the Federal Republic of Germany and vicinity.

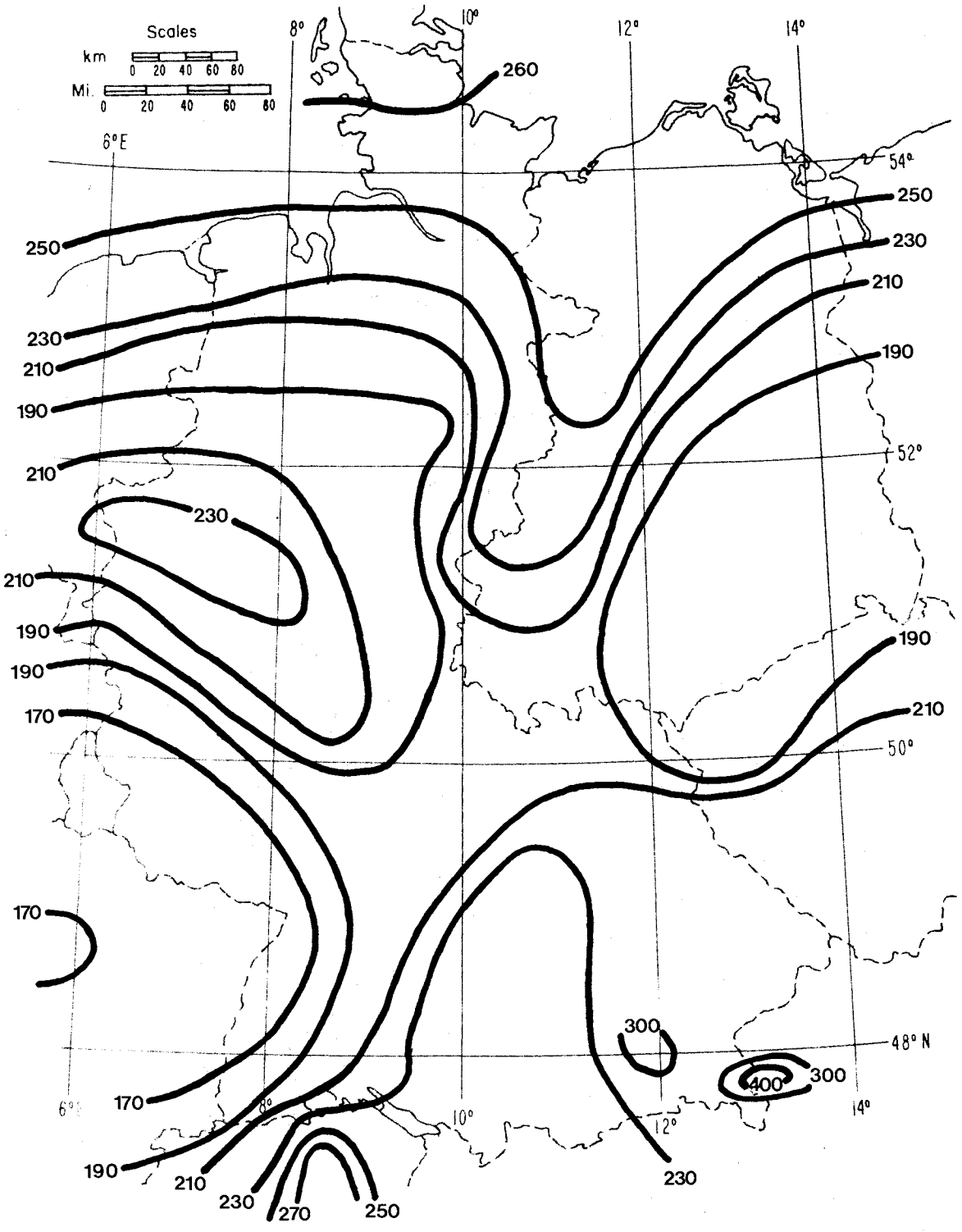

Figure 22. Contour map of the greatest monthly precipitation, M_m, in 30 consecutive years, in millimeters, for the Federal Republic of Germany and vicinity.

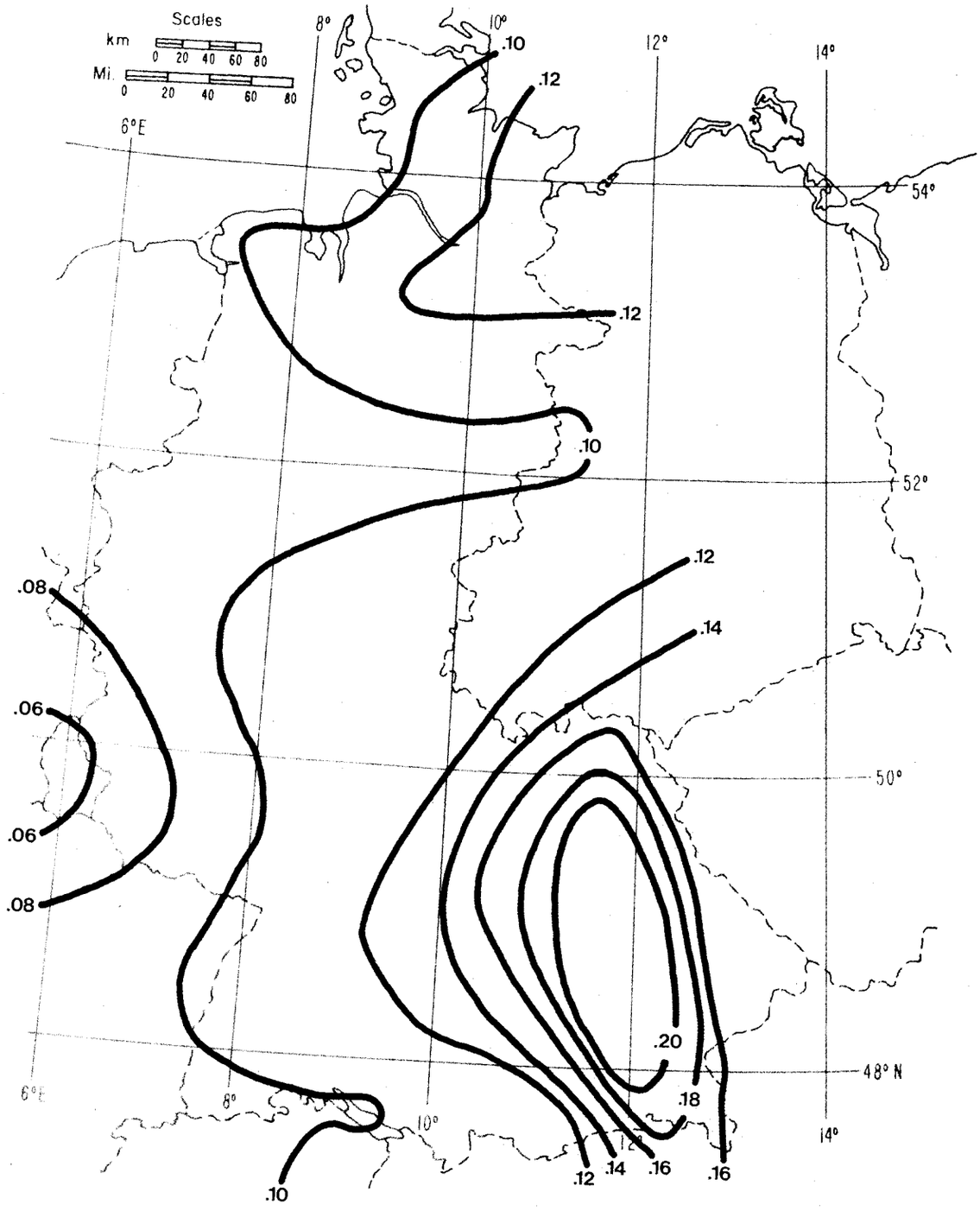

Figure 23. Contour map of the thunderstorm ratio, β, for the Federal Republic of Germany and vicinity.

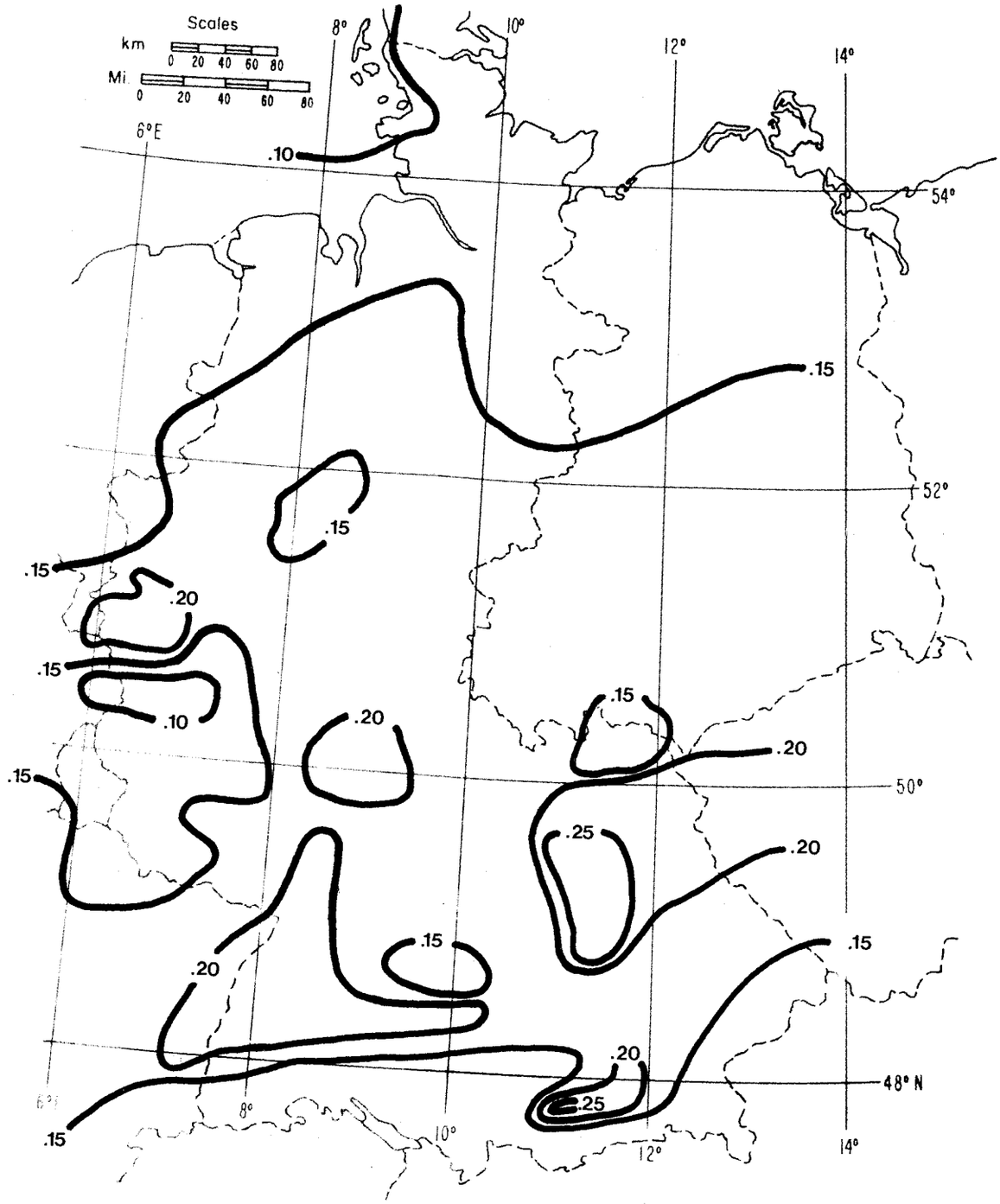

Figure 24. Contour map of the thunderstorm ratio, $U/D_{.01}$, for the Federal Republic of Germany and vicinity.

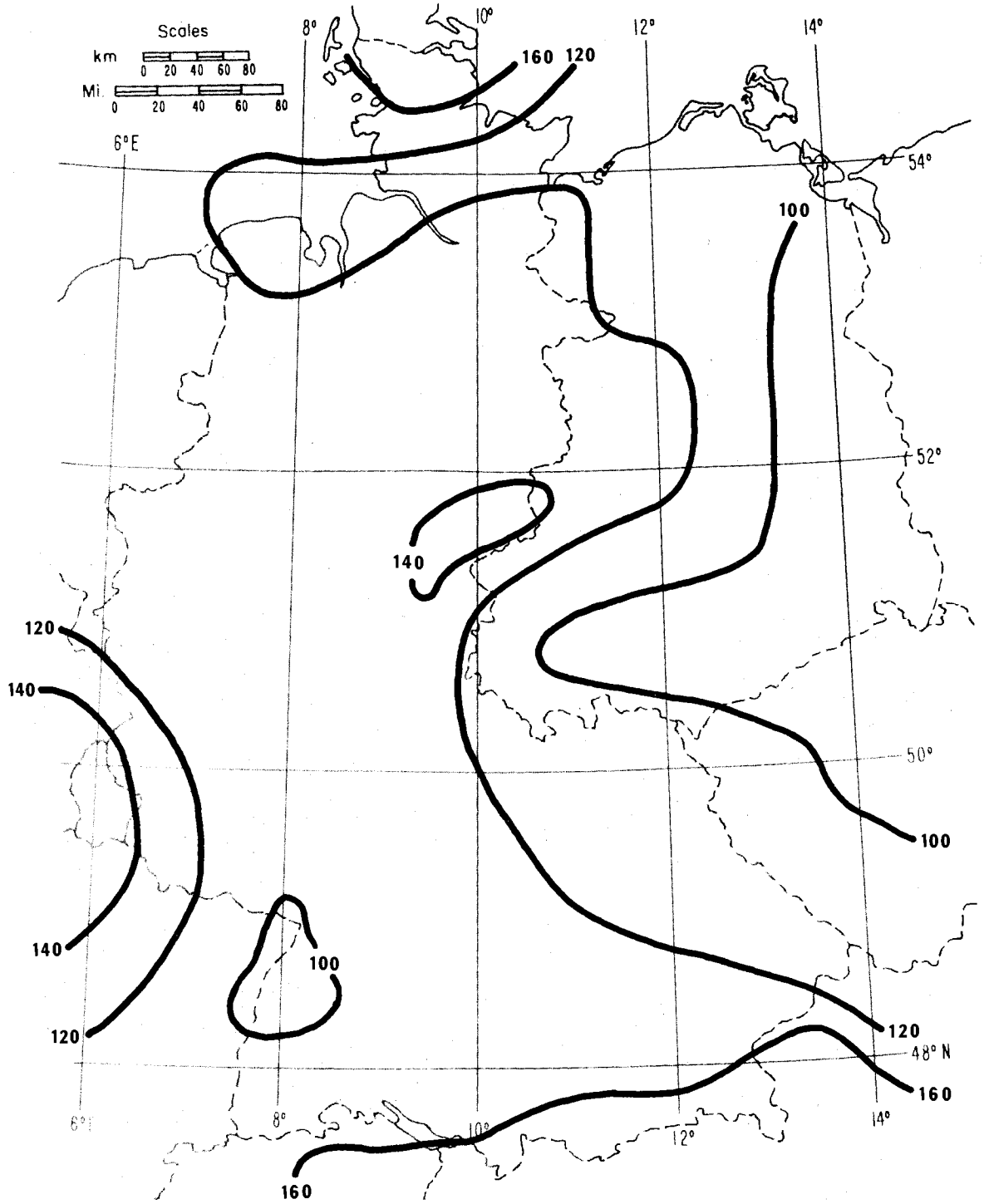

Figure 25. Contour map of the year-to-year standard deviation, s_M, in millimeters, of total annual precipitation for the Federal Republic of Germany and vicinity.

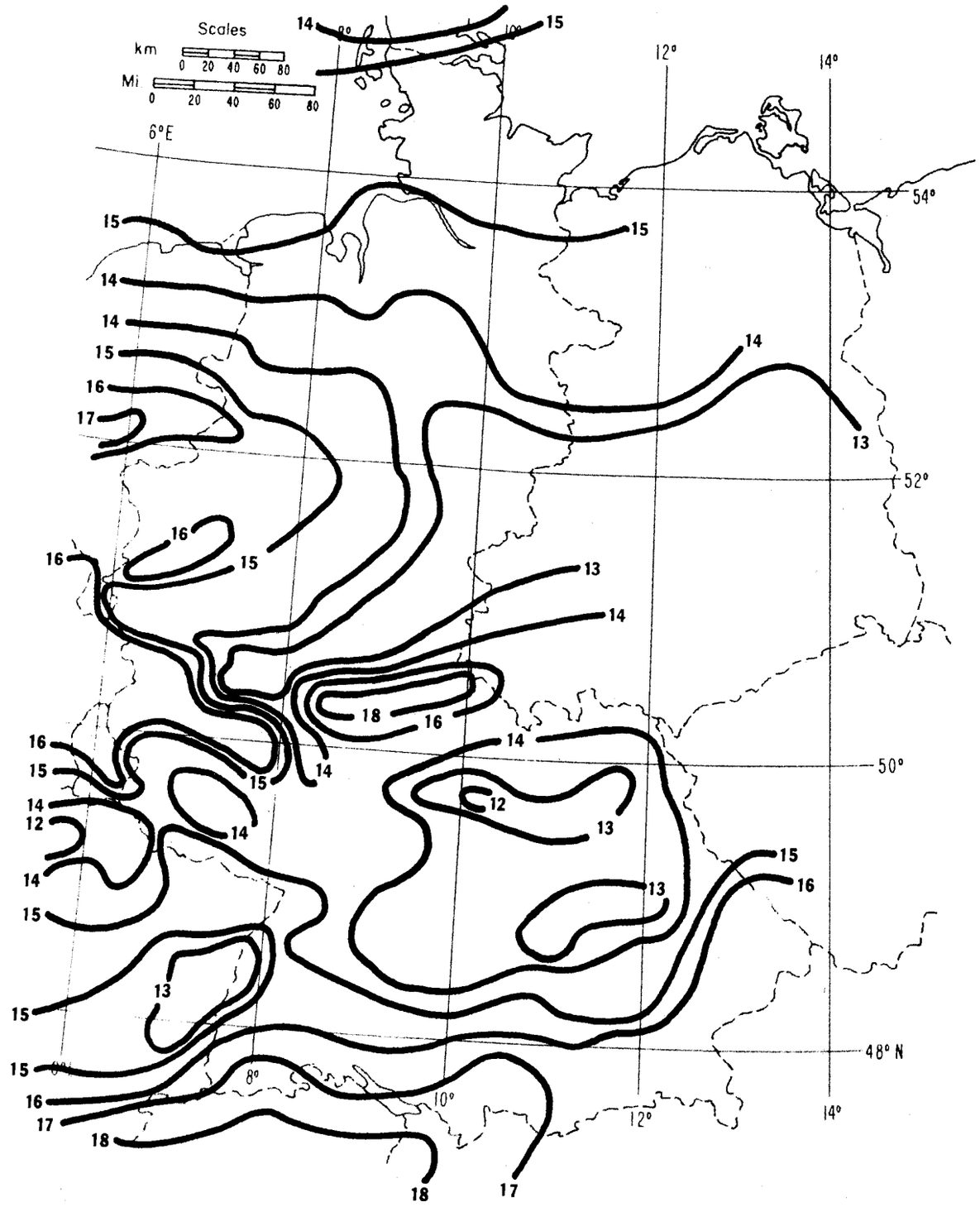

Figure 26. Contour map of the year-to-year standard deviation, s_D, of the annual number of days with precipitation greater than .01 in. for the Federal Republic of Germany and vicinity.

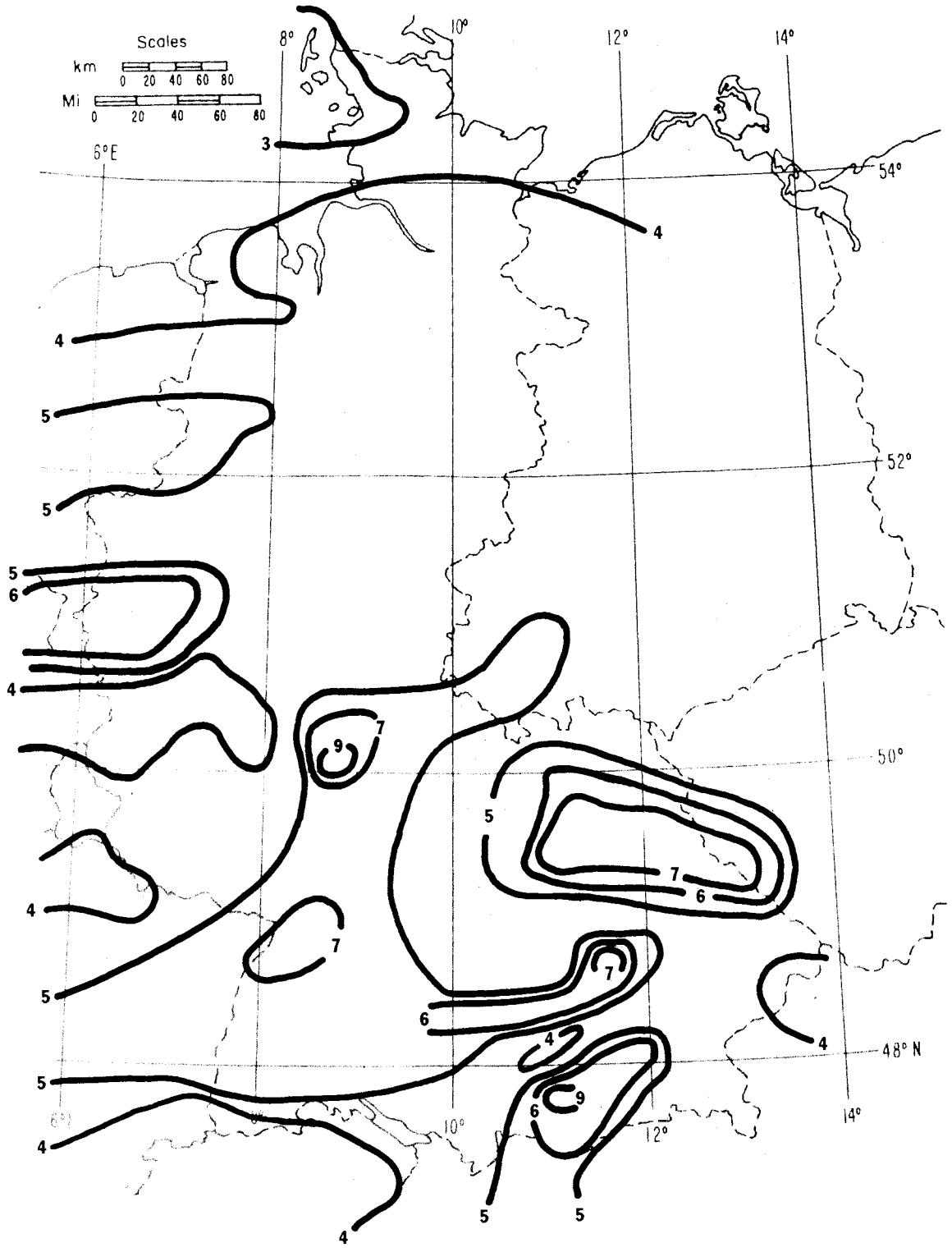

Figure 27. Contour map of the year-to-year standard deviation, s_U, of the annual number of days with thunderstorms for the Federal Republic of Germany and vicinity.

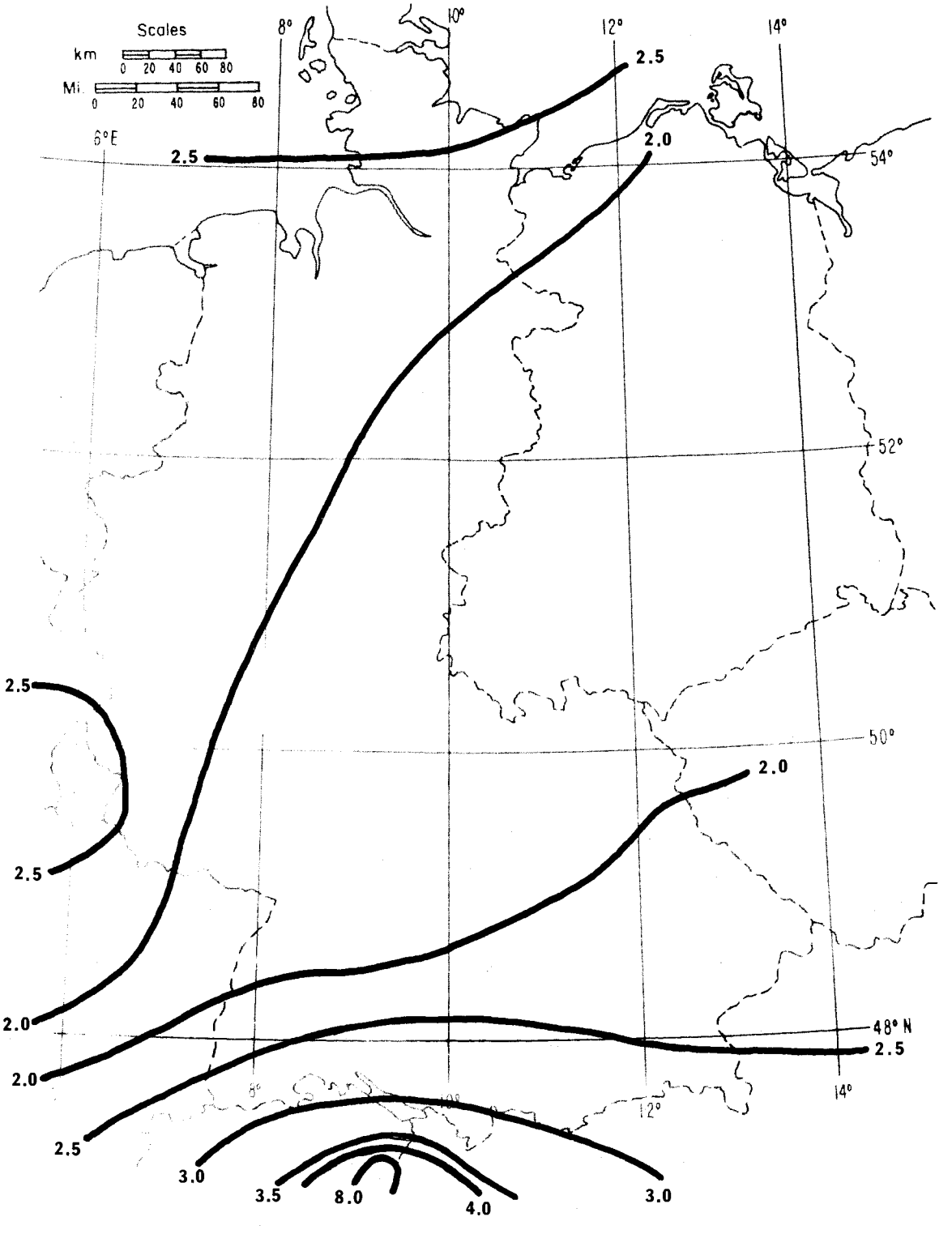

Figure 28. Contour map of rain rate, $R_1(\beta)$, in millimeters per hour, expected to be exceeded 1 percent of an average year and derived using the thunderstorm ratio, β, for the Republic of Germany and vicinity.

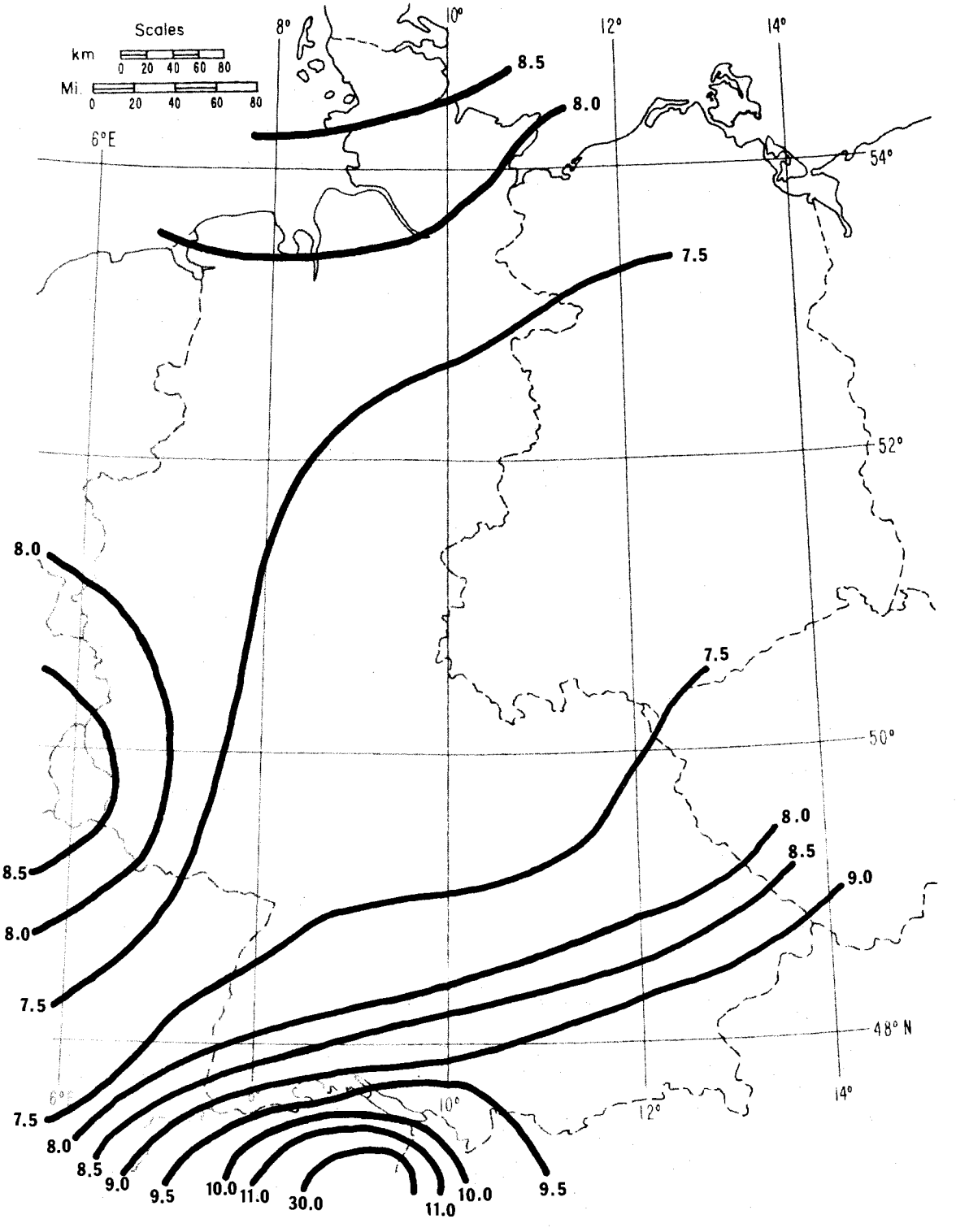

Figure 29. Contour map of the rain rate, $R_{0.1}(\beta)$, in millimeters per hour, expected to be exceeded 0.1 percent of an average year and derived using the thunderstorm ratio, β, for the Federal Republic of Germany and vicinity.

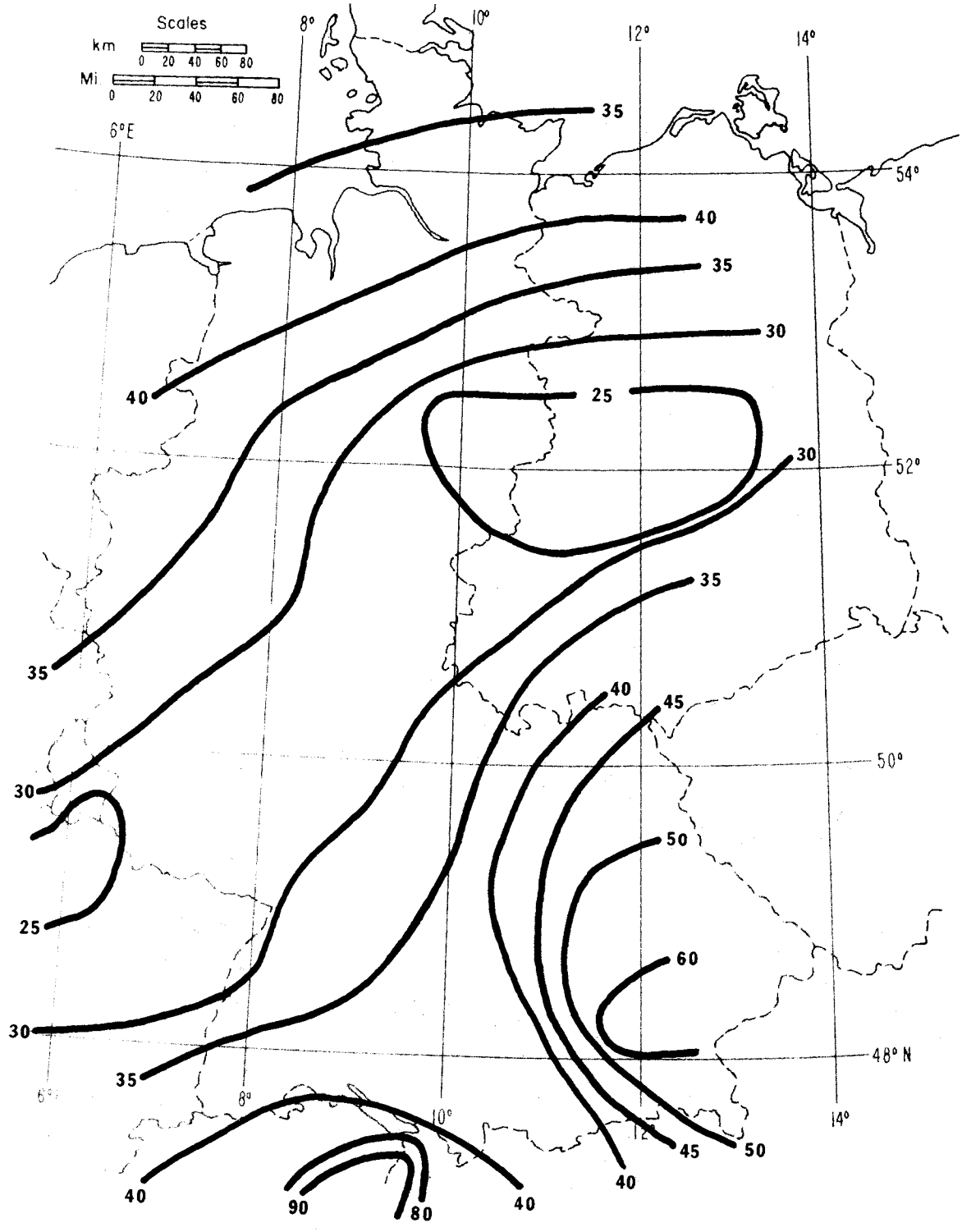

Figure 30. Contour map of the rain rate, $R_{.01}(\beta)$, in millimeters per hour, expected to be exceeded 0.01 percent of an average year and derived using the thunderstorm ratio, β, for the Federal Republic of Germany and vicinity.

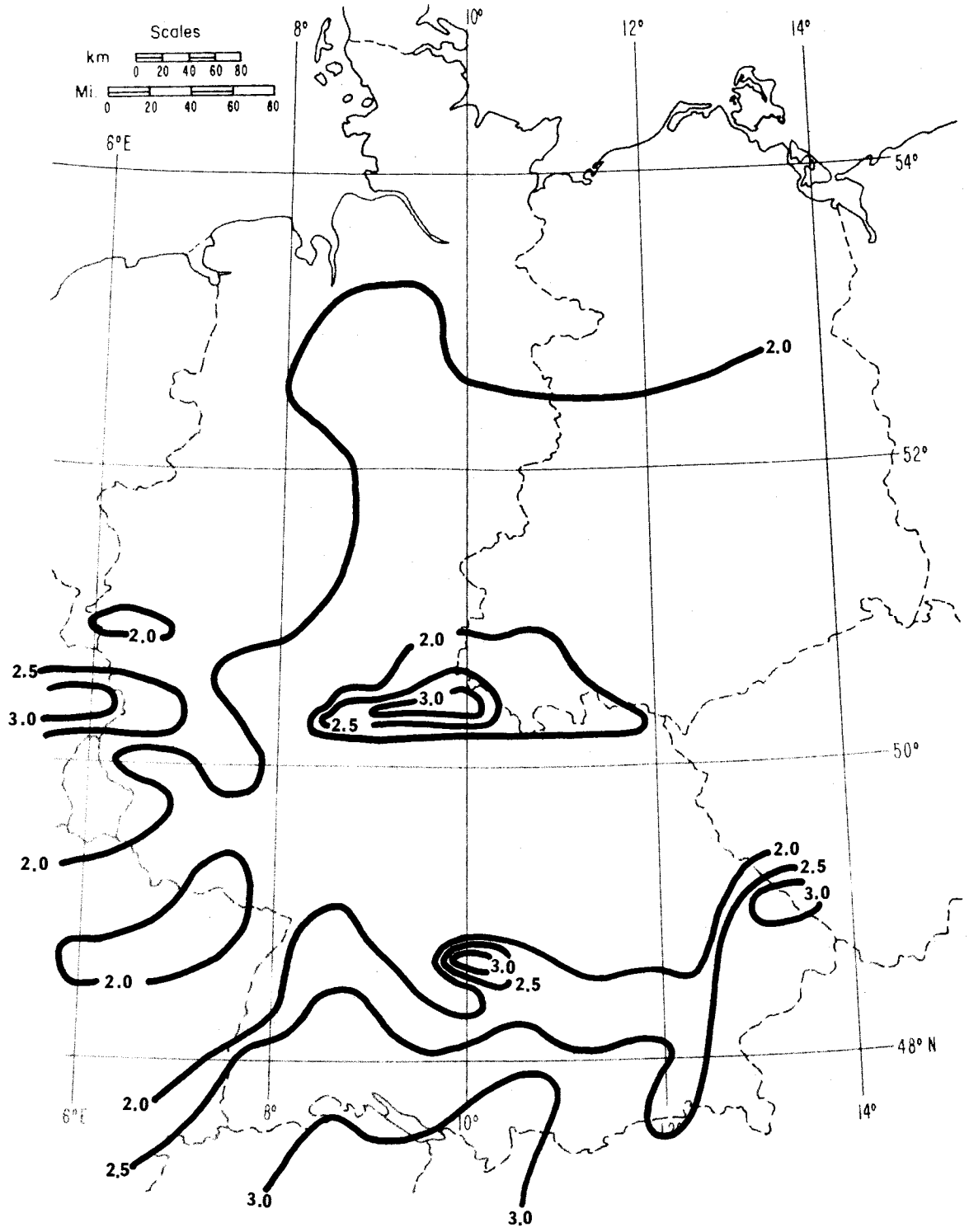

Figure 31. Contour map of the rain rate, $R_1(U/D)$, in millimeters per hour, expected to be exceeded 1 percent of an average year and derived using the thunderstorm ratio, $U/D_{.01}$, for the Federal Republic of Germany and vicinity.

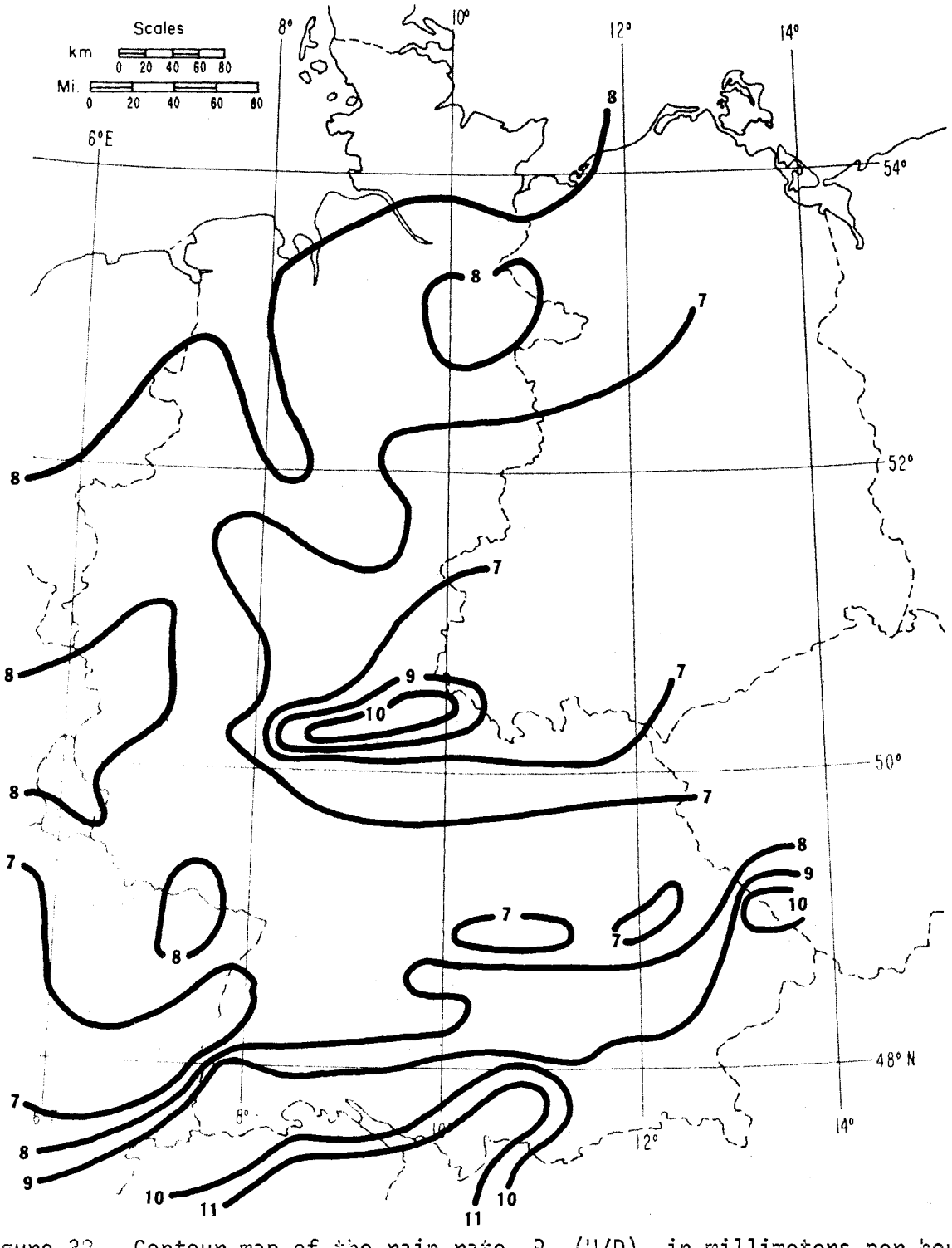

Figure 32. Contour map of the rain rate, $R_{.1}(U/D)$, in millimeters per hour, expected to be exceeded 0.1 percent of an average year and derived using the thunderstorm ratio, $U/D_{.01}$, for the Federal Republic of Germany and vicinity.

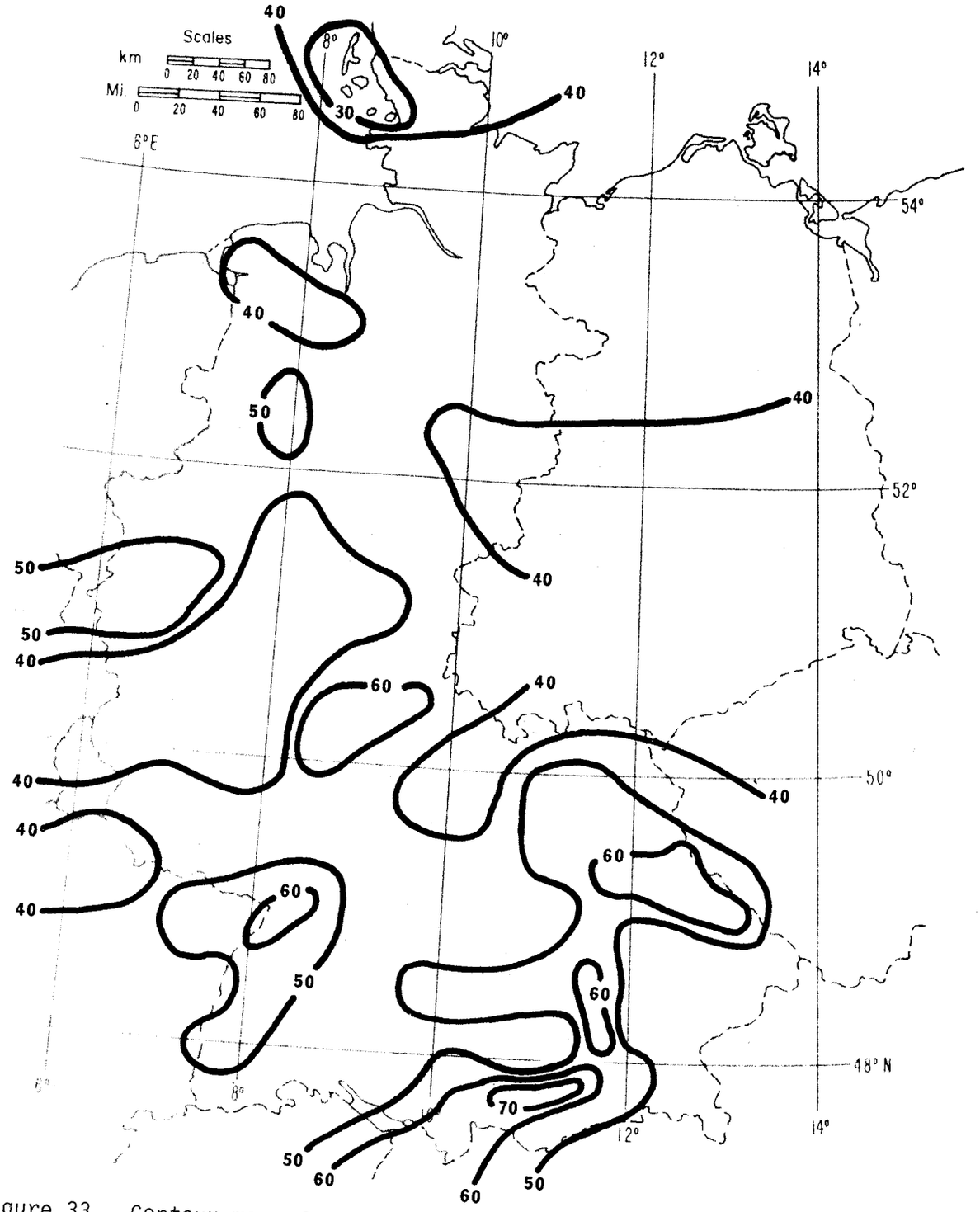

Figure 33. Contour map of the rain rate, $R_{.01}(U/D)$, in millimeters per hour, expected to be exceeded 0.01 percent of an average year and derived using the thunderstorm ratio, $U/D_{.01}$, for the Federal Republic of Germany and vicinity.

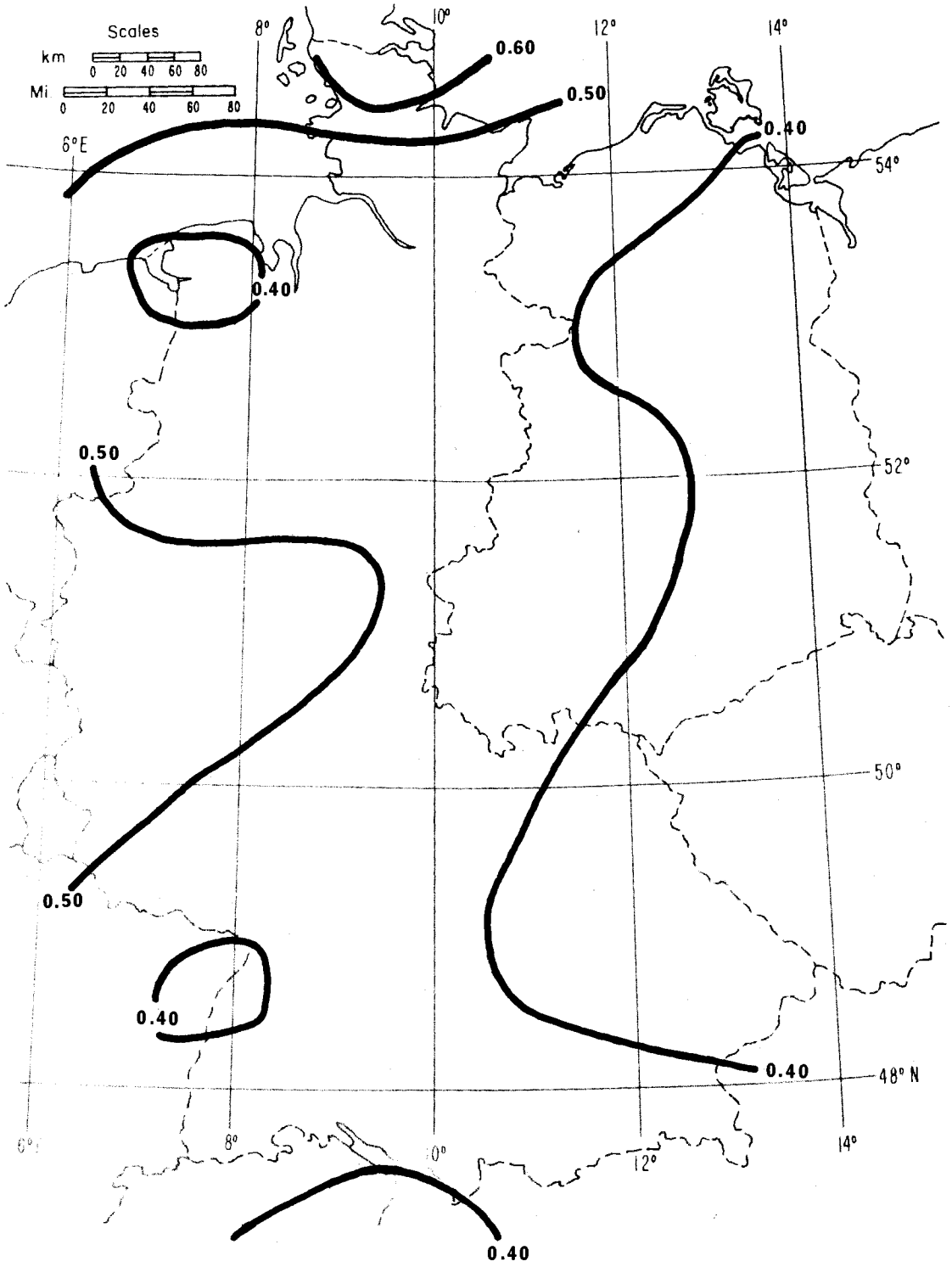

Figure 34. Contour map of the estimated year-to-year standard deviation, s_{R_1}, in millimeters per hour, of rain rate expected at the 1 percent exceedance level for the Federal Republic of Germany and vicinity.

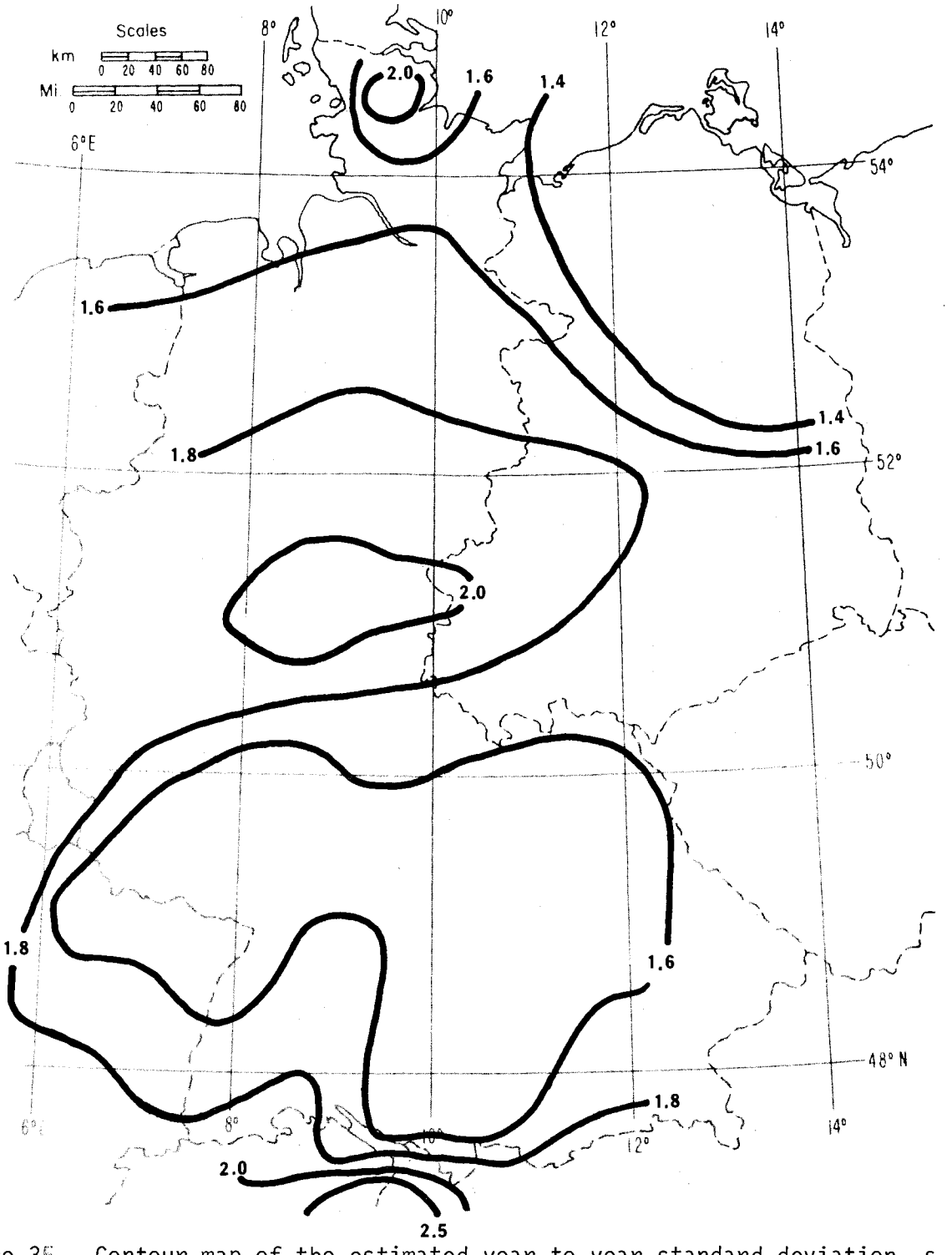

Figure 35. Contour map of the estimated year-to-year standard deviation, $s_{R_{.1}}$, in millimeters per hour, of rain rate expected at the 0.1 percent exceedance level for the Federal Republic of Germany and vicinity.

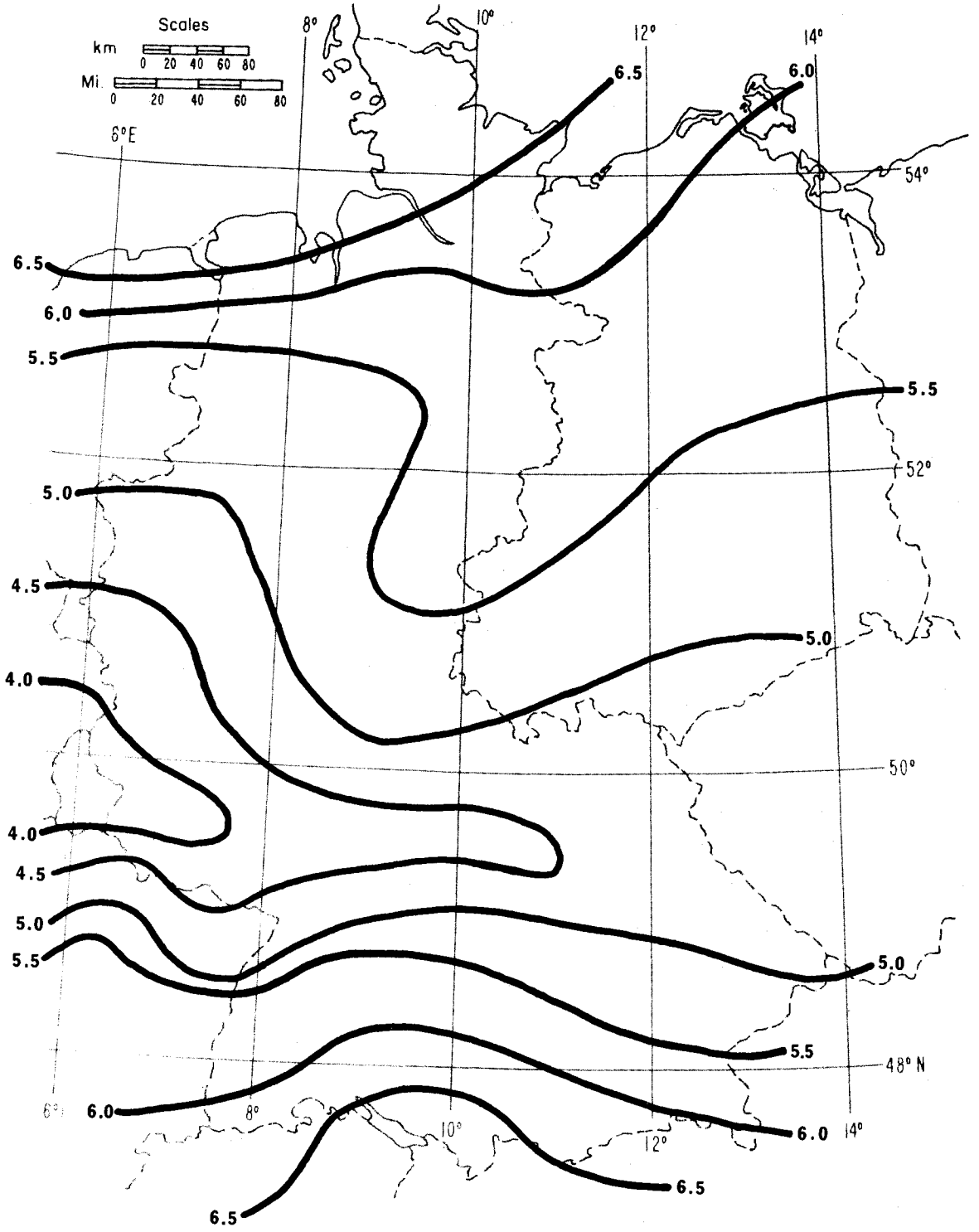

Figure 36. Contour map of the estimated year-to-year standard deviation, $s_{R_{.01}}$, in millimeters per hour, of rain rate expected at the 0.01 percent exceedance level for the Federal Republic of Germany and vicinity.

and

$$s_U = \overline{\left(\frac{s_U}{U}\right)}_{U.S.} U \quad . \tag{21}$$

The mean ratios in (20) and (21) were obtained from the U.S.A. data base, again on the Köppen (1918) zonal basis.

At this time it should be noted that values of M_m often cannot be obtained as well, although for the FRG and vicinity they are available. In this case we have chosen not to use a method such as (19), (20), or (21) to obtain M_m, but rather just denote missing data on maps. This is because in the case of M_m, however, partial maps (except in the case of Okinawa, which is an unusual case, anyway, as discussed in Section 3.2) were often able to be drawn.

3.2 Okinawa

Table 4 summarizes results from Okinawa, in the one departure from contour mapping. There were only four data locations, as shown in Table 4, on Okinawa, all of which were military installations. Furthermore, all four locations are very close to one another on the west side of Okinawa. As a consequence, a meaningful map of all of Okinawa could simply not be drawn. The values of $R_1(\beta)$, $R_{.1}(\beta)$, and $R_{.01}(\beta)$ could not be obtained because of unavailable M_m information. As was the case for the FRG and vicinity, $D_{.01}$, s_D, and s_U were estimated using the approach of (19), (20), and (21), respectively. Okinawa was determined as lying in Köppen (1918) zone C for purposes of this analysis.

3.3 Republic of Korea and Vicinity

Figure 37 shows the 33 data locations used for contouring maps in the Republic of Korea (ROK/South Korea) and vicinity. With the exception of one location, located in the People's Democratic Republic of Korea (North Korea), all data came from the ROK. Figures 38 to 50 show M, $D_{.01}$, U, $U/D_{.01}$, s_M, s_D, s_U, $R_1(U/D)$, $R_{.1}(U/D)$, $R_{.01}(U/D)$, s_{R_1}, $s_{R_{.1}}$, and $s_{R_{.01}}$, in that order.

There were only four values of M_m available for the ROK; hence, it was decided that this constituted an insufficient data base from which to draw a contour map. With no M_m map, there are correspondingly, then, no maps of β or the rain rates predicted from the thunderstorm ratio, β. Thus we were once again obliged to rely upon $U/D_{.01}$ for rain rate predictions, which also, once again, shows its value as an alternative thunderstorm ratio. As in previous areas analyzed, the parameters

Table 4
Rain Rate and Rain Attenuation Prediction Parameters for Okinawa

LOCATION	M (mm)	$D_{.01}$ (days)	U (days)	β	$U/D_{.01}$
Naha	2103.1	171.8	18.6	0.3	0.108
Futema	2037.1	136.2	17.3	0.3	0.127
Kadena	2039.6	140.3	18.6	0.3	0.133
Hamby	2037.1	136.2	17.3	0.3	0.127

LOCATION	S_M (mm)	s_D (days)	s_U (days)
Naha	581.8	18.55	3.24
Futema	581.8	14.71	3.01
Kadena	581.8	15.15	3.24
Hamby	581.8	14.71	3.01

LOCATION	$R_1(U/D)$ (mm/hr)	$R_{.1}(U/D)$ (mm/hr)	$R_{.01}(U/D)$ (mm/hr)
Naha	5.776	28.320	99.945
Futema	5.703	29.567	99.066
Kadena	5.705	29.284	99.100
Hamby	5.703	29.567	99.066

LOCATION	s_{R_1} (mm/hr)	$s_{R_{.1}}$ (mm/hr)	$s_{R_{.01}}$ (mm/hr)
Naha	1.934	7.627	7.266
Futema	1.978	8.418	7.777
Kadena	1.998	8.118	7.227
Hamby	1.978	8.418	7.777

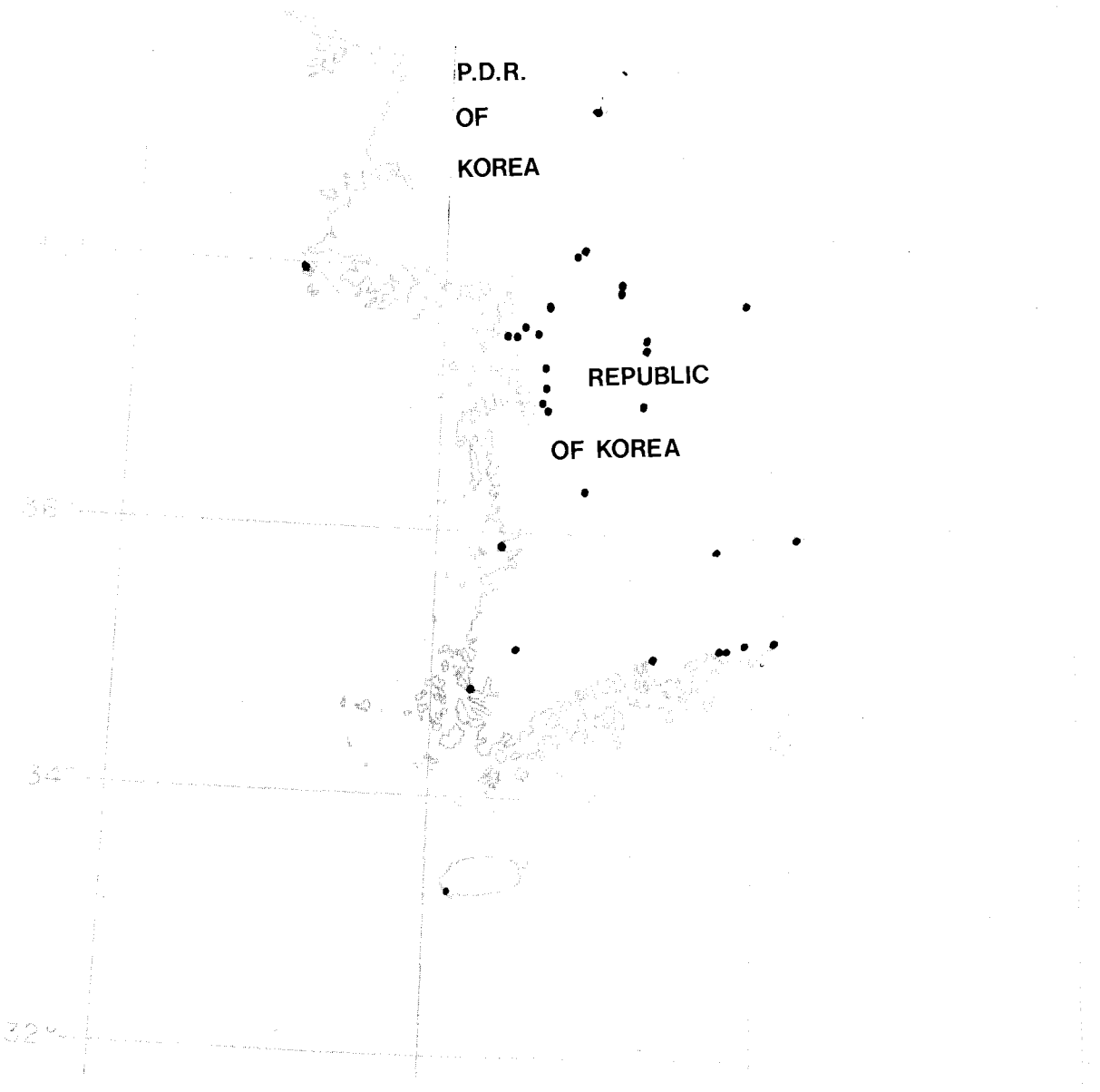

Figure 37. Map of data locations in the Republic of Korea and vicinity.

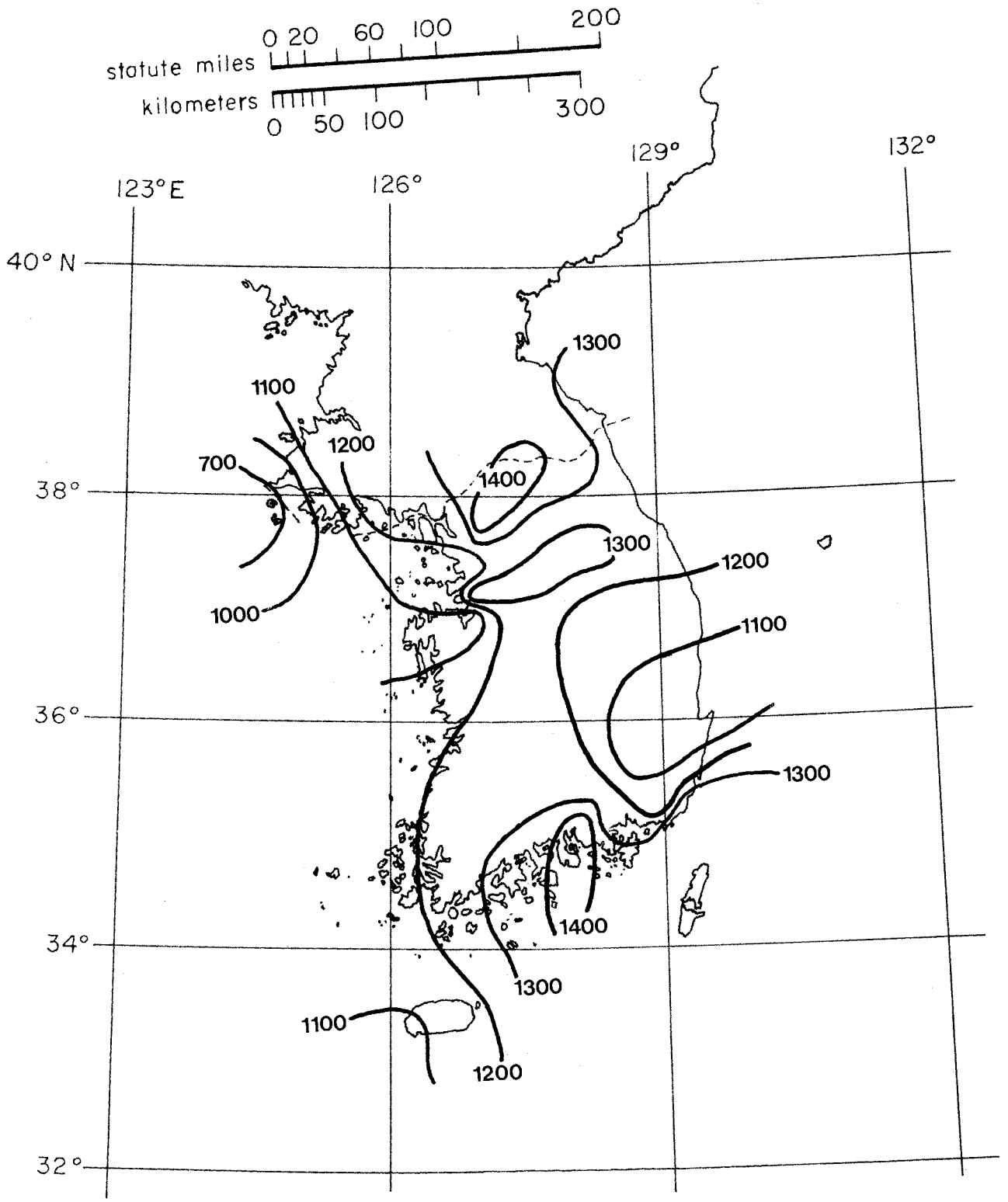

Figure 38. Contour map of the average annual precipitation, M, in millimeters, for the Republic of Korea and vicinity.

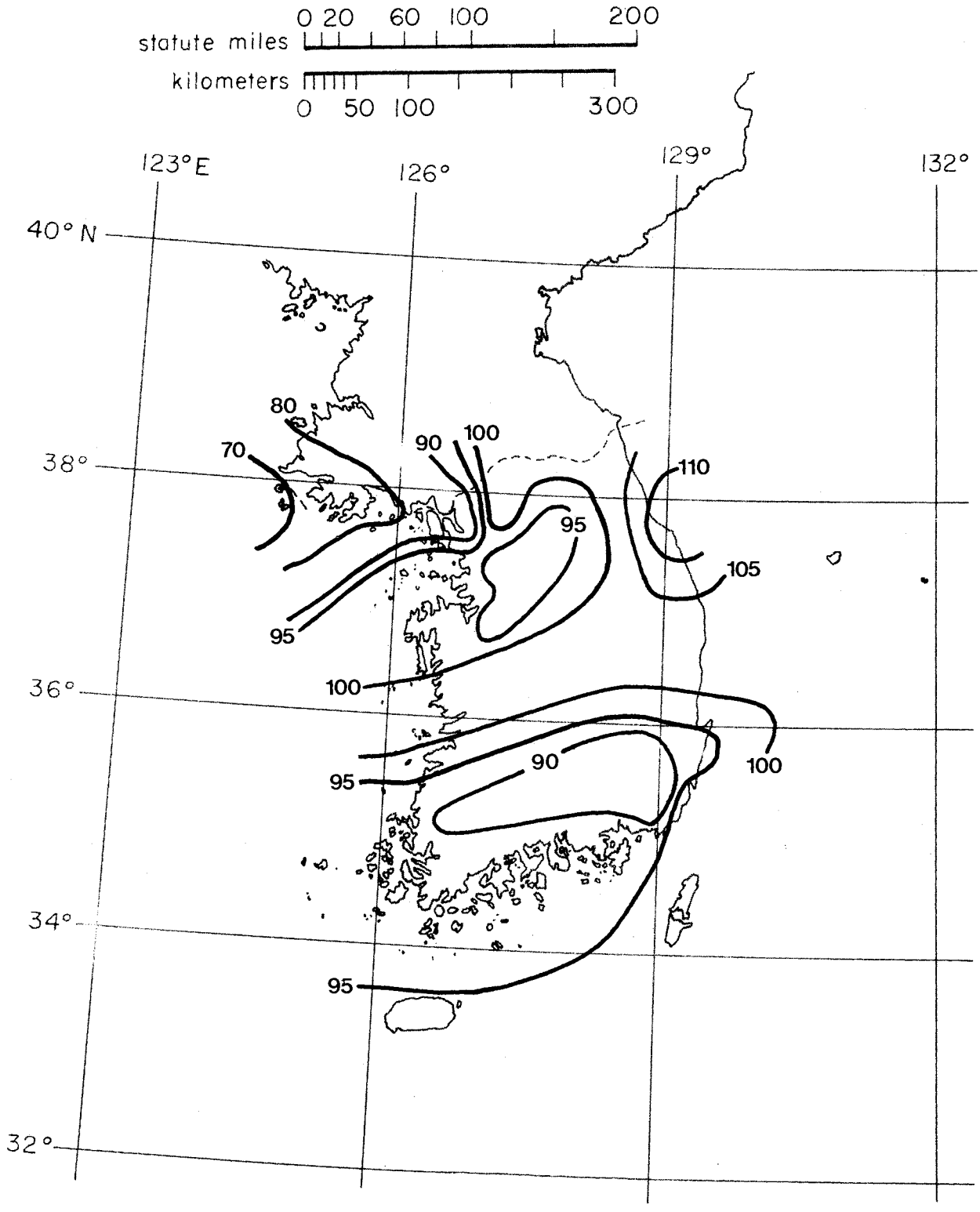

Figure 39. Contour map of the average annual number of days, $D_{.01}$, with precipitation greater than .01 in. for the Republic of Korea and vicinity.

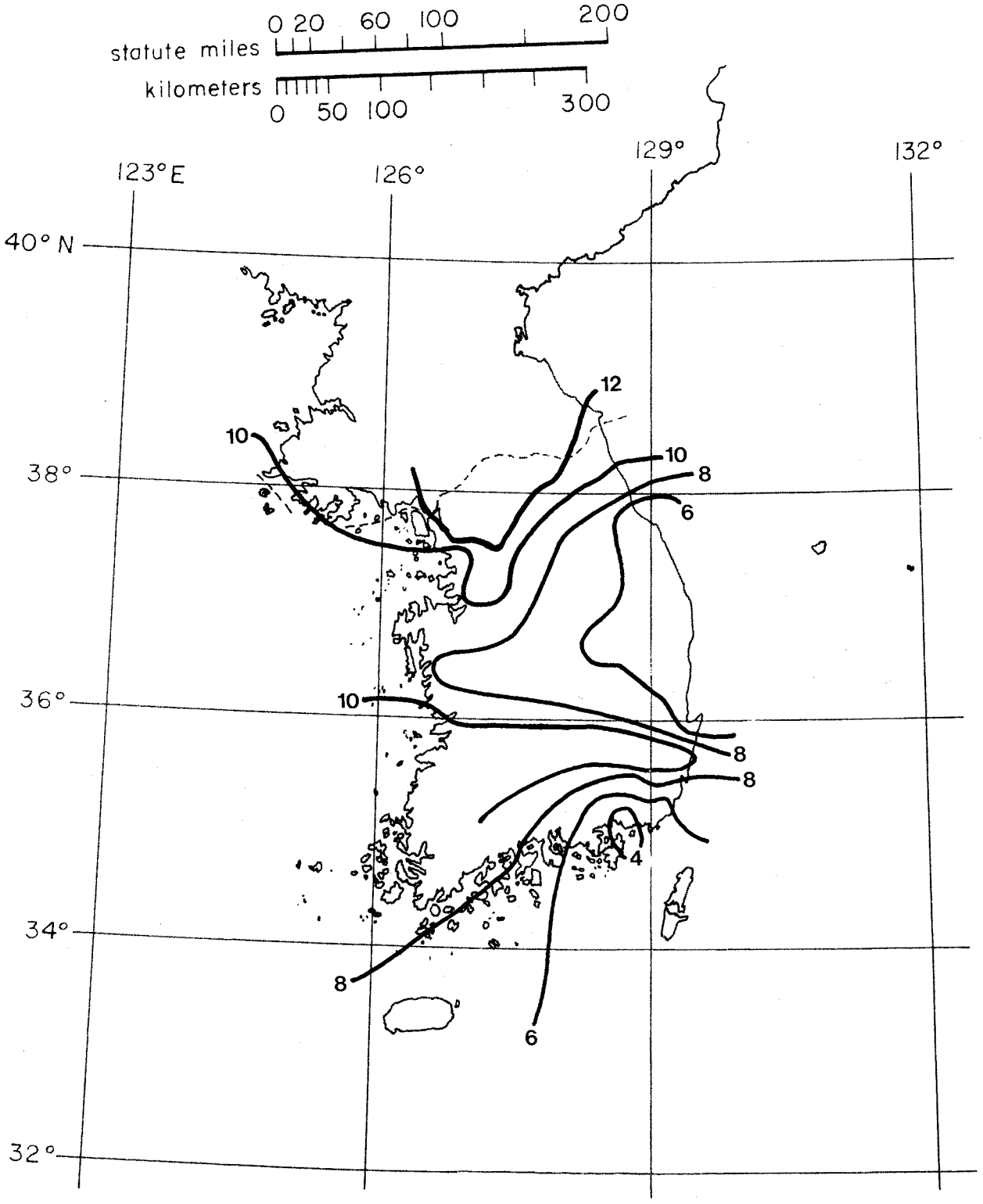

Figure 40. Contour map of the average annual number of days, U, with thunderstorms for the Republic of Korea and vicinity.

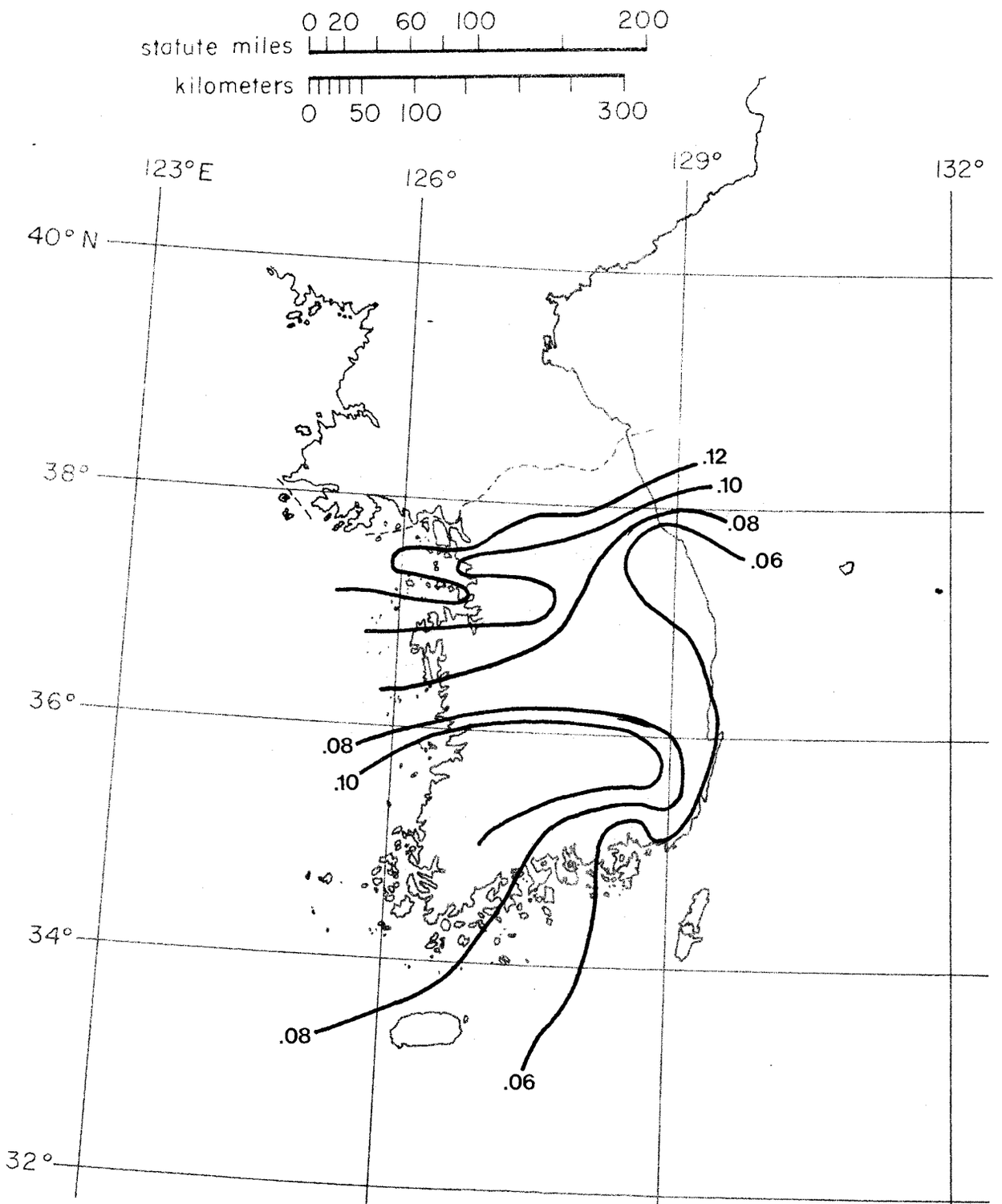

Figure 41. Contour map of the thunderstorm ratio, $U/D_{.01}$, for the Republic of Korea and vicinity.

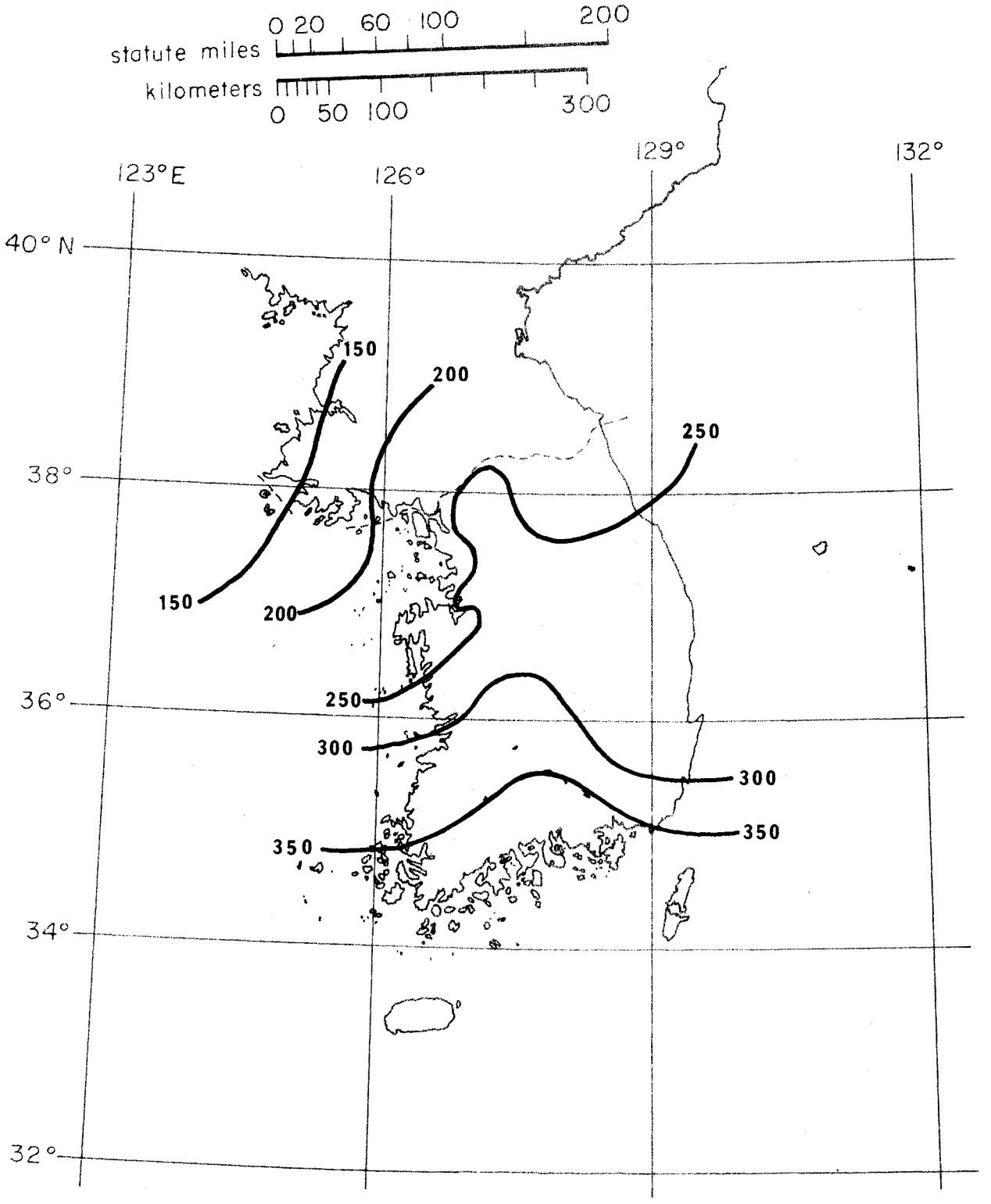

Figure 42. Contour map of the year-to-year standard deviation, s_M, in millimeters, of total annual precipitation for the Republic of Korea and vicinity.

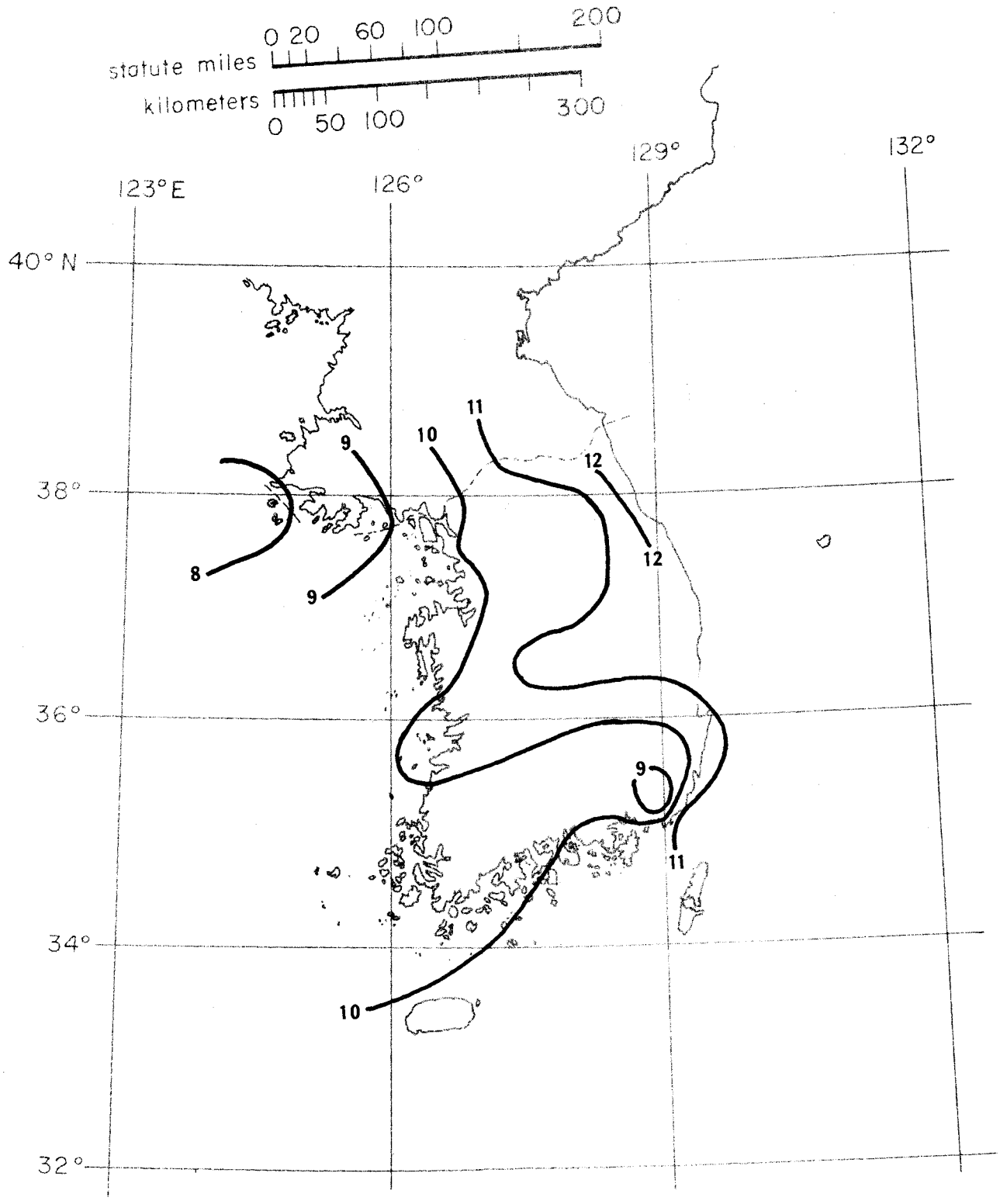

Figure 43. Contour map of the year-to-year standard deviation, s_D, of the annual number of days with precipitation greater than .01 in., for the Republic of Korea and vicinity.

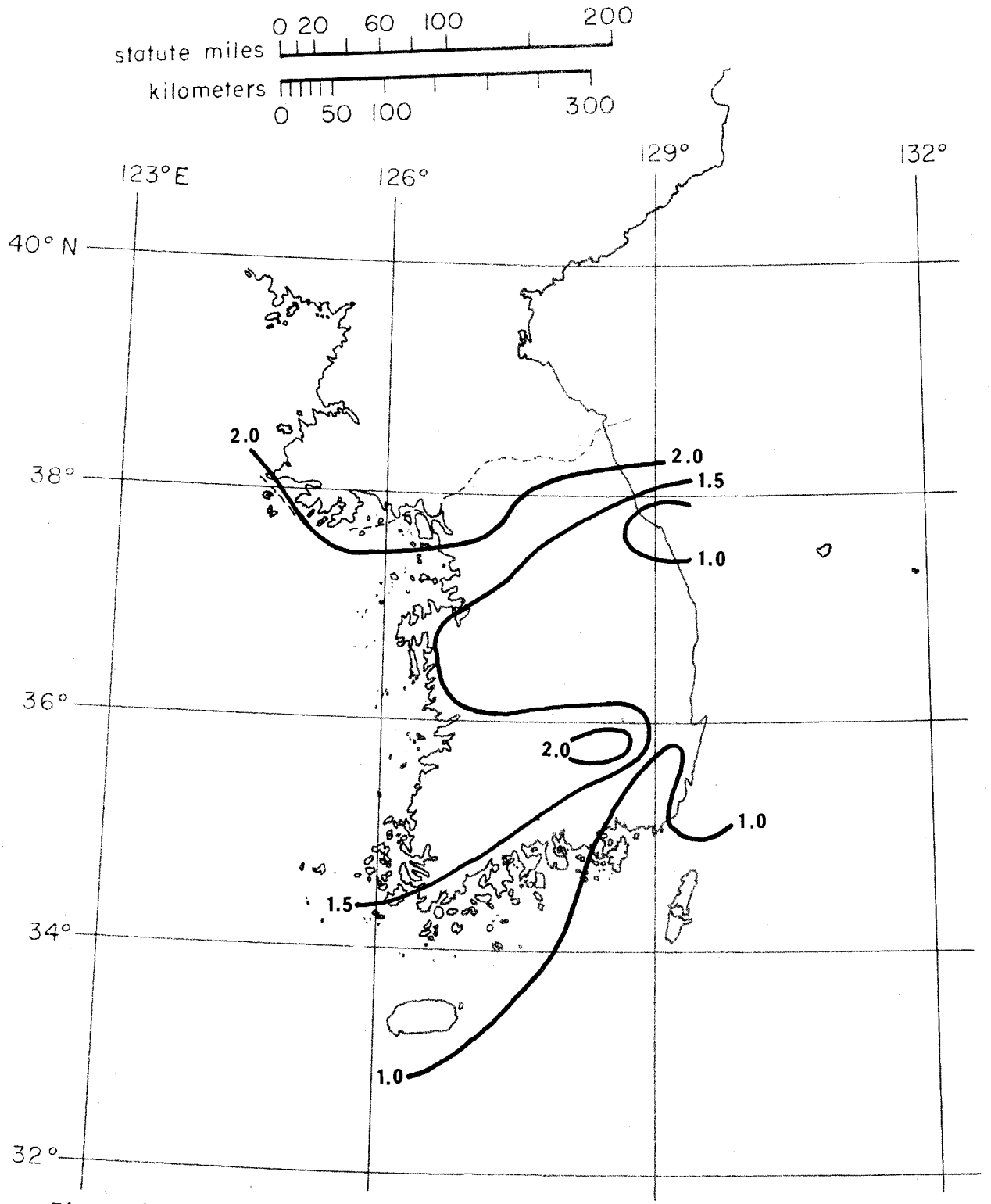

Figure 44. Contour map of the year-to-year standard deviation, s_U, of the annual number of days with thunderstorms for the Republic of Korea and vicinity.

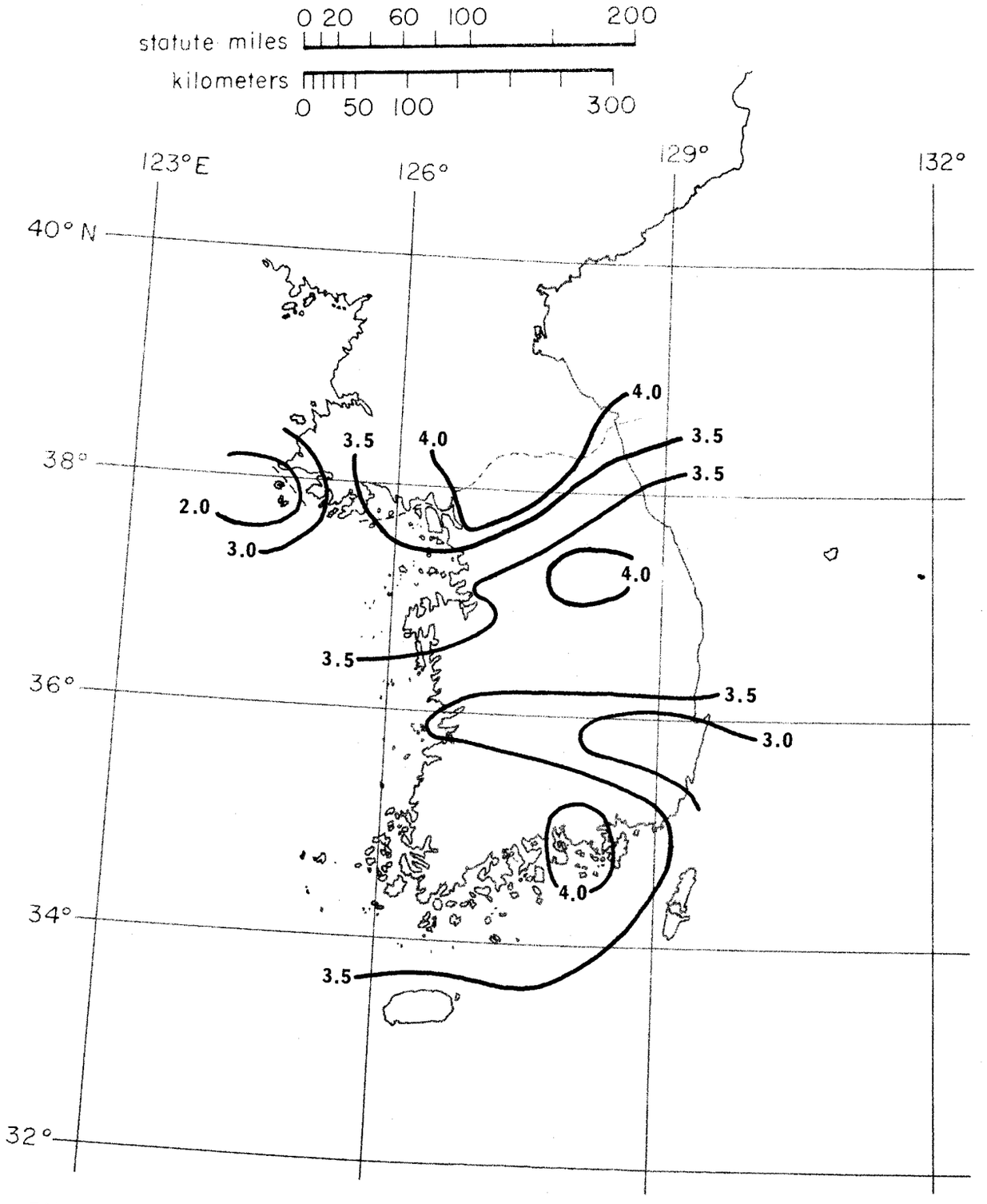

Figure 45. Contour map of the rain rate, $R_1(U/D)$, in millimeters per hour, expected to be exceeded 1 percent of an average year and derived using the thunderstorm ratio, $U/D_{.01}$, for the Republic of Korea and vicinity.

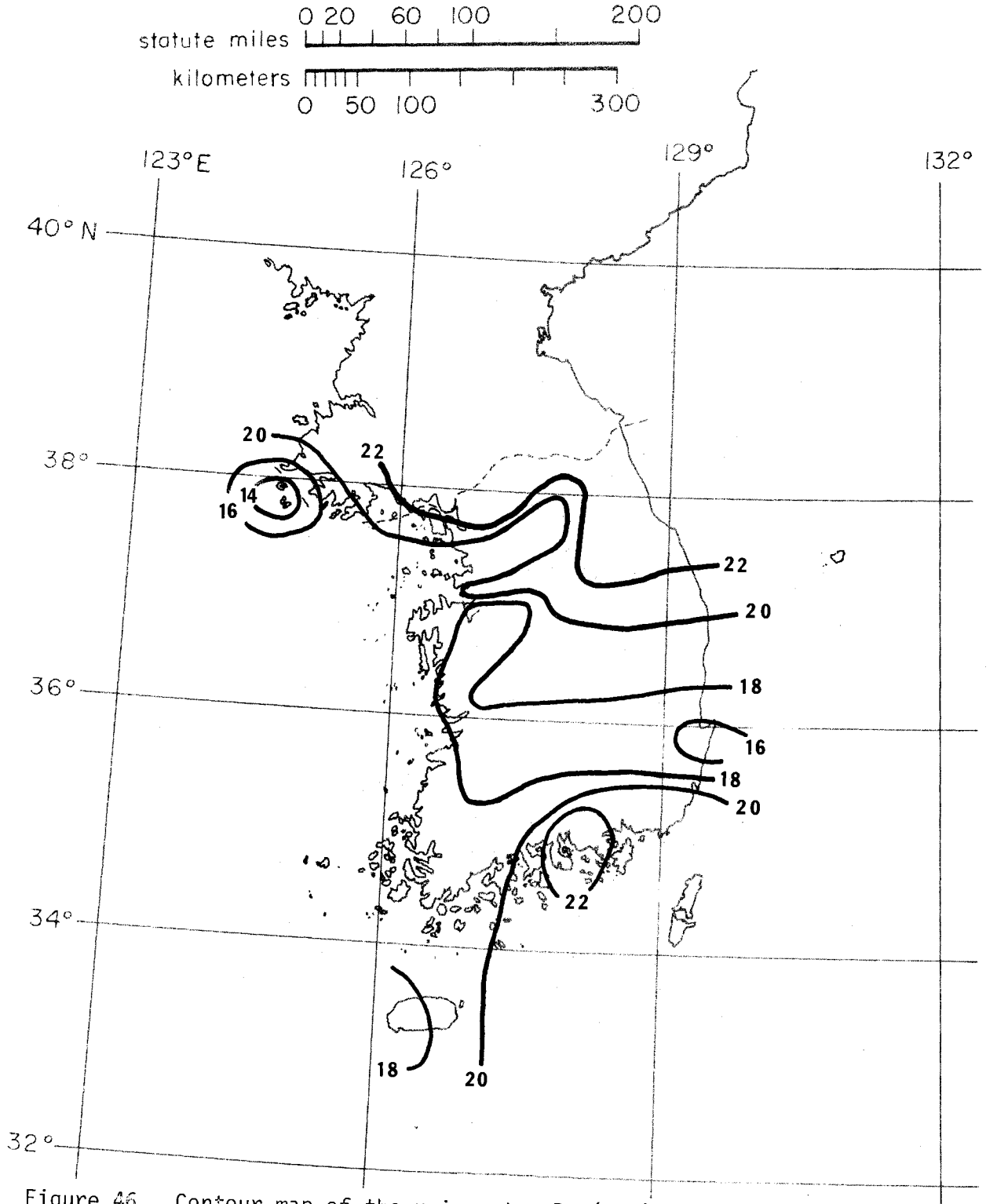

Figure 46. Contour map of the rain rate, $R_{.1}(U/D)$, in millimeters per hour, expected to be exceeded 0.1 percent of an average year and derived using the thunderstorm ratio, $U/D_{.01}$, of the Republic of Korea and vicinity.

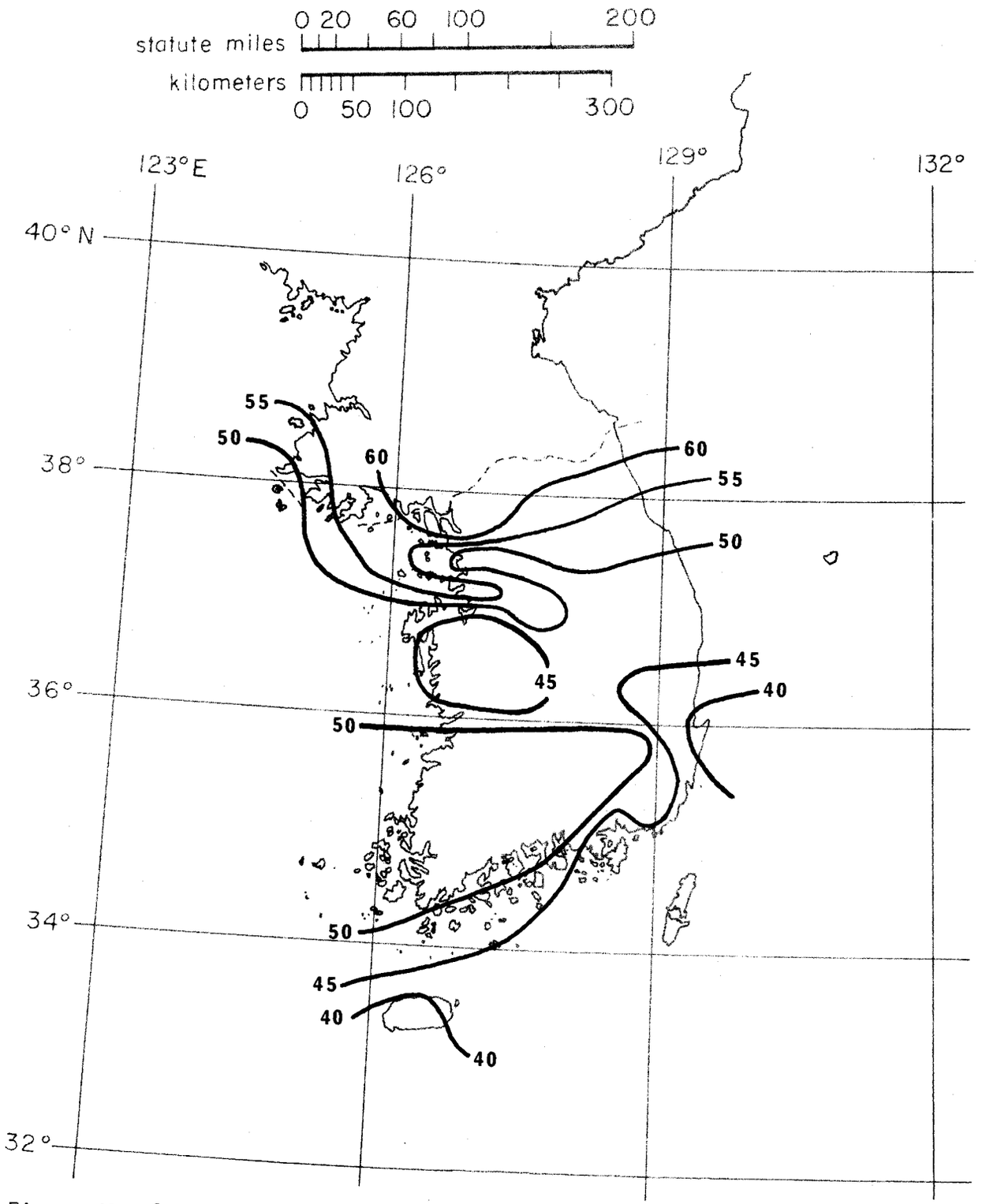

Figure 47. Contour map of the rain rate, $R_{.01}(U/D)$, in millimeters per hour, expected to be exceeded 0.01 percent of an average year and derived using the thunderstorm ratio, $U/D_{.01}$, for the Republic of Korea and vicinity.

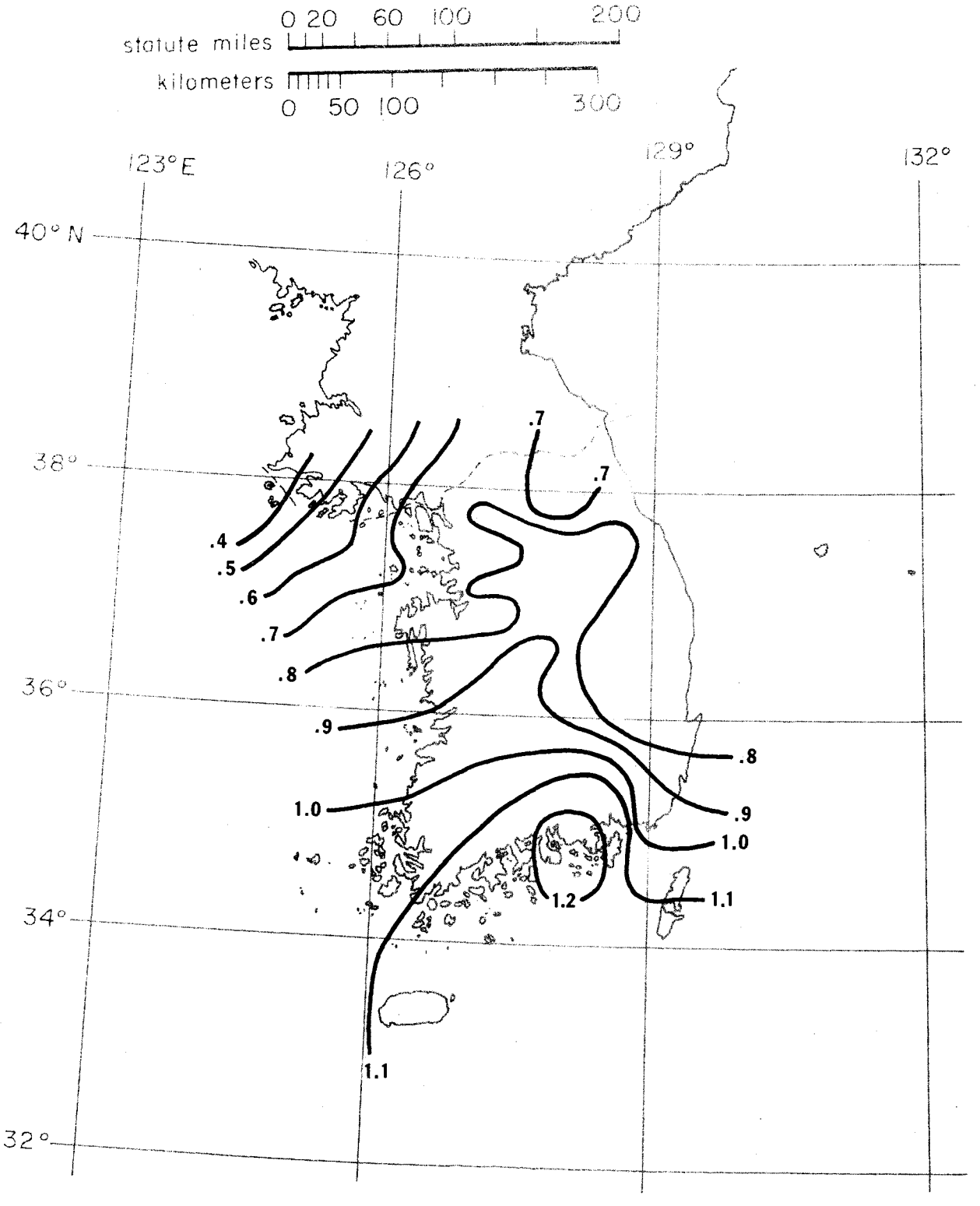

Figure 48. Contour map of the estimated year-to-year standard deviation, s_{R_1}, in millimeters per hour, of rain rate expected at the 1 percent exceedance level for the Republic of Korea and vicinity.

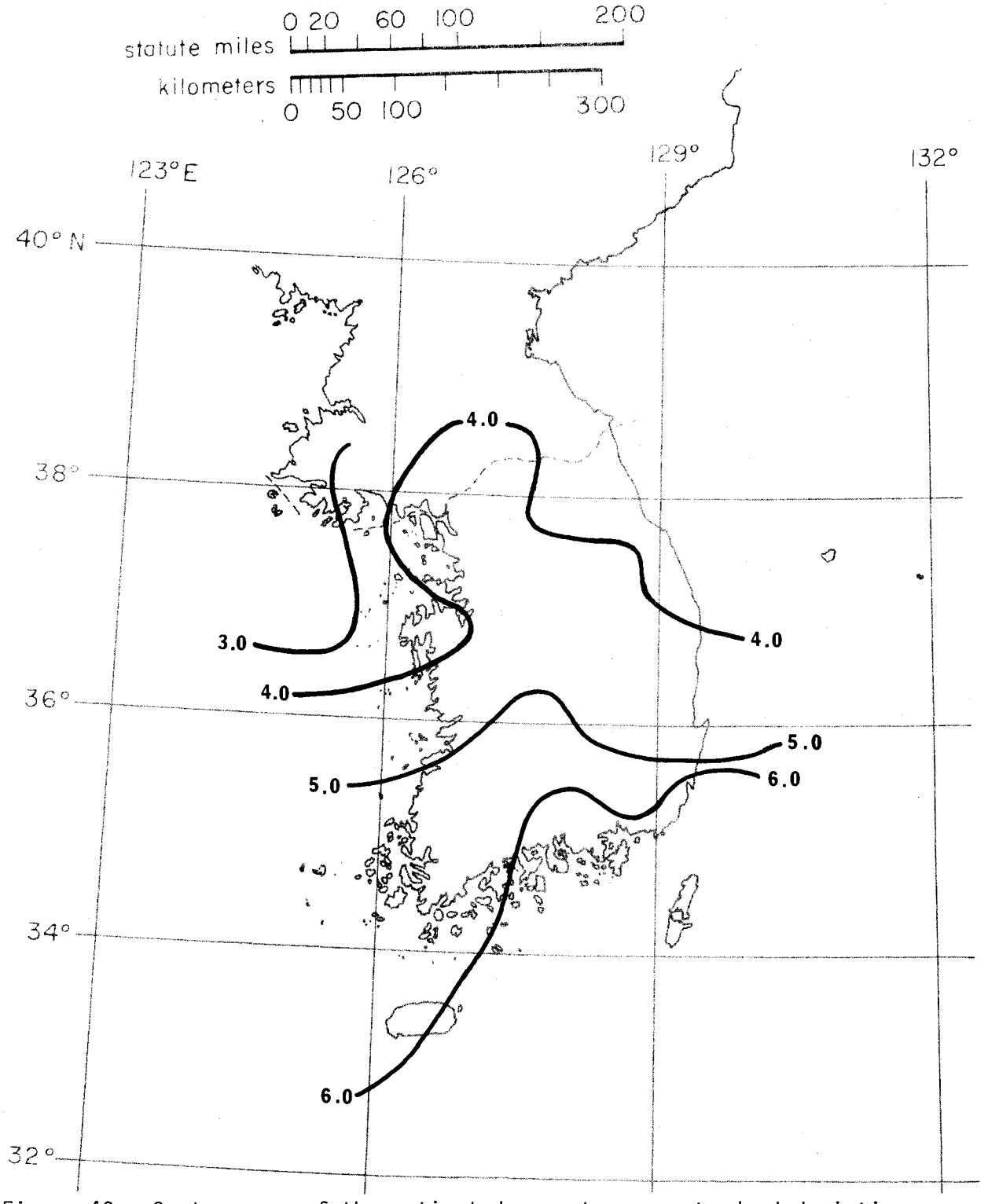

Figure 49. Contour map of the estimated year-to-year standard deviation, $s_{R_{.1}}$, in millimeters per hour, of rain rate expected at the 0.1 percent exceedance level for the Republic of Korea and vicinity.

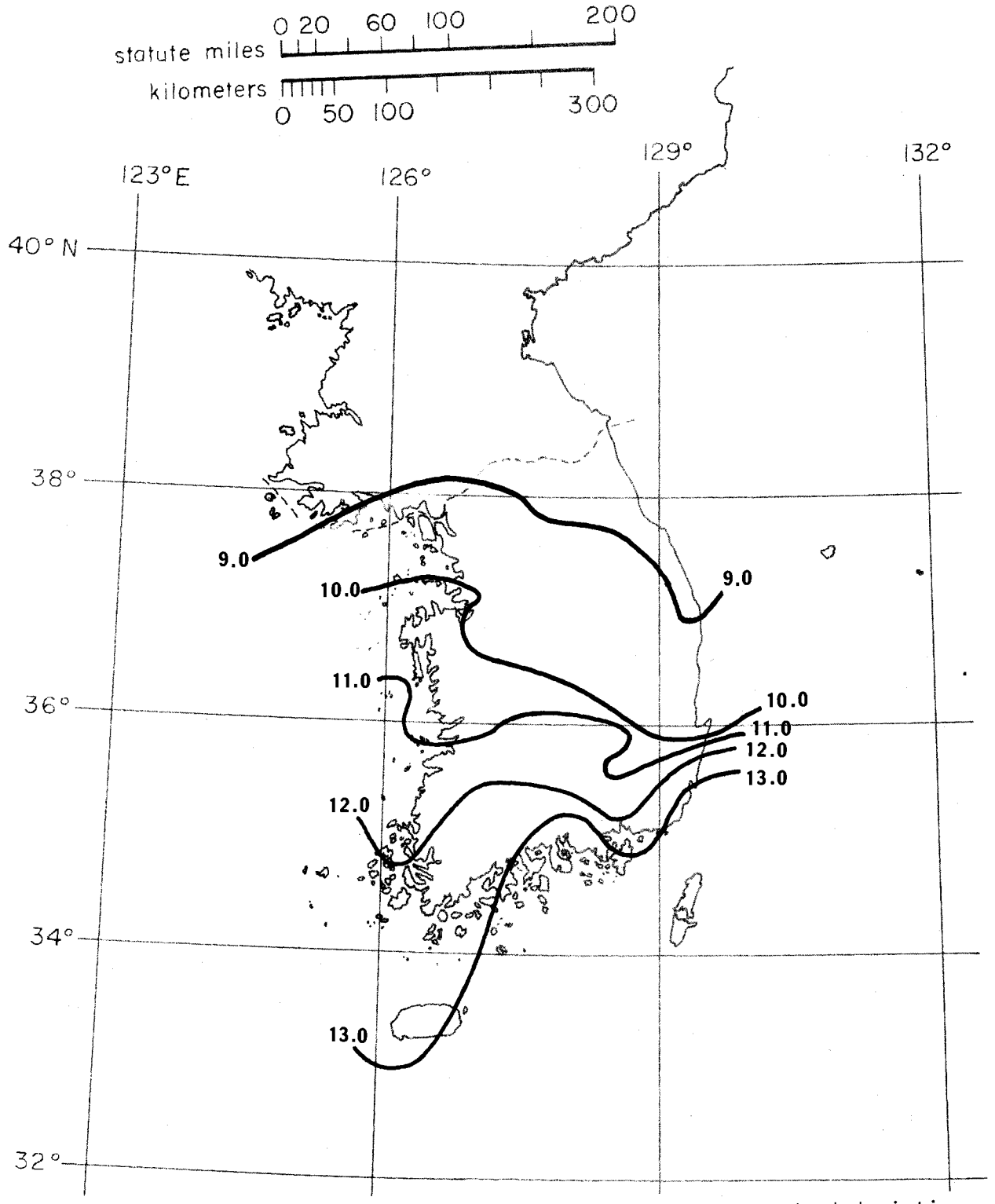

Figure 50. Contour map of the estimated year-to-year standard deviation, $s_{R_{.01}}$, in millimeters per hour, of rain rate expected at the 0.01 percent exceedance level for the Republic of Korea and vicinity.

$D_{.01}$, s_D, and s_U were estimated from (19), (20), and (21), by determining that the ROK and vicinity are in Köppen (1918) zone C.

3.4 Southwest Asia

Figure 51 shows the 185 data locations used for contouring maps in the Southwest Asia area, including the Middle East. Locations appear to be spread relatively uniformly over the area, encompassing a variety of climatic types. In spite of this, many locations did not contain complete data sets, as can be seen from Figures 52 to 69. Figures 52 to 69 show M, $D_{.01}$, U, M_m, β, $U/D_{.01}$, s_M, s_D, s_U, $R_1(\beta)$, $R_{.1}(\beta)$, $R_{.01}(\beta)$, $R_1(U/D)$, $R_{.1}(U/D)$, $R_{.01}(U/D)$, s_{R_1}, $s_{R_{.1}}$, and $s_{R_{.01}}$, in that order. Figure 55 shows that a discontinuity, marked "NO DATA," exists in the contouring of M_m in the Iran-Afghanistan region. This lack of data for M_m also carries over to any parameters derived from M_m; namely, β, $R_1(\beta)$, $R_{.1}(\beta)$, and $R_{.01}(\beta)$. Hence, Figures 56, 61, 62, and 63 have the same "NO DATA" region indicated thereon. Values of s_R, $s_{R_{.1}}$, and $s_{R_{.01}}$ were derived from $U/D_{.01}$ rather than from β because of the more complete data base.

As in earlier cases, $D_{.01}$, s_D, and s_U were estimated using (19), (20), and (21), respectively, in southwest Asia. In this situation, however, southwest Asia encompasses Köppen (1918) zones A, B, C, and D. This required the calculation and use of four different ratios in the U.S.A. for use with (19) through (21), instead of only one ratio as has been the case in previously mapped areas. While the prevailing perception of southwest Asia and the Middle East is that of a dry, hot climate, many parts of the region can be quite cold, and others, such as western India, extremely wet.

3.5 Central America

Figure 70 shows the 47 data locations used for contouring maps in Central America. There are few data stations just above the isthmus region in Costa Rica and Nicaragua. As a consequence, there is often a total void of data in that region, resulting in a "NO DATA" indication on many of the contour maps for Central America. Figures 71 to 83 show M, $D_{.01}$, U, $U/D_{.01}$, s_M, s_D, s_U, $R_1(U/D)$, $R_{.1}(U/D)$, $R_{.01}(U/D)$, s_{R_1}, $s_{R_{.1}}$, and $s_{R_{.01}}$, in that order.

As in some earlier cases, there were insufficiently few (five) values of M_m available; whence, it was decided not to base any contour maps of M_m, or any of the parameters dependent upon it (β, $R_1(\beta)$, etc.) on such a limited sample. It was, however, possible once again to substitute the "thunderstorm ratio," $U/D_{.01}$, for

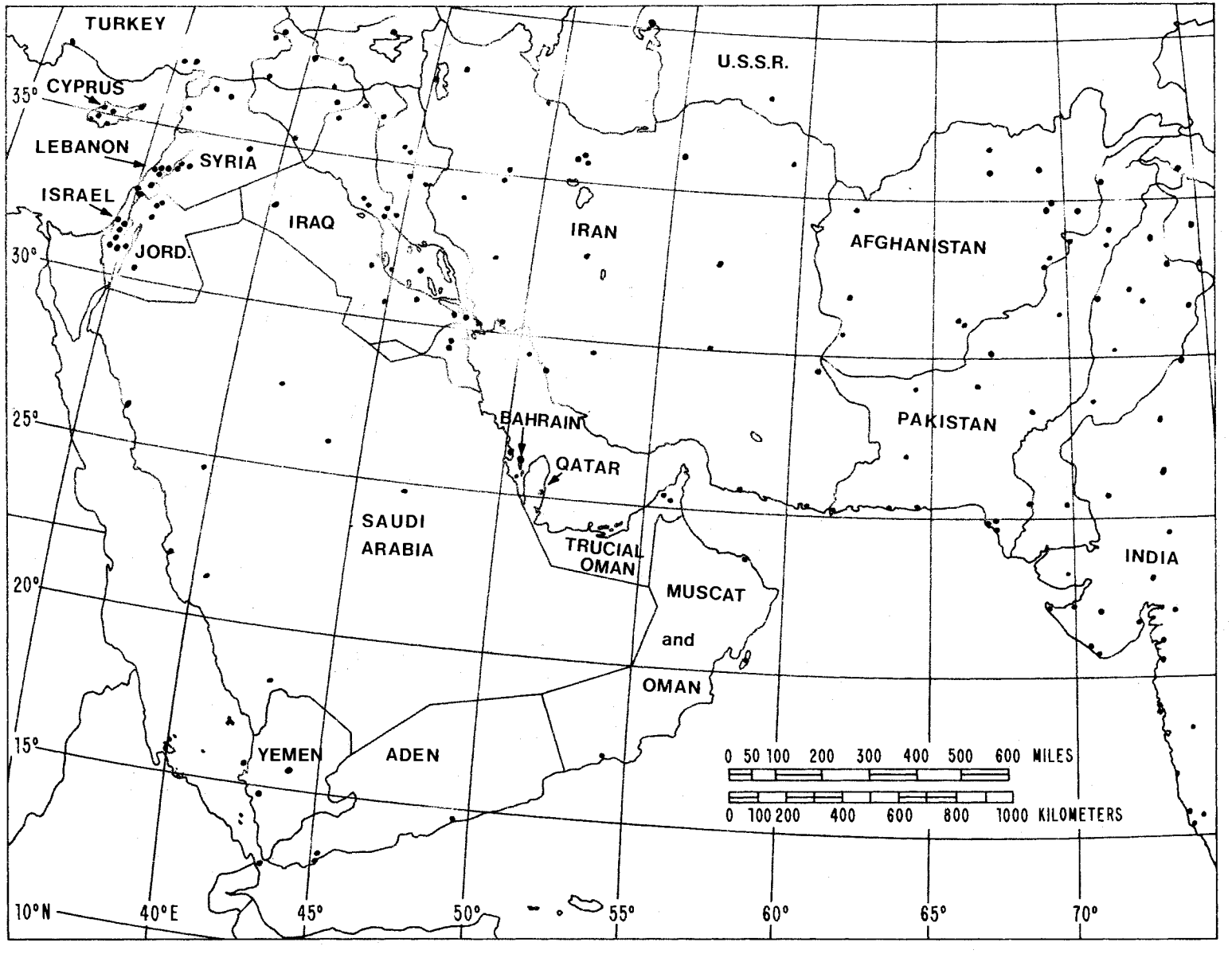

Figure 51. Map of data locations in Southwest Asia.

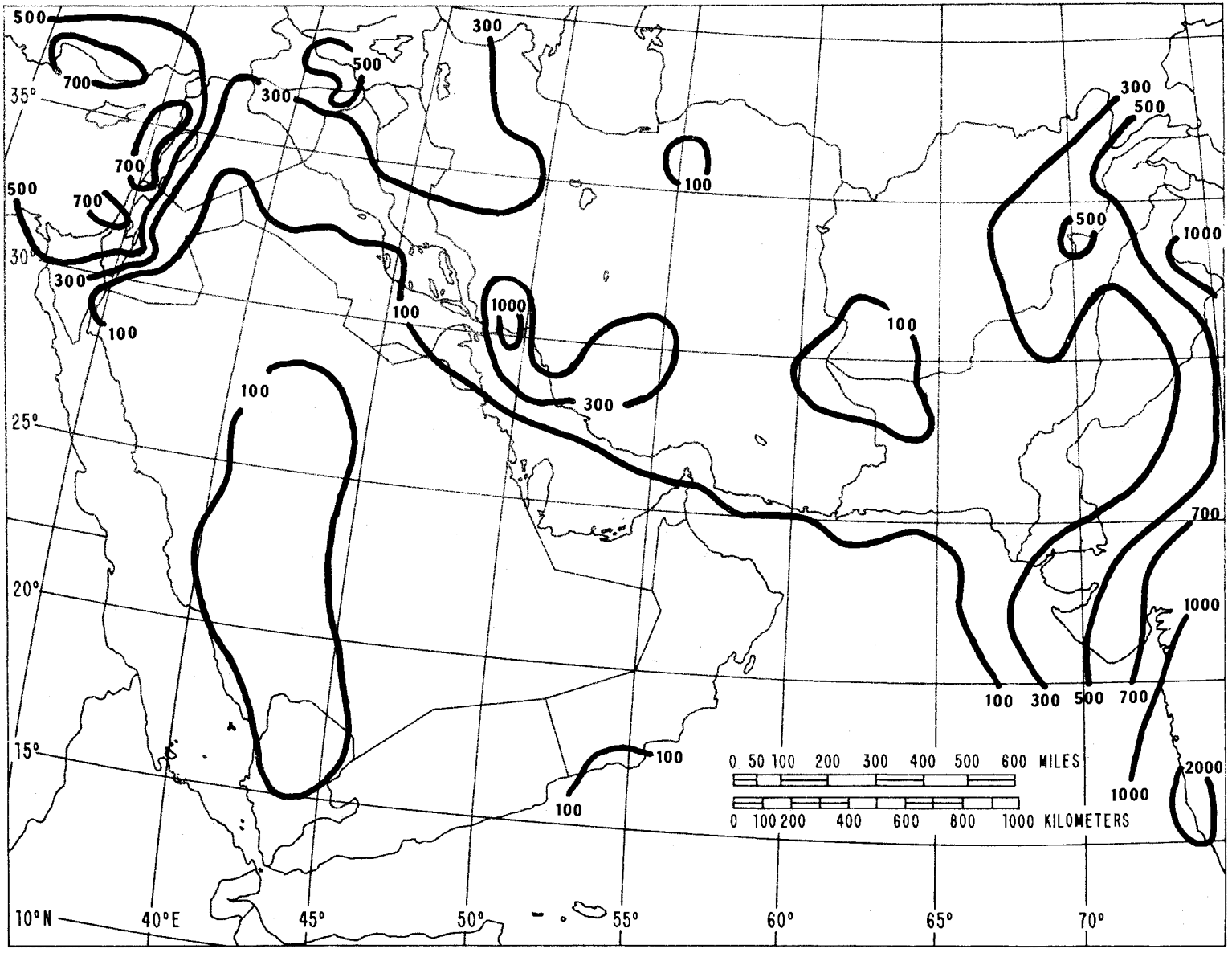

Figure 52. Contour map of the average annual precipitation, M, in millimeters, for Southwest Asia.

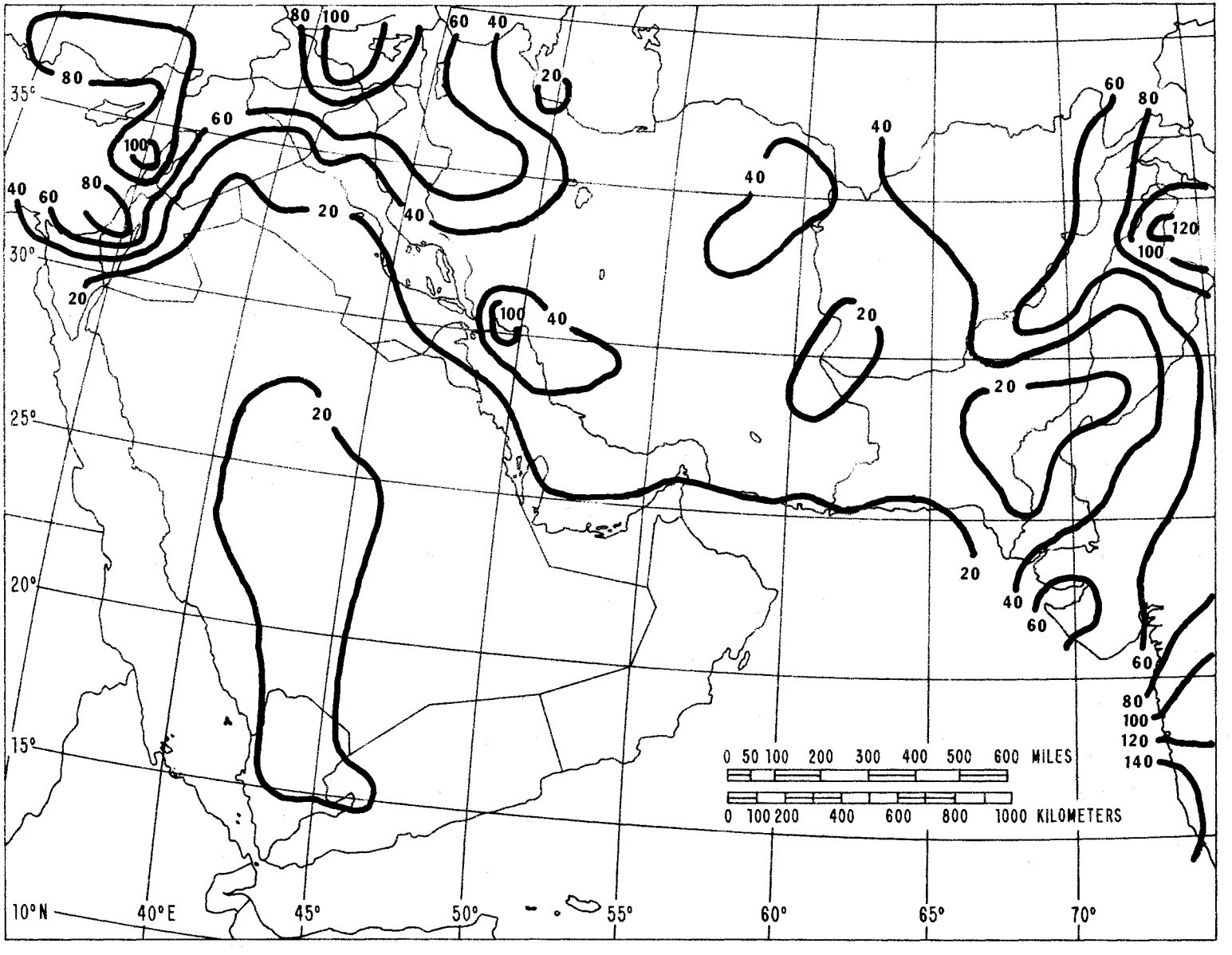

Figure 53. Contour map of the average annual number of days, $D_{.01}$, with precipitation greater than .01 in., for Southwest Asia.

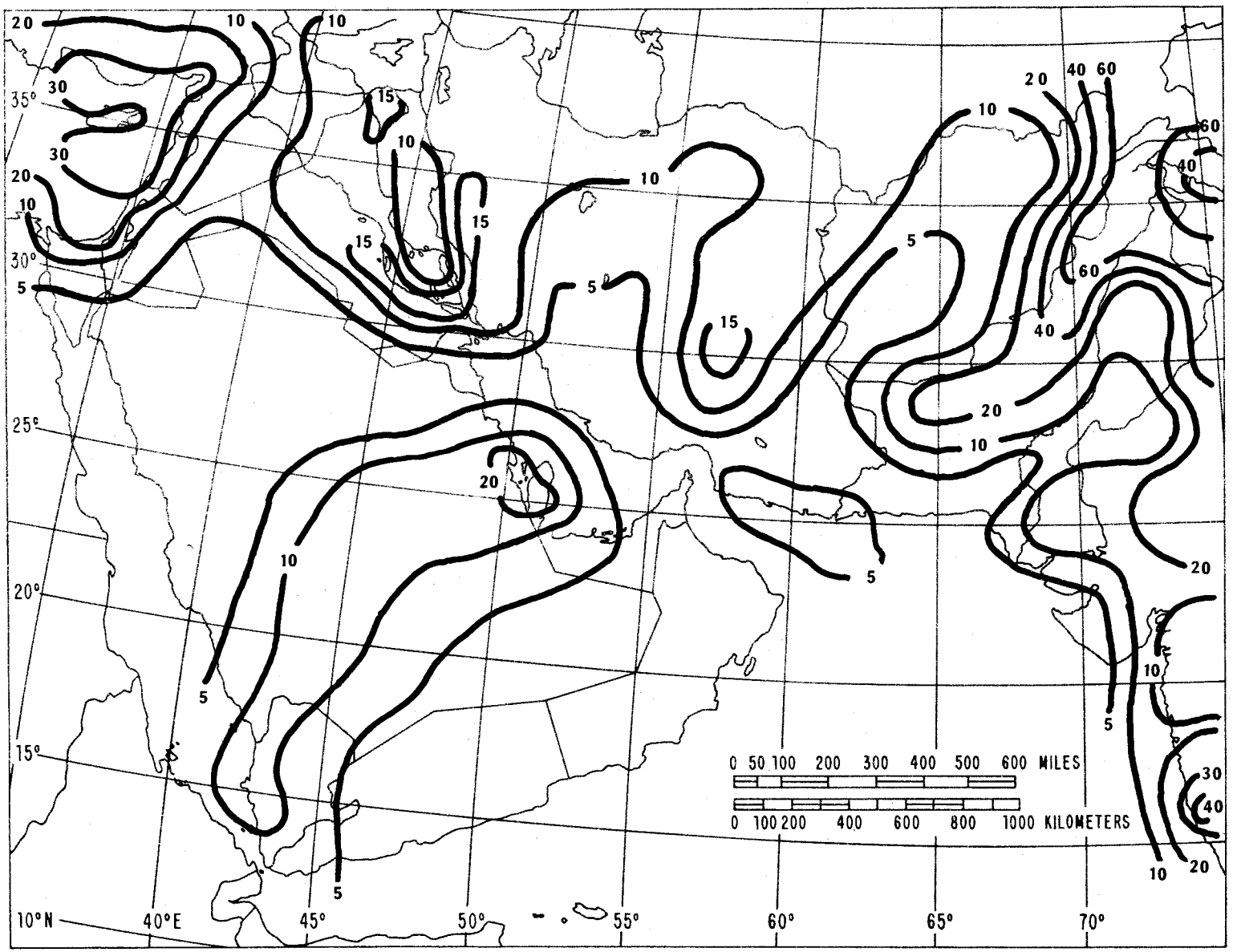

Figure 54. Contour map of the average annual number of days, U, with thunderstorms for Southwest Asia.

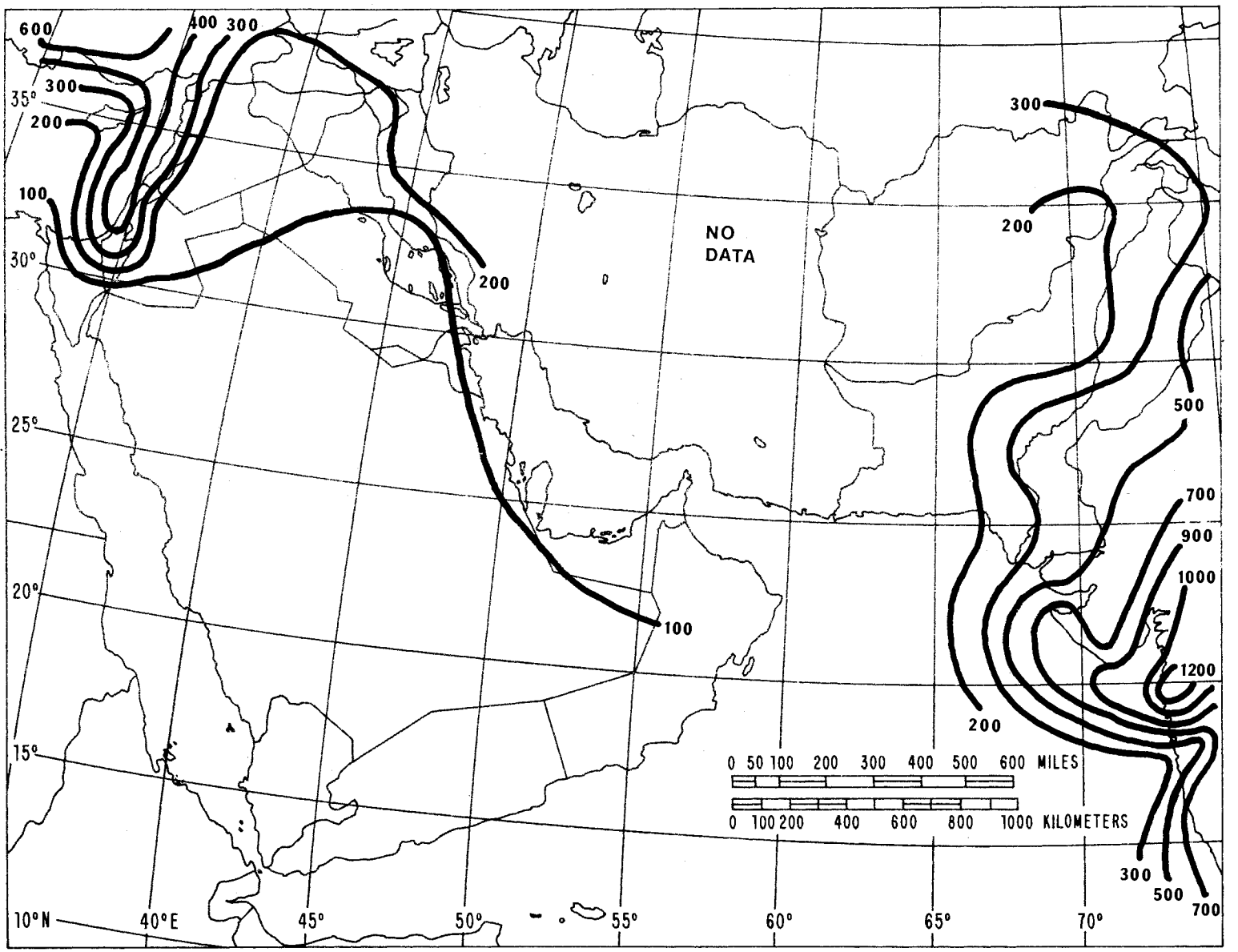

Figure 55. Contour map of the greatest monthly precipitation, M_m, in 30 consecutive years, in millimeters, for Southwest Asia.

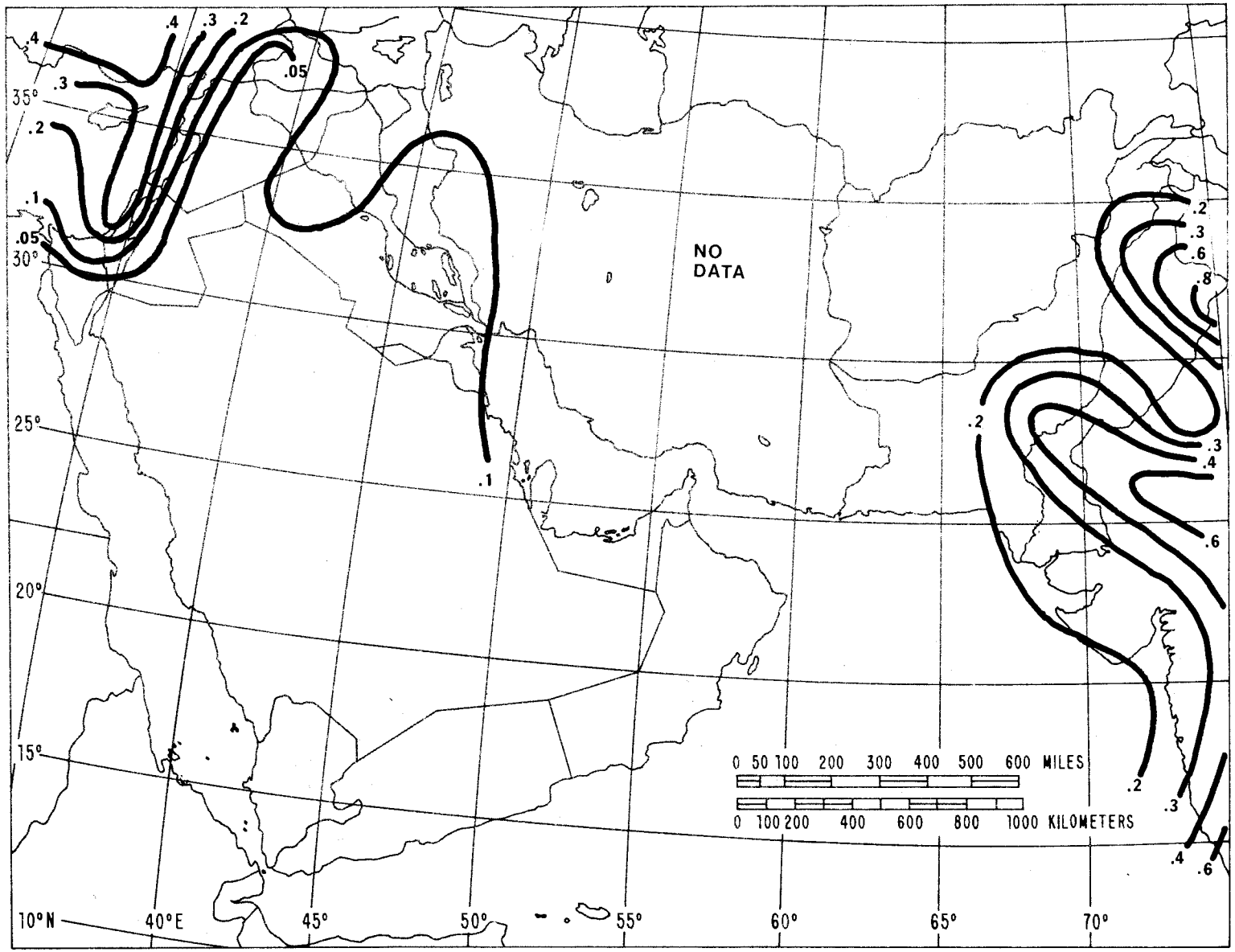

Figure 56. Contour map of the thunderstorm ratio, β, for Southwest Asia.

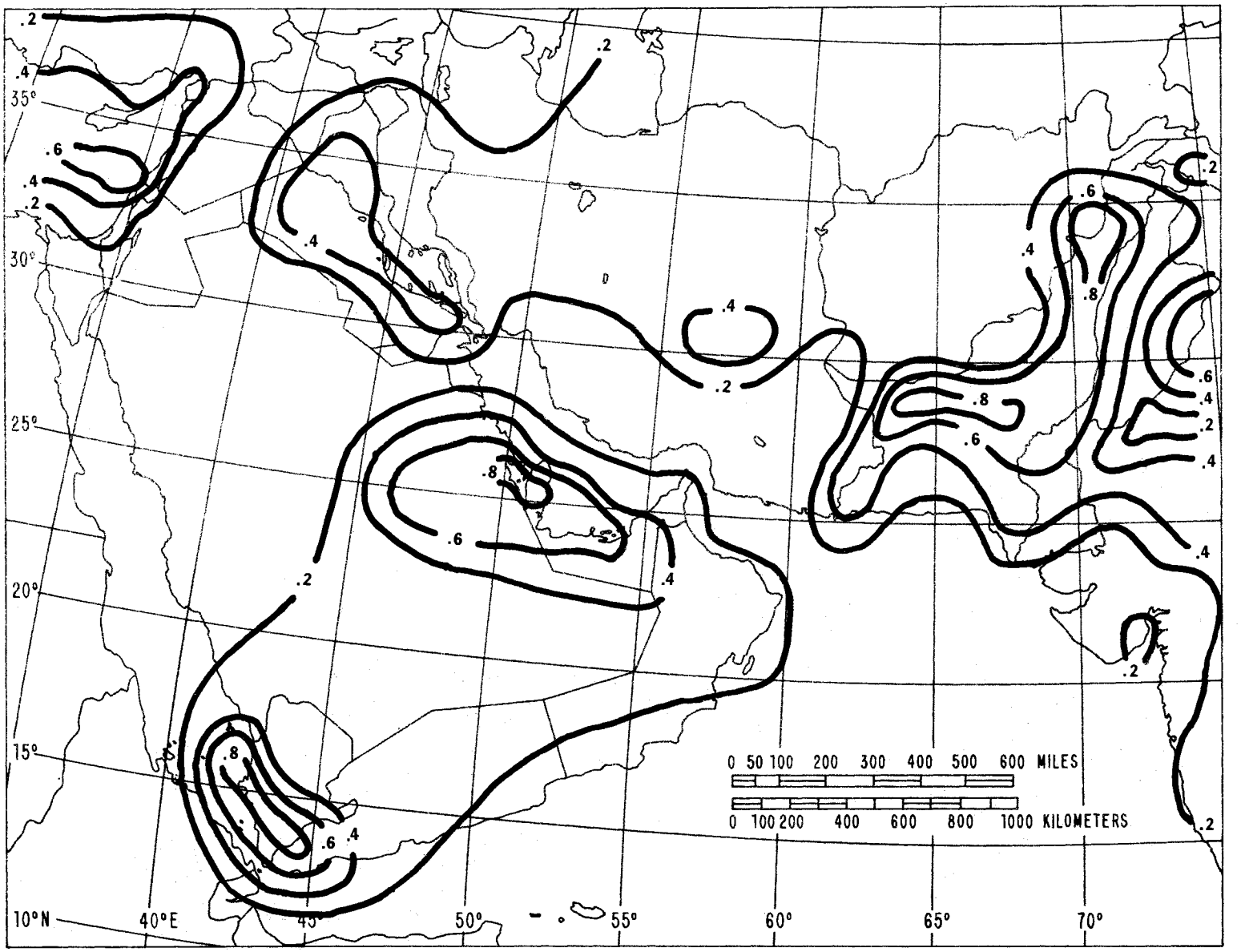

Figure 57. Contour map of the thunderstorm ratio, $U/D_{.01}$, for Southwest Asia.

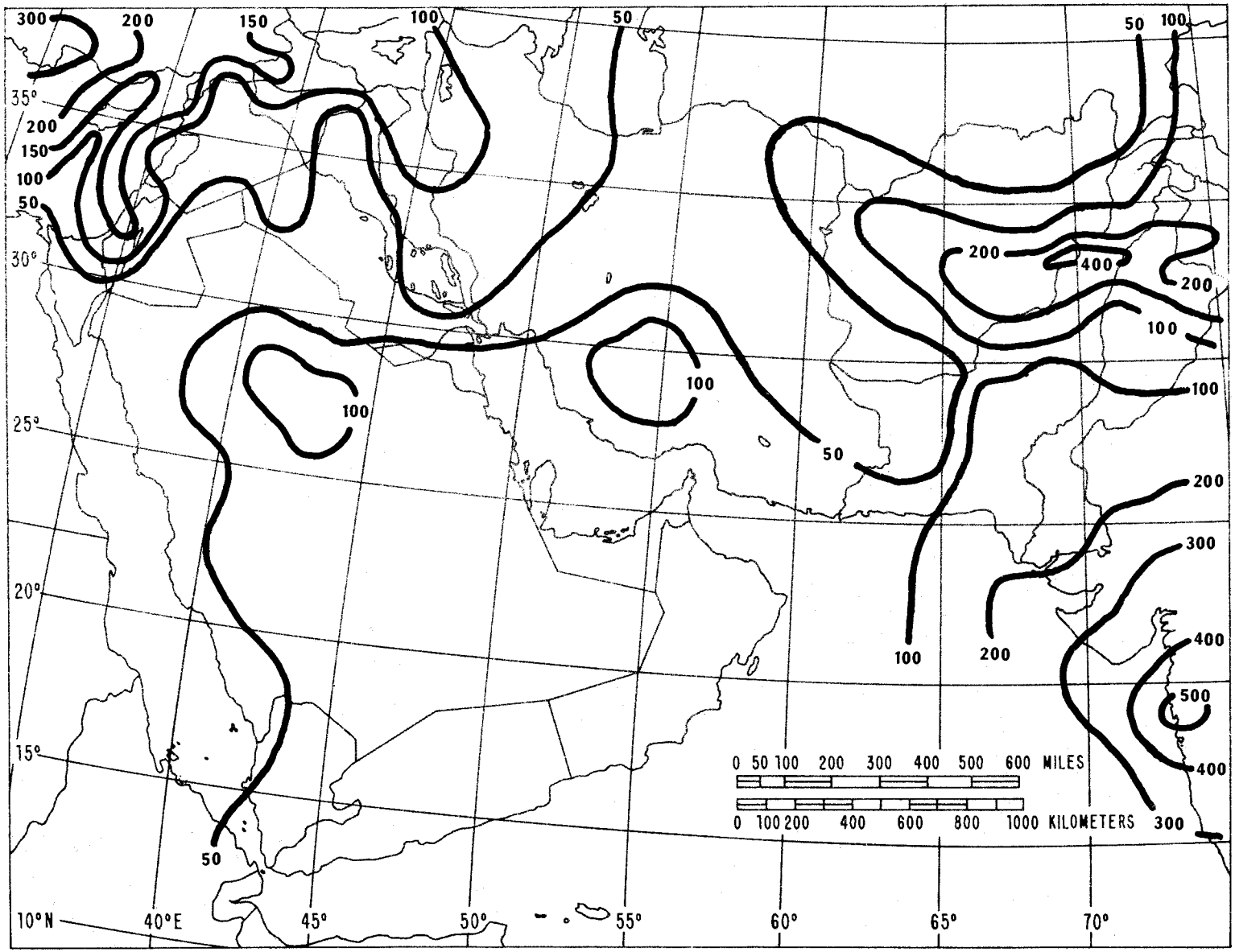

Figure 58. Contour map of the year-to-year standard deviation, s_M, in millimeters, of total annual precipitation for Southwest Asia.

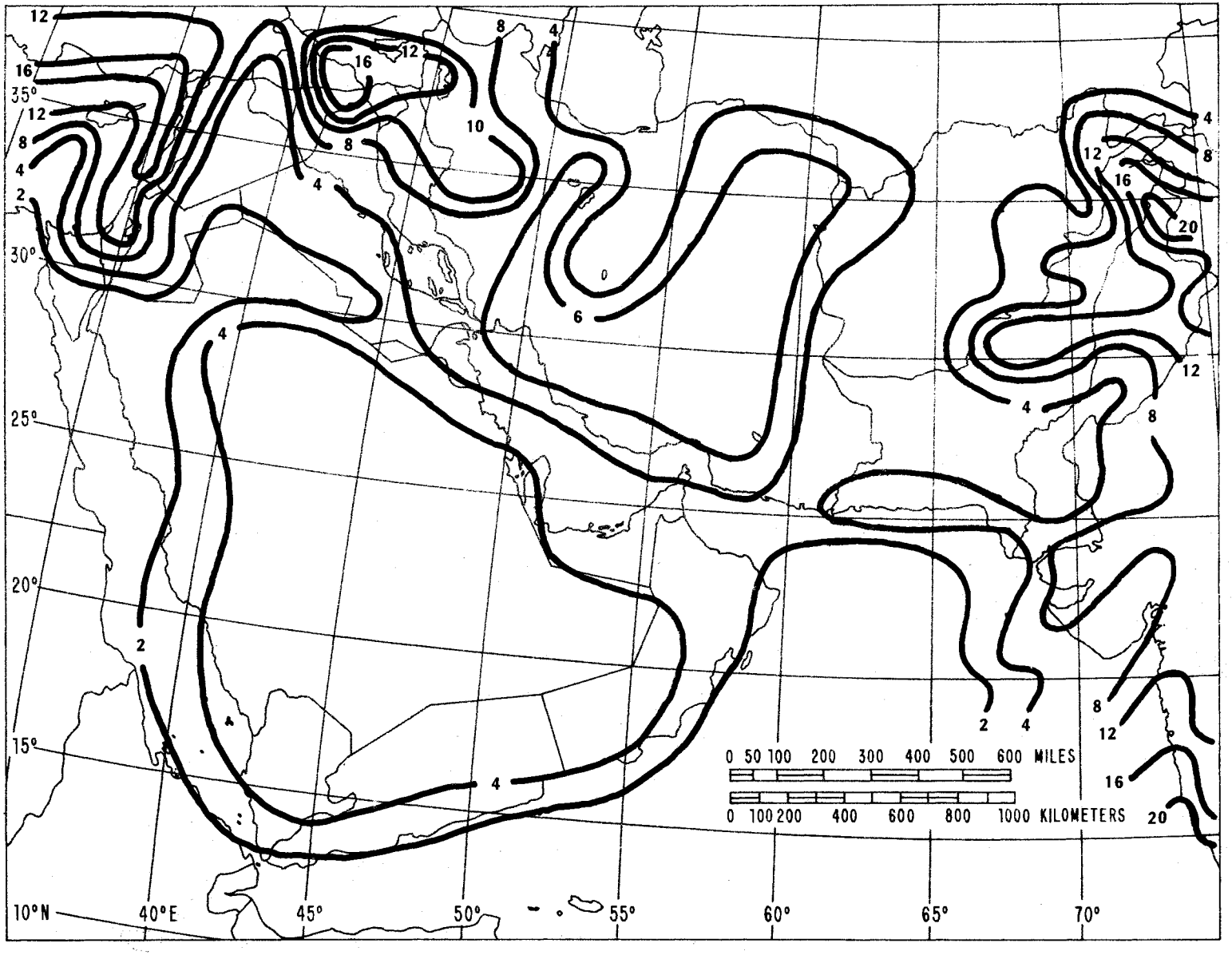

Figure 59. Contour map of the year-to-year standard deviation, s_D, of the annual number of days with precipitation greater than .01 in., for Southwest Asia.

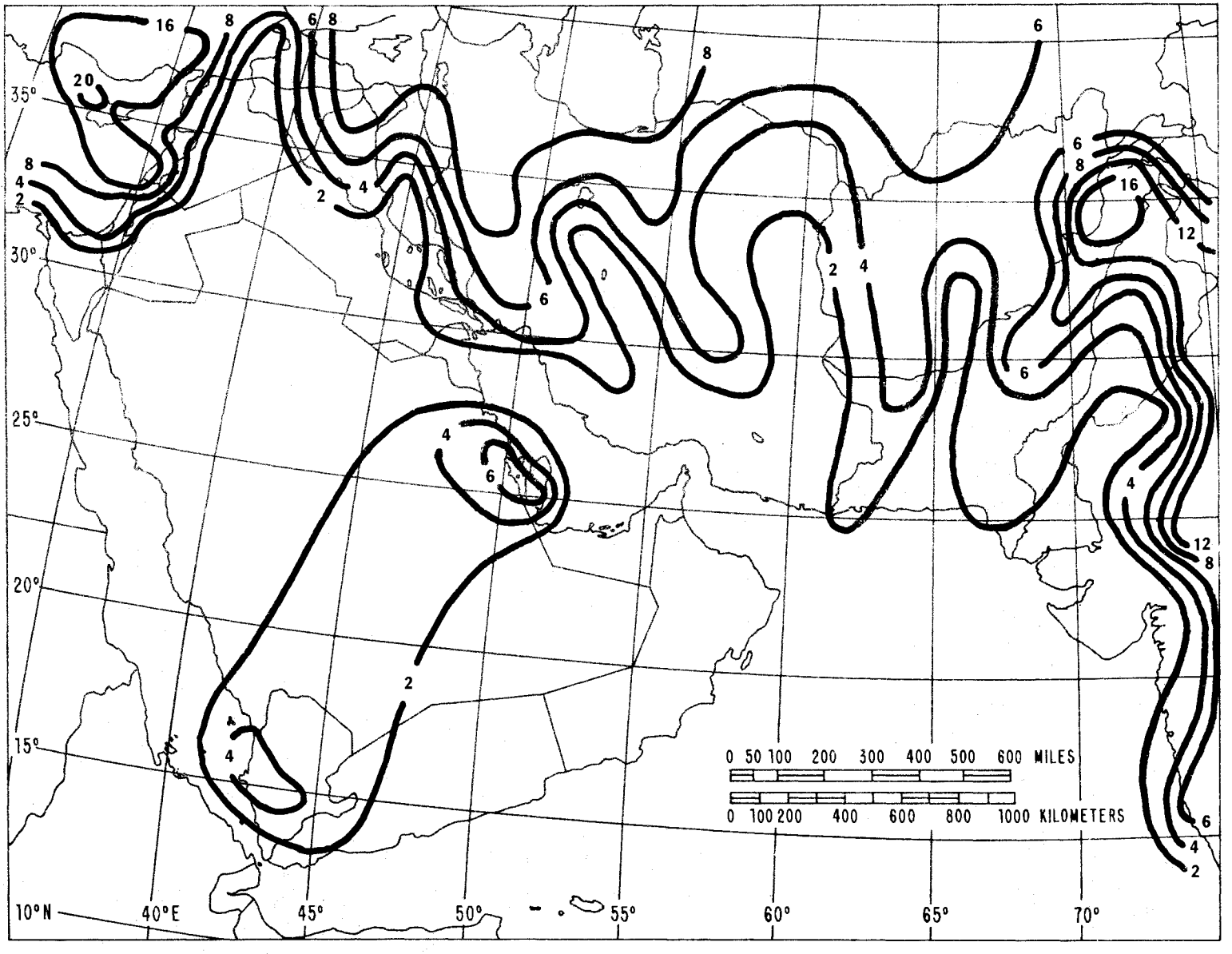

Figure 60. Contour map of the year-to-year standard deviation, s_U, of the annual number of days with thunderstorms for Southwest Asia.

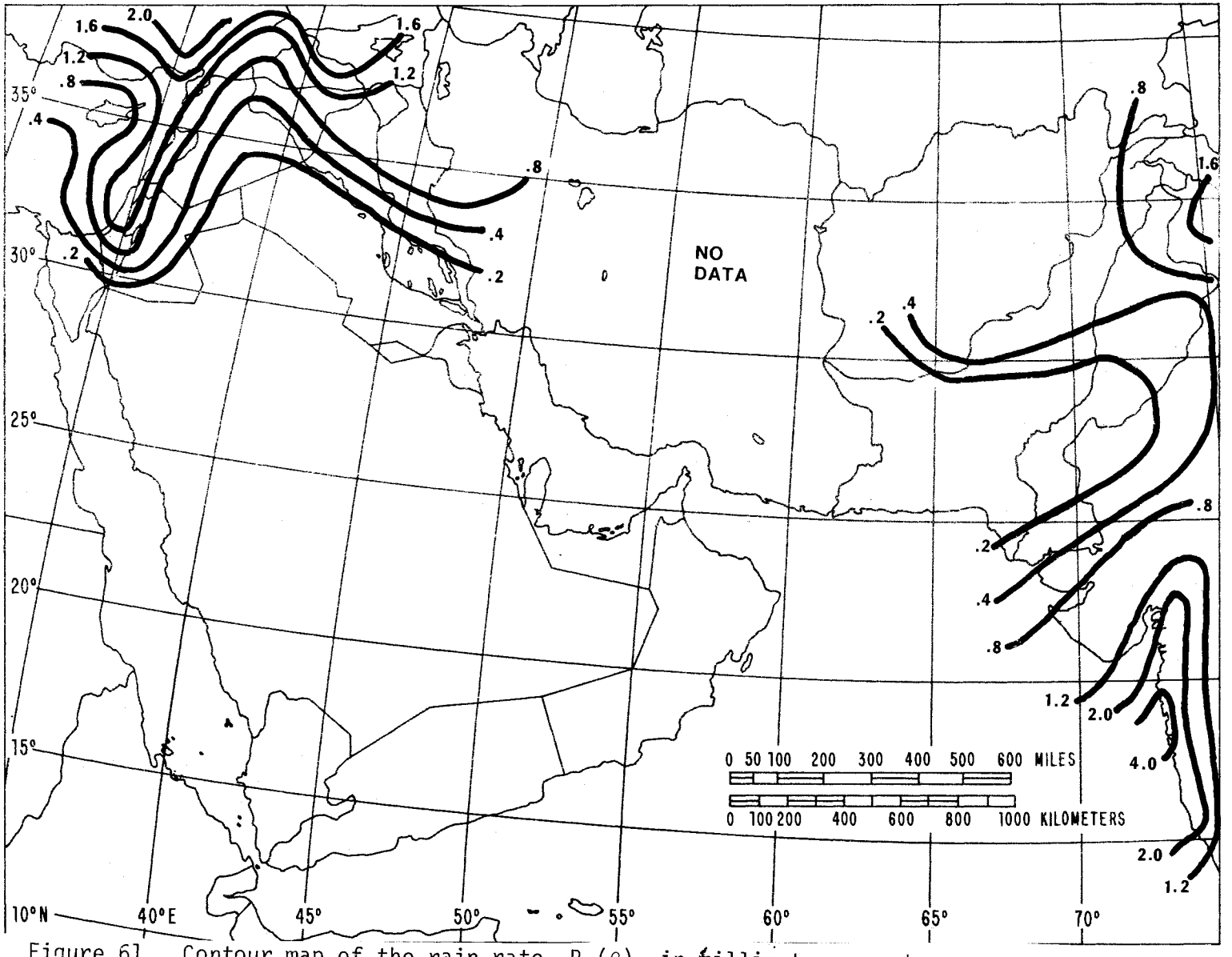

Figure 61. Contour map of the rain rate, $R_1(\beta)$, in millimeters per hour, expected to be exceeded 1 percent of an average year and derived using the thunderstorm ratio, β, for Southwest Asia.

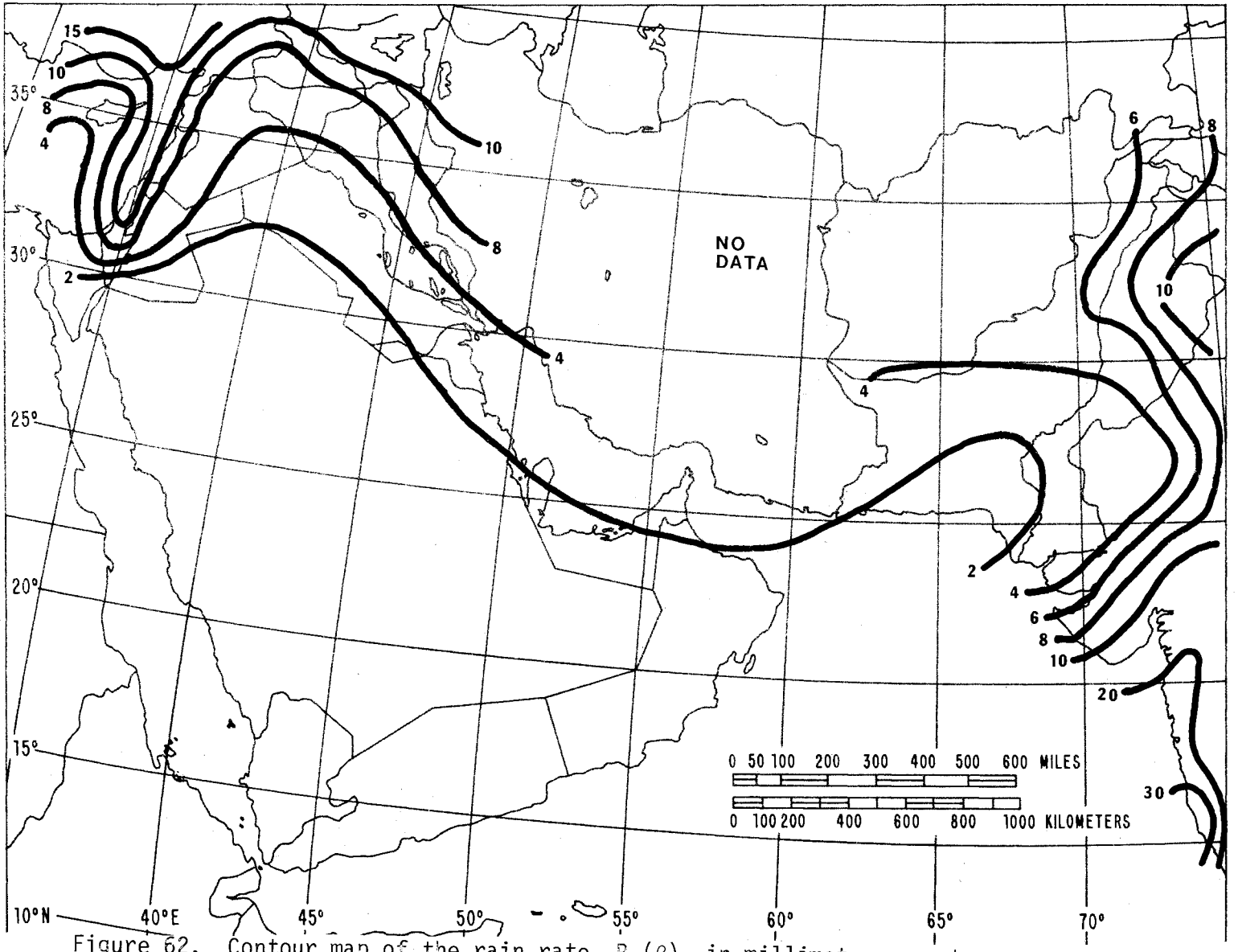

Figure 62. Contour map of the rain rate, $R_1(\beta)$, in millimeters per hour, expected to be exceeded 0.1 percent of an average year and derived using the thunderstorm ratio, β, for Southwest Asia.

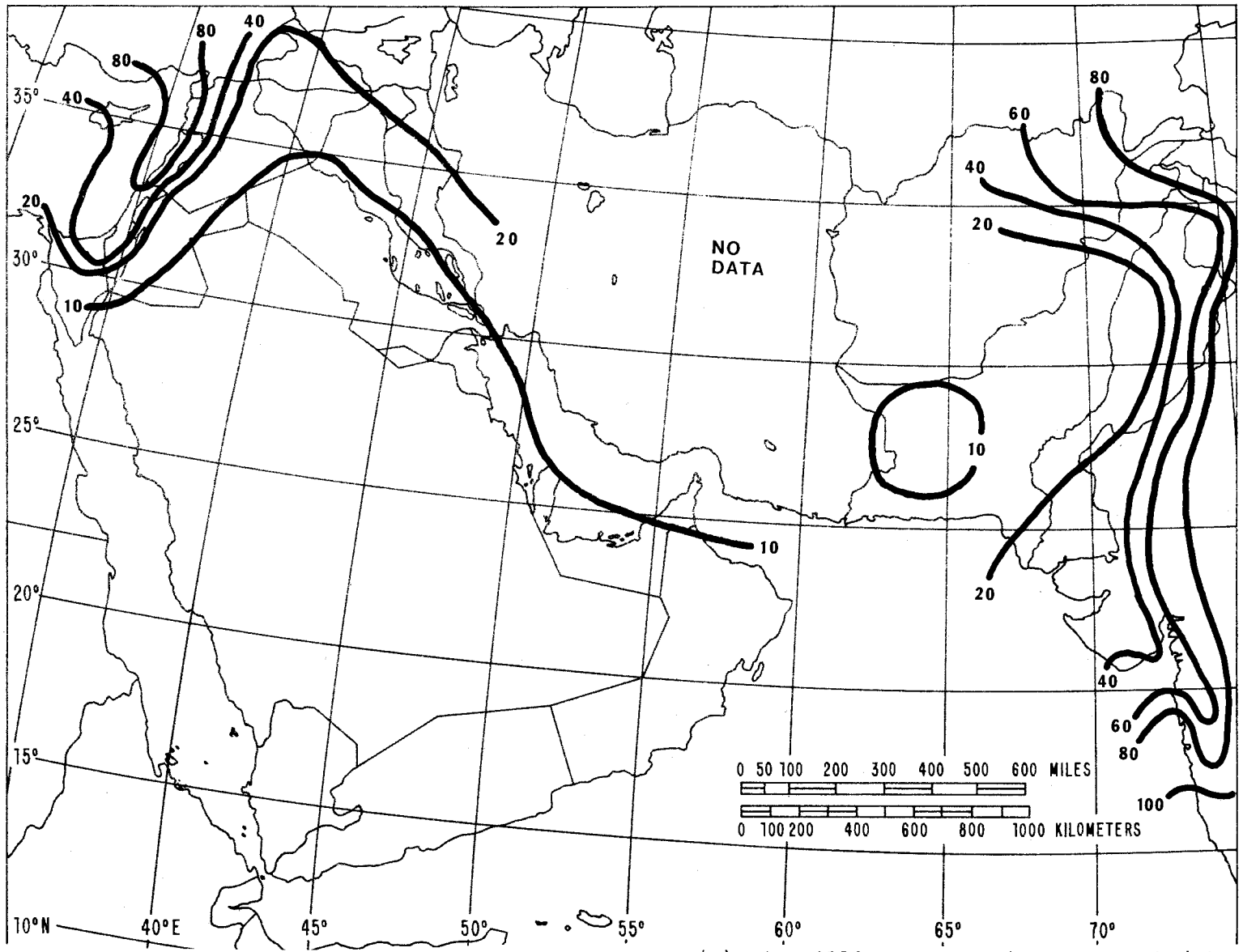

Figure 63. Contour map of the rain rate, $R_{.01}(\beta)$, in millimeters per hour, expected to be exceeded 0.01 percent of an average year and derived using the thunderstorm ratio, β, for Southwest Asia.

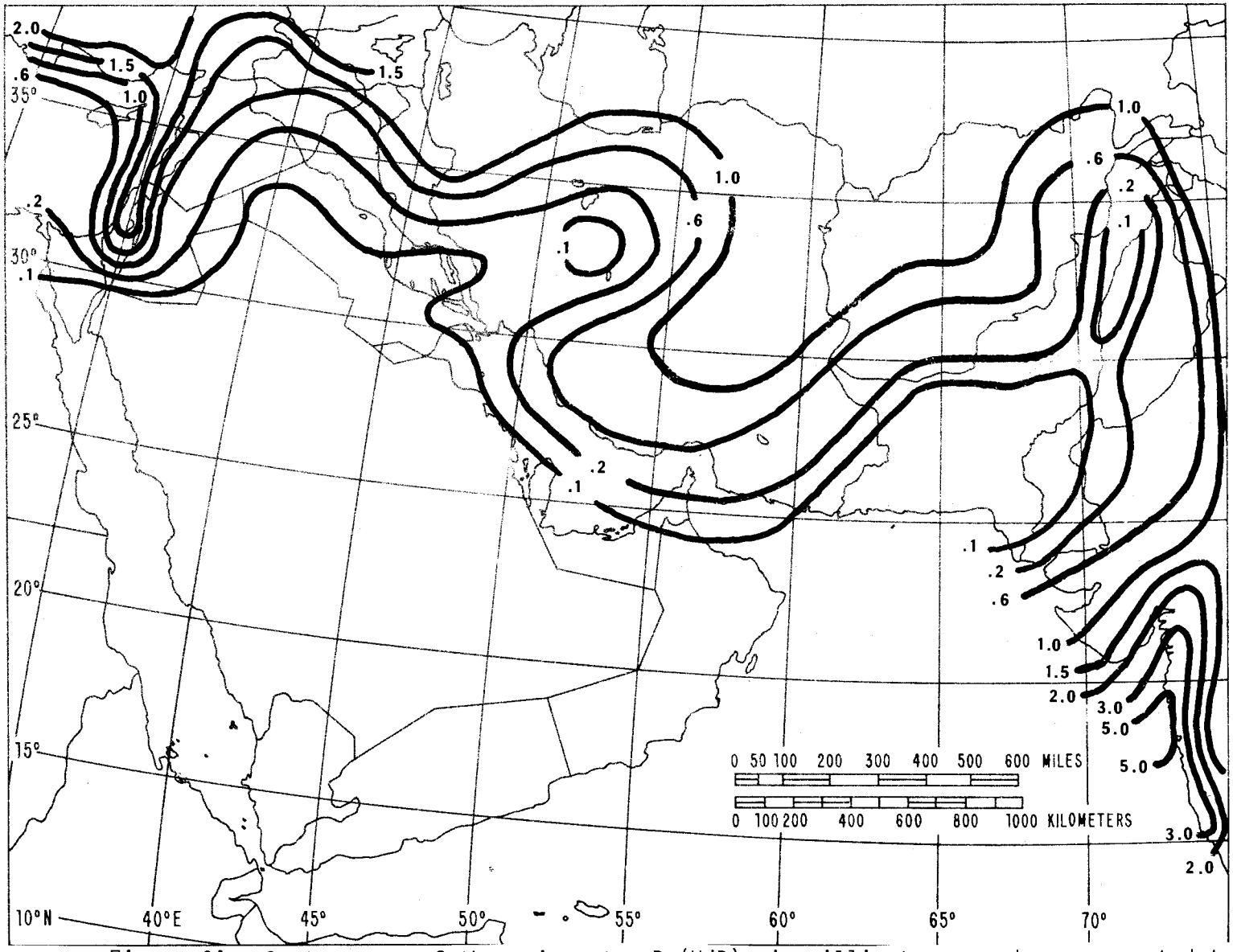

Figure 64. Contour map of the rain rate, $R_1(U/D)$, in millimeters per hour, expected to be exceeded 1 percent of an average year and derived using the thunderstorm ratio, $U/D_{.01}$, for Southwest Asia.

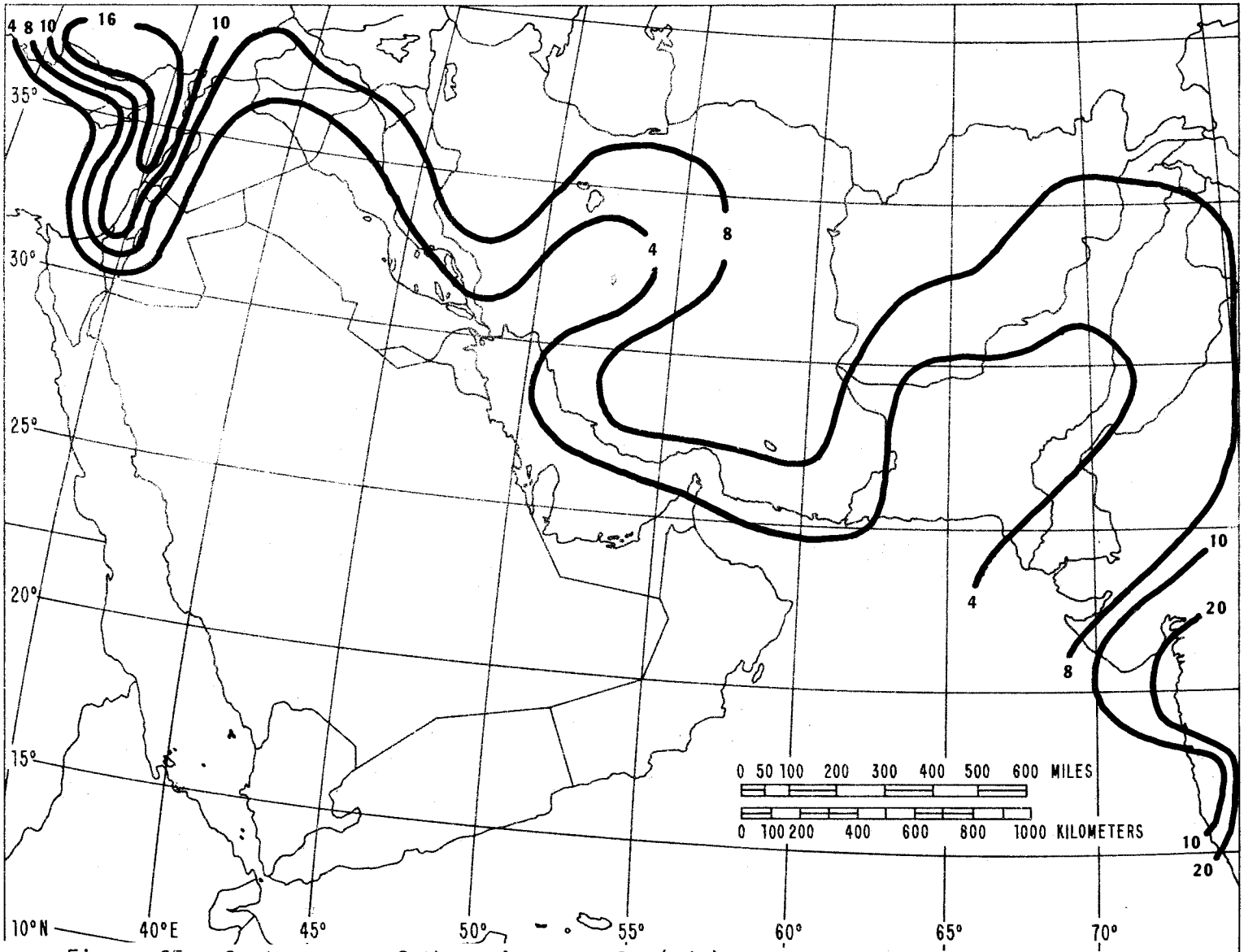

Figure 65. Contour map of the rain rate, $R_{.1}(U/D)$, in millimeters per hour, expected to be exceeded 0.1 percent of an average year and derived using the thunderstorm ratio, $U/D_{.01}$, for Southwest Asia.

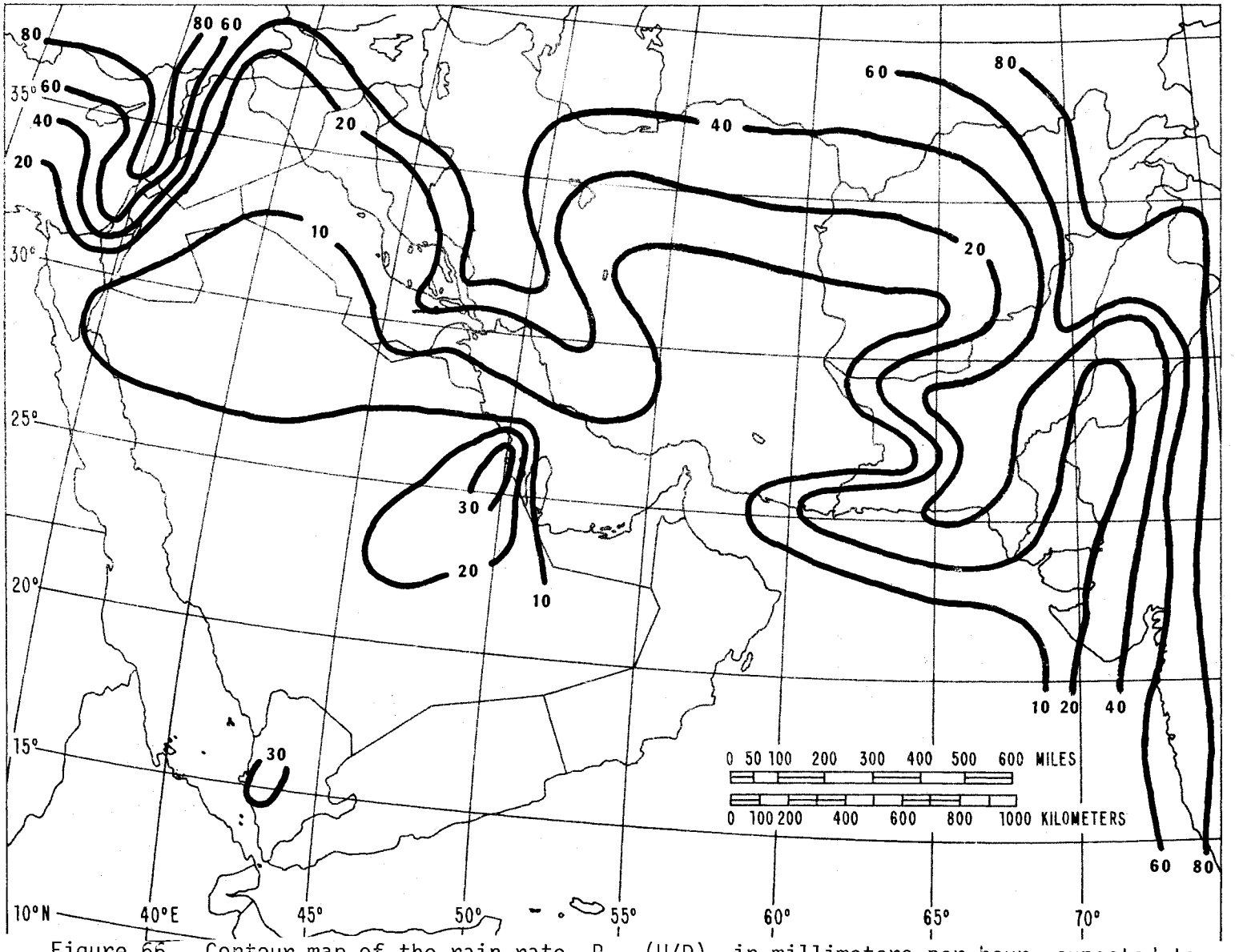

Figure 66. Contour map of the rain rate, $R_{.01}(U/D)$, in millimeters per hour, expected to be exceeded 0.01 percent of an average year and derived using the thunderstorm ratio, $U/D_{.01}$, for Southwest Asia.

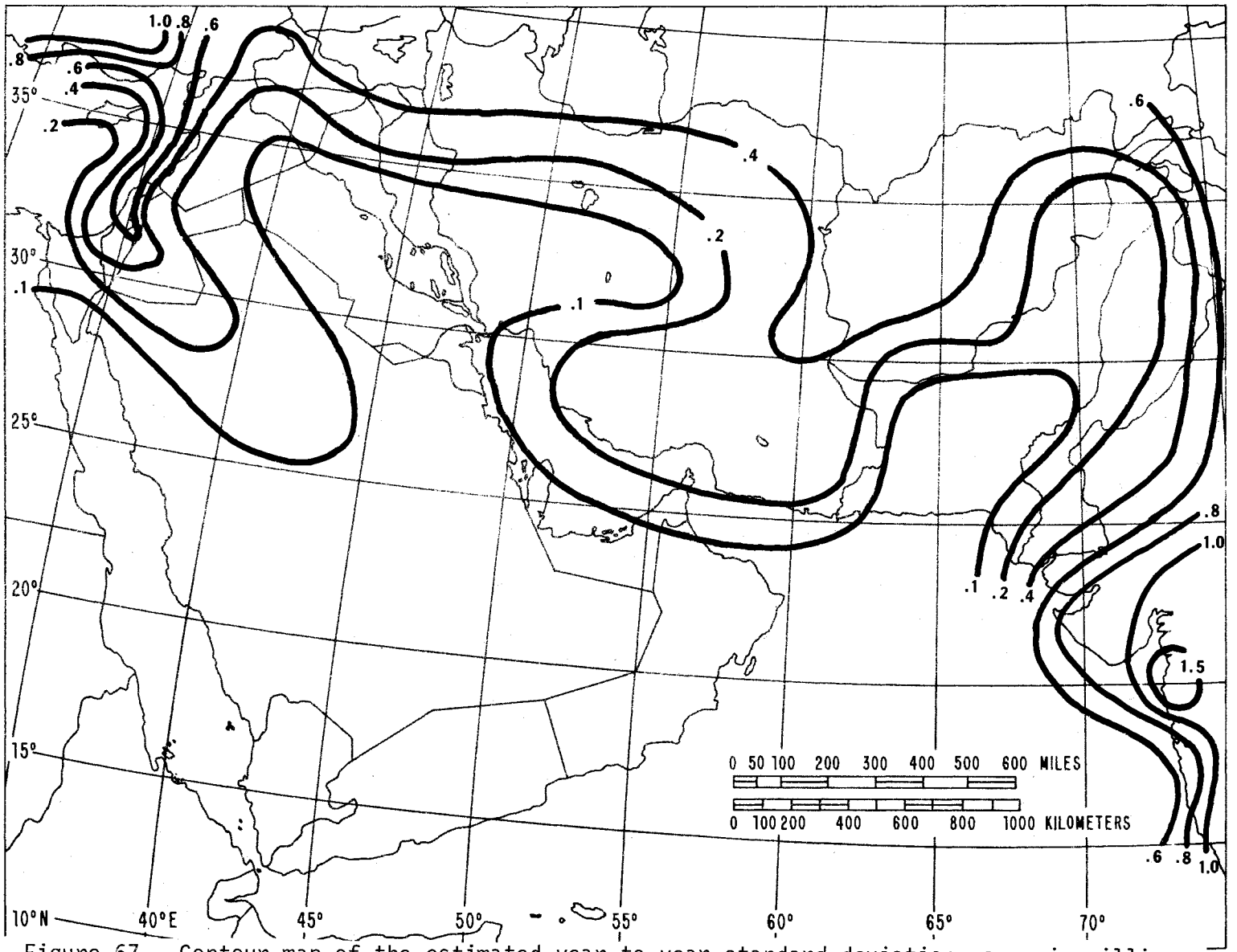

Figure 67. Contour map of the estimated year-to-year standard deviation, s_{R_1}, in millimeters per hour, of rain rate expected at the 1 percent exceedance level for Southwest Asia.

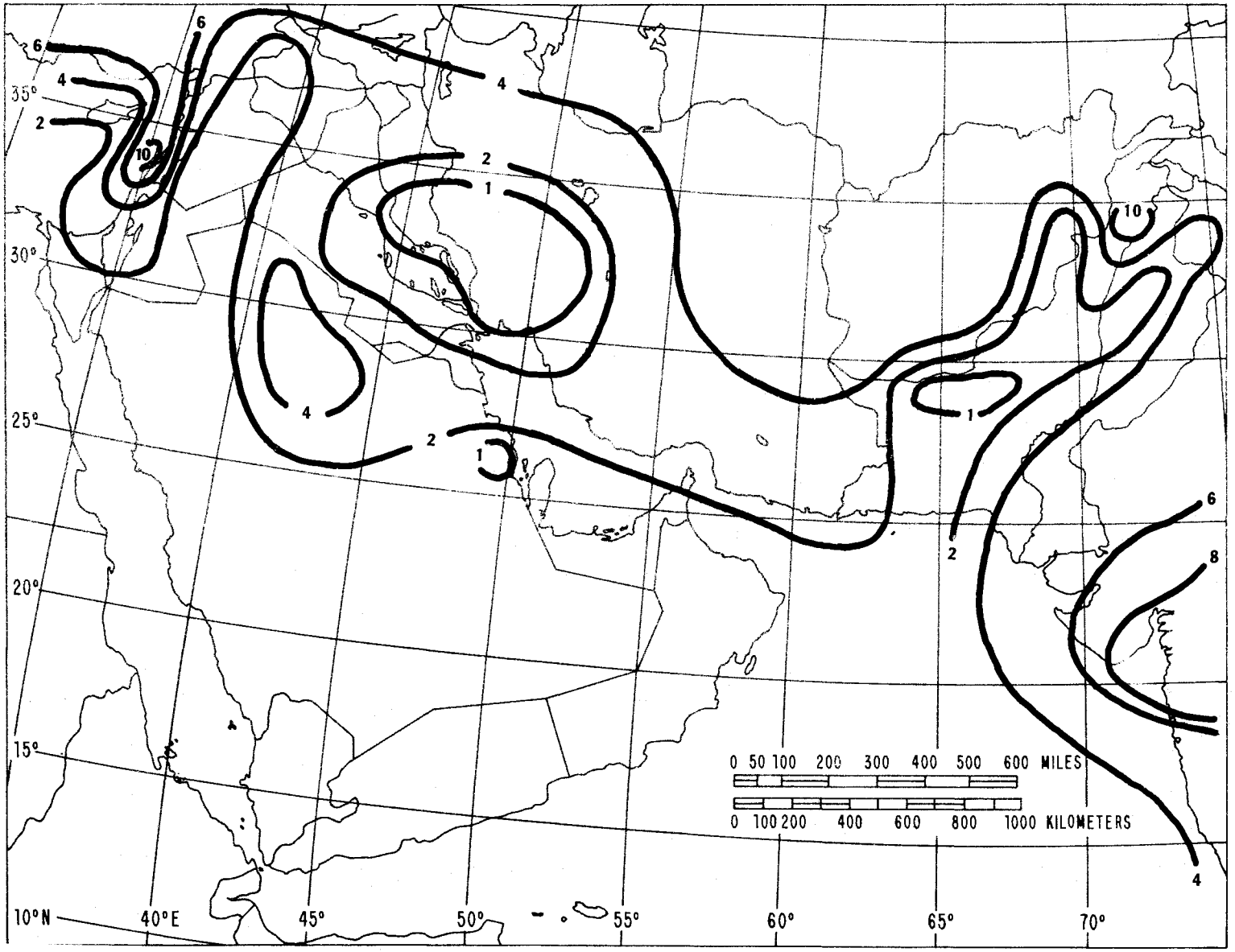

Figure 63. Contour map of the estimated year-to-year standard deviation, $s_{R_{.1}}$, in millimeters per hour, of rain rate expected at the 0.1 percent exceedance level for Southwest Asia.

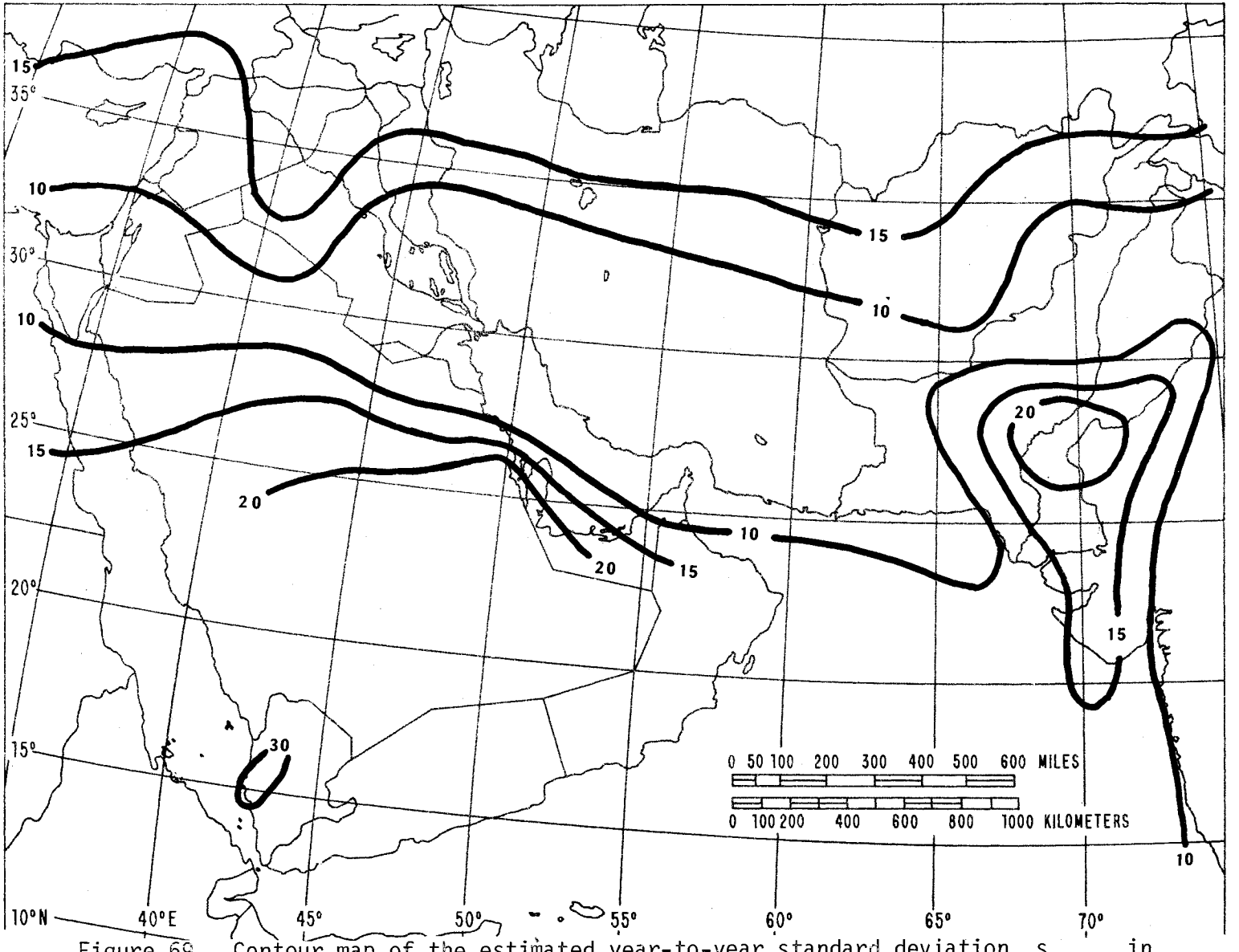

Figure 69. Contour map of the estimated year-to-year standard deviation, $s_{R_{.01}}$, in millimeters per hour, of rain rate expected at the 0.01 percent exceedance level for Southwest Asia.

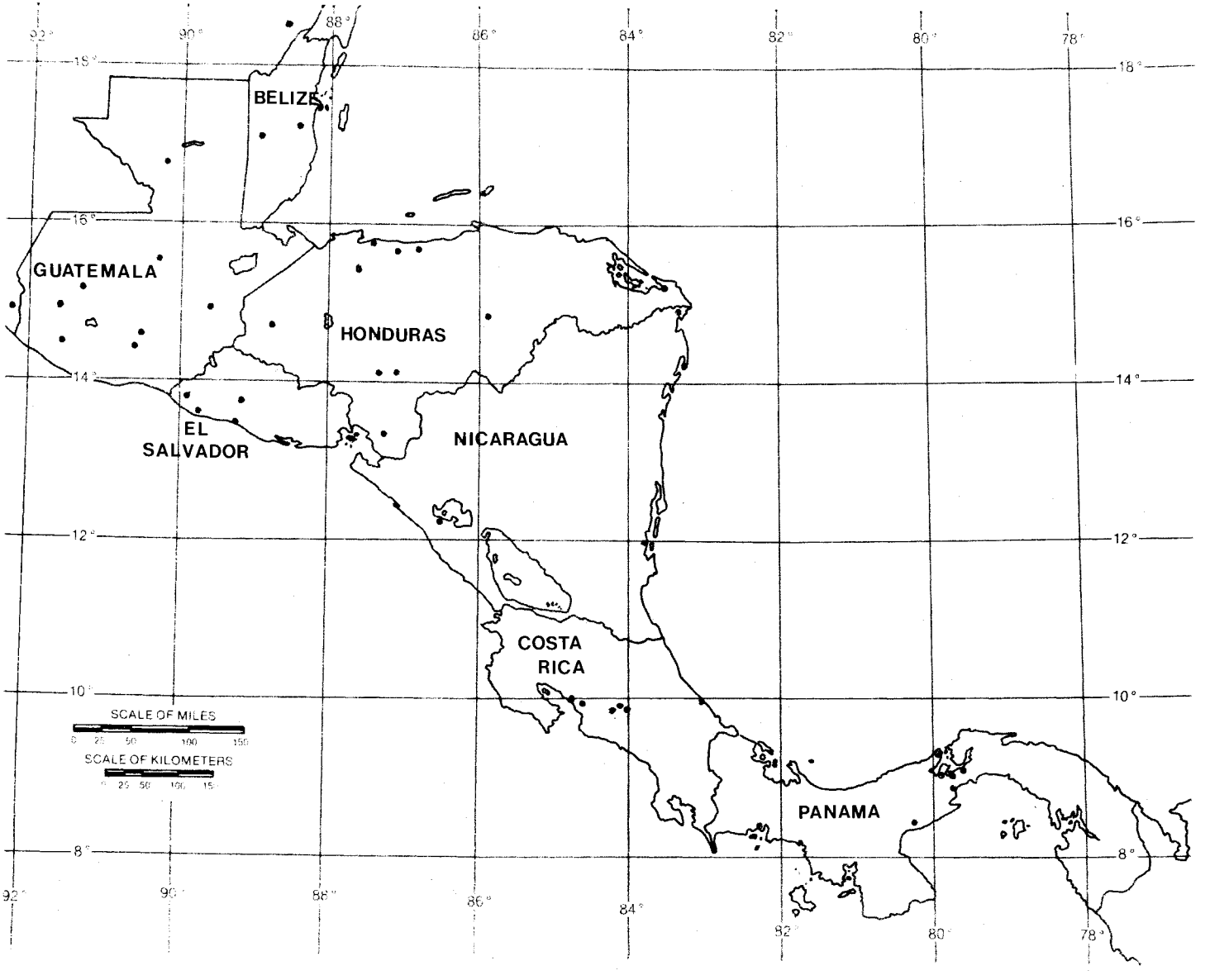

Figure 70. Map of data locations in Central America.

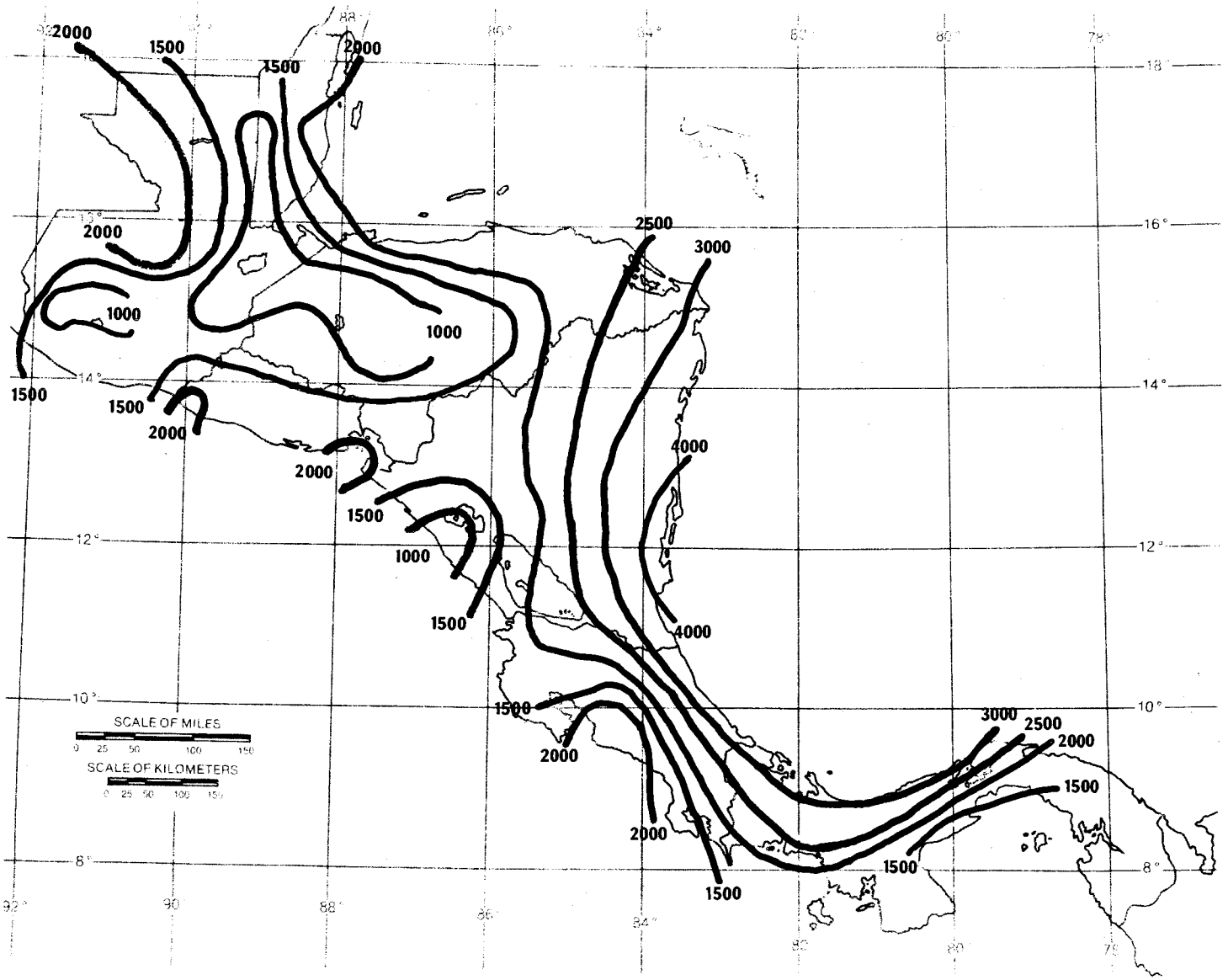

Figure 71. Contour map of the average annual precipitation, M, in millimeters, for Central America.

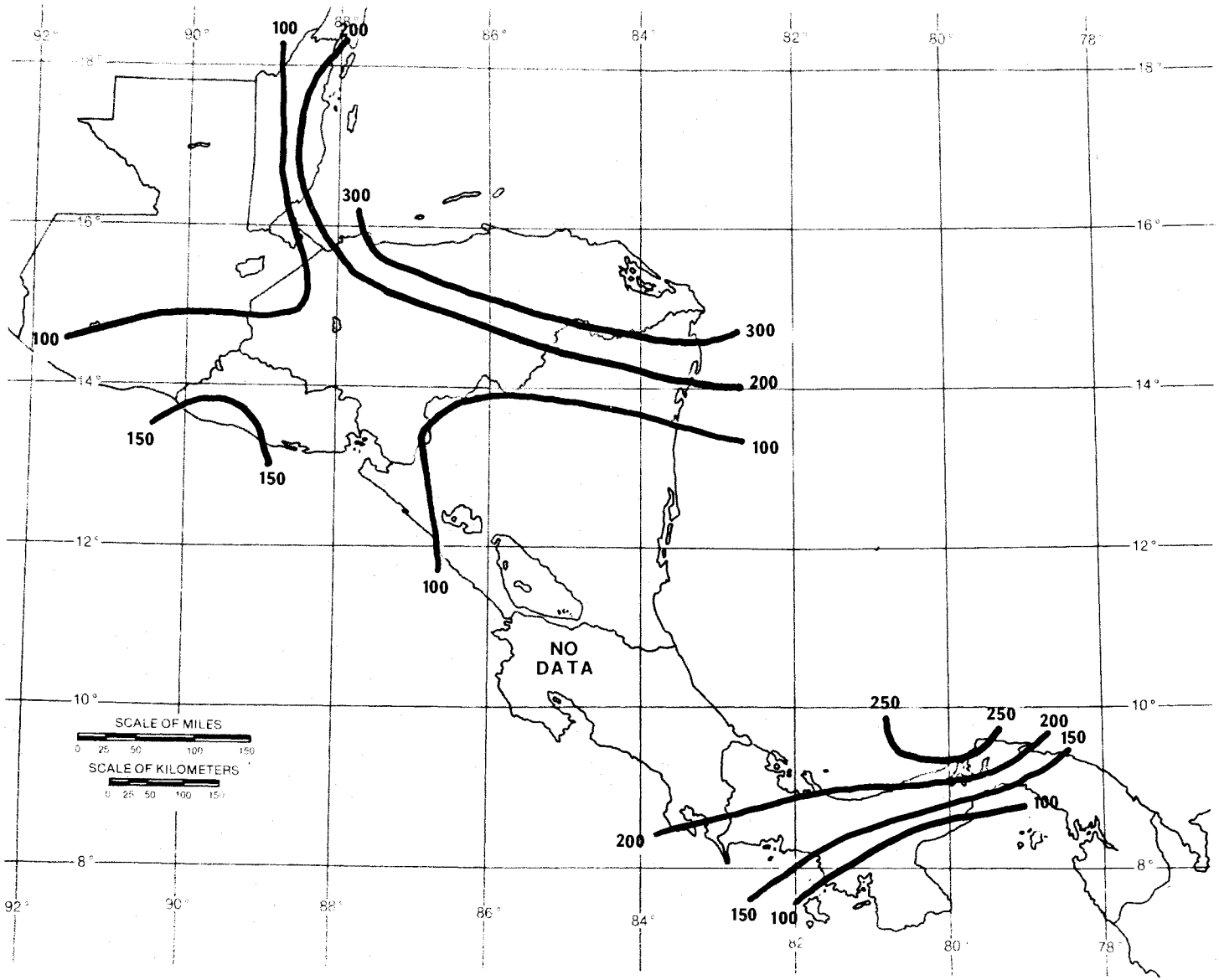

Figure 72. Contour map of the average annual number of days, $D_{.01}$, with precipitation greater than .01 in., for Central America.

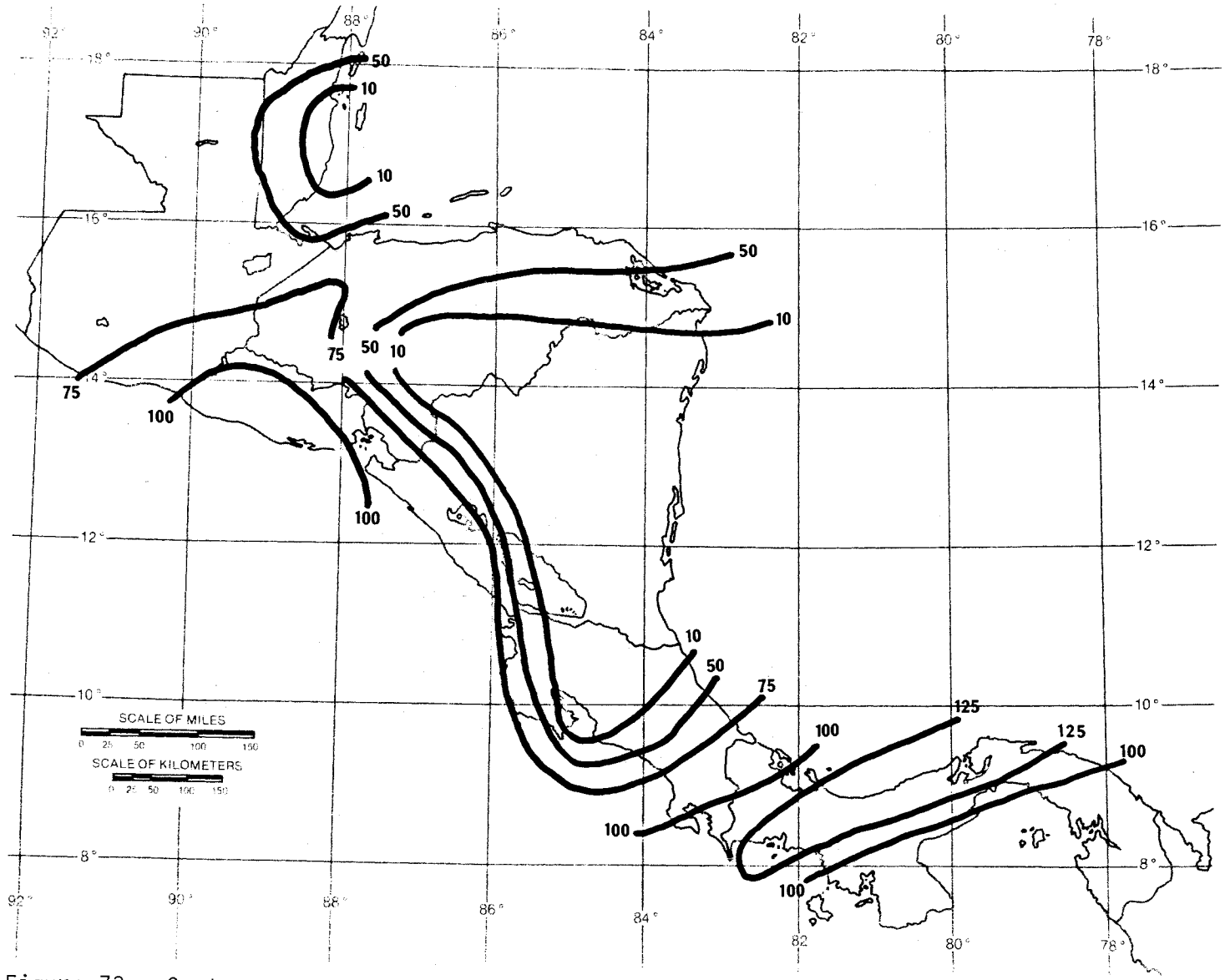

Figure 73. Contour map of the average annual number of days, U, with thunderstorms for Central America.

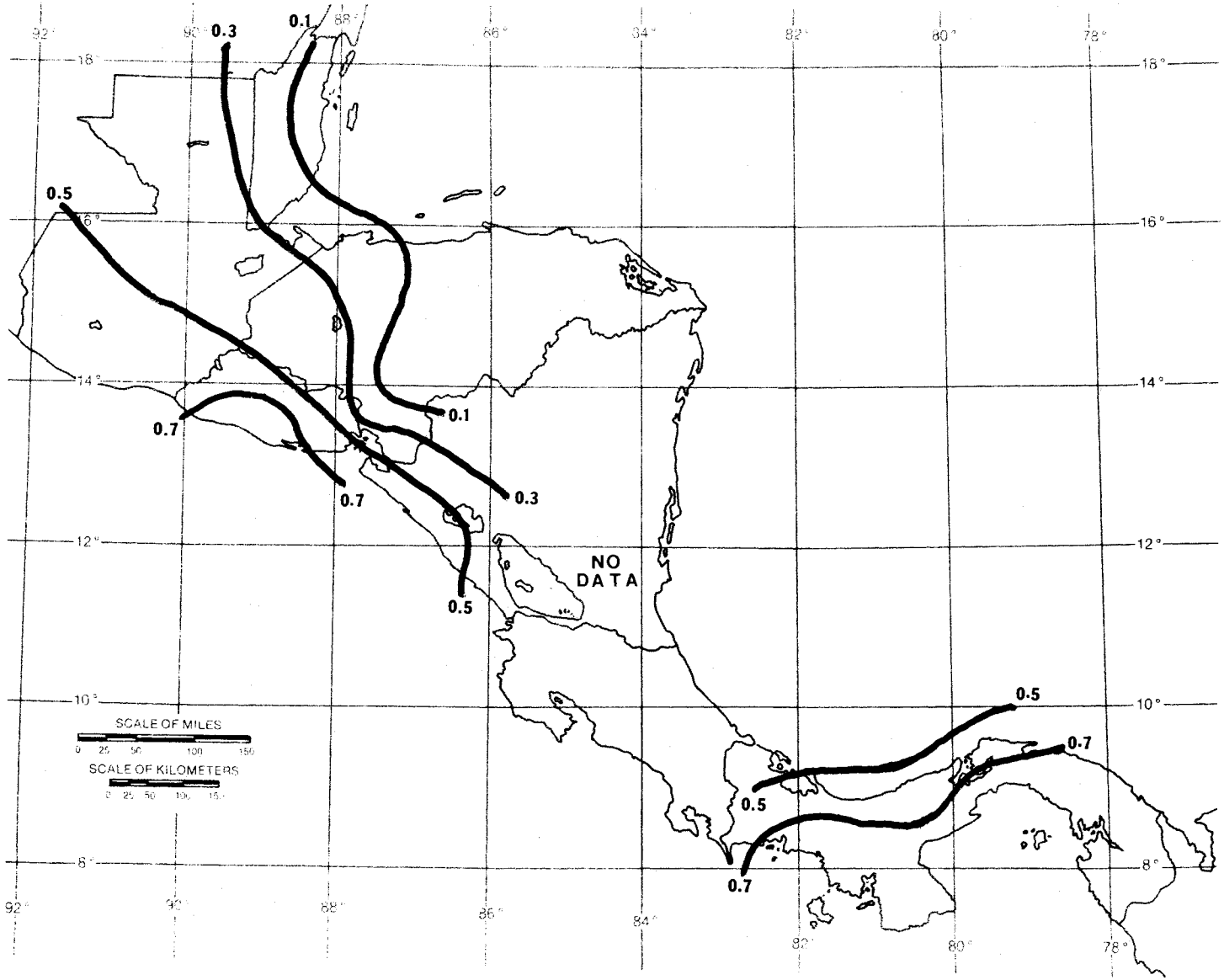

Figure 74. Contour map of the thunderstorm ratio, $U/D_{.01}$, for Central America.

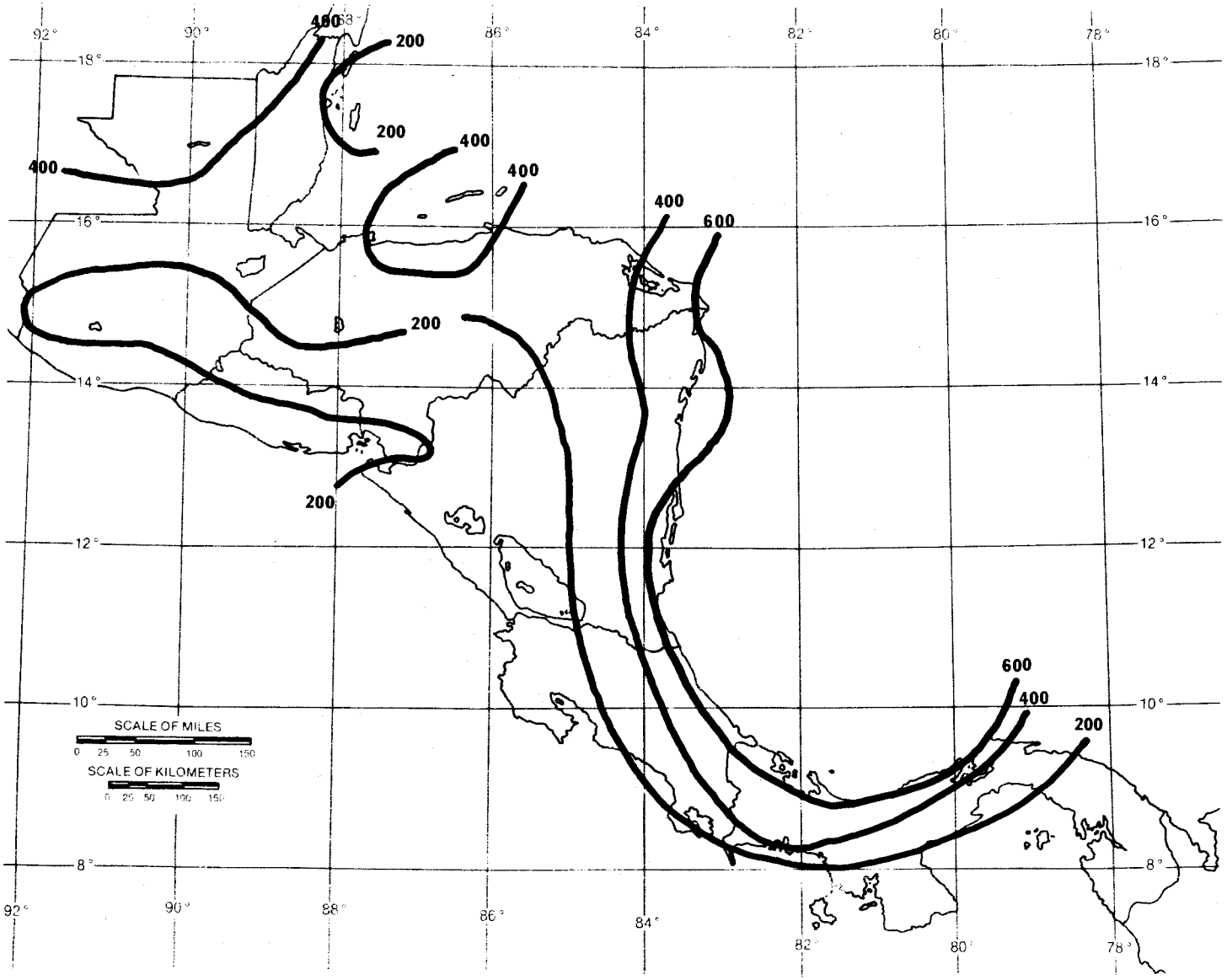

Figure 75. Contour map of the year-to-year standard deviation, s_M, in millimeters, of total annual precipitation for Central America.

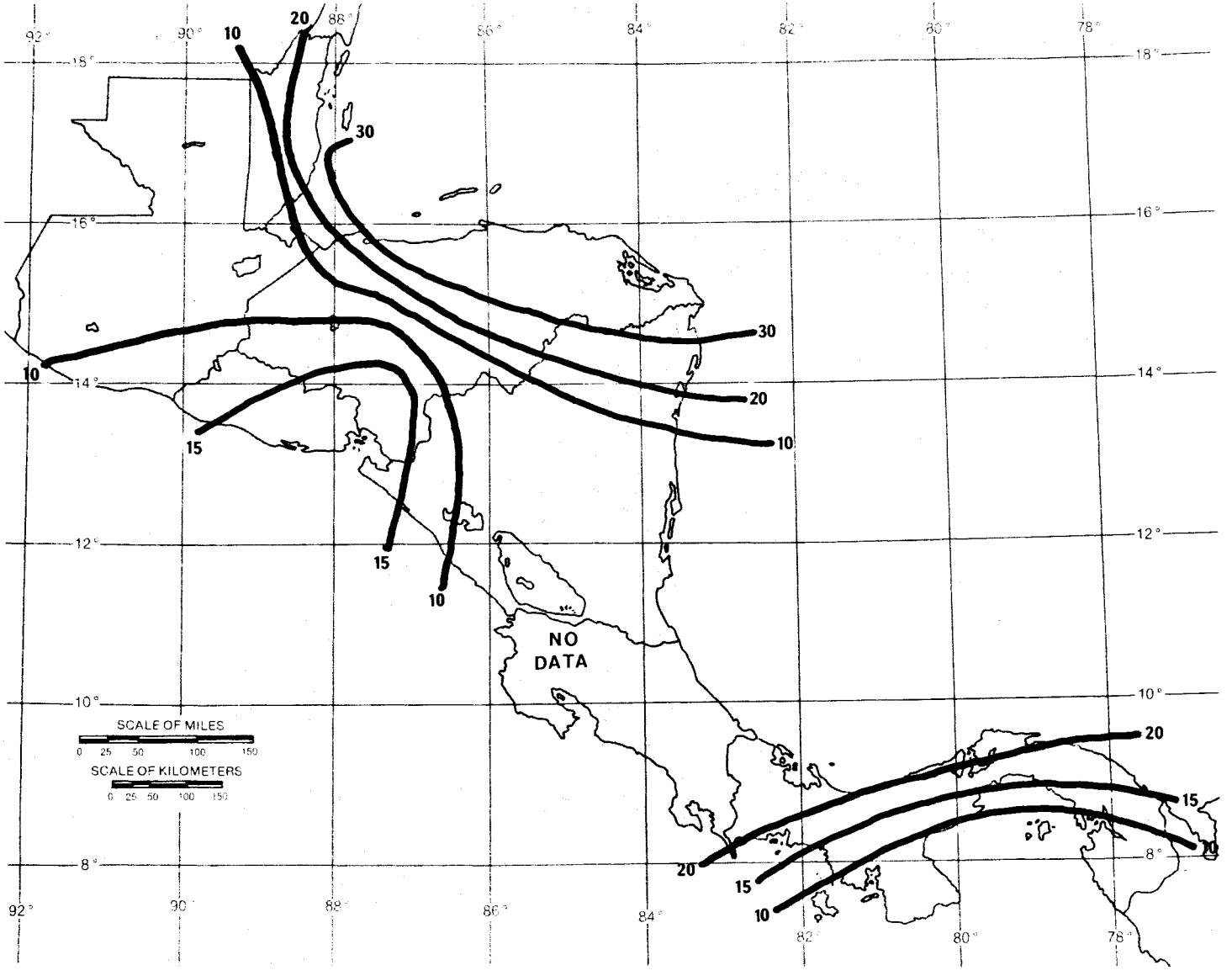

Figure 76. Contour map of the year-to-year standard deviation, s_D, of the annual number of days with precipitation greater than .01 inch, for Central America.

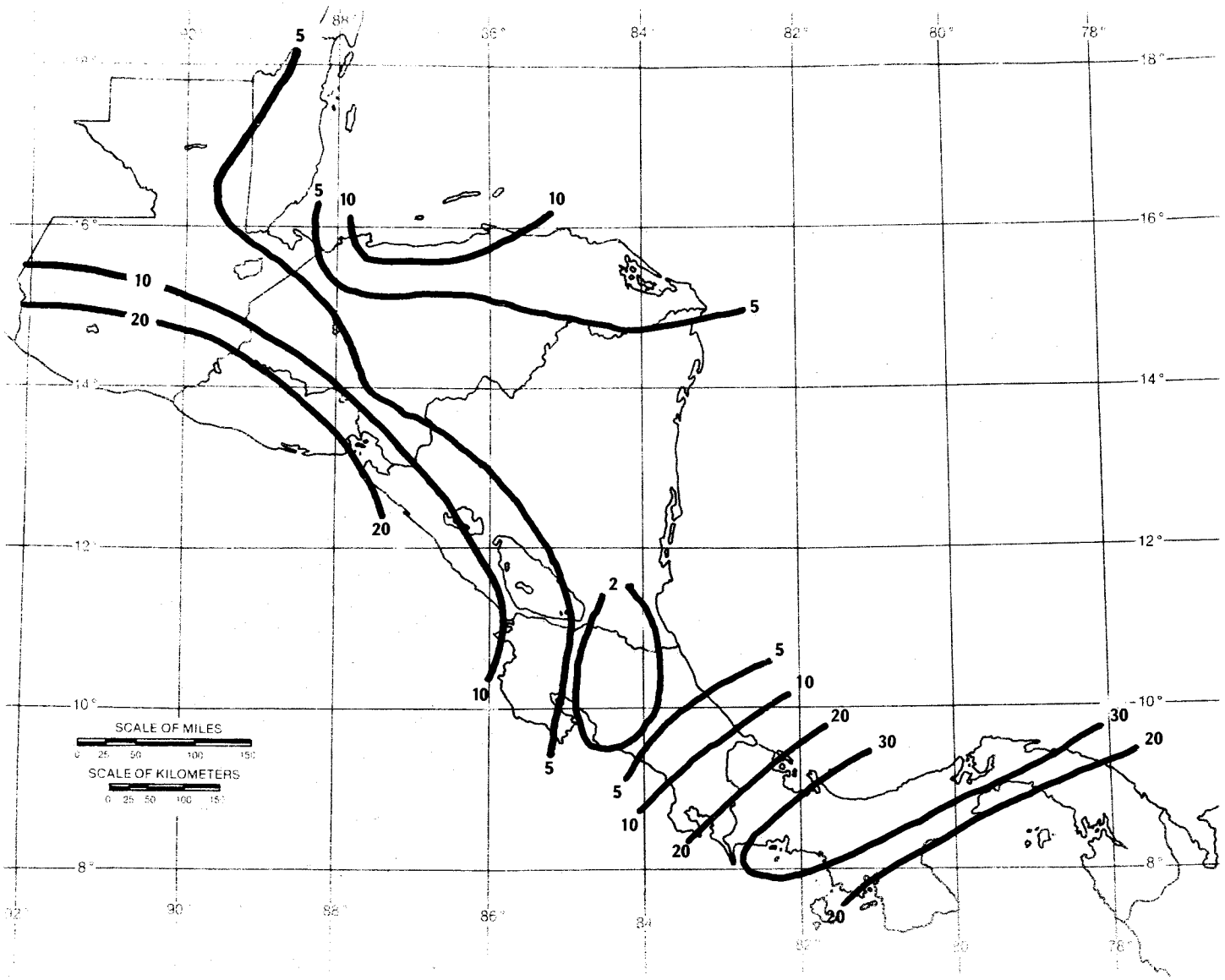

Figure 77. Contour map of the year-to-year standard deviation, s_U, of the annual number of days with thunderstorms for Central America.

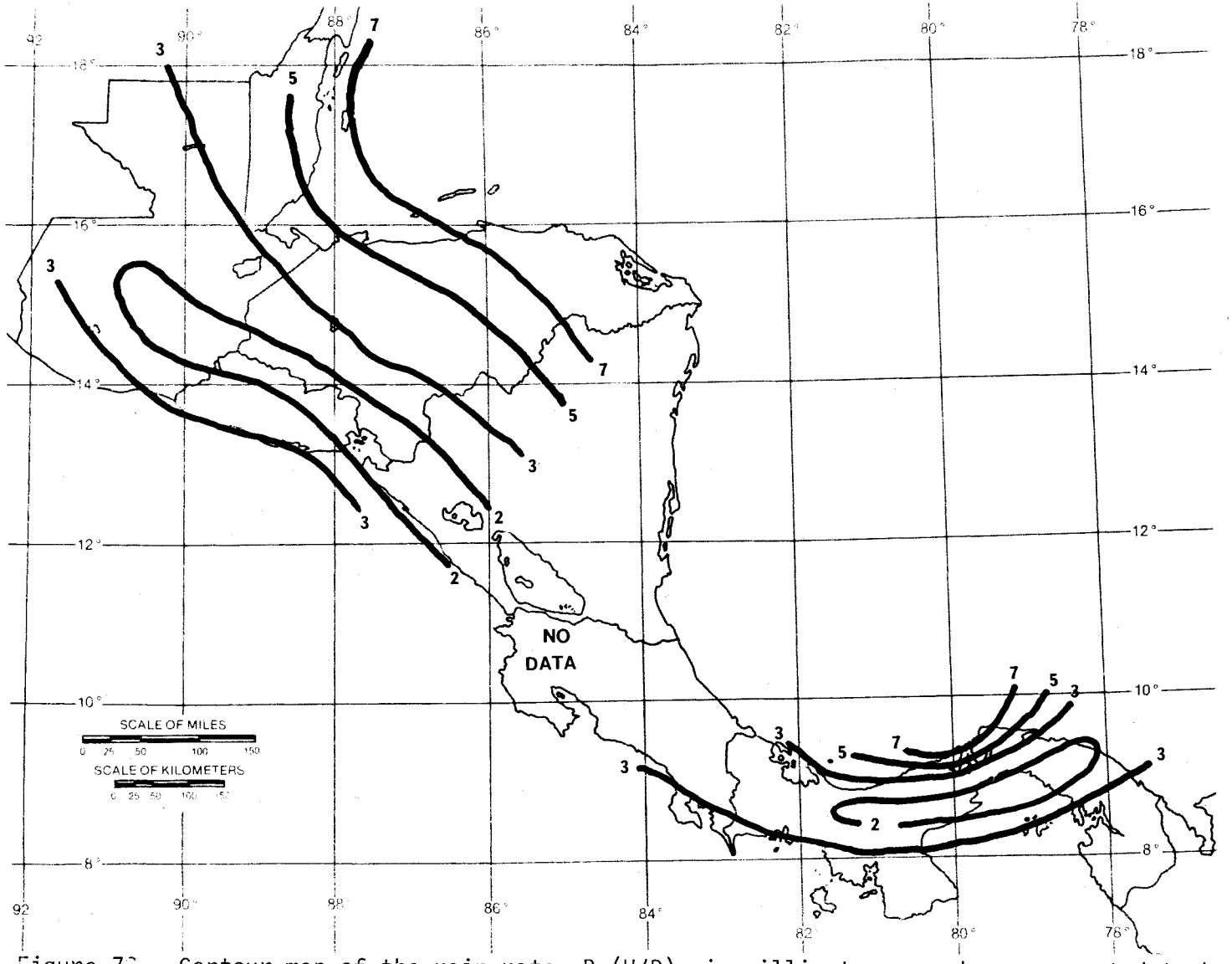

Figure 73. Contour map of the rain rate, $R_{.01}$(U/D), in millimeters per hour, expected to be exceeded 1 percent of an average year and derived using the thunderstorm ratio, $U/D_{.01}$, for Central America.

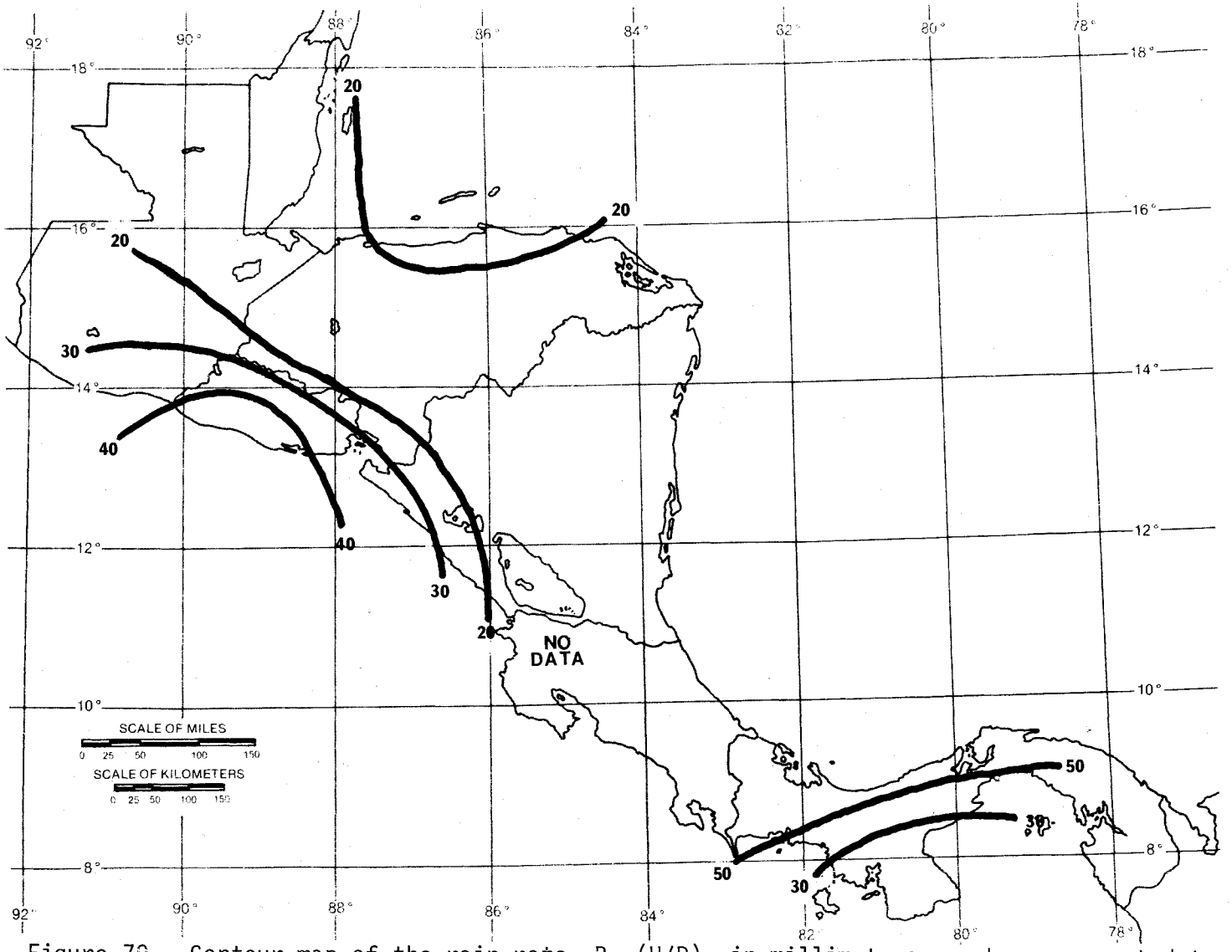

Figure 79. Contour map of the rain rate, $R_{.1}(U/D)$, in millimeters per hour, expected to be exceeded 0.1 percent of an average year and derived using the thunderstorm ratio, $U/D_{.01}$ for Central America.

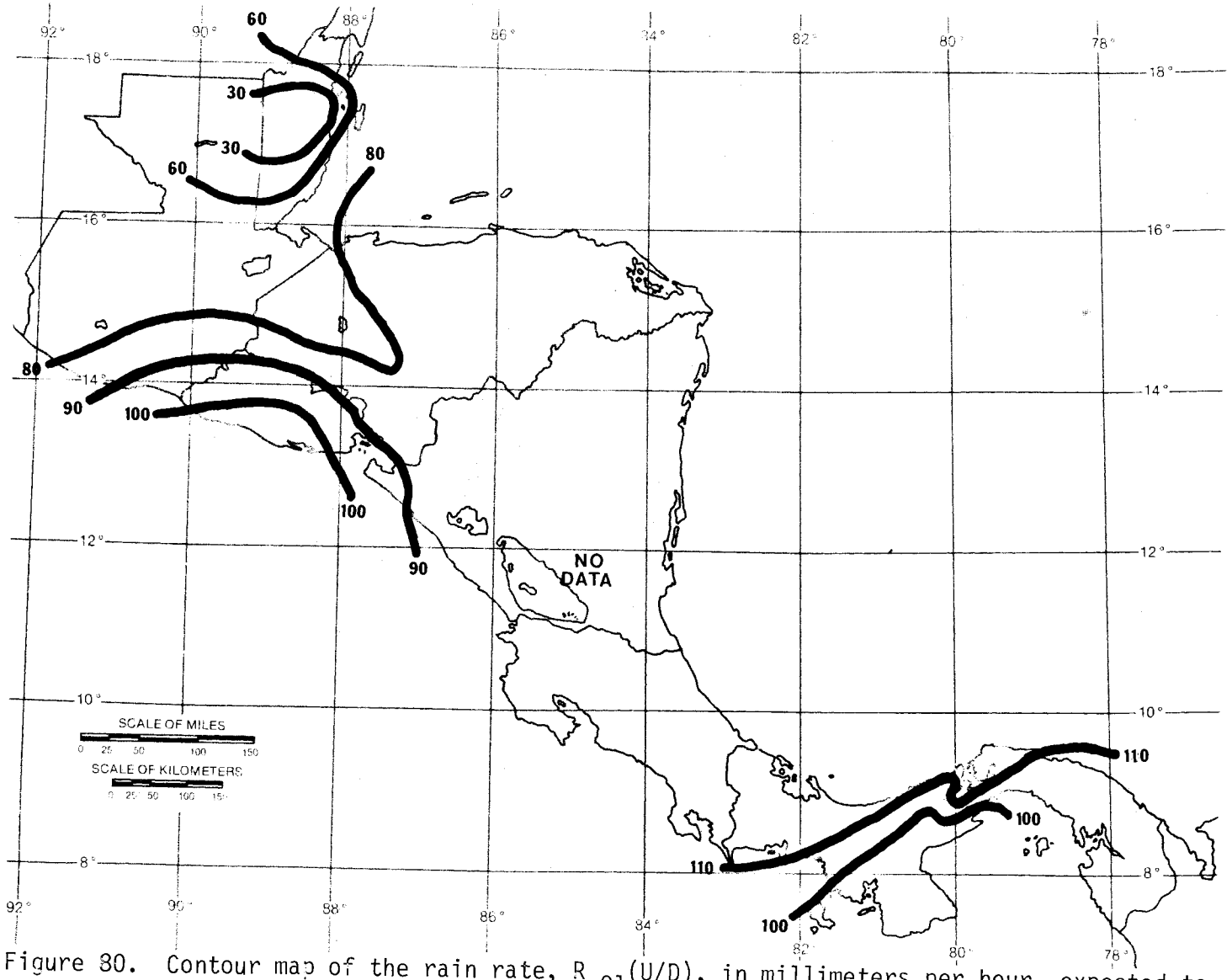

Figure 80. Contour map of the rain rate, $R_{.01}(U/D)$, in millimeters per hour, expected to be exceeded 0.01 percent of an average year and derived using the thunderstorm ratio, $U/D_{.01}$, for Central America.

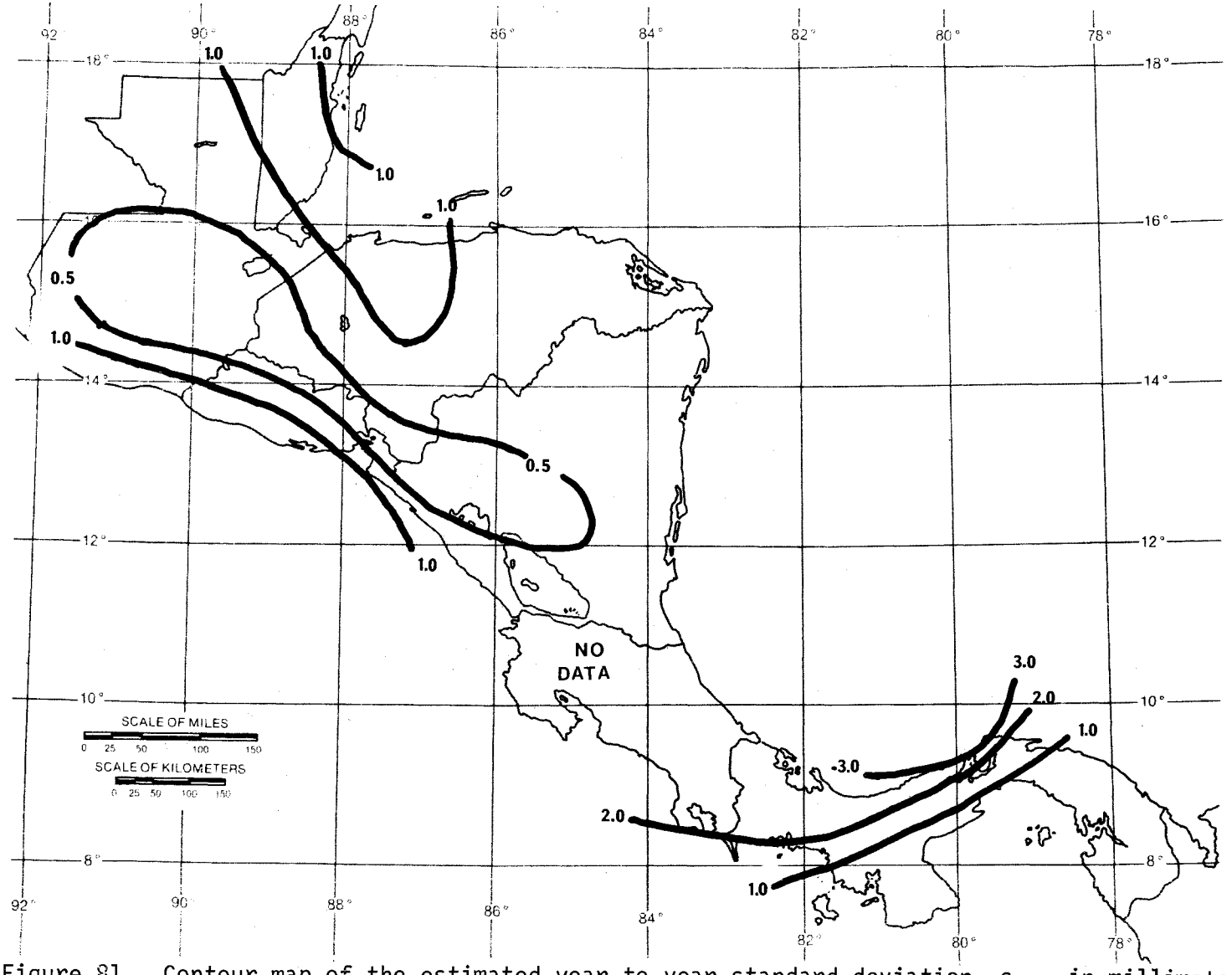

Figure 81. Contour map of the estimated year-to-year standard deviation, s_{R_1}, in millimeters per hour, of rain rate expected at the 1 percent exceedance level for Central America.

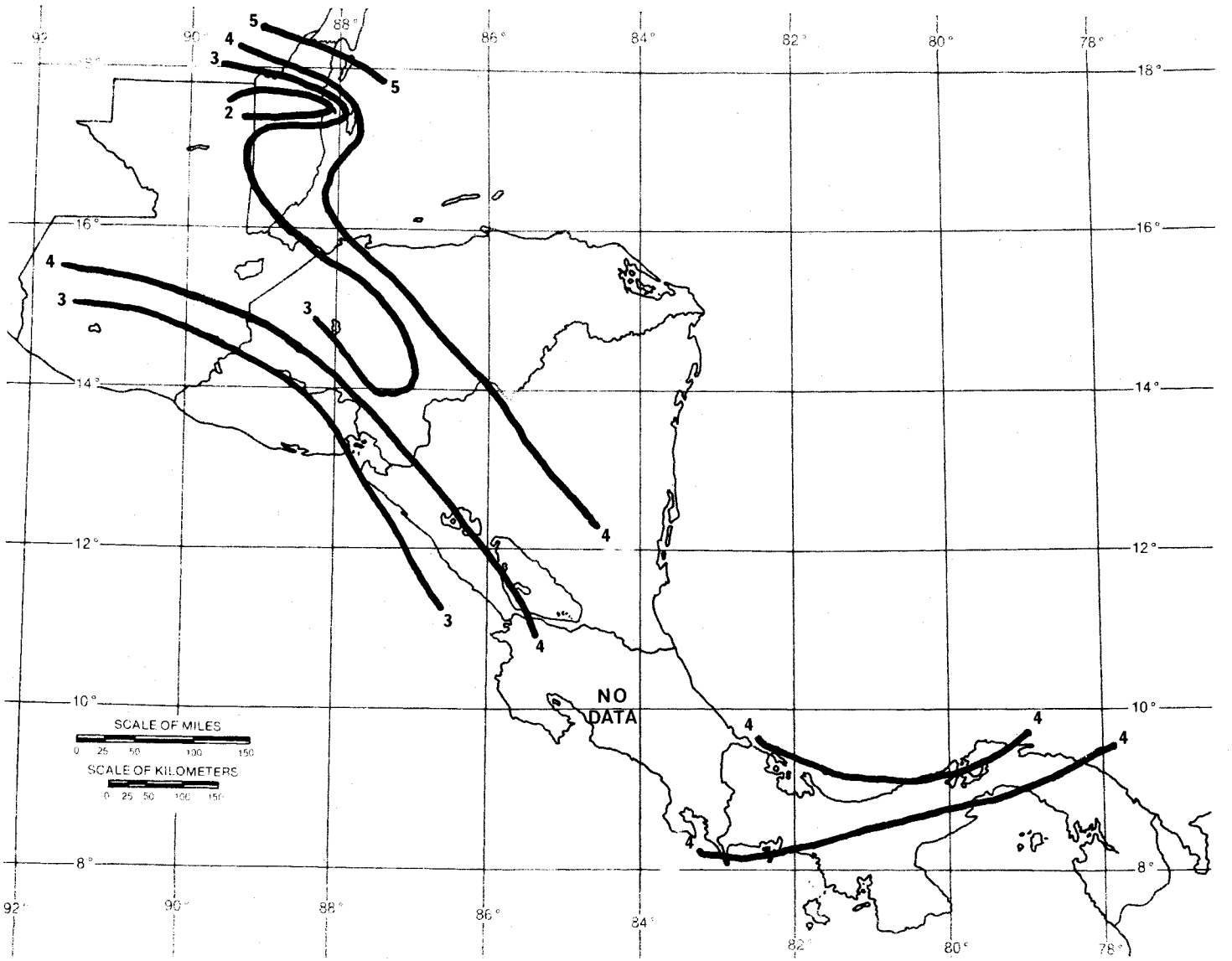

Figure 32. Contour map of the estimated year-to-year standard deviation, s_{R_1}, in millimeters per hour, of rain expected at the 0.1 percent exceedance level for Central America.

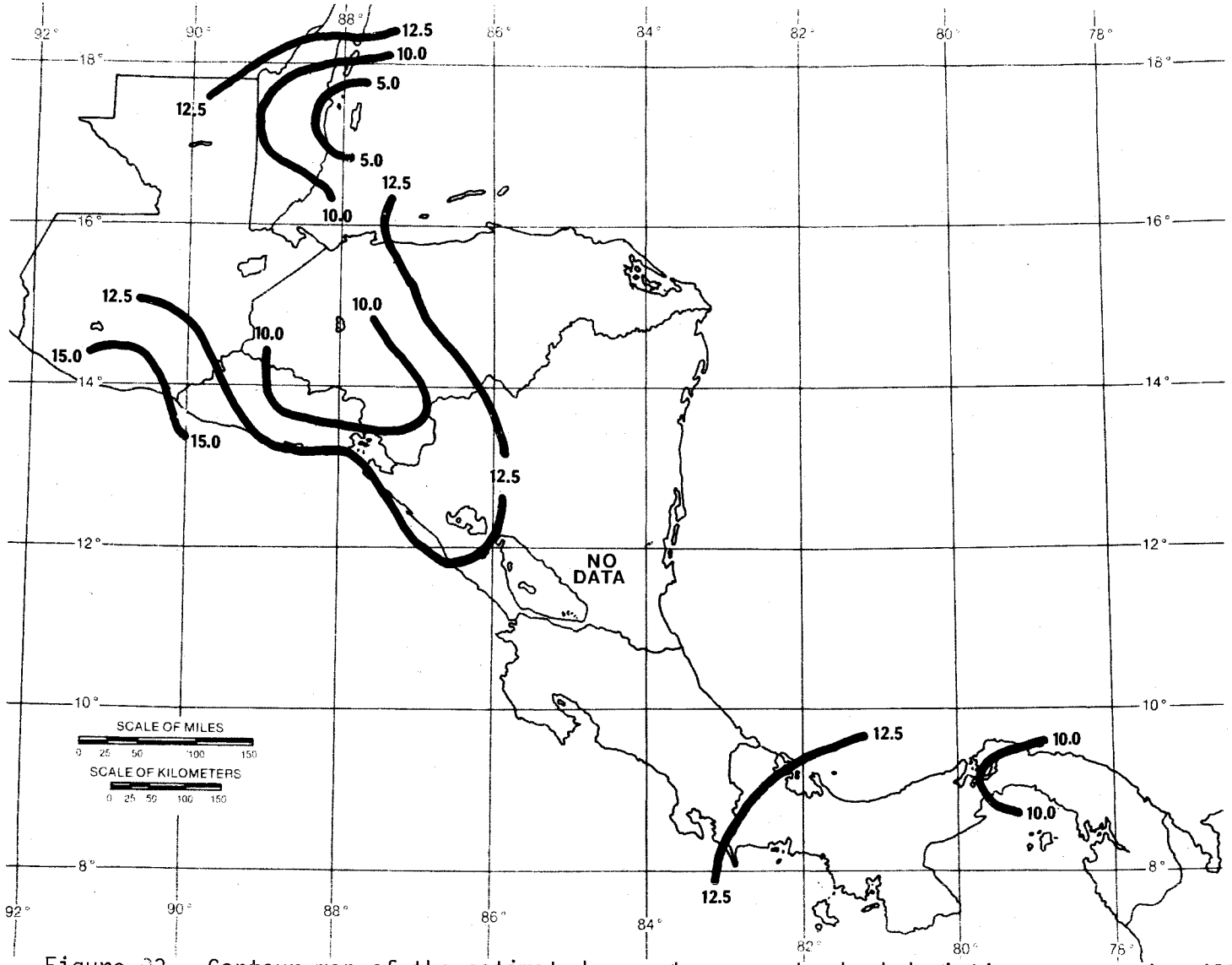

Figure 33. Contour map of the estimated year-to-year standard deviation, $s_{R_{.01}}$, in millimeters per hour, of the rain rate expected at the 0.01 exceedance level for Central America.

β, and obtain an alternative set of maps for the various rain rates (Figures 78 to 80) and their year-to-year standard deviations (Figures 81 to 83). As in previous cases, the values of $D_{.01}$, s_D, and s_U were estimated from (19) through (21). These results were based on the conclusion that most of Central America is represented by Köppen (1918) zone A, with some of the interior portions represented by zone C.

3.6 The United States of America

The United States of America (USA), as discussed herein, consists of the conterminous ("lower 48") United States, or CONUS, Alaska, and Hawaii. A good deal more usable data are available for the USA. As a matter of fact, all of the 18 parameters discussed in Section 3 are directly available, and do not need to be estimated from formulations such as (19) through (21). An earlier report (Dutton, 1977b) presented much of this material, yet all of the maps, with the exception of Figure 88 for M_m, required revision to account for additional data now available.

Figure 84 shows the 304 data locations used for contouring maps in the U.S.A. There are 275 locations in CONUS, 25 locations in Alaska, and 4 locations in Hawaii. Figures 85 through 105 show M, $D_{.01}$, U, M_m, β, $U/D_{.01}$, s_M, s_D, s_U, $R_1(\beta)$, $R_{.1}(\beta)$, $R_{.01}(\beta)$, $R_1(U/D)$, $R_{.1}(U/D)$, $R_{.01}(U/D)$, $s_{R_1}(\beta)$, $s_{R_{.1}}(\beta)$, $s_{R_{.01}}(\beta)$, $s_{R_1}(U/D)$, $s_{R_{.1}}(U/D)$, and $s_{R_{.01}}(U/D)$, in that order. Because of the sufficiency of data in the USA, it is possible to present contour maps of the rain-rate year-to-year standard deviation (s_R's) as derived both from β, Figures 100 through 102, and from $U/D_{.01}$, in Figures 103 through 105.

3.7 Southeast Asia

Southeast Asia, as can be seen from Figure 106, is taken here to include many of the large islands in the Pacific Ocean (Sumatra, Borneo, New Guinea, etc.) now part of Indonesia. In this area of Southeast Asia, usable data are often lacking; as a consequence, many of the contour maps for Southeast Asia contain a "NO DATA" region indicated thereon.

Figure 106 shows the 243 data locations used for the purpose of contouring maps of rain rate prediction parameters, and predicted rain rates and their year-to-year variability in Southeast Asia. Figures 107 through 119 show M, $D_{.01}$, U, $U/D_{.01}$, s_M, s_D, s_U, $R_1(U/D)$, $R_{.1}(U/D)$, $R_{.01}(U/D)$, s_{R_1}, $s_{R_{.1}}$, and $s_{R_{.01}}$, in that order. Once again there were insufficient data from which to prepare maps of M_m,

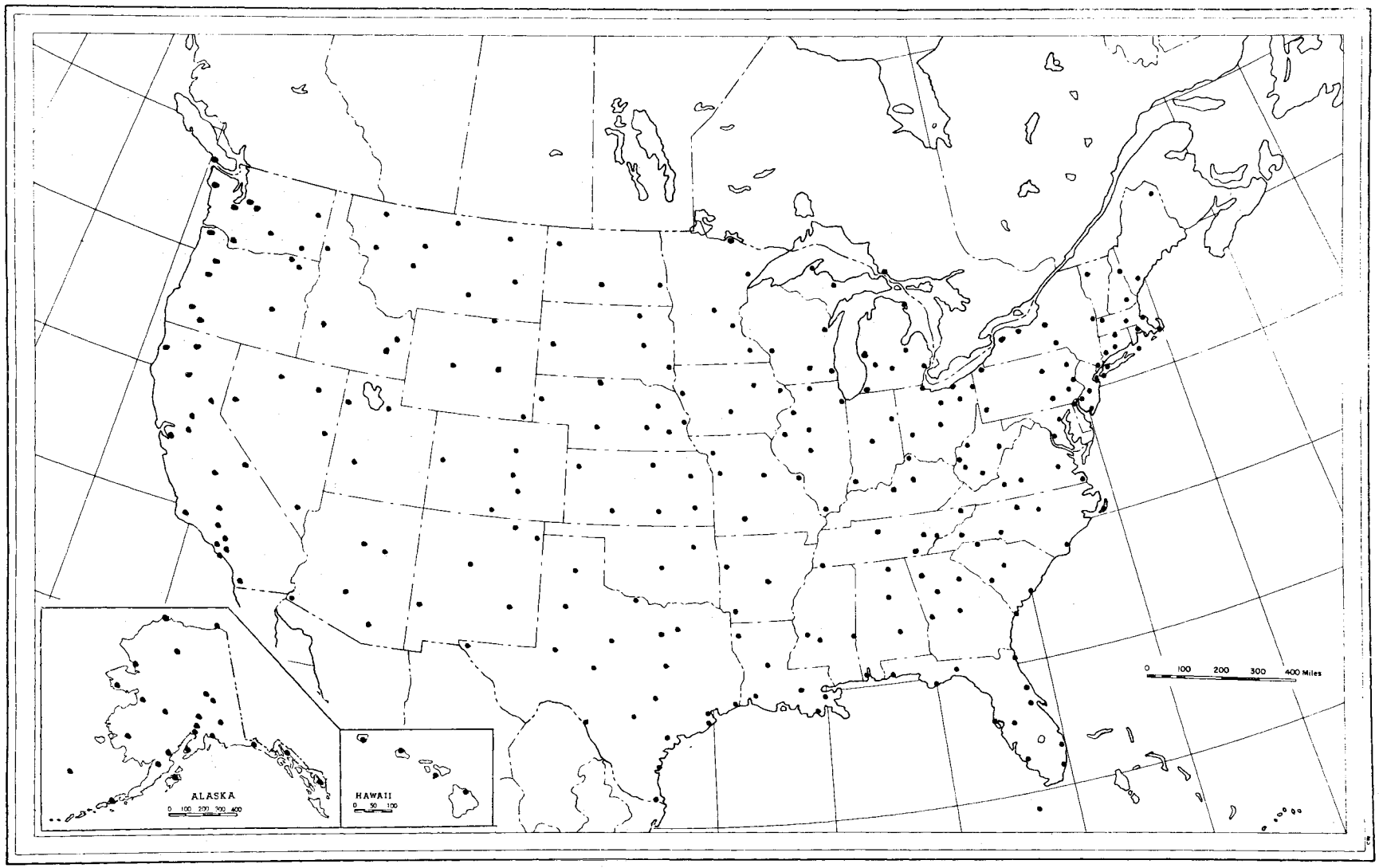

Figure 84. Map of data locations in the United States of America.

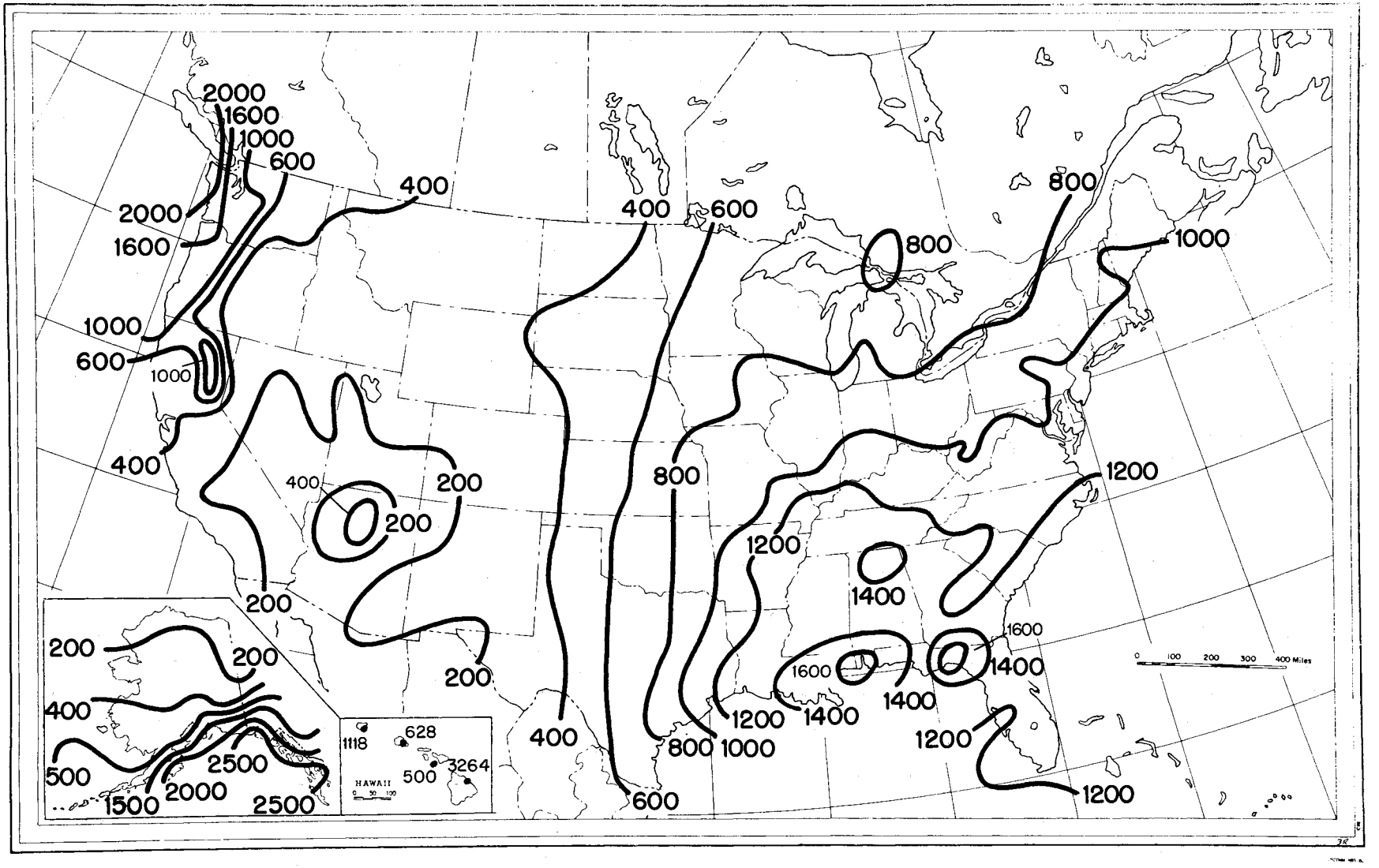

Figure 85. Contour map of the average annual precipitation, M, in millimeters, for the United States of America.

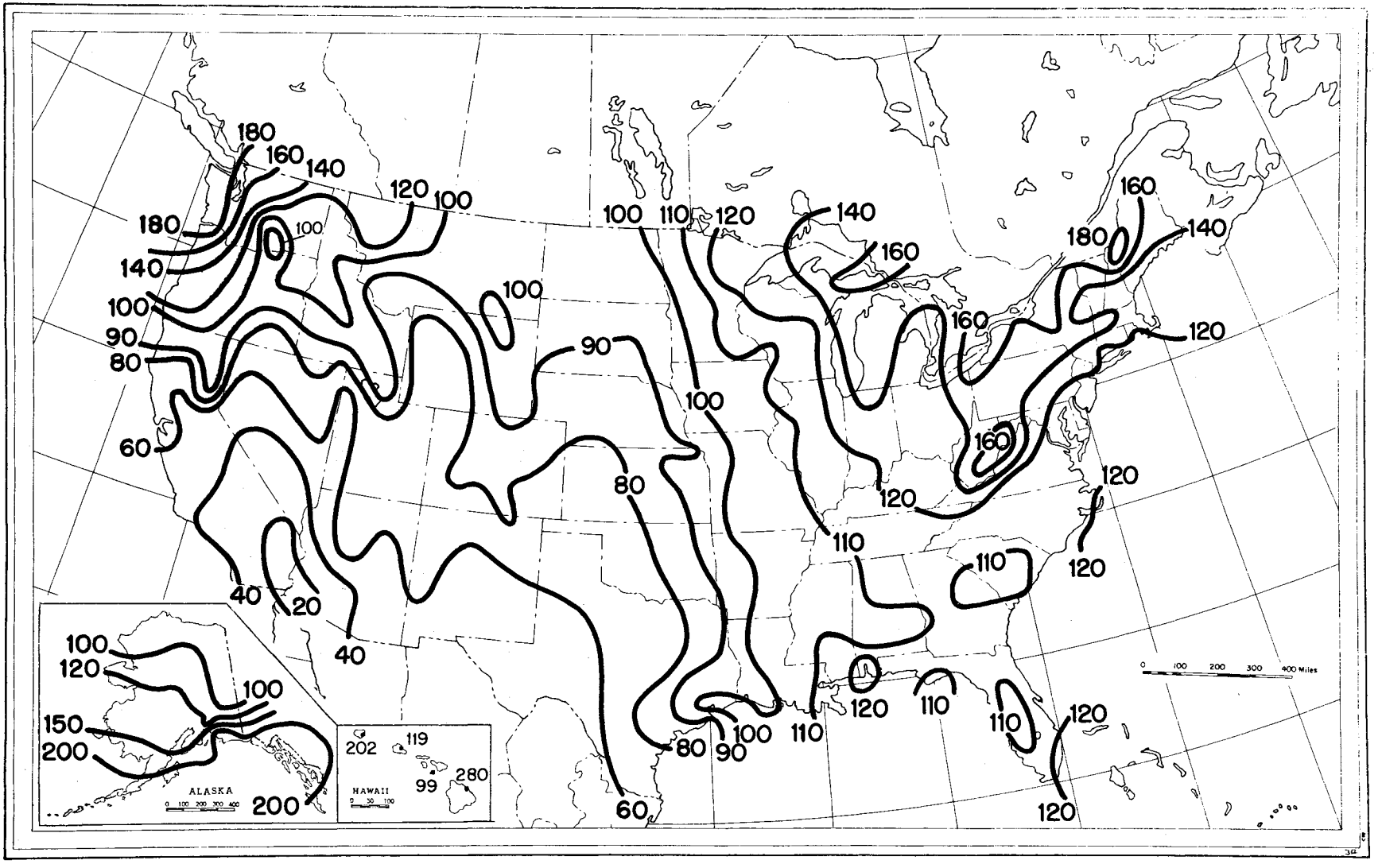

Figure 86. Contour map of the average annual number of days, $D_{.01}$, with precipitation greater than .01 in., for the United States of America.

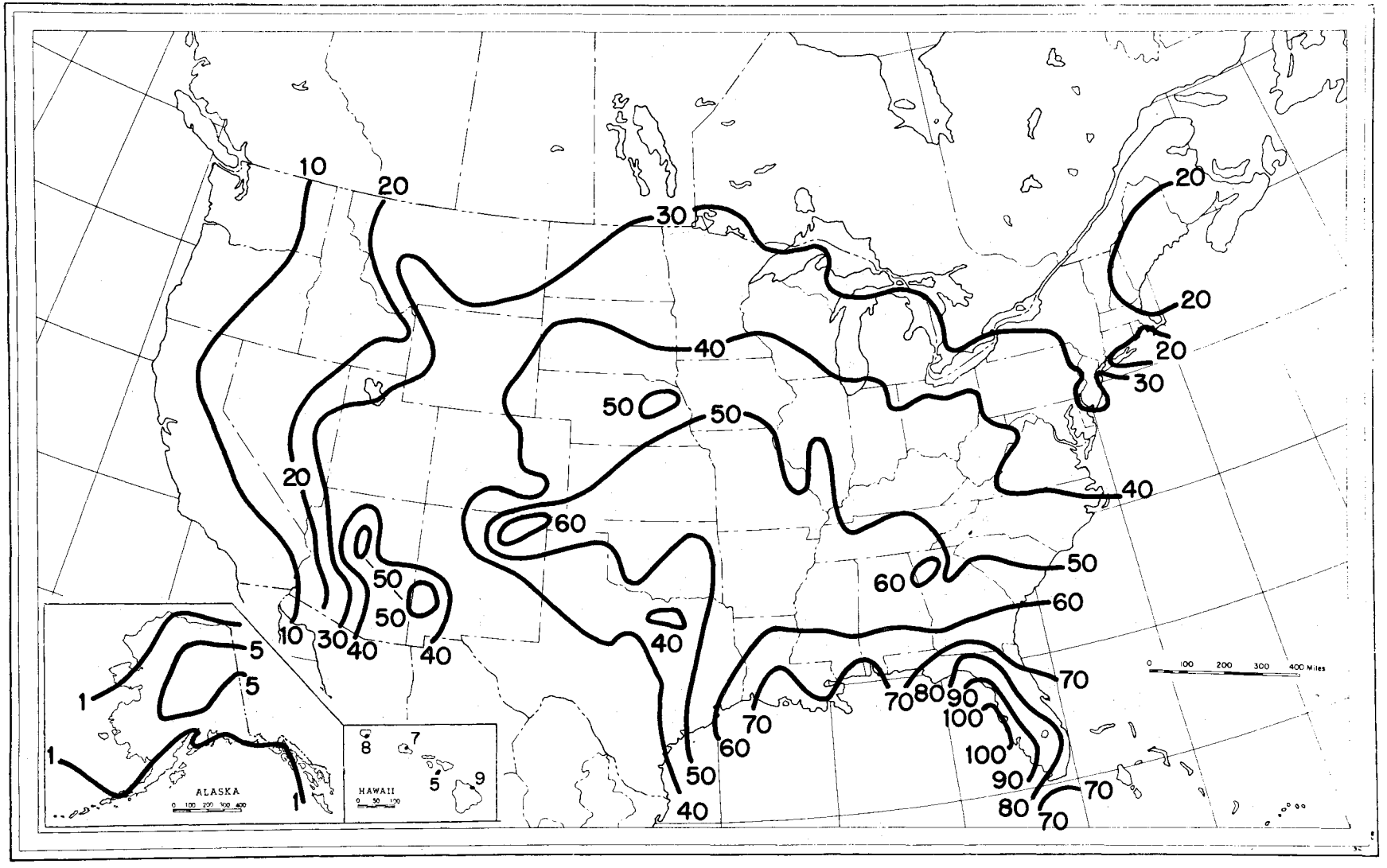

Figure 87. Contour map of the average annual number of days, U, with thunderstorms for the United States of America.

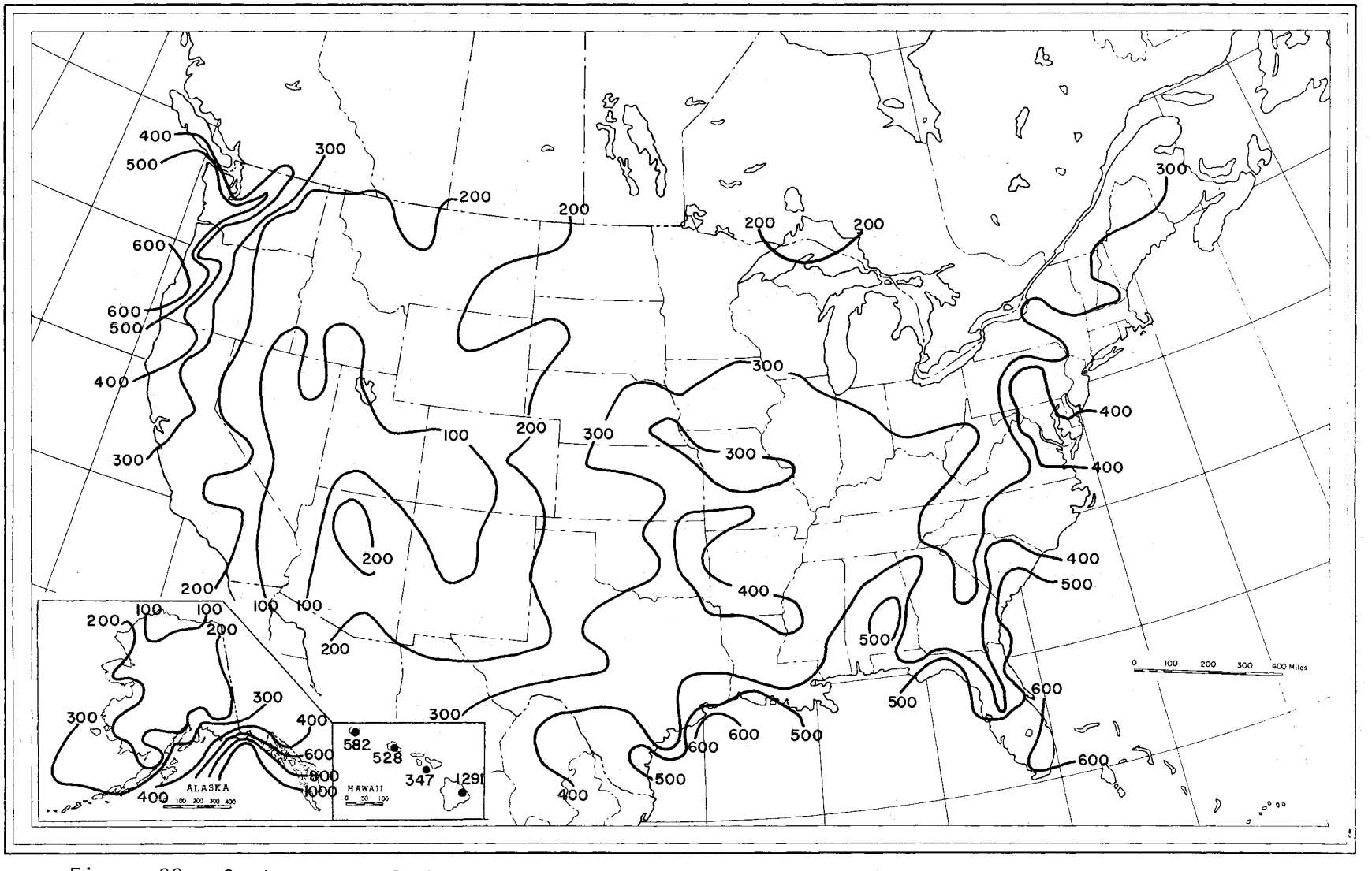

Figure 88. Contour map of the greatest monthly precipitation, M_m, in 30 consecutive years, in millimeters, for the United States of America.

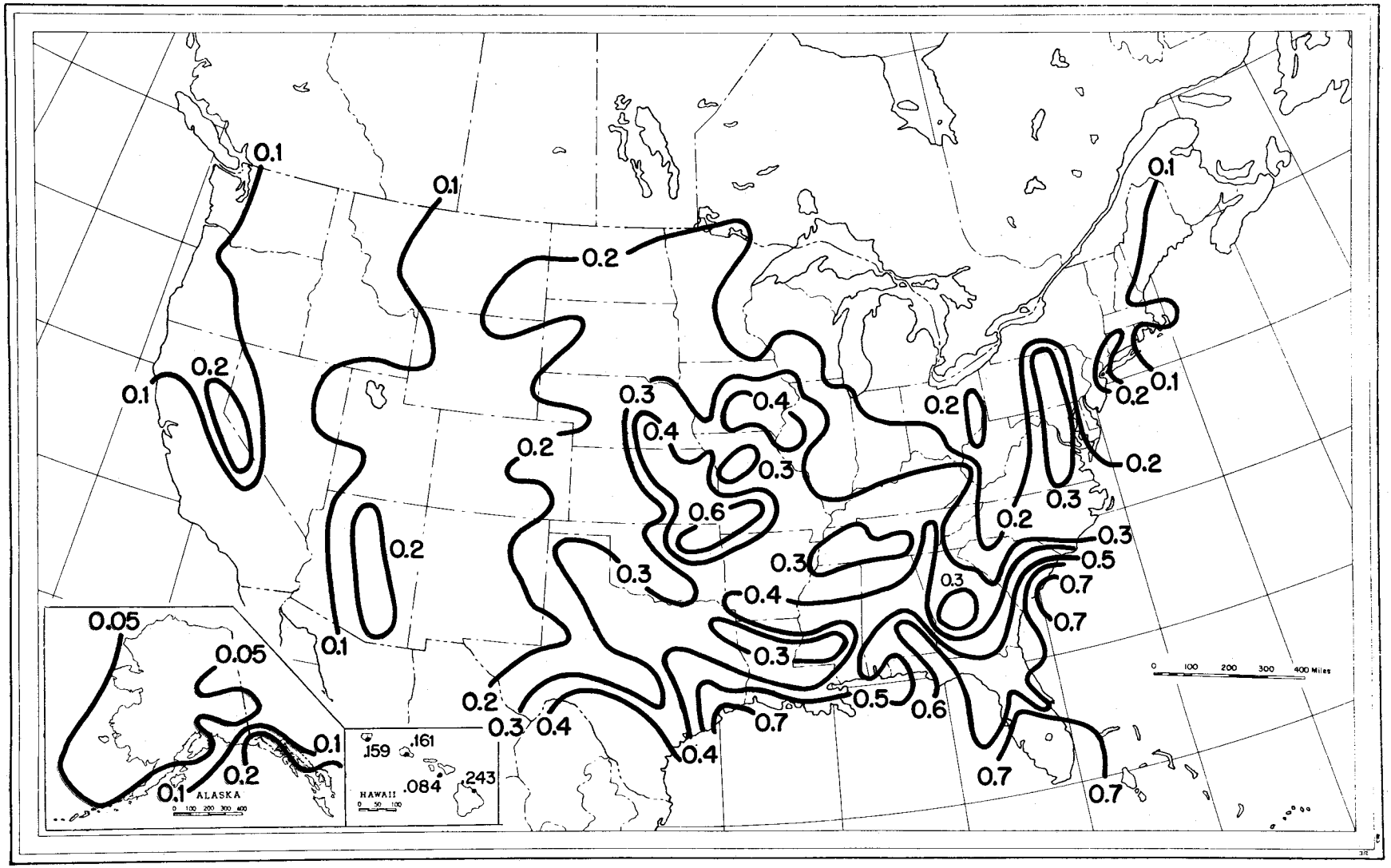

Figure 89. Contour map of the thunderstorm ratio, β, for the United States of America.

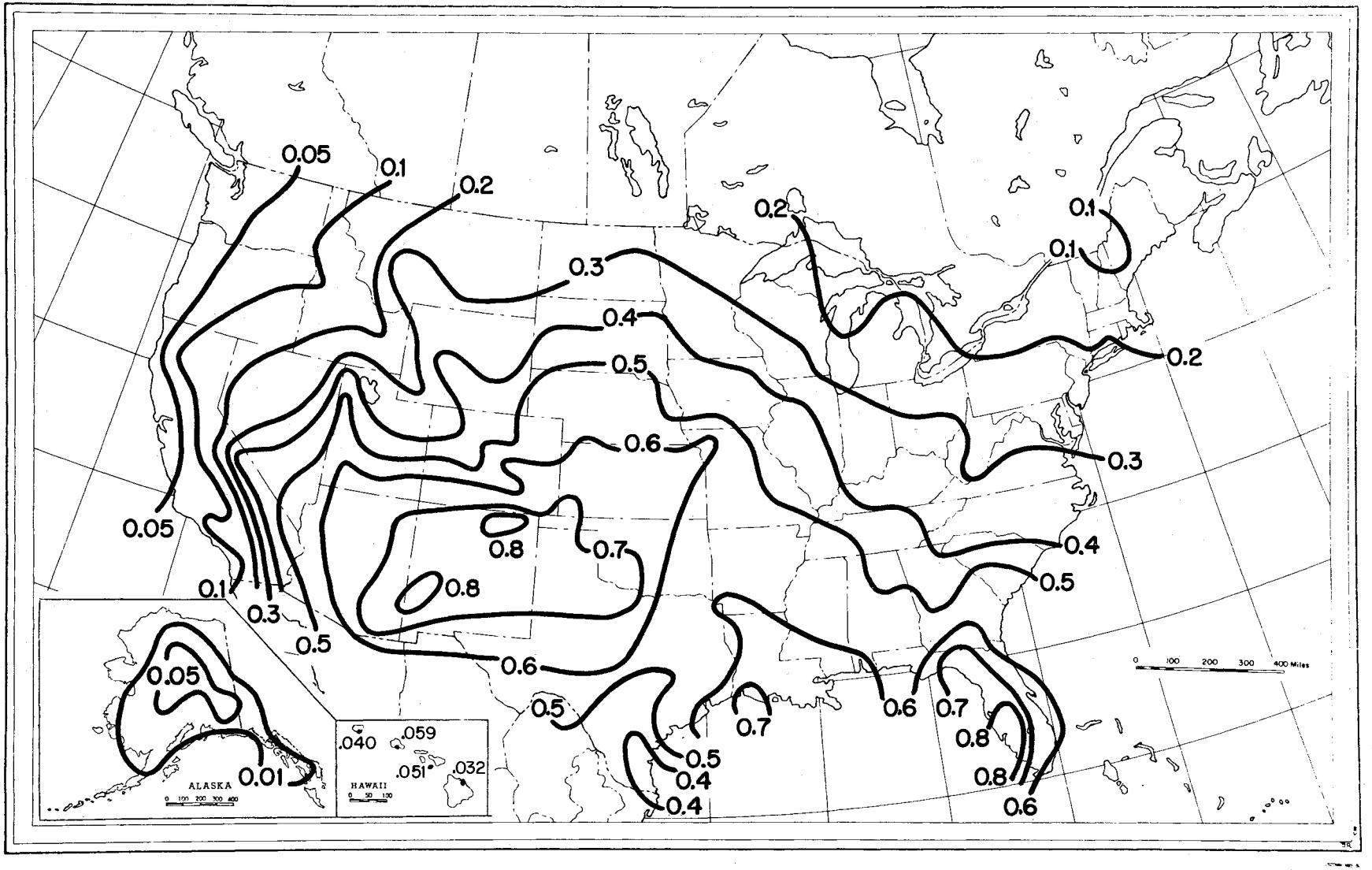

Figure 90. Contour map of the thunderstorm ratio, $U/D_{.01}$, for the United States of America.

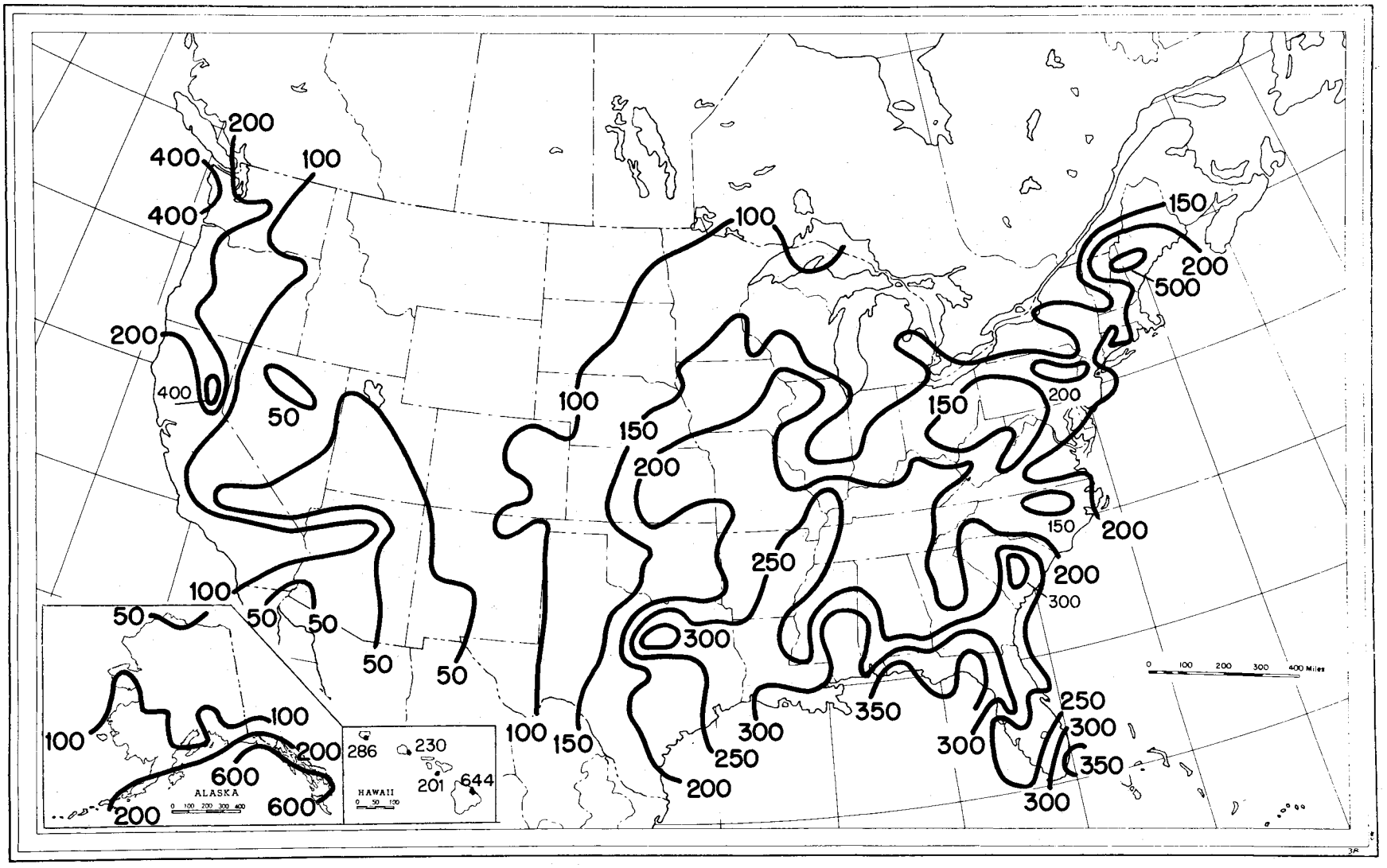

Figure 91. Contour map of the year-to-year standard deviation, s_M, in millimeters, of total annual precipitation for the United States of America.

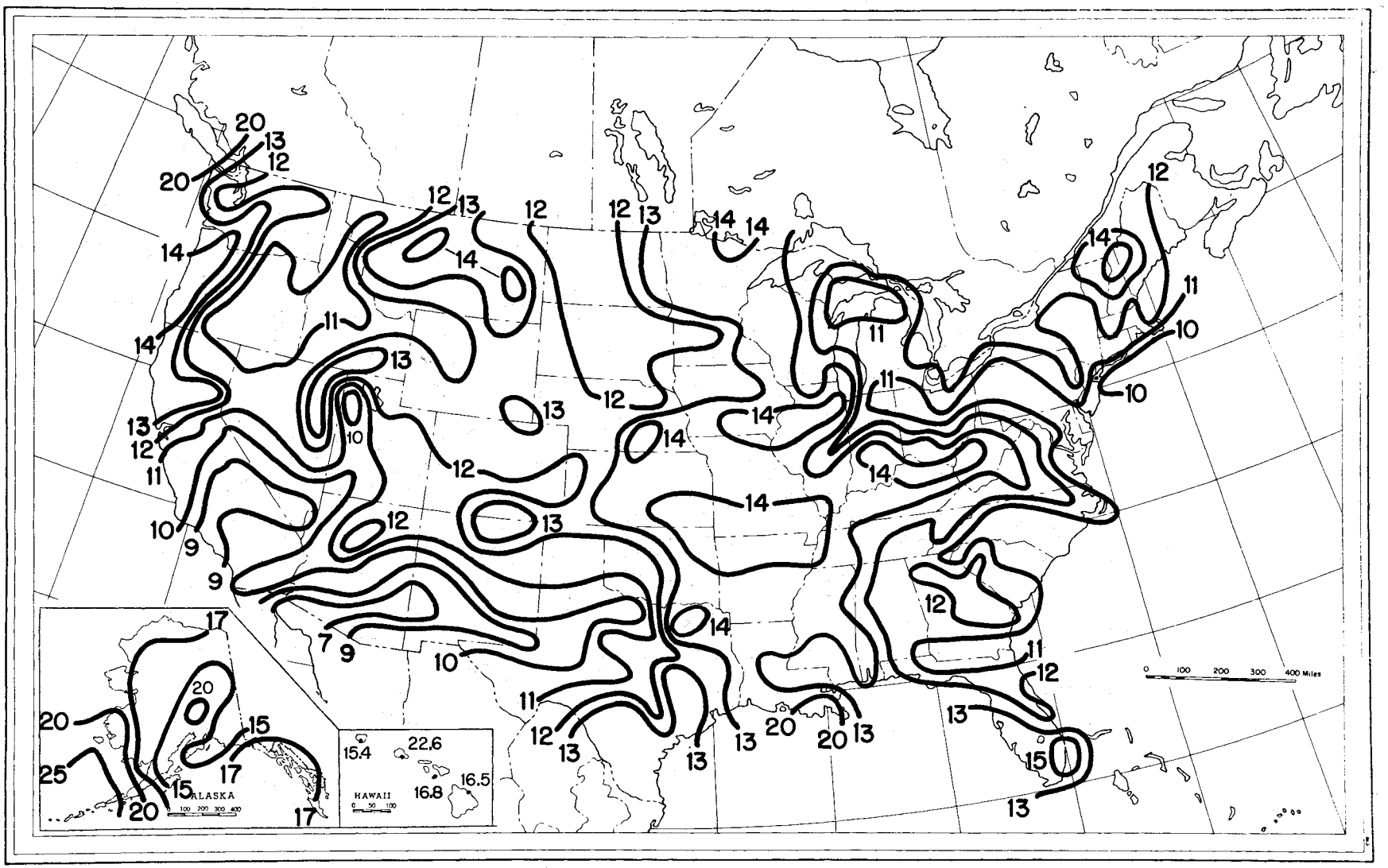

Figure 92. Contour map of the year-to-year standard deviation, s_D, of the annual number of days with precipitation greater than .01 in., for the United States of America.

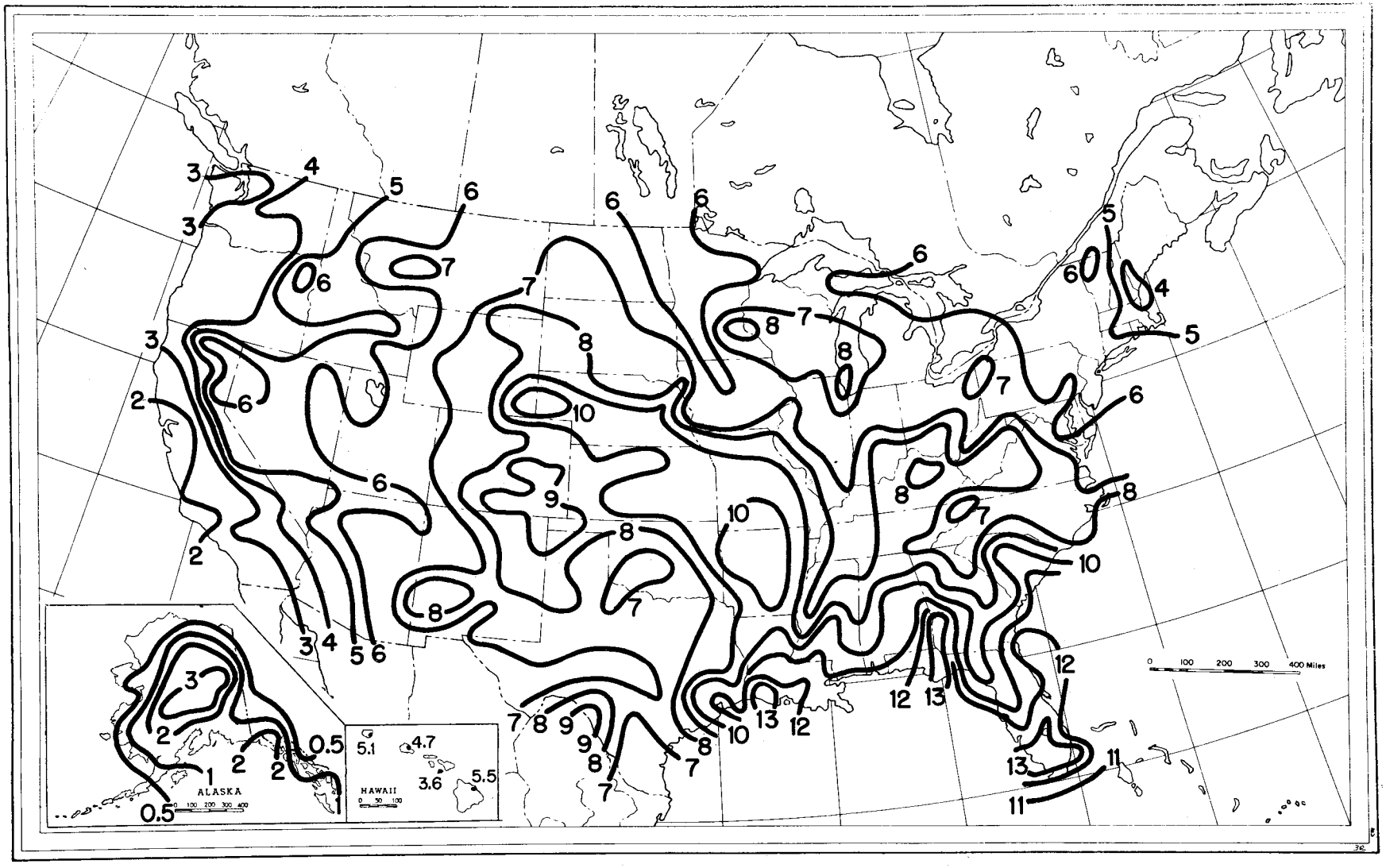

Figure 93. Contour map of the year-to-year standard deviation, s_U, of the annual number of days with thunderstorms for the United States of America.

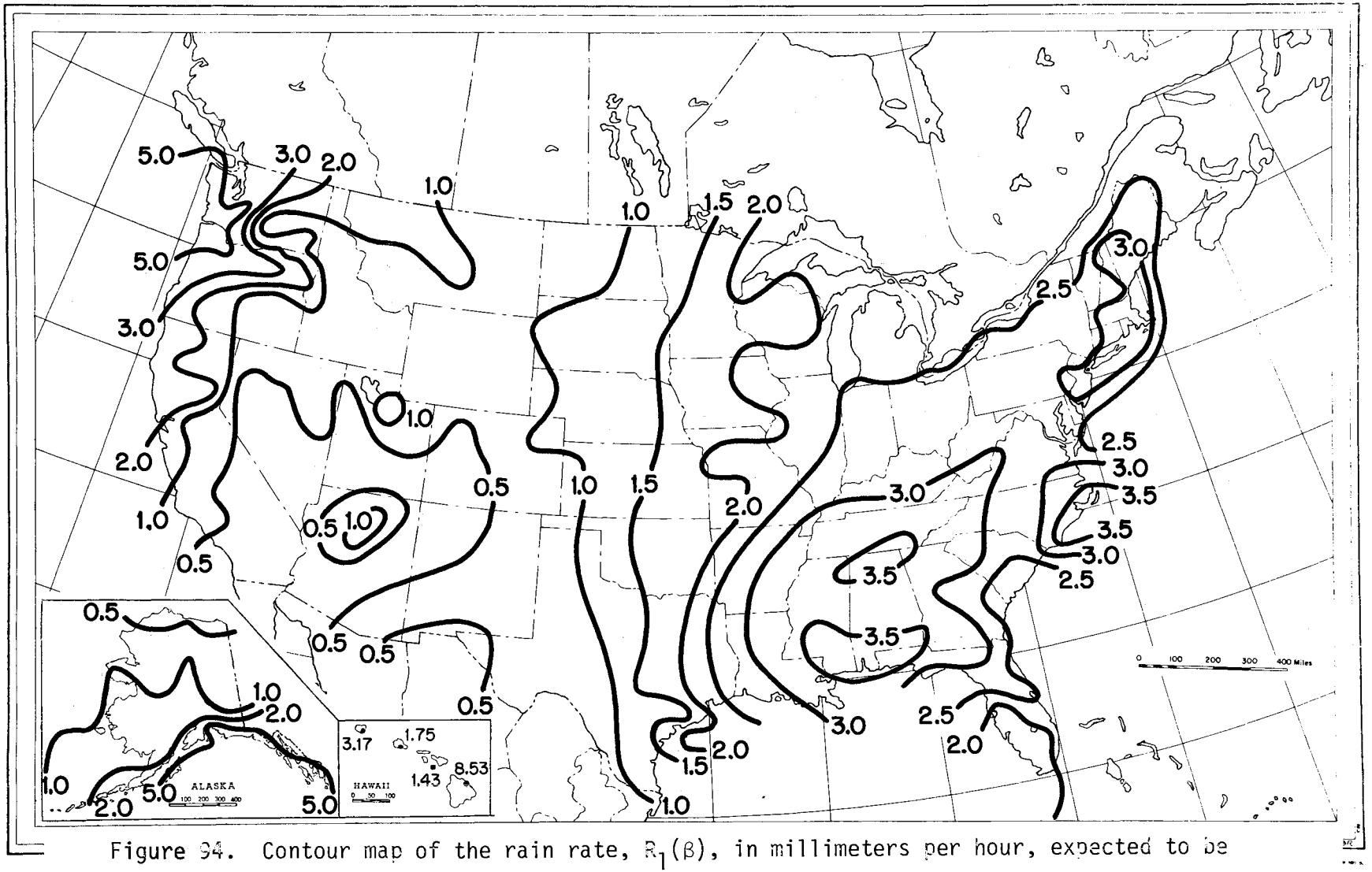

Figure 94. Contour map of the rain rate, $R_1(\beta)$, in millimeters per hour, expected to be exceeded 1 percent of an average year and derived from the thunderstorm ratio, β, for the United States of America.

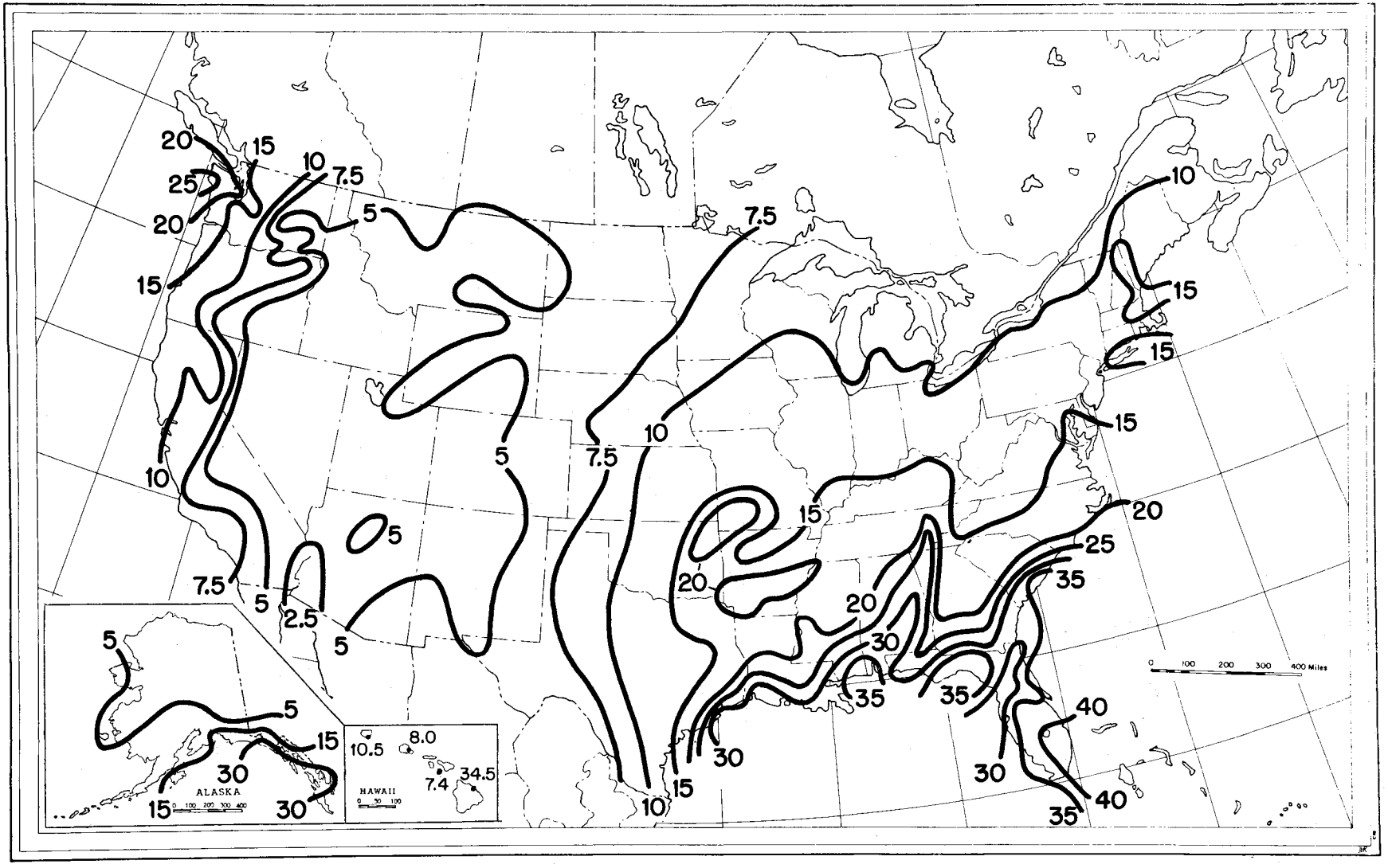

Figure 95. Contour map of the rain rate, $R_{.1}(\beta)$, in millimeters per hour, expected to be exceeded 0.1 percent of an average year and derived from the thunderstorm ratio, β, for the United States of America.

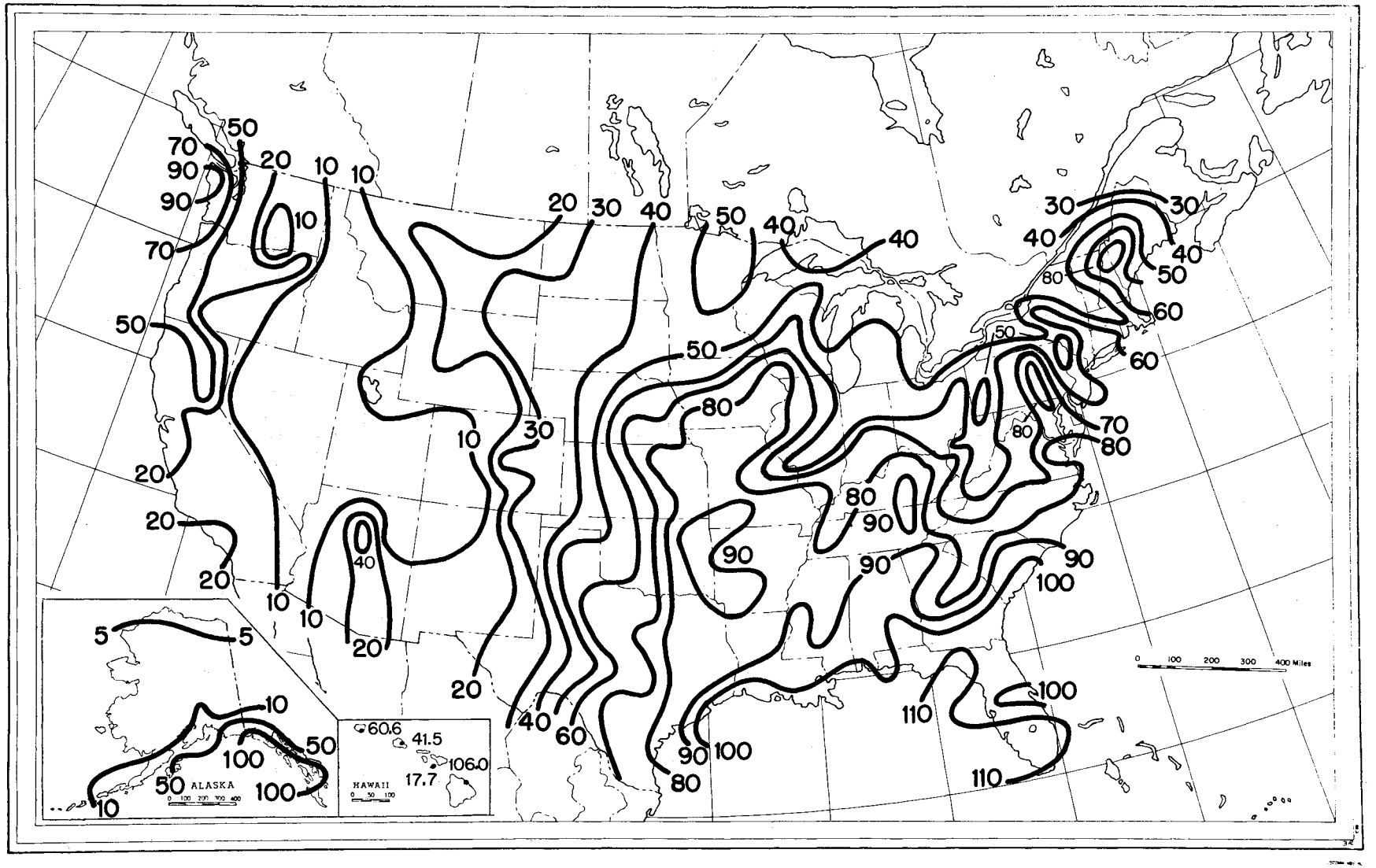

Figure 96. Contour map of the rain rate, $R_{.01}(\beta)$, in millimeters per hour, expected to be exceeded 0.01 percent of an average year and derived from the thunderstorm ratio, β, for the United States of America.

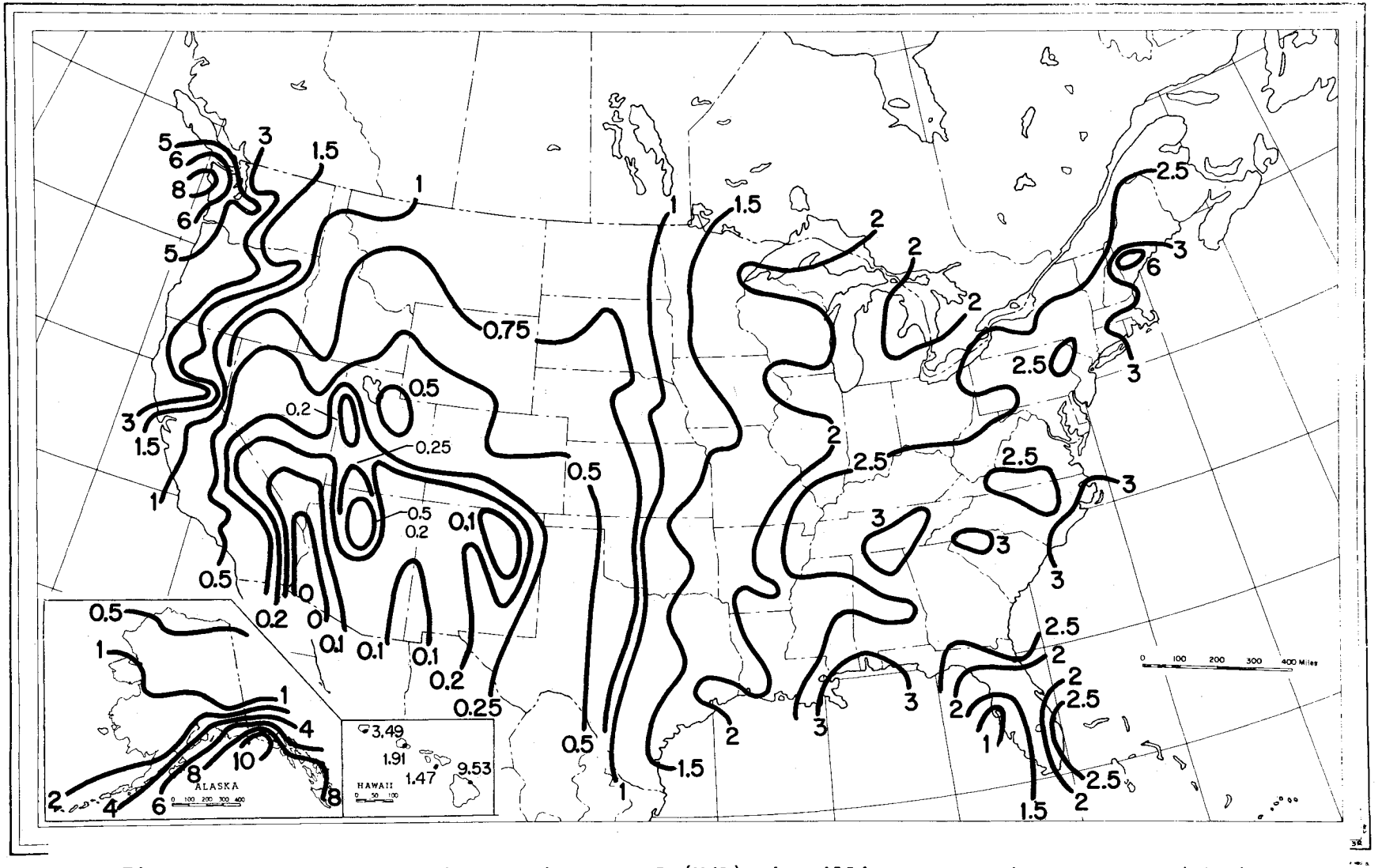

Figure 97. Contour map of the rain rate, $R_1(U/D)$, in millimeters per hour, expected to be exceeded 1 percent of an average year and derived from the thunderstorm ratio, $U/D_{.01}$, for the United States of America.

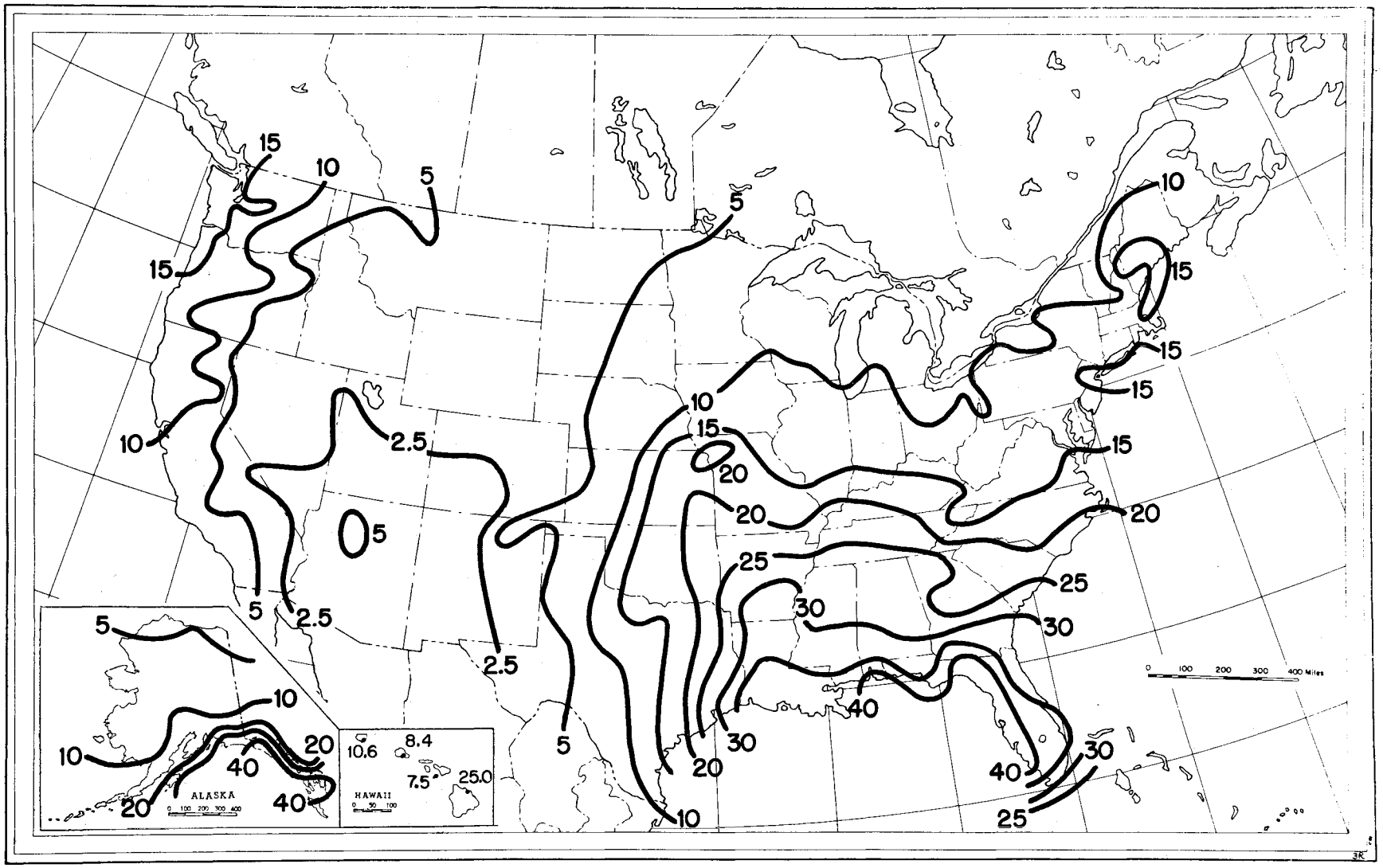

Figure 98. Contour map of the rain rate, $R_{.1}(U/D)$, in millimeters per hour, expected to be exceeded 0.1 percent of an average year and derived from the thunderstorm ratio, $U/D_{.01}$, for the United States of America.

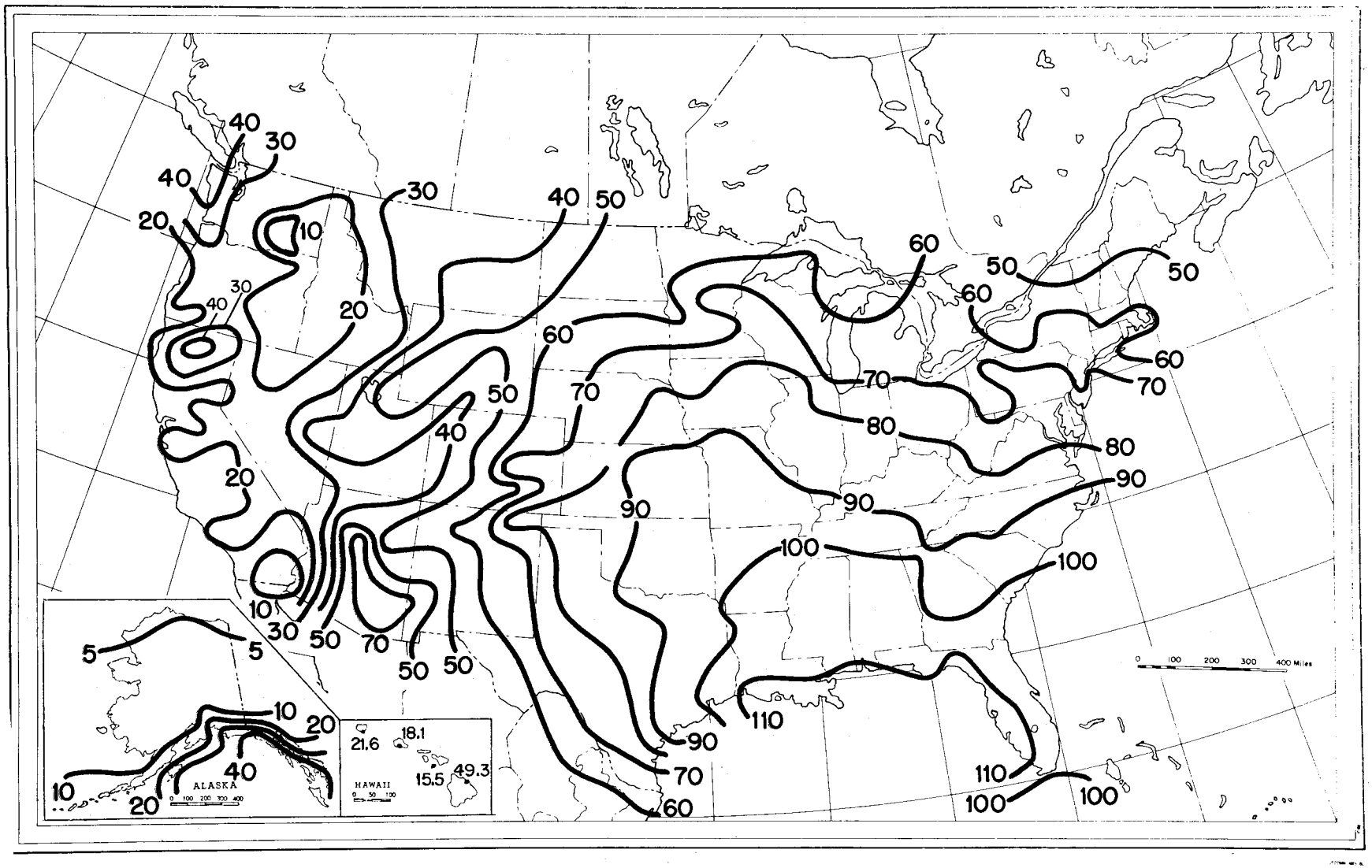

Figure 99. Contour map of the rain rate, $R_{.01}(U/D)$, in millimeters per hour, expected to be exceeded 0.01 percent of an average year and derived from the thunderstorm ratio, $U/D_{.01}$, for the United States of America.

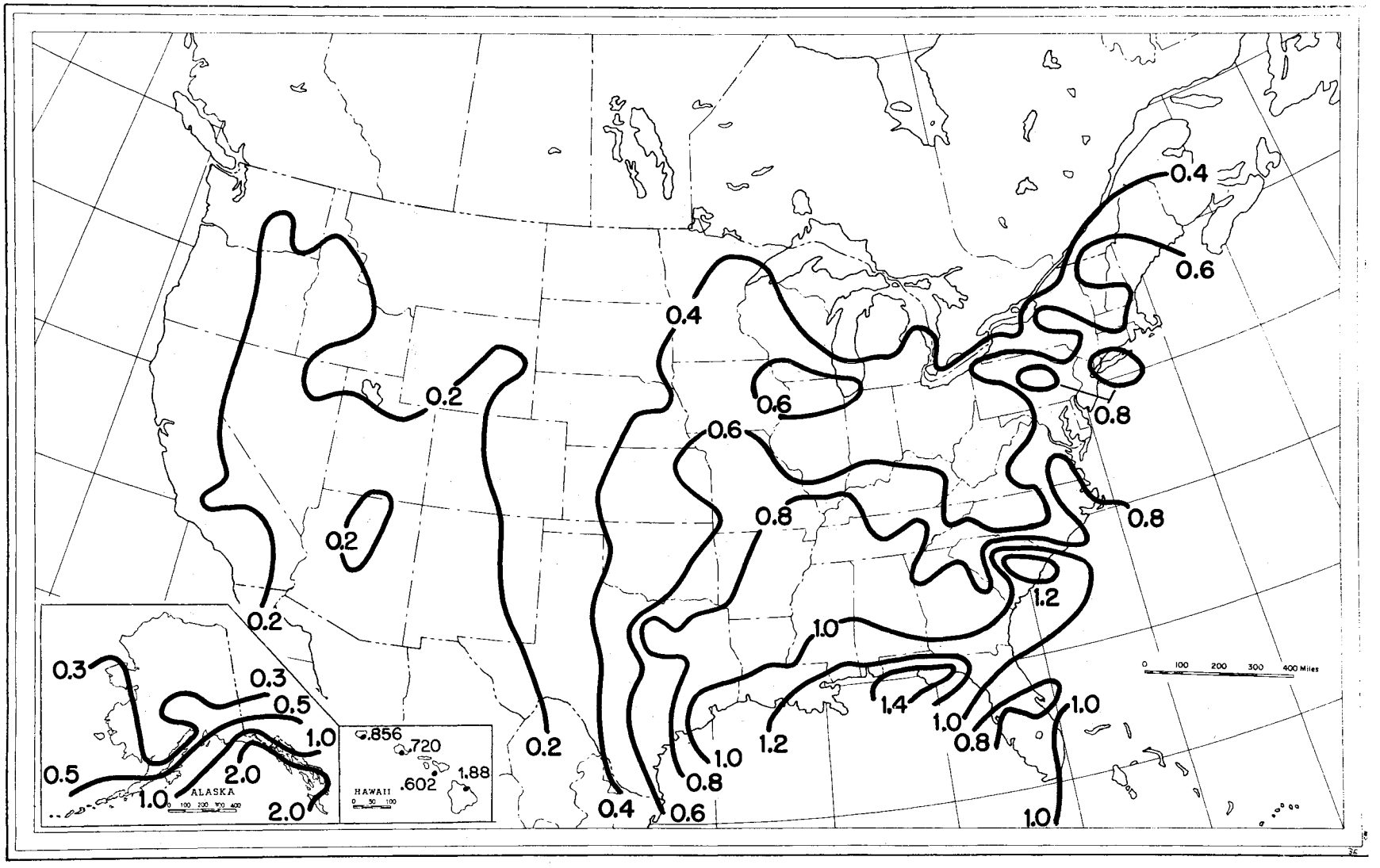

Figure 100. Contour map of the estimated year-to-year standard deviation, $s_{R_1}(\beta)$, in millimeters per hour, of rain rate expected at the 1 percent exceedance level, derived from the thunderstorm ratio, β, for the United States of America.

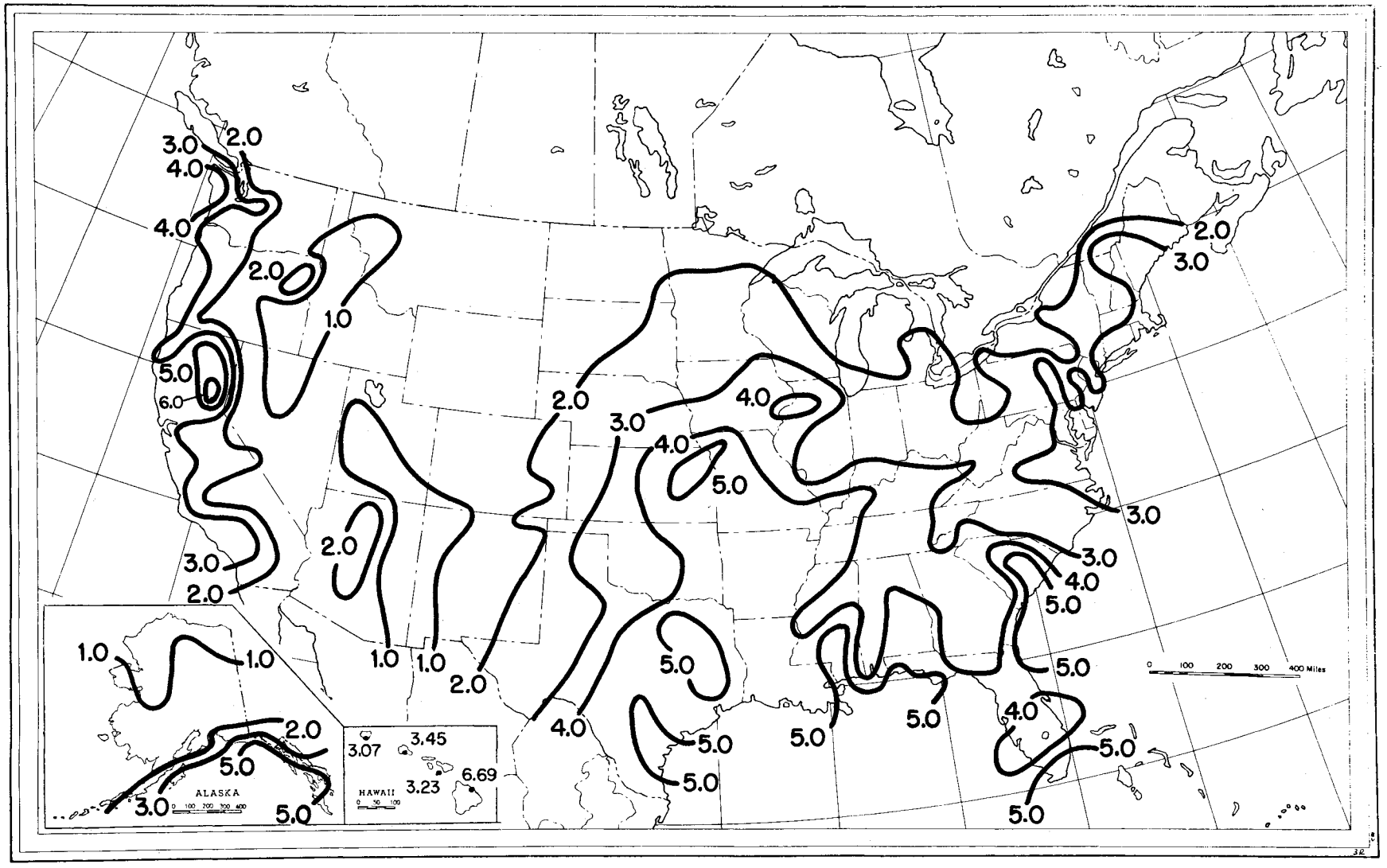

Figure 101. Contour map of the estimated year-to-year standard deviation $s_{R_{.1}}(\beta)$, in millimeters per hour, of rain rate expected at the 0.1 percent exceedance level from the thunderstorm ratio, β, for the United States of America.

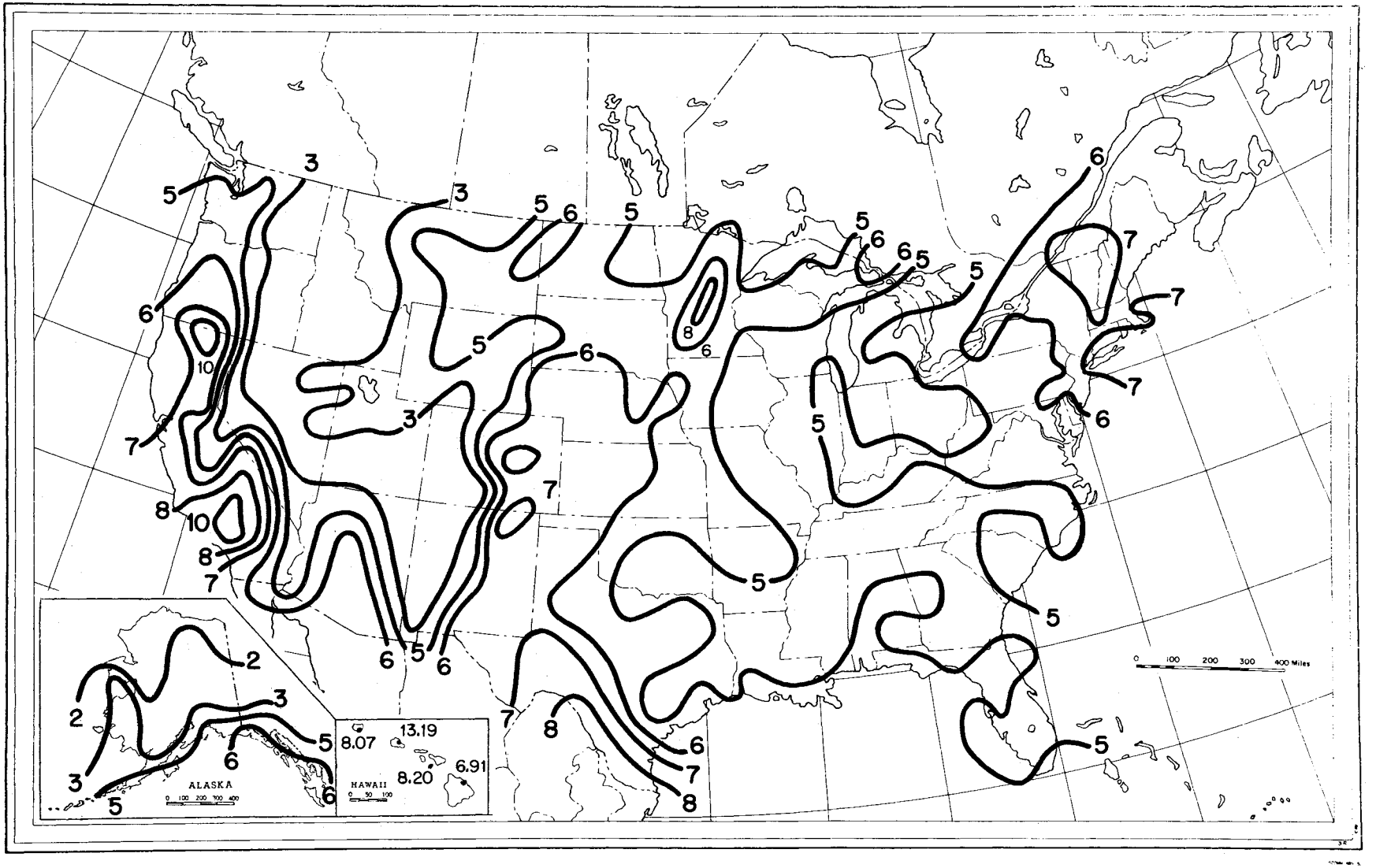

Figure 102. Contour map of the estimated year-to-year standard deviation, $s_{R_{.01}}(\beta)$, in millimeters per hour, of rain rate expected at the 0.01 percent exceedance level, derived from the thunderstorm ratio, β, for the United States of America.

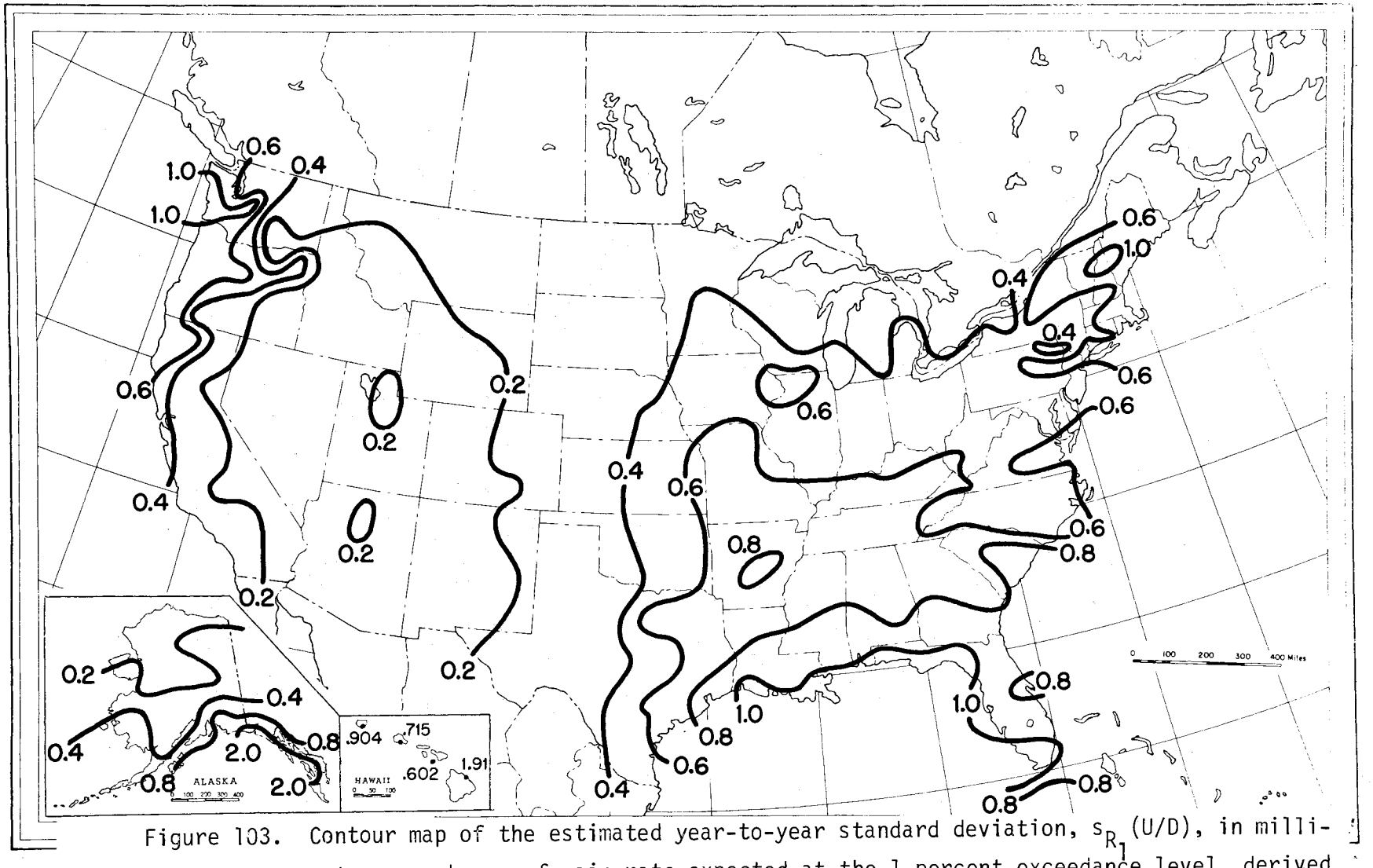

Figure 103. Contour map of the estimated year-to-year standard deviation, $s_{R_1}(U/D)$, in millimeters per hour, of rain rate expected at the 1 percent exceedance level, derived from the thunderstorm ratio, $U/D_{.01}$, for the United States of America.

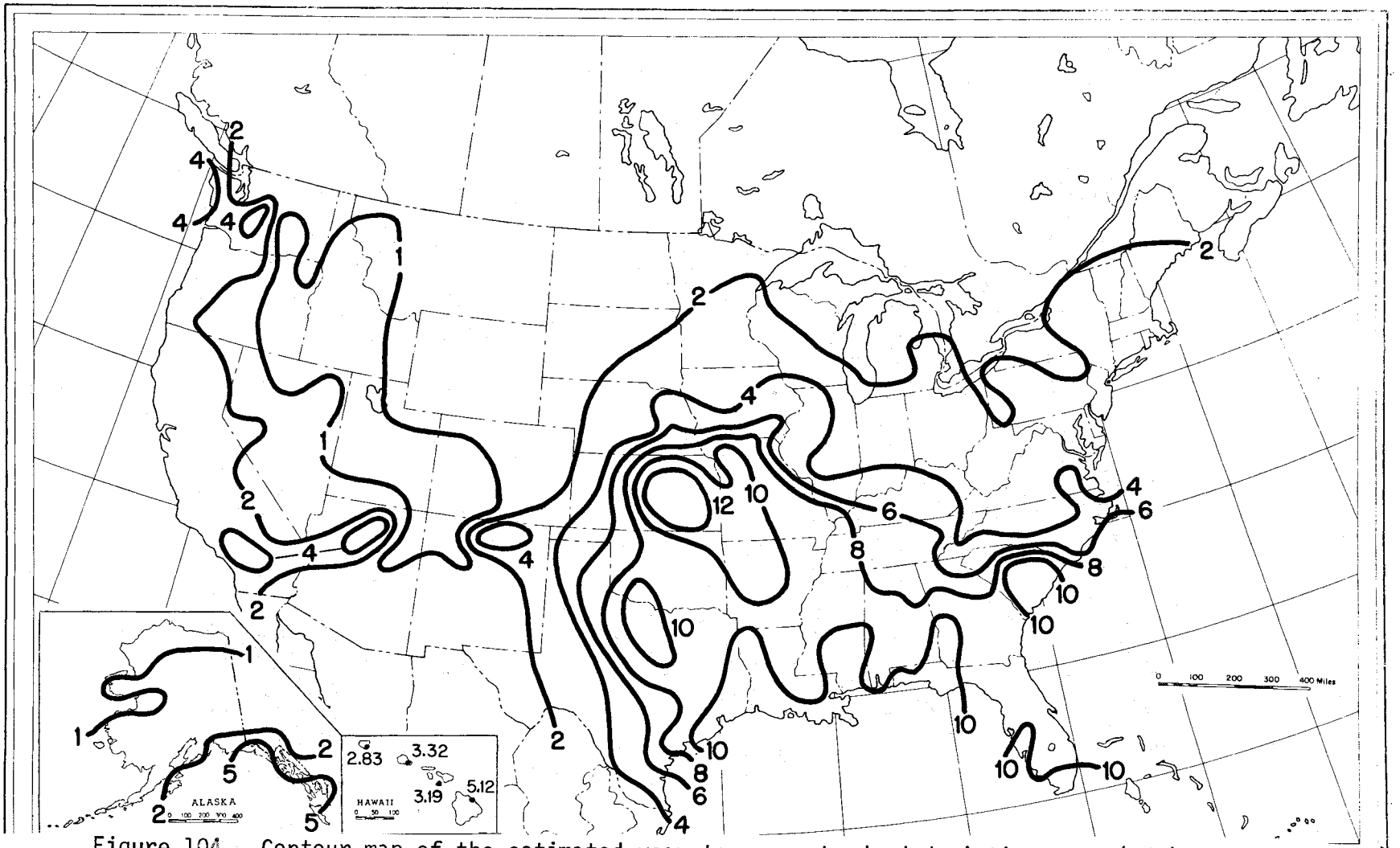

Figure 104. Contour map of the estimated year-to-year standard deviation, $s_{R_{.1}}$ (U/D), in millimeters per hour, of rain rate expected at the 0.1 percent exceedance level, derived from the thunderstorm ratio, $U/D_{.01}$, for the United States of America.

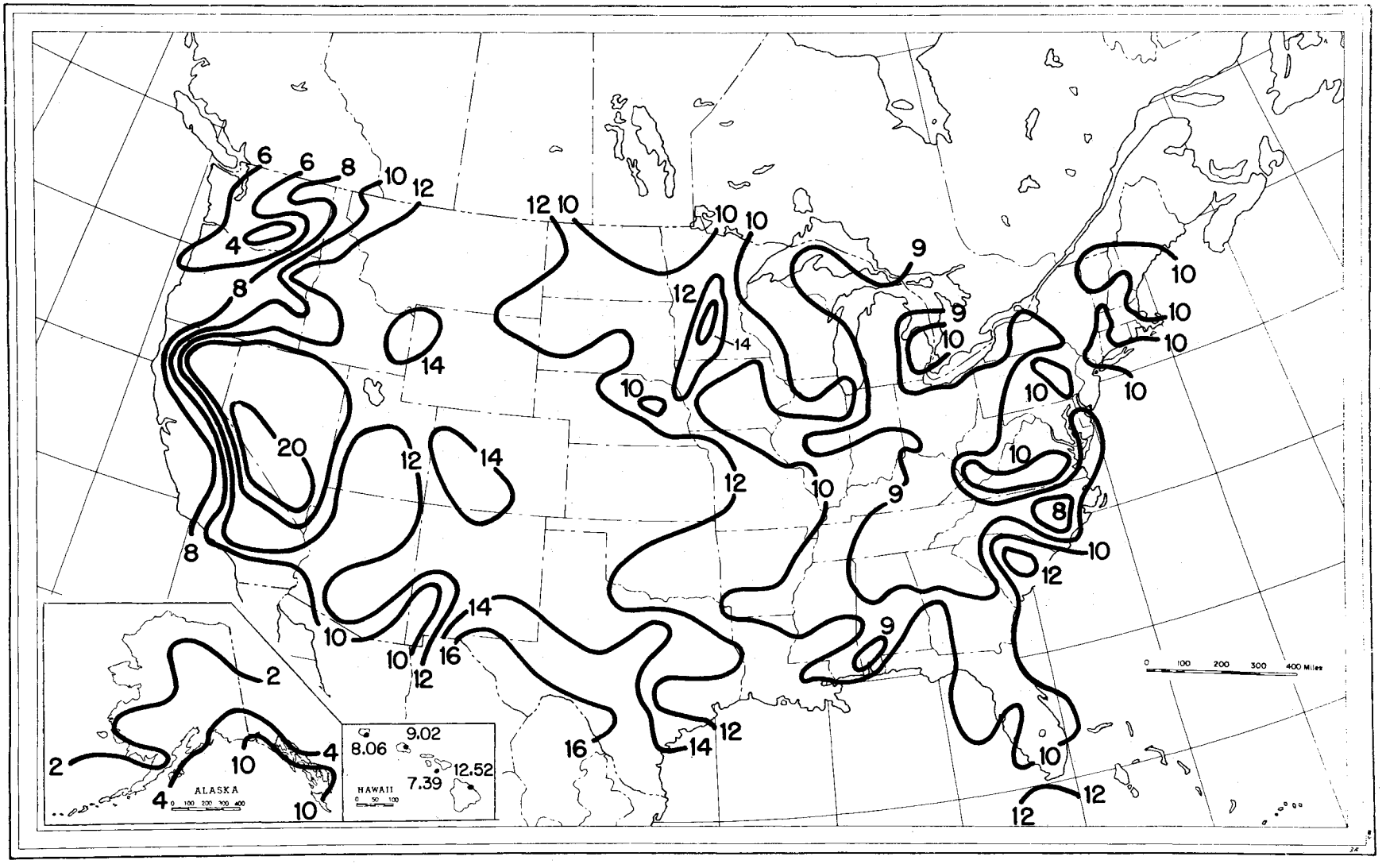

Figure 105. Contour map of the estimated year-to-year standard deviation, $s_{R_{.01}}(U/D)$, in millimeters per hour, of rain rate expected at the 0.01 percent exceedance level, derived from the thunderstorm ratio, $U/D_{.01}$, for the United States of America.

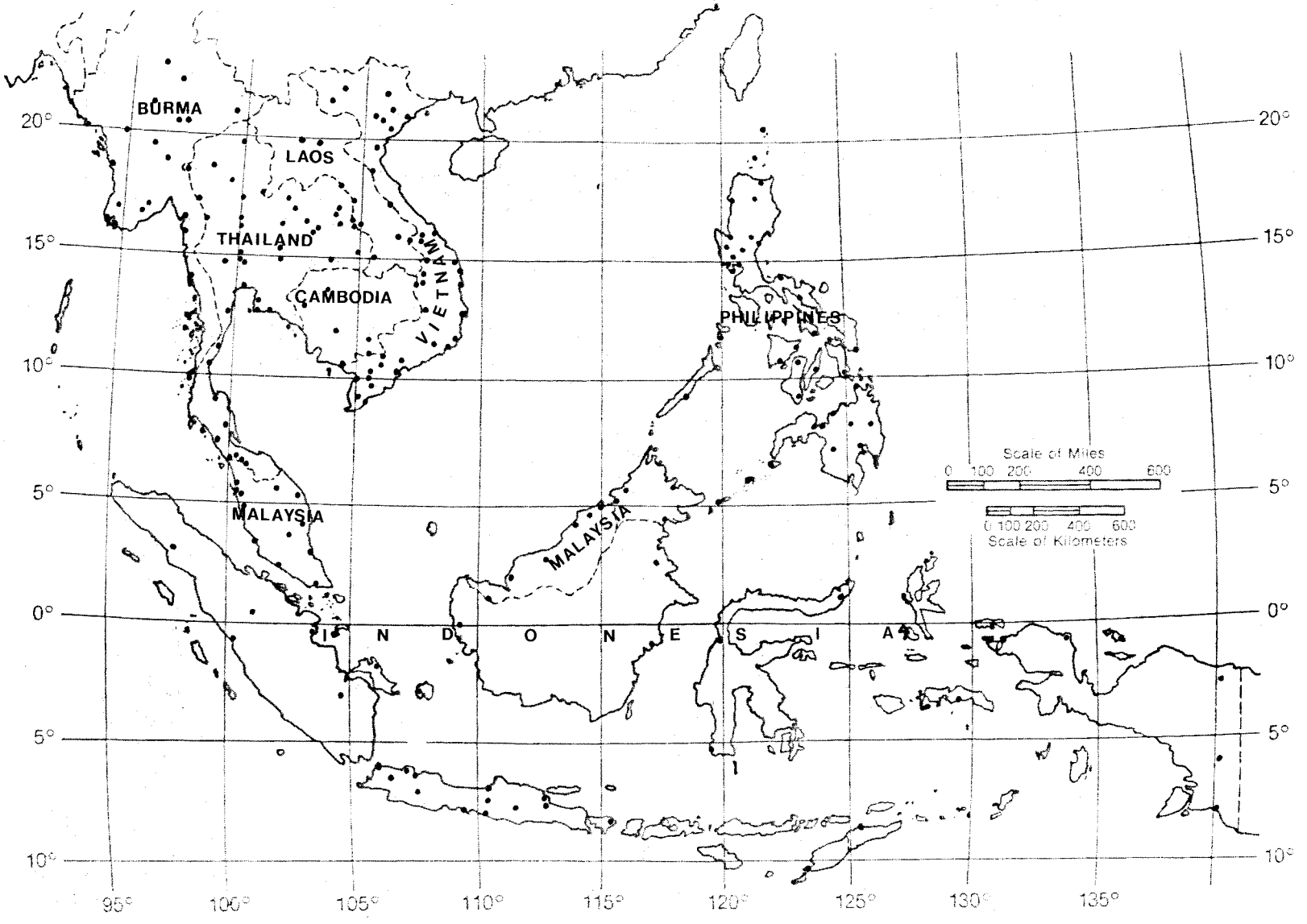

Figure 106. Map of data locations in Southeast Asia.

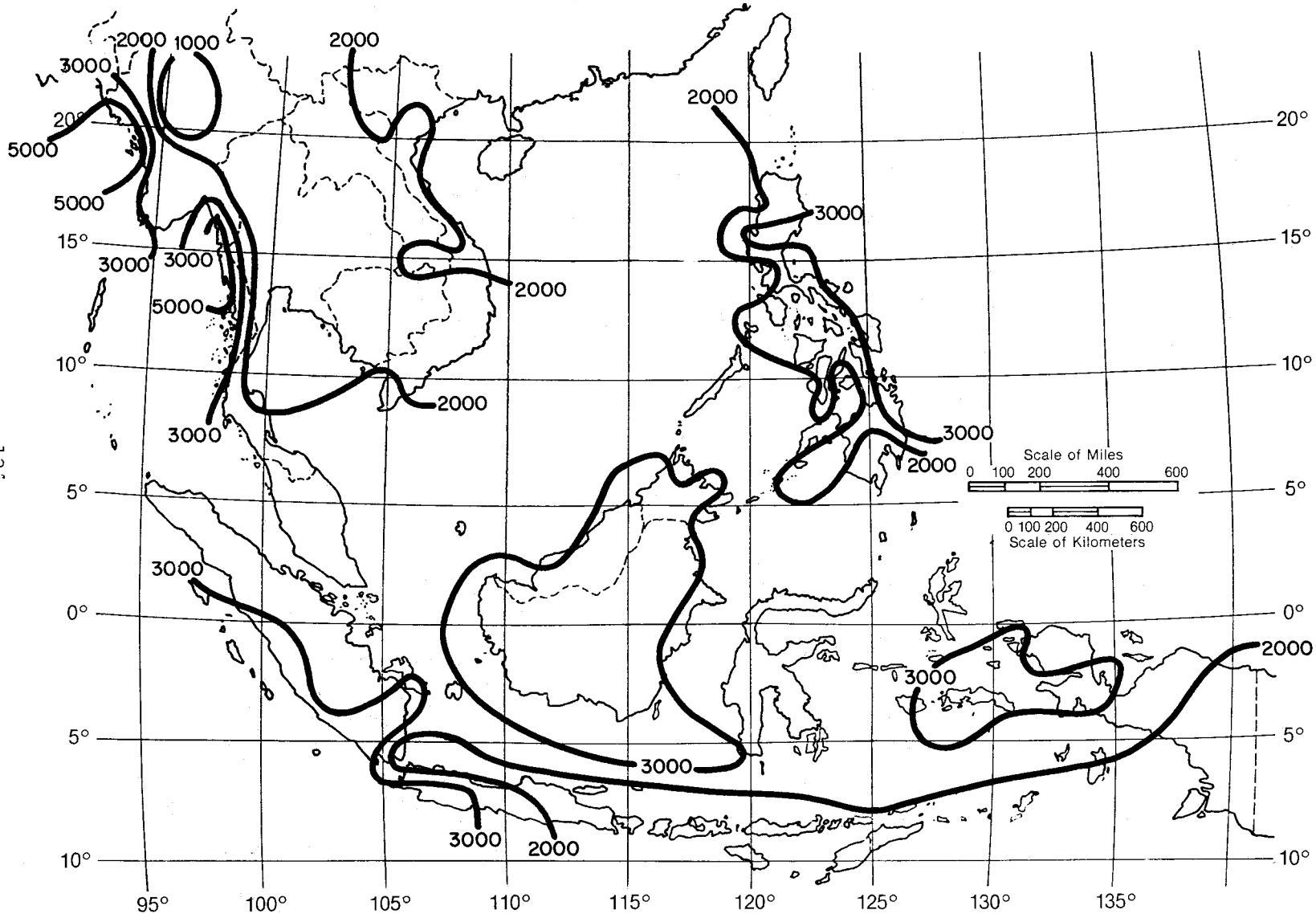

Figure 107. Contour map of the average annual precipitation, M, in millimeters, for Southeast Asia.

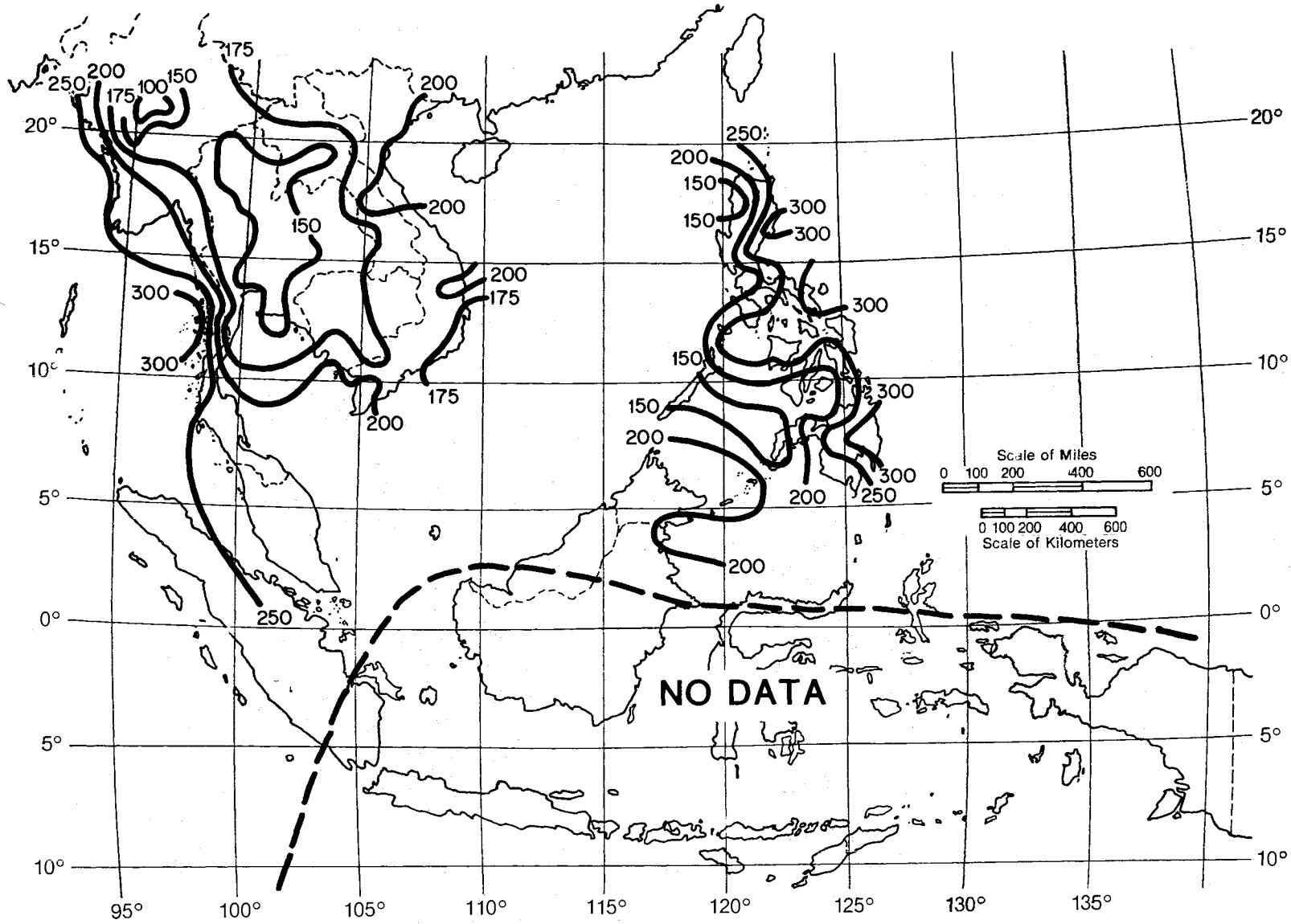

Figure 108. Contour map of the average annual number of days, $D_{.01}$, with precipitation greater than .01 in., for Southeast Asia.

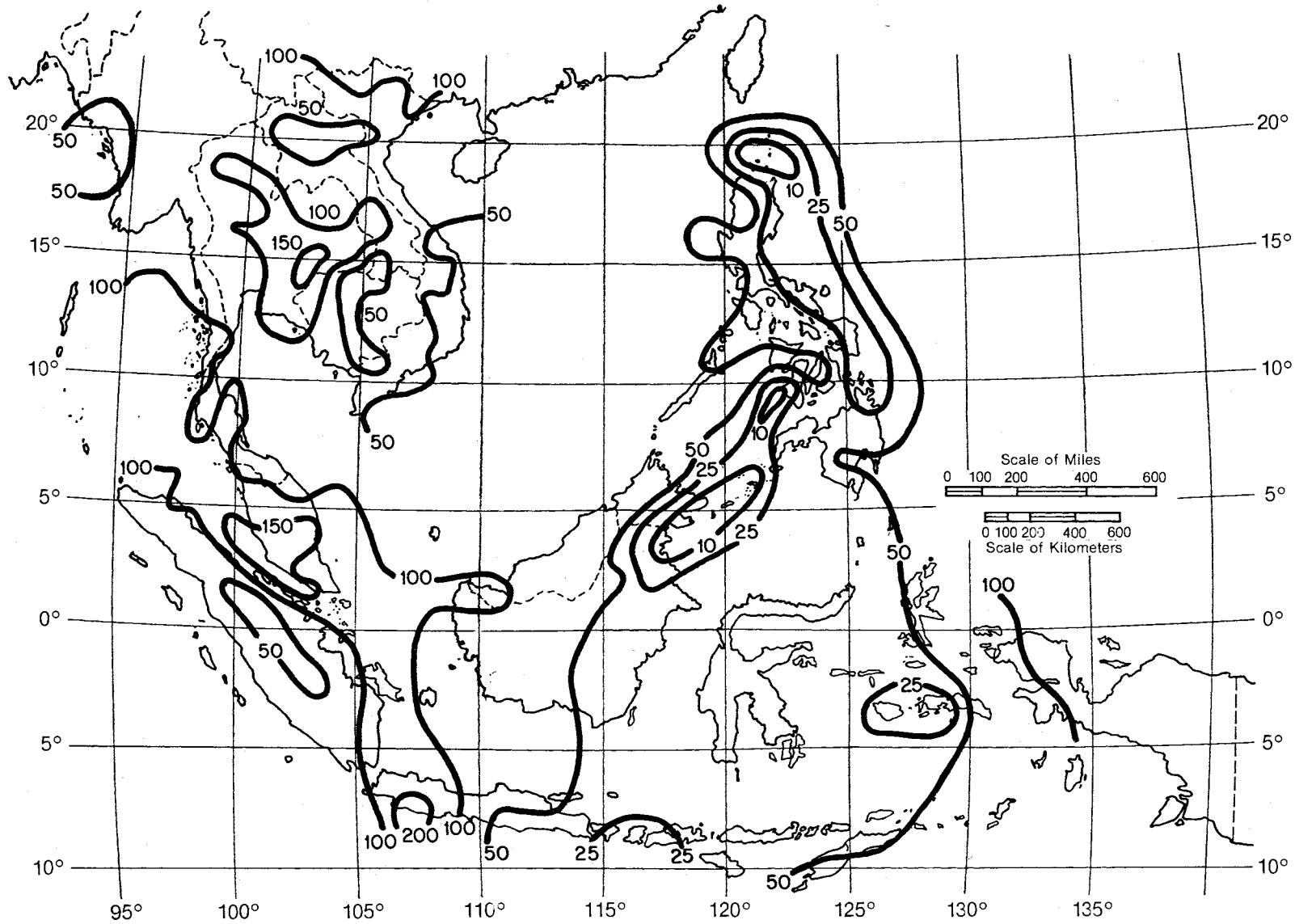

Figure 109. Contour map of the average annual number of days, U, with thunderstorms for Southeast Asia.

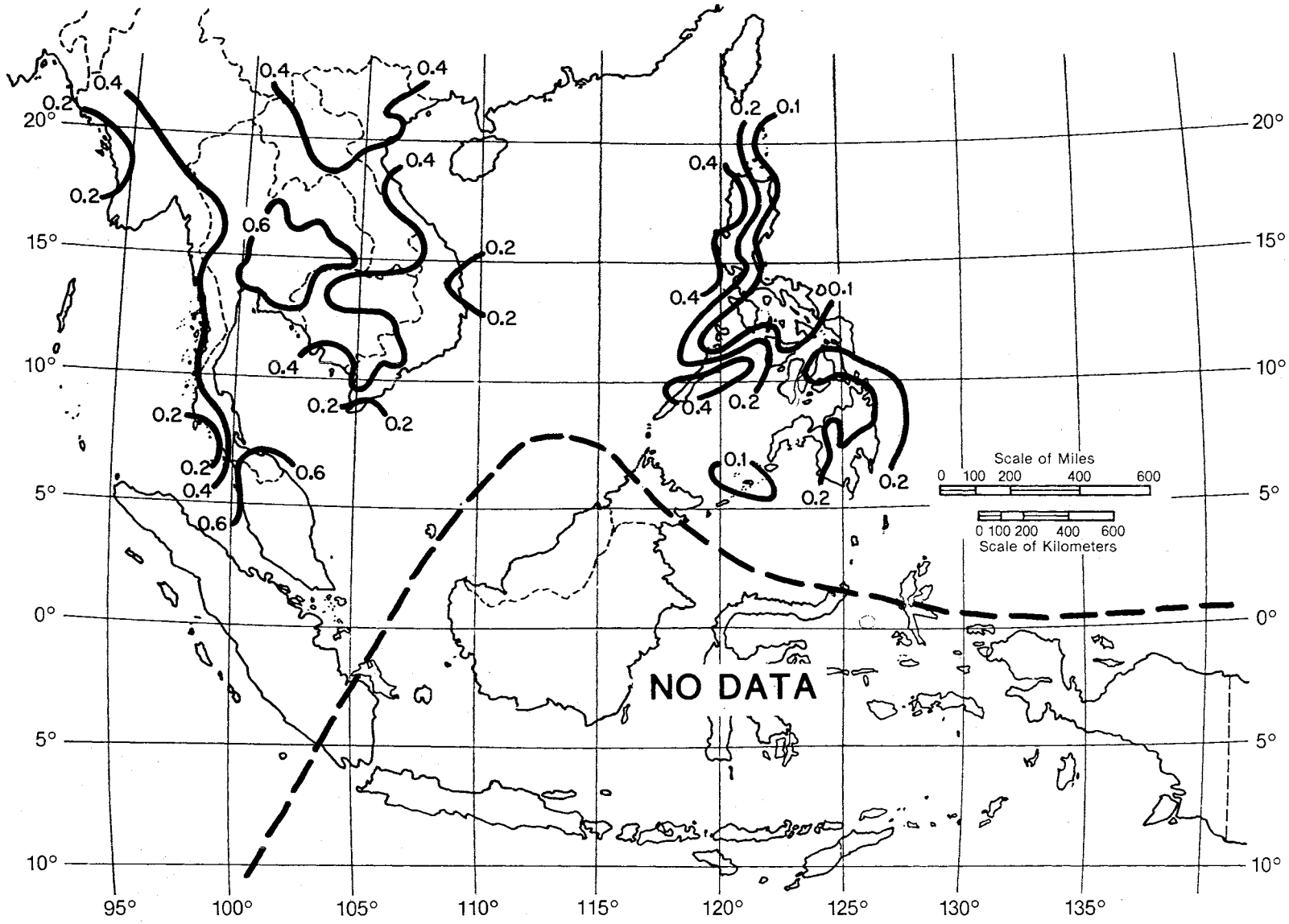

Figure 110. Contour map of the thunderstorm ratio, $U/D_{.01}$, for Southeast Asia.

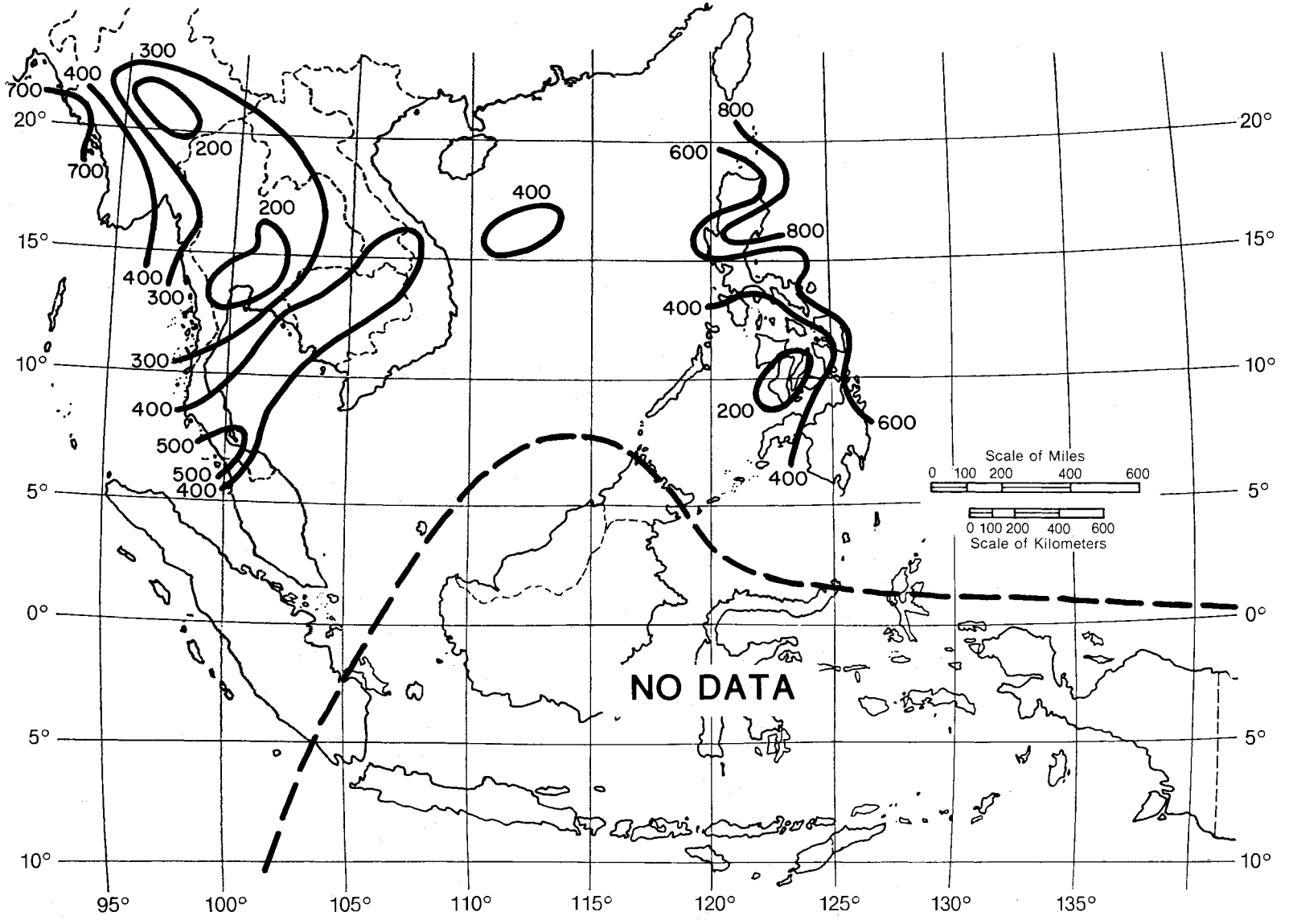

Figure 111. Contour map of the year-to-year standard deviation, s_M, in millimeters, of total annual precipitation for Southeast Asia.

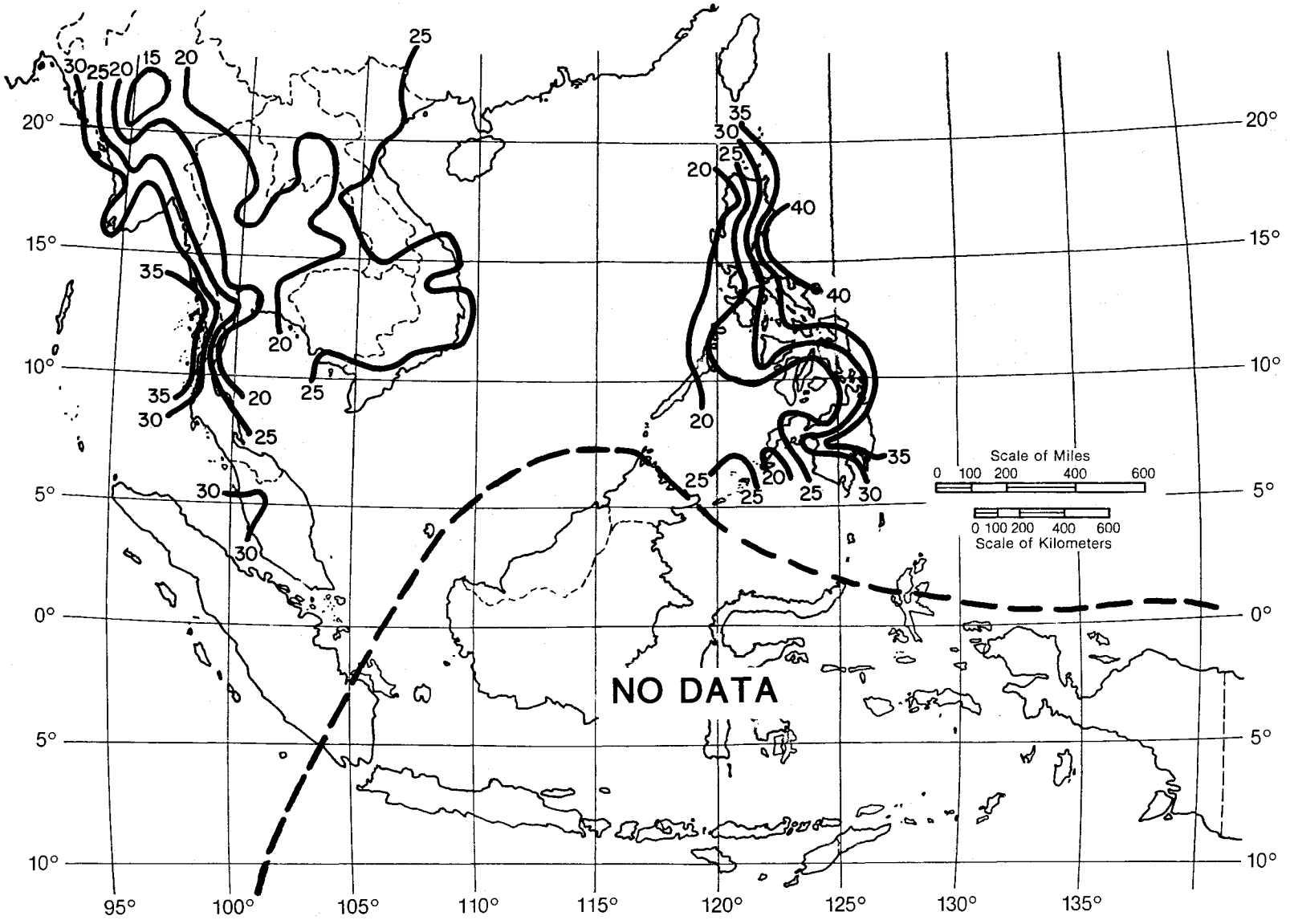

Figure 112. Contour map of the year-to-year standard deviation, s_D, of the annual number of days with precipitation greater than .01 in., for Southeast Asia.

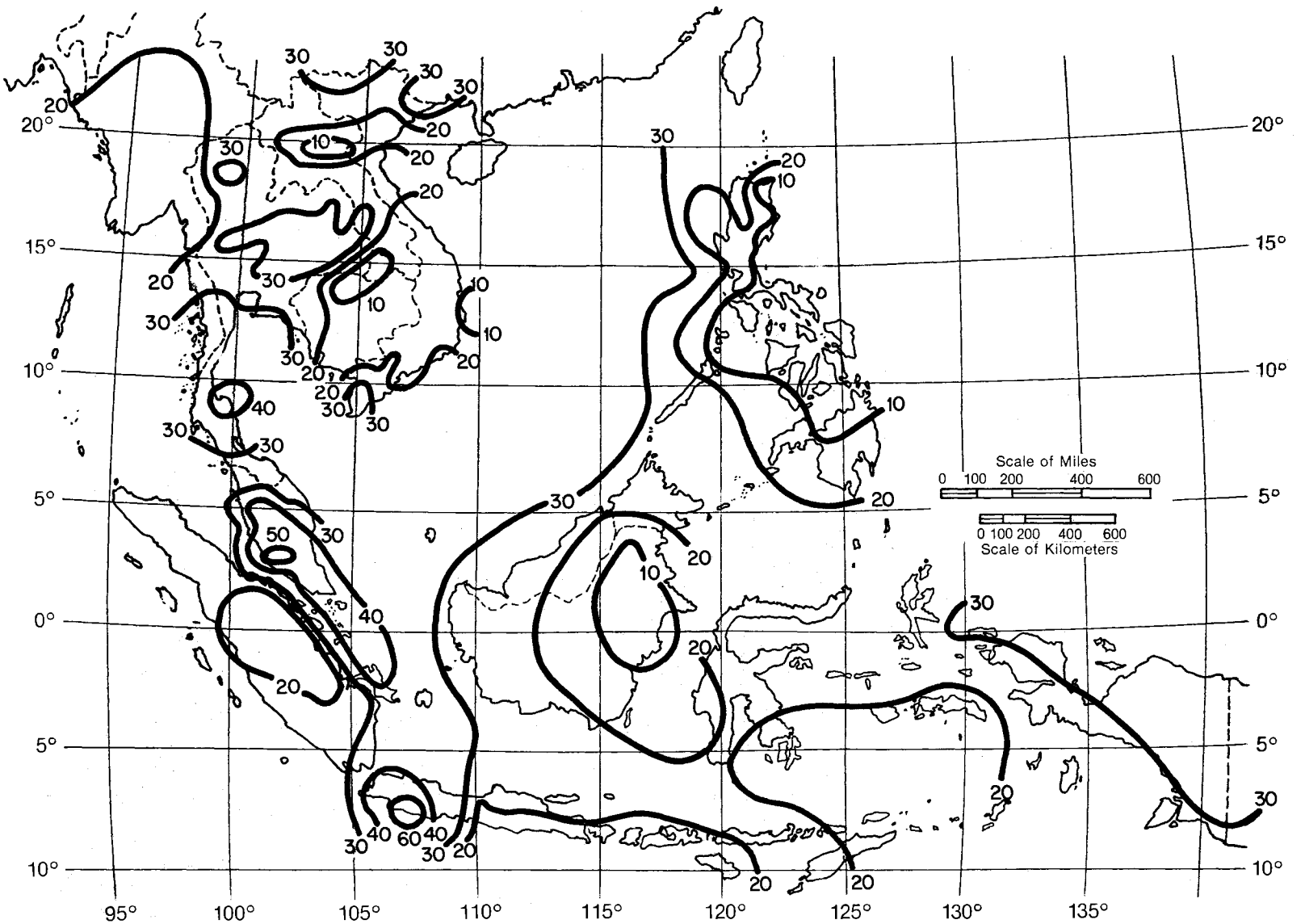

Figure 113. Contour map of the year-to-year standard deviation, s_U, of the annual number of days with thunderstorms for Southeast Asia.

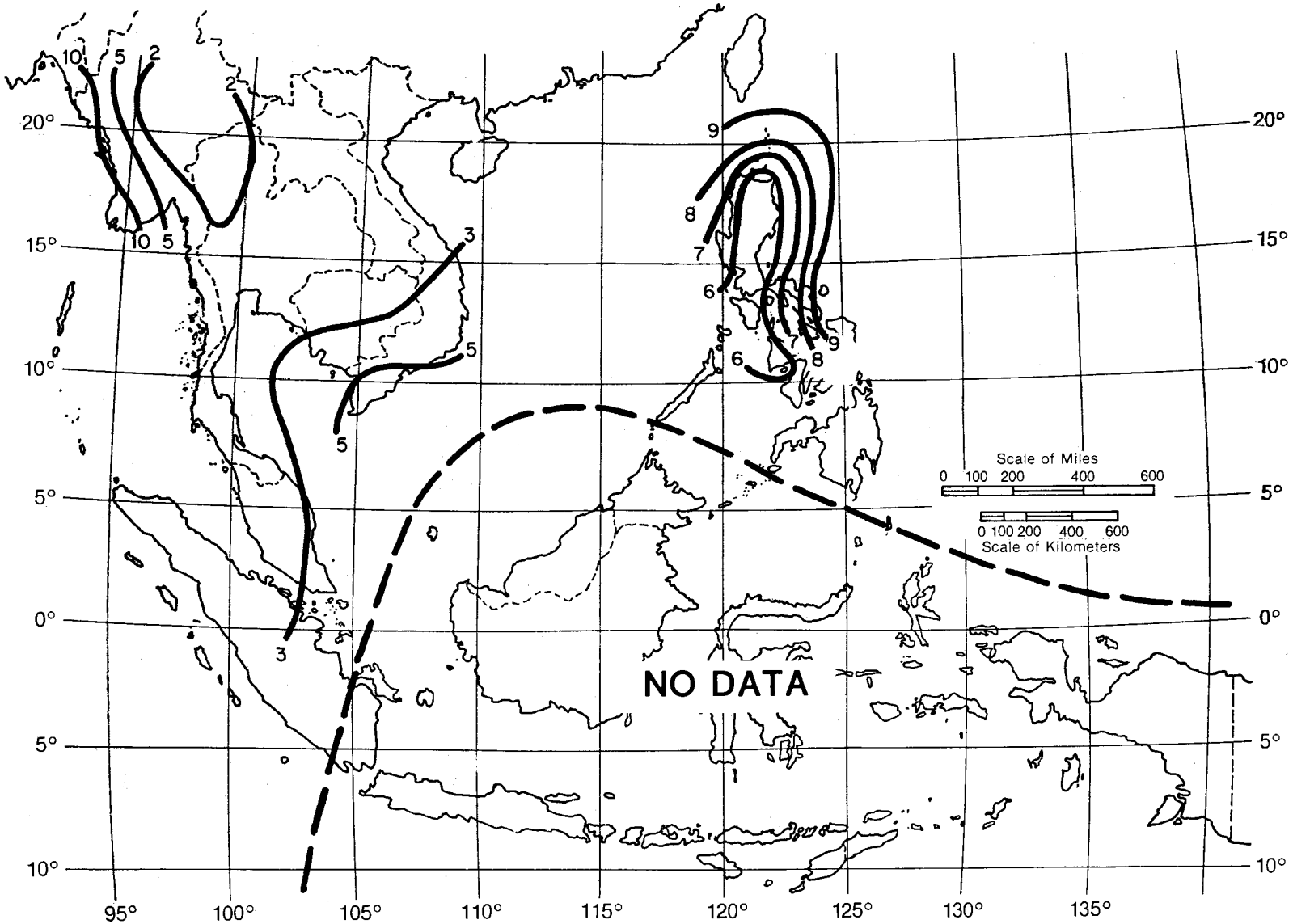

Figure 114. Contour map of the rain rate, $R_1(U/D)$, in millimeters per hour, expected to be exceeded 1 percent of an average year and derived from the thunderstorm ratio, $U/D_{.01}$, for Southeast Asia.

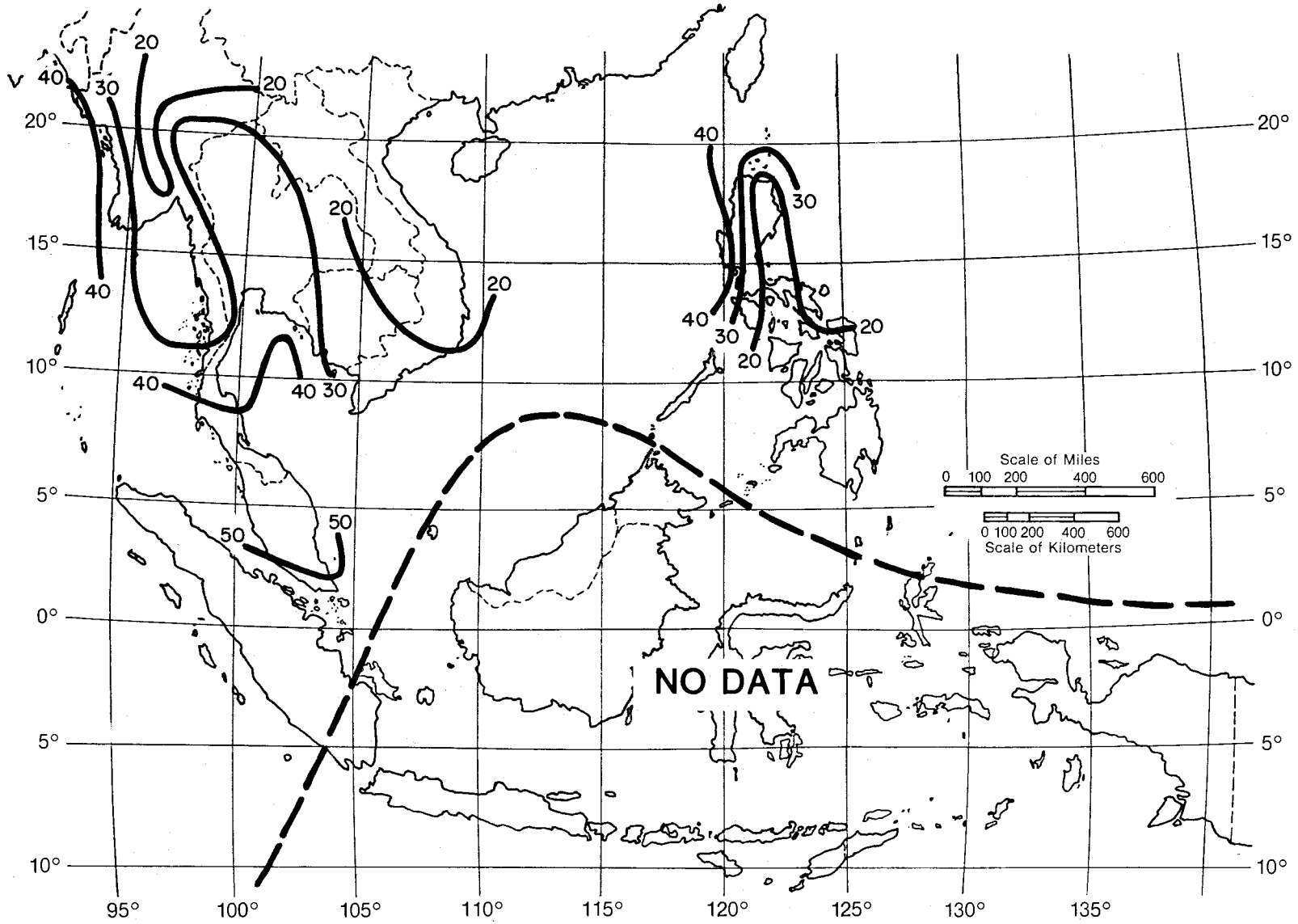

Figure 115. Contour map of the rain rate, $R_{.1}(U/D)$, in millimeters per hour, expected to be exceeded 0.1 percent of an average year and derived from the thunderstorm ratio, $U/D_{.01}$, for Southeast Asia.

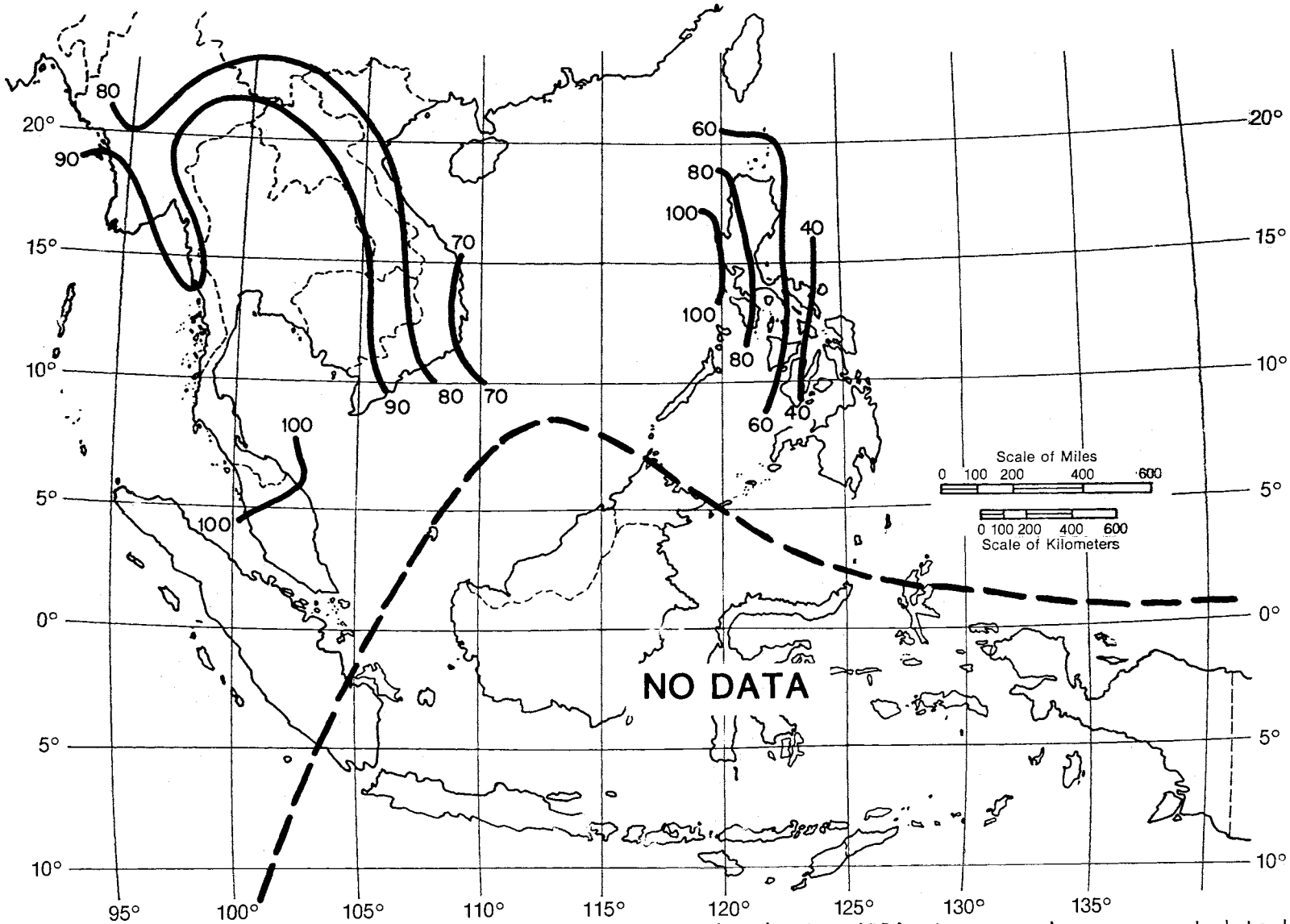

Figure 116. Contour map of the rain rate, $R_{.01}(U/D)$, in millimeters per hour, expected to be exceeded 0.01 percent of an average year and derived from the thunderstorm ratio, $U/D_{.01}$, for Southeast Asia.

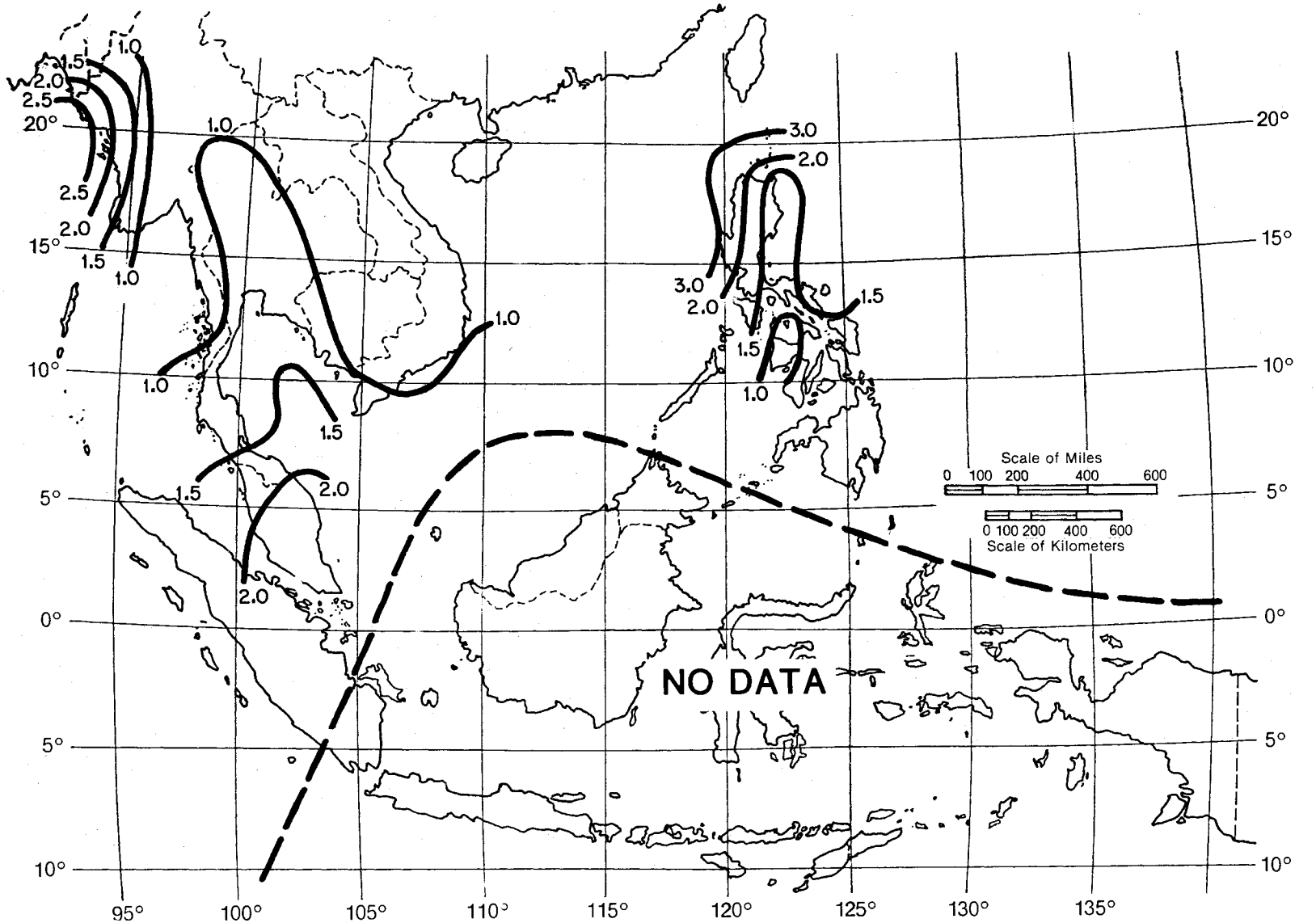

Figure 117. Contour map of the estimated year-to-year standard deviation, s_{R_1}, in millimeters per hour, of rain rate expected at the 1 percent exceedance level for Southeast Asia.

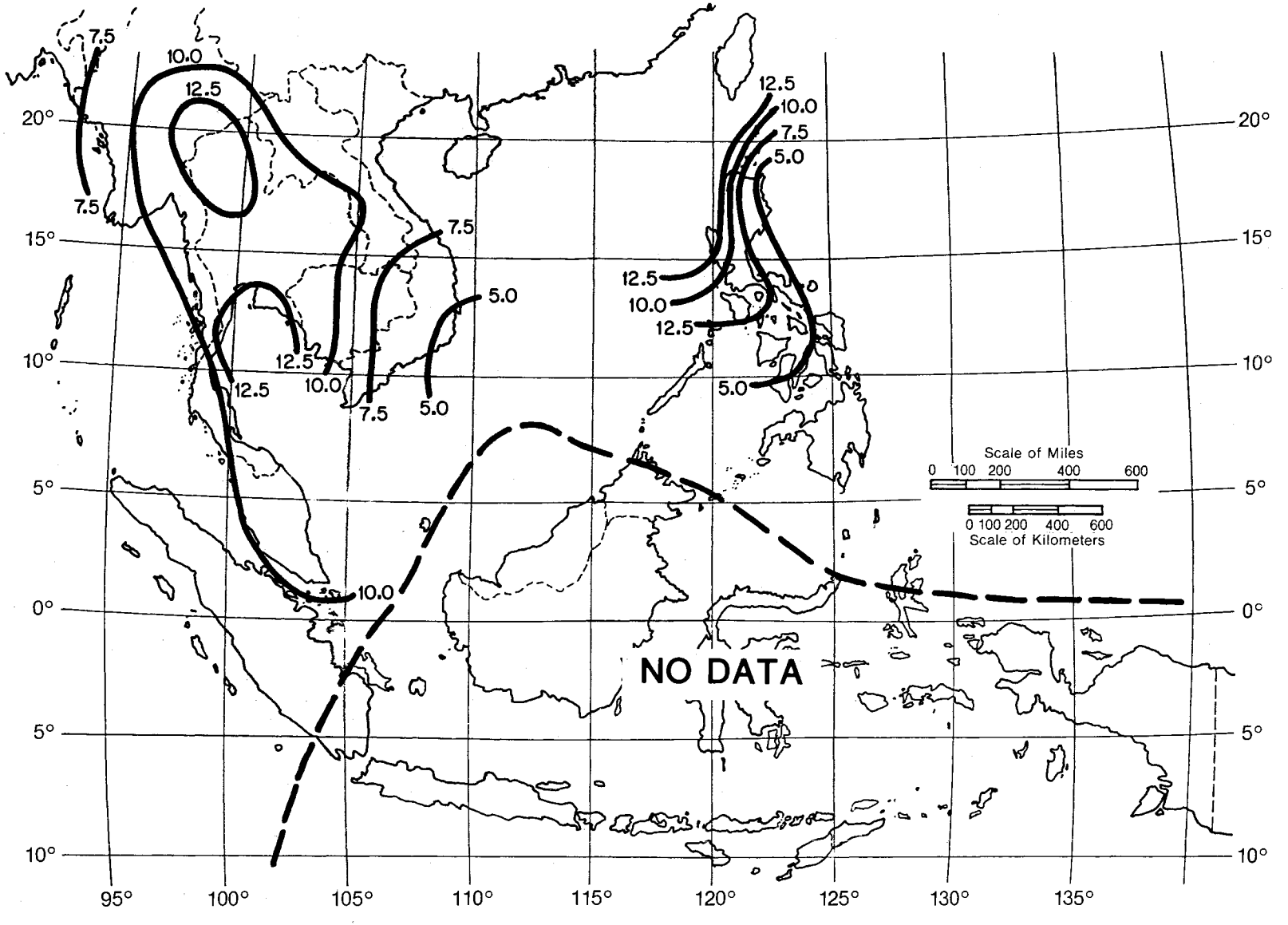

Figure 118. Contour map of the estimated year-to-year standard deviation, $s_{R_{.1}}$, in millimeters per hour, of rain rate expected at the 0.1 exceedance level for Southeast Asia.

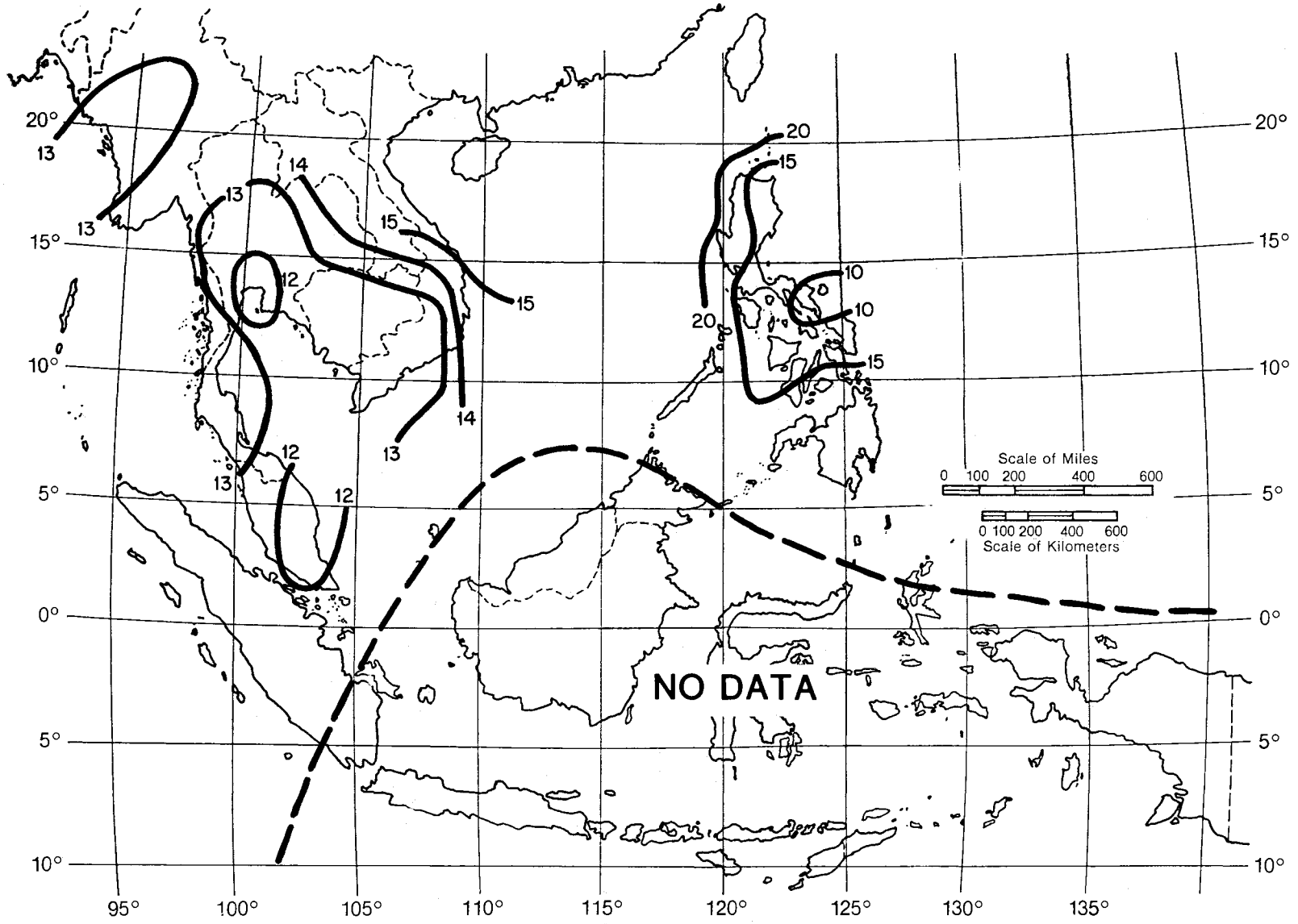

Figure 119. Contour map of the estimated year-to-year standard deviation, $s_{R_{.01}}$, in millimeters per hour, of rain rate expected at the 0.01 exceedance level for Southeast Asia.

β, and any of the modeled rain rate results dependent on the β parameter. Also, the values of $D_{.01}$, s_D, and s_U were estimated using (19) through (21), and were based on the assumption that the entire Southeast Asia area can be classified as a Köppen (1918) zone A.

4. SYNOPSIS

Prediction of annual rain rate distributions and their consequent attenuation distributions on microwave terrestrial links have been extended and examined in quite some detail in this report. Although there are seven geographical areas covered rather exhaustively, there remains the rest of the world that has not been examined herein. For such areas, the likely best procedure at the present for obtaining rain rate and rain attenuation prediction results is from the worldwide zonal maps presented by the CCIR (1982). The CCIR (1982) results, however, are presented on a good deal coarser geographical variability scale than has been presented here, and are presented without the essential ingredient of year-to-year variability.

5. REFERENCES

Barsis, A. P., C. A. Samson, and H. T. Dougherty (1973), Microwave communication links at 15 GHz, U. S. Army Communications Command Tech. Report ACC-ACO-2-73 (NTIS Acces. No. 767-545).

Battesti, J., L. Boithais, and P. Misme (1971), Determination de l'affaiblissement du a la pluie pour les frequencies superieures a 10 GHz, Ann. Telecom. (France), 26, No. 11-12, pp. 439-444.

CCIR (1981), Statistics of rainfall rate and rain attenuation on a line-of-sight radio relay link operating at 11 GHz, CCIR Document 5/316-E, Brazil, 4 June 1981.

CCIR (1982), Recommendations and Reports of the CCIR, 1982; Volume V: Propagation in Non-ionized Media, Report 338-4: Propagation data required for line-of-sight radio-relay systems, ITU, Geneva, Switzerland, pp. 291-292.

Crane, R. K. (1980), Prediction of attenuation by rain, IEEE Trans. Commun., COM-28, No. 9, pp. 1717-1733.

Crane, R. K. (1982), A two-component rain model for the prediction of attenuation statistics, Radio Sci. 17, No. 6, pp. 1371-1387.

Crow, E. L., F. A. Davis, and M. W. Maxfield (1960), Statistics Manual (Dover Publications, Inc., New York, NY).

Dougherty, H. T., and E. J. Dutton (1984), The evaluation of prediction models for microwave attenuation by rainfall, NTIA Report 84-145.

Dutton, E. J. (1977a), Earth-space attenuation prediction procedures at 4 to 16 GHz, Office of Telecommunications Report 77-123 (NTIS Acces. No. PB 269-228/AS).

Dutton, E. J. (1977b), Precipitation variability in the U. S. A. for microwave terrestrial system design, Office of Telecom. Report 77-134 (NTIS Acces. No. AD A049041).

Dutton, E. J., H. T. Dougherty, and R. F. Martin, Jr. (1974), Prediction of European rainfall and link performance and coefficients at 8 to 30 GHz, USACC Tech. Report No. ACC-ACO-16-74 (NTIS Acces. No. A000804).

Dutton, E. J., H. K. Kobayashi, and H. T. Dougherty (1982), An improved model for earth-space microwave attenuation distribution prediction, Radio Sci. 17, No. 6, pp. 1360-1370.

Goldhirsh, J. (1982), Yearly variations of rain rate statistics at Wallops Island, and their impact on predicted slant path attenuations, The Johns Hopkins University/Applied Physics Laboratory Report SIR82U-031, November.

Jones, D. M. A., and A. L. Sims (1971), Climatology of instantaneous precipitation rates, Report AFCRL-72-0430, prepared by the Illinois State Water Survey/U. of Illinois, Urbana, Illinois 61801, for the Air Force Cambridge Research Labs., Bedford, MA 01730, December.

Köppen, W. (1918), Klassification der klimate nach temperatur, niederschlag und jahreslauf, Petermanns Mitt. aus Justus Perthes' Geog. Anst. 64, pp. 193-248.

Kanellopoulos, J. D. (1983), Extension of Lin empirical formula for the prediction of rain attenuation, Radio Sci. 18, No. 2, pp. 237-240.

Lin, S. H. (1975), A method for calculating rain attenuation distributions on microwave paths, Bell System Tech. J. 54, No. 6, pp. 1051-1086.

Lin, S. H. (1977), Nationwide long-term rain rate statistics and empirical calculation of 11-GHz microwave rain attenuation, Bell System Tech. J. 56, No. 9, pp. 1581-1604.

Medhurst, R. G. (1965), Rainfall attenuation of centimeter waves: comparison of theory and measurement, IEEE Trans. Ant. Prop. AP-13, No. 4, pp. 550-564.

Misme, P., and J. Fimbel (1975), Theoretical and experimental determination of attenuation due to rain on a radio-path, Ann. Telecom. (France) 30, Nos. 5-6, pp. 149-158.

Misme, P., and P. Waldteufel (1980), A model for attenuation by precipitation on a microwave earth-space link, Radio Sci. 15, No. 3, pp. 655-665.

Morita, K., and I. Higuti (1976), Prediction methods for rain attenuation distributions of micro and millimeter waves, Rev. Elect. Comm. Labs. (Japan) 24, Nos. 7-8, pp. 651-668.

Olsen, R. C., D. V. Rogers, and D. B. Hodge (1978), The aR^b relation in the calculation of rain attenuation, IEEE Trans. Ant. Prop. AP-26, No. 2, pp. 318-329.

Rice, P. L., and N. R. Holmberg (1973), Cumulative time statistics of surface point-rainfall rates, IEEE Trans. Commun. COM-21 No. 10, pp. 1131-1136.

Ryde, J. W. (1946), The attenuation and radar echoes produced at centimetre wavelengths by various meteorological phenomena, in Meteorological Factors in Radio Wave Propagation (The Physical Society, London, U. K.), pp. 169-188.

APPENDIX: IDENTIFICATION OF SITES USED IN THE PREPARATION OF CONTOUR MAPS IN SECTION 3

THE FEDERAL REPUBLIC OF GERMANY (FRG) AND VICINITY

	LOCATION	LATITUDE	LONGITUDE
1.	Sylt, FRG	54°54'N	8°20'E
2.	List, FRG	55°01'N	8°26'E
3.	Leck, FRG	54°47'N	8°56'E
4.	Husum, FRG	54°31'N	9°08'E
5.	Eggebeck, FRG	54°37'N	9°20'E
6.	Schleswig, FRG	54°27'N	9°30'E
7.	Jever, FRG	53°32'N	7°53'E
8.	Wittmundhaven, FRG	53°32'N	7°40'E
9.	Nordholz, FRG	53°46'N	8°39'E
10.	Hamburg, FRG	53°38'N	10°00'E
11.	Emden, FRG	53°22'N	7°13'E
12.	Oldenburg, FRG	53°10'N	8°10'E
13.	Ahlhorn, FRG	52°53'N	8°13'E
14.	Bremen, FRG	53°02'N	8°47'E
15.	Fassburg, FRG	52°55'N	10°11'E
16.	Hopsten, FRG	52°20'N	7°32'E
17.	Gutersloh, RAF,FRG	51°56'N	8°19'E
18.	Diepholz, FRG	52°35'N	8°20'E
19.	Wunstorf, FRG	52°27'N	9°25'E
20.	Buckeburg, FRG	52°16'N	9°05'E
21.	Hannover, FRG	52°27'N	9°41'E
22.	Celle, FRG	52°35'N	10°01'E
23.	Dusseldorf, FRG	51°16'N	6°45'E
24.	Bruggen, FRG	51°12'N	6°08'E
25.	Wildenrath, FRG	51°06'N	6°13'E
26.	Laarbruch, FRG	51°36'N	6°08'E
27.	Geilenkirchen, FRG	50°57'N	6°02'E
28.	Norvenich, FRG	50°49'N	6°39'E
29.	Butzweilerhof, FRG	50°58'N	6°54'E
30.	Köln-Bonn, FRG	50°51'N	7°08'E

The Federal Republic of Germany (FRG) and Vicinity (Continued)

	LOCATION	LATITUDE	LONGITUDE
31.	Niedermendig, FRG	50°22'N	7°18'E
32.	Wiesbaden, FRG	50°02'N	8°19'E
33.	Kleiner Feldberg, FRG	50°13'N	8°27'E
34.	Rhein-Main, FRG	50°02'N	8°35'E
35.	Darmstadt, FRG	49°51'N	8°41'E
36.	Sollingen, FRG	48°46'N	8°04'E
37.	Karlsruhe, FRG	49°01'N	8°23'E
38.	Freiburg, FRG	48°00'N	7°51'E
39.	Lahr, FRG	48°22'N	7°49'E
40.	Bremgarten, FRG	47°54'N	7°35'E
41.	Kassel, FRG	51°19'N	9°27'E
42.	Giessen, FRG	50°36'N	8°44'E
43.	Wasserkuppe, FRG	50°30'N	9°57'E
44.	Ohringen, FRG	49°12'N	9°31'E
45.	Nurburg, FRG	50°21'N	6°57'E
46.	Spangdahlem AB, FRG	49°58'N	6°42'E
47.	Trier, FRG	49°43'N	6°36'E
48.	Bitburg, FRG	49°56'N	6°33'E
49.	Buchel, FRG	50°10'N	7°03'E
50.	Ramstein, FRG	49°26'N	7°36'E
51.	Hahn, FRG	49°56'N	7°15'E
52.	Pferdsfeld City, FRG	49°51'N	7°36'E
53.	Sembach, FRG	49°30'N	7°52'E
54.	Zweibrucken, FRG	49°12'N	7°24'E
55.	Hoppstadten, FRG	49°36'N	7°11'E
56.	Giebelstadt, FRG	49°38'N	9°57'E
57.	Wurzburg, FRG	49°48'N	9°54'E
58.	Bamberg, FRG	49°53'N	10°52'E
59.	Hof, FRG	50°19'N	11°55'E
60.	Weiden, FRG	49°41'N	12°11'E
61.	Stuttgart, FRG	48°41'N	9°12'E
62.	Weissenberg, FRG	49°02'N	10°58'E
63.	Nurnberg, FRG	49°29'N	11°04'E

The Federal Republic of Germany (FRG) and Vicinity (Continued)

	LOCATION	LATITUDE	LONGITUDE
64.	Regensberg, FRG	49°02'N	12°04'E
65.	Grosser Falkenstein, FRG	49°05'N	13°17'E
66.	Stotten, FRG	48°40'N	9°52'E
67.	Ulm, FRG	48°24'N	9°59'E
68.	Leipheim, FRG	48°26'N	10°14'E
69.	Augsburg, FRG	48°23'N	10°51'E
70.	Neuburg, FRG	48°42'N	11°12'E
71.	Lechfeld, FRG	48°11'N	10°52'E
72.	Landsberg, FRG	48°04'N	10°54'E
73.	Furstenfeldbruck, FRG	48°12'N	11°16'E
74.	Ingolstadt-Manching, FRG	48°43'N	11°31'E
75.	München-Neubiberg, FRG	48°04'N	11°38'E
76.	München-Riem, FRG	48°08'N	11°42'E
77.	Erding, FRG	48°19'N	11°56'E
78.	Passau, FRG	48°35'N	13°29'E
79.	Memmingen, FRG	47°59'N	10°13'E
80.	Kitzingen, FRG	49°44'N	10°12'E
81.	Bayreuth, FRG	49°58'N	11°34'E
82.	Oberpfaffenhofen, FRG	48°05'N	11°17'E
83.	Friedrichshafen, FRG	47°39'N	9°29'E
84.	Kaufbeuren, FRG	47°51'N	10°36'E
85.	Zugspitze, FRG	47°25'N	10°59'E
86.	Hohenpeissenberg, FRG	47°48'N	11°01'E
87.	Garmisch, FRG	47°03'N	11°06'E
88.	Berlin-Tegel, West Berlin	52°33'N	13°18'E
89.	Berlin-Tempelhof, West Berlin	52°28'N	13°24'E
90.	Gatow, West Berlin	52°28'N	13°08'E
91.	Essen, FRG	51°24'N	6°58'E
92.	Geisenheim, FRG	49°59'N	7°58'E
93.	Zurich, Switzerland	47°23'N	8°33'E
94.	Santis, Switzerland	47°15'N	9°20'E
95.	Innsbruck, Austria	47°16'N	11°21'E
96.	Salzburg, Austria	47°48'N	13°00'E
97.	Etain-Rouvres, France	49°14'N	5°40'E

The Federal Republic of Germany (FRG) and Vicinity (Continued)

	LOCATION	LATITUDE	LONGITUDE
98.	Metz-Frescaty, France	49°04'N	6°08'E
99.	Toul-Rosieres, France	48°47'N	5°59'E
100.	Nancy-Essey, France	48°42'N	6°14'E
101.	Nancy-Ochey, France	48°34'N	5°56'E
102.	Phalsbourg, France	48°46'N	7°12'E
103.	Strasbourg, France	48°32'N	7°37'E
104.	Colmar-Meyerheim, France	47°55'N	7°23'E
105.	Bale-Mulhouse, France	47°35'N	7°31'E
106.	Chambley, France	49°01'N	5°52'E
107.	Gros Tenquin, France	49°01'N	6°43'E
108.	Montmedy-Marville, France	49°27'N	5°25'E
109.	Bree, Belgium	51°07'N	5°35'E
110.	Spa, Belgium	50°28'N	5°55'E
111.	Deelen, The Netherlands	52°03'N	5°52'E
112.	Volkel, The Netherlands	51°39'N	5°42'E
113.	Zuid Limburg, The Netherlands	50°55'N	5°46'E
114.	DePeel, The Netherlands	51°31'N	5°51'E
115.	Twenthe, The Netherlands	52°16'N	6°53'E
116.	Clervaux, Luxembourg	50°03'N	6°01'E
117.	Luxembourg City, Luxembourg	49°37'N	6°03'E
118.	Luxembourg, Luxembourg	49°37'N	6°12'E
119.	Echternach, Luxembourg	49°49'N	6°25'E
120.	Berle, Luxembourg	49°57'N	5°51'E
121.	Ettelbruck, Luxembourg	49°51'N	6°06'E
122.	Mondorf-des-Bains, Luxembourg	49°30'N	6°17'E
123.	Cheb, Czechoslovakia	50°05'N	12°24'E
124.	Wernigerode, GDR	51°51'N	10°46'E
125.	Meiningen, GDR	50°33'N	10°22'E
126.	Kaltennordheim, GDR	50°39'N	10°09'E
127.	Brocken, GDR	51°48'N	10°37'E
128.	Magdeburg, GDR	52°06'N	11°35'E
129.	Leipzig, GDR	51°25'N	12°14'E
130.	Erfurt-Blindersleben, GDR	50°59'N	10°58'E
131.	Praha-Ruzyne, Czechoslovakia	50°06'N	14°17'E

OKINAWA

	LOCATION	LATITUDE	LONGITUDE
1.	Naha AB, Okinawa	26°11'N	127°38'E
2.	Kadena AB, Okinawa	26°20'N	127°46'E
3.	Futema MCAF, Okinawa	26°16'N	127°45'E
4.	Hamby AAF, Okinawa	26°17'N	127°45'E

REPUBLIC OF KOREA (ROK) AND VICINITY

	LOCATION	LATITUDE	LONGITUDE
1.	Airfield (R-401), ROK	37°26'N	127°58'E
2.	Chunchon, ROK	37°53'N	127°43'E
3.	Kangnung, ROK	37°45'N	128°57'E
4.	Hoengsung, ROK	37°27'N	127°58'E
5.	Chipo-Ri, ROK	38°09'N	127°19'E
6.	Airfield (A-210), ROK	37°44'N	127°02'E
7.	Airfield (A-306), ROK	37°52'N	127°43'E
8.	Airfield (A-511), ROK	36°57'N	127°02'E
9.	Airfield (R-237), ROK	38°08'N	127°18'E
10.	Chunju West, ROK	36°58'N	127°55'E
11.	Seoul, ROK	37°31'N	126°55'E
12.	Airfield (A-102), ROK	37°30'N	126°42'E
13.	Suwon AB, ROK	37°14'N	127°00'E
14.	Osan AB, ROK	37°05'N	127°01'E
15.	Pyong Taek, ROK	36°57'N	127°02'E
16.	Taejon, ROK	36°20'N	127°23'E
17.	Kunsan AB, ROK	35°54'N	126°37'E
18.	Paengnyong do, ROK	37°59'N	124°40'E
19.	Kimpo International, ROK	37°33'N	126°47'E
20.	Airfield (R-813), ROK	35°08'N	128°41'E
21.	Airfield (R-814), ROK	35°05'N	128°04'E
22.	Airfield (R-815), ROK	35°59'N	129°25'E
23.	Pohang Dong, ROK	35°59'N	129°25'E
24.	Taegu, ROK	35°53'N	128°39'E
25.	Kimhae, ROK	35°10'N	128°56'E
26.	Pusan, ROK	35°10'N	129°07'E
27.	Kwangju AB, ROK	35°07'N	126°48'E

Republic of Korea (ROK) and Vicinity (Continued)

	LOCATION	LATITUDE	LONGITUDE
28.	Chinhae, ROK	35°08'N	128°42'E
29.	Sachon, ROK	35°05'N	128°04'E
30.	Mosulpo, ROK	33°12'N	126°13'E
31.	Inchon, ROK	37°29'N	126°38'E
32.	Mokpo, ROK	34°47'N	126°23'E
33.	Wosan, North Korea	39°11'N	127°26'E

SOUTHWEST ASIA AND THE MIDDLE EAST

	LOCATION	LATITUDE	LONGITUDE
1.	Riyan, Aden	14°39'N	49°19'E
2.	Aden City, Aden	12°49'N	45°01'E
3.	Mazar-I-Sharif, Afghanistan	36°42'N	67°14'E
4.	Kunduz, Afghanistan	36°41'N	68°54'E
5.	Dehdadi, Afghanistan	36°39'N	67°00'E
6.	Herot, Afghanistan	34°20'N	62°10'E
7.	Farah, Afghanistan	32°24'N	62°06'E
8.	Kandahar East, Afghanistan	31°37'N	65°46'E
9.	Kandahar International, Afghan.	31°30'N	65°51'E
10.	Jalalabad, Afghanistan	34°26'N	70°28'E
11.	Kabul International, Afghanistan	34°33'N	69°12'E
12.	Bagram, Afghanistan	34°57'N	69°16'E
13.	Mirzakai, Afghanistan	33°45'N	69°25'E
14.	Ghazni, Afghanistan	33°07'N	69°07'E
15.	Bahrain-Muharraq	26°16'N	50°37'E
16.	Paphos, Cyprus	34°45'N	32°24'E
17.	Akrotiri, Cyprus	34°35'N	32°59'E
18.	Morphou Bay, Cyprus	35°18'N	32°57'E
19.	Nicosia, Cyprus	35°09'N	33°16'E
20.	Cape Andreas, Cyprus	35°40'N	34°34'E
21.	Gangagar, India	29°55'N	73°53'E
22.	Bikaner-Nal, India	28°03'N	73°12'E
23.	Jodhpur, India	26°15'N	73°03'E
24.	Barmer, India	25°45'N	71°23'E
25.	Udaipur, India	24°35'N	73°24'E

Southwest Asia and the Middle East (Continued)

	LOCATION	LATITUDE	LONGITUDE
26.	Bhuj, India	23°16'N	69°40'E
27.	Ahmedabad, India	23°03'N	72°37'E
28.	Dwarka, India	22°22'N	69°05'E
29.	Jamnager, India	22°27'N	70°00'E
30.	Rajkot, India	22°18'N	70°47'E
31.	Baroda, India	22°19'N	73°13'E
32.	Bhavnagar, India	21°45'N	72°11'E
33.	Surat, India	21°12'N	72°50'E
34.	Veraval, India	20°54'N	70°22'E
35.	Diu, India	20°43'N	70°55'E
36.	Damao, India	20°26'N	72°51'E
37.	Bombay-Juhu, India	19°05'N	72°50'E
38.	Bombay-Santa Cruz, India	19°06'N	72°51'E
39.	Poona, India	18°34'N	73°55'E
40.	Vengurla, India	15°52'N	73°38'E
41.	Marmagao, India	15°22'N	73°49'E
42.	Belgaum, India	15°51'N	74°37'E
43.	Sinjar, Iraq	36°19'N	41°50'E
44.	Tabriz, Iran	38°07'N	46°14'E
45.	Mashhad, Iran	36°16'N	59°38'E
46.	Diwaniya, Iraq	31°59'N	44°59'E
47.	Najaf, Iraq	31°59'N	44°19'E
48.	Mosul, Iraq	36°18'N	43°08'E
49.	Airfield (K-1), Iraq	35°30'N	44°17'E
50.	Kirkuk (Military), Iraq	35°28'N	44°21'E
51.	Eski Kifri, Iraq	34°37'N	44°53'E
52.	Khanaqin, Iraq	34°18'N	45°26'E
53.	Rashid, Iraq	33°16'N	44°29'E
54.	Baghdad, Iraq	33°15'N	44°13'E
55.	Baghdad West, Iraq	33°19'N	44°21'E
56.	Kutel Hai, Iraq	32°10'N	46°02'E
57.	Nasiriya, Iraq	31°01'N	46°14'E
58.	Shaibah, Iraq	30°25'N	47°38'E
59.	Basra, Iraq	30°34'N	47°46'E
60.	Rutba, Iraq	33°02'N	40°17'E

Southwest Asia and the Middle East (Continued)

	LOCATION	LATITUDE	LONGITUDE
61.	Habbaniyah-Plate, Iraq	33°20'N	43°35'E
62.	Habbaniyah, Iraq	33°22'N	43°33'E
63.	As Salman, Iraq	30°28'N	44°43'E
64.	Bandar Pahlevi, Iraq	37°28'N	49°29'E
65.	Abadan, Iran	30°21'N	48°13'E
66.	Khark Island, Iran	29°15'N	50°20'E
67.	Bushehr, Iran	28°57'N	50°49'E
68.	Jask, Iran	25°45'N	57°45'E
69.	Tabas, Iran	33°36'N	56°45'E
70.	Rezaiyeh, Iran	37°32'N	45°05'E
71.	Shahrud, Iran	36°25'N	55°01'E
72.	Meshed, Iran	36°17'N	59°38'E
73.	Teheran-Mehrabad, Iran	35°41'N	51°19'E
74.	Teheran-Doshan, Iran	35°42'N	51°28'E
75.	Teheran City, Iran	35°38'N	51°22'E
76.	Shahroki AFB, Iran	35°11'N	48°41'E
77.	Kermanshah, Iran	34°19'N	47°07'E
78.	Hamadan, Iran	34°38'N	48°31'E
79.	Vahdati AFB, Iran	32°26'N	48°24'E
80.	Isfahan, Iran	32°37'N	51°41'E
81.	Kerman, Iran	30°15'N	56°57'E
82.	Shiraz (New), Iran	29°32'N	52°35'E
83.	Zahedan, Iran	29°27'N	60°54'E
84.	Eilat, Israel	29°33'N	34°57'E
85.	Haifa, Israel	32°48'N	35°02'E
86.	Ramat David, Israel	32°39'N	35°10'E
87.	Tel Aviv, Israel	32°06'N	34°46'E
88.	Kfir Sirkin, Israel	32°05'N	34°54'E
89.	Lod, Israel	31°59'N	34°53'E
90.	Egron, Israel	31°50'N	34°49'E
91.	Jerusalem, Israel	31°47'N	35°13'E
92.	Hatzor, Israel	31°45'N	34°43'E
93.	Beersheba, Israel	31°14'N	34°47'E
94.	Harkenaan, Israel	33°59'N	35°31'E
95.	Gilgit, Kashmir	35°55'N	74°23'E

Southwest Asia and the Middle East (Continued)

	LOCATION	LATITUDE	LONGITUDE
96.	Srinagar, Kashmir	33°58'N	74°46'E
97.	Jammu, Jammu	32°41'N	74°50'E
98.	Jerusalem, Jordan	31°52'N	35°13'E
99.	King Hussein, Jordan	32°21'N	36°15'E
100.	Mofraq, Jordan	32°20'N	36°14'E
101.	Amman, Jordan	31°58'N	35°59'E
102.	Kuwait, Kuwait	29°14'N	47°58'E
103.	Nigra, Kuwait	29°21'N	47°59'E
104.	Beirut, Lebanon	33°48'N	35°29'E
105.	Riyaq, Lebanon	33°51'N	35°59'E
106.	Ksarah, Lebanon	33°50'N	35°53'E
107.	Al Qurayyah	33°49'N	35°40'E
108.	Muscat, Oman	23°45'N	58°35'E
109.	Masirah-Rashilf, Oman	20°40'N	58°53'E
110.	Salalah, Oman	17°01'N	54°06'E
111.	Drosh, Pakistan	35°34'N	71°47'E
112.	Peshawar, Pakistan	33°59'N	71°30'E
113.	Risalpur, Pakistan	34°04'N	71°58'E
114.	Kohat, Pakistan	33°34'N	71°26'E
115.	Rawalpindi, Pakistan	33°35'N	73°03'E
116.	Chaklala, Pakistan	33°36'N	73°06'E
117.	Khushab, Pakistan	32°18'N	72°21'E
118.	Sargodha, Pakistan	32°02'N	72°39'E
119.	Fort Sandaman, Pakistan	31°21'N	69°27'E
120.	Quetta/Samungli, Pakistan	30°15'N	66°56'E
121.	Dalbandin, Pakistan	28°53'N	64°24'E
122.	Panjgur, Pakistan	26°58'N	64°04'E
123.	Lahore, Pakistan	31°31'N	74°24'E
124.	Multan, Pakistan	30°11'N	71°25'E
125.	Jacobabab, Pakistan	28°18'N	68°28'E
126.	Khanpur, Pakistan	28°39'N	70°41'E
127.	Hyderabad, Pakistan	25°23'N	68°25'E
128.	Jiwani, Pakistan	25°04'N	61°48'E
129.	Ormara, Pakistan	25°15'N	64°39'E
130.	Karachi Civil, Pakistan	24°54'N	67°09'E

Southwest Asia and the Middle East (Continued)

	LOCATION	LATITUDE	LONGITUDE
131.	Mauripur, Pakistan	24°54'N	66°57'E
132.	Drigh Road, Pakistan	24°54'N	67°06'E
133.	Doha, Qatar	25°16'N	51°33'E
134.	Jidda, Saudi Arabia	21°30'N	39°12'E
135.	Hail, Saudi Arabia	27°30'N	42°02'E
136.	Dhahran, Saudi Arabia	26°16'N	50°10'E
137.	Riyadh, Saudi Arabia	24°43'N	46°43'E
138.	Wejh, Saudi Arabia	26°14'N	36°26'E
139.	Ma'An, Jordan	30°10'N	35°47'E
140.	Medina, Saudi Arabia	24°31'N	39°42'E
141.	Taif, Saudi Arabia	21°29'N	40°32'E
142.	Dumayr, Syria	33°36'N	36°45'E
143.	Damascus, Syria	33°28'N	36°13'E
144.	Humaymim, Syria	33°28'N	36°13'E
145.	Sahles Sahra, Syria	33°34'N	36°10'E
146.	Qamieliye, Syria	37°01'N	41°11'E
147.	Aleppo, Syria	36°11'N	37°13'E
148.	Rasin el Aboud, Syria	36°11'N	37°35'E
149.	Deier Ez Zor, Syria	35°19'N	40°09'E
150.	Dubai, Trucial Oman	25°15'N	55°20'E
151.	Sharja, Trucial Oman	25°20'N	55°23'E
152.	Antalya, Turkey	36°53'N	30°44'E
153.	Adana Civil, Turkey	36°58'N	35°16'E
154.	Incirlik, Turkey	37°00'N	35°25'E
155.	Malatya, Turkey	38°21'N	38°15'E
156.	Erhac, Turkey	38°26'N	38°05'E
157.	Diyarbakir, Turkey	37°55'N	40°13'E
158.	Batman, Turkey	37°55'N	41°07'E
159.	Kamaran I, Yemen	15°20'N	42°37'E
160.	Sana South, Yemen	15°31'N	44°11'E
161.	Al Hudayah, Yemen	14°44'N	42°59'E
162.	Gassim, Saudi Arabia	26°17'N	43°51'E
163.	Ratnagiri, India	16°59'N	73°18'E
164.	Bandar Abbas, Iran	37°28'N	49°29'E
165.	Chahbar, Iran	25°17'N	60°37'E

Southwest Asia and the Middle East (Continued)

	LOCATION	LATITUDE	LONGITUDE
166.	Seistan, Iran	31°00'N	61°30'E
167.	Pasni, Pakistan	25°16'N	63°29'E
168.	Khormaksar, Saudi Arabia	12°50'N	45°01'E
169.	Perim Island, Saudi Arabia	12°39'N	43°24'E
170.	Urfa, Turkey	37°07'N	38°46'E
171.	Van, Turkey	38°30'N	43°23'E
172.	Kamis Mushait, Saudi Arabia	18°18'N	42°48'E
173.	Len Koran, U.S.S.R.	38°46'N	48°52'E
174.	Ashkabad, U.S.S.R.	37°58'N	58°20'E
175.	Krasnovodsk, U.S.S.R.	40°02'N	52°59'E
176.	Famagusta, Cyprus	35°07'N	33°57'E
177.	Prodromos, Cyprus	34°57'N	32°50'E
178.	Kamishli, Syria	37°03'N	41°13'E
179.	Palmyra, Syria	34°33'N	38°18'E
180.	Lattakia, Syria	35°32'N	35°48'E
181.	Chhor, Pakistan	25°31'N	69°47'E
182.	Parachinar, Pakistan	33°52'N	70°05'E
183.	Dera Ismail Khan, Pakistan	31°49'N	70°55'E
184.	Jhelum, Pakistan	32°56'N	73°44'E
185.	Kalat, Pakistan	29°02'N	66°35'E

CENTRAL AMERICA

	LOCATION	LATITUDE	LONGITUDE
1.	Salina Cruz, Mexico	16°12'N	95°12'W
2.	Tapachula, Mexico	14°54'N	92°15'W
3.	Coatzcolacos, Mexico	18°09'N	94°24'W
4.	Chetumal, Mexico	18°28'N	88°19'W
5.	Los Andes, El Salvador	13°52'N	89°39'W
6.	San Salvador, El Salvador	13°40'N	89°05'W
7.	Acajulta, El Salvador	13°36'N	89°50'W
8.	Labor Oualle, Guatemala	14°51'N	91°30'W
9.	Guatemala City, Guatemala	14°35'N	90°32'W
10.	La Fragua, Guatemala	14°58'N	89°32'W
11.	Huehuetengo, Guatemala	15°19'N	91°28'W
12.	Caban, Guatemala	15°29'N	90°20'W

Central America (Continued)

	LOCATION	LATITUDE	LONGITUDE
13.	El Provenir, Guatemala	16°31'N	90°29'W
14.	Santa Rosa, Honduras	14°47'N	88°47'W
15.	Tegucigalpa, Honduras	14°02'N	87°15'W
16.	Amapala, Honduras	13°18'N	87°38'W
17.	Choluteca, Honduras	13°18'N	87°11'W
18.	La Mesa, Honduras	15°27'N	87°56'W
19.	Catacamas, Honduras	14°51'N	85°55'W
20.	Tela, Honduras	15°46'N	87°27'W
21.	Ceiba, Honduras	15°44'N	86°52'W
22.	Guanaja, Honduras	16°28'N	85°54'W
23.	Puerto Lempira, Honduras	15°13'N	83°48'W
24.	Belize, Belize	17°32'N	88°18'W
25.	San Jose, Costa Rica	9°59'N	84°13'W
26.	Puerto Limon, Costa Rica	9°58'N	84°50'W
27.	Puentarenas, Costa Rica	9°58'N	84°49'W
28.	Stanley International, Belize	17°32'N	88°18'W
29.	El Cayo, Belize	17°10'N	89°04'W
30.	El Coco, Costa Rica	9°59'N	84°12'W
31.	La Sabana, Costa Rica	9°56'N	84°06'W
32.	Limon, Costa Rica	9°58'N	83°01'W
33.	Ilopango, El Salvador	13°41'N	89°07'W
34.	Albrook AFB, Panama	8°58'N	79°33'W
35.	LaAurora, Guatemala	14°34'N	90°31'W
36.	Retalhuleu, Guatemala	14°31'N	91°41'W
37.	Toncotin, Honduras	14°03'N	87°13'W
38.	Las Mercedes, Nicaragua	12°08'N	86°10'W
39.	Cape Gracias, Nicaragua	15°00'N	83°10'W
40.	Puerto Cabezas, Nicaragua	14°03'N	83°23'W
41.	Bluefields, Nicaragua	12°00'N	83°43'W
42.	Colon, Panama	9°22'N	79°54'W
43.	David, Panama	8°23'N	82°26'W
44.	Rio Hato, Panama	8°22'N	80°07'W
45.	Tocumen National, Panama	9°05'N	79°22'W
46.	Marcos a Gelaber, Panama	8°58'N	79°30'W
47.	Howard AFB, Panama	8°54'N	79°36'W

THE UNITED STATES OF AMERICA (USA)

	LOCATION	LATITUDE	LONGITUDE
1.	Birmingham, AL	33°03'N	86°55'W
2.	Huntsville, AL	34°44'N	86°35'W
3.	Mobile, AL	30°04'N	80°05'W
4.	Montgomery, AL	32°22'N	86°20'W
5.	Anchorage, AK	61°10'N	150°00'W
6.	Anchorage, AK *	61°10'N	150°00'W
7.	Annette, AK	55°02'N	131°36'W
8.	Barrow, AK	71°16'N	156°50'W
9.	Barter Island, AK	70°07'N	143°40'W
10.	Bethel, AK	60°49'N	161°49'W
11.	Bettles, AK	66°53'N	151°51'W
12.	Big Delta, AK	64°10'N	145°55'W
13.	Cold Bay, AK	55°10'N	162°47'W
14.	Fairbanks, AK	64°50'N	147°50'W
15.	Gulkana, AK	62°15'N	145°30'W
16.	Homer, AK	59°40'N	151°37'W
17.	Juneau, AK	58°20'N	134°20'W
18.	King Salmon, AK	58°40'N	156°40'W
19.	Kodiak, AK	57°49'N	152°30'W
20.	Kutzebue, AK	66°51'N	162°40'W
21.	McGrath, AK	62°58'N	155°40'W
22.	Nome, AK	64°30'N	165°30'W
23.	St. Paul Island, AK	57°09'N	170°18'W
24.	Shemya, AK	52°45'N	174°05'W
25.	Summit, AK	63°19'N	149°19'W
26.	Talkeetna, AK	62°20'N	150°09'W
27.	Unalakleet, AK	63°52'N	160°50'W
28.	Valdez, AK	61°07'N	146°17'W
29.	Yakutat, AK	59°29'N	139°49'W
30.	Flagstaff, AZ	35°12'N	111°38'W

* There are occasions in the USA when two locations appear identical but are actually slightly separated.

The United States of America (USA) (Continued)

	LOCATION	LATITUDE	LONGITUDE
31.	Phoenix, AZ	33°30'N	112°03'W
32.	Tucson, AZ	32°15'N	110°57'W
33.	Winslow, AZ	35°01'N	110°43'W
34.	Yuma, AZ	32°40'N	114°39'W
35.	Fort Smith, AR	35°22'N	94°27'W
36.	Little Rock, AR	34°42'N	92°17'W
37.	Texarkana, AR	33°28'N	94°02'W
38.	Bakersfield, CA	35°20'N	118°52'W
39.	Bishop, CA	37°20'N	118°24'W
40.	Blue Canyon, CA	39°06'N	118°45'W
41.	Eureka, CA	40°49'N	124°10'W
42.	Fresno, CA	36°41'N	119°47'W
43.	Long Beach, CA	33°47'N	118°15'W
44.	Los Angeles, CA	34°00'N	118°15'W
45.	Los Angeles, CA	34°00'N	118°15'W
46.	Mt. Shasta, CA	41°19'N	122°20'W
47.	Oakland, CA	37°50'N	122°15'W
48.	Red Bluff, CA	40°11'N	122°16'W
49.	Sacramento, CA	38°32'N	121°50'W
50.	Sandberg Ranch, CA	34°42'N	118°36'W
51.	San Diego, CA	32°45'N	117°10'W
52.	San Francisco, CA	37°45'N	122°27'W
53.	San Francisco, CA	37°45'N	122°27'W
54.	Santa Catalina, CA	33°25'N	118°25'W
55.	Santa Maria, CA	34°56'N	120°25'W
56.	Stockton, CA	37°59'N	121°20'W
57.	Alamosa, CO	37°28'N	105°54'W
58.	Colorado Springs, CO	38°50'N	104°50'W
59.	Denver, CO	39°45'N	105°00'W
60.	Grand Junction, CO	39°04'N	108°33'W
61.	Pueblo, CO	38°17'N	104°38'W
62.	Bridgeport, CT	41°12'N	73°12'W
63.	Hartford, CT	41°45'N	72°42'W
64.	New Haven, CT	41°18'N	72°55'W

The United States of America (USA) (Continued)

	LOCATION	LATITUDE	LONGITUDE
65.	Wilmington, DE	39°46'N	75°31'W
66.	Washington, DC	38°55'N	77°00'W
67.	Washington, DC	38°55'N	77°00'W
68.	Appalachicola, FL	29°43'N	85°01'W
69.	Daytona Beach, FL	29°11'N	81°01'W
70.	Ft. Myers, FL	26°39'N	81°51'W
71.	Jacksonville, FL	30°20'N	81°40'W
72.	Key West, FL	24°34'N	81°48'W
73.	Lakeland, FL	28°02'N	81°59'W
74.	Miami, FL	25°45'N	80°15'W
75.	Orlando, FL	28°33'N	81°21'W
76.	Pensacola, FL	30°26'N	87°12'W
77.	Tallahassee, FL	30°26'N	84°19'W
78.	Tampa, FL	27°58'W	82°38'W
79.	West Palm Beach, FL	26°42'N	80°05'W
80.	Athens, GA	33°57'N	83°24'W
81.	Atlanta, GA	33°45'N	84°23'W
82.	Augusta, GA	33°29'N	82°00'W
83.	Columbus, GA	32°28'N	84°59'W
84.	Macon, GA	32°49'N	83°37'W
85.	Rome, GA	34°01'N	85°02'W
86.	Savannah, GA	32°04'N	81°07'W
87.	Hilo, HI	19°42'N	155°04'W
88.	Honolulu, HI	21°19'N	157°50'W
89.	Kahului, HI	20°56'N	156°29'W
90.	Lihue, HI	21°59'N	159°23'W
91.	Boise, ID	43°38'N	116°12'W
92.	Idaho Falls, ID	43°30'N	112°01'W
93.	Idaho Falls, ID	43°30'N	112°01'W
94.	Lewiston, ID	46°25'N	117°00'W
95.	Pocatello, ID	42°53'N	112°26'W
96.	Cairo, IL	37°01'N	89°09'W
97.	Chicago-O'Hare, IL	41°57'N	87°53'W
98.	Chicago-Midway, IL	41°50'N	87°45'W
99.	Moline, IL	41°31'N	90°26'W

The United States of America (USA) (Continued)

	LOCATION	LATITUDE	LONGITUDE
100.	Peoria, IL	40°43'N	89°38'W
101.	Rockford, IL	42°16'N	89°06'W
102.	Springfield, IL	39°49'N	89°39'W
103.	Evansville, IN	38°00'N	87°33'W
104.	Fort Wayne, IN	41°05'N	85°08'W
105.	Indianapolis, IN	39°45'N	86°10'W
106.	South Bend, IN	41°40'N	86°15'W
107.	Burlington, IA	40°50'N	91°07'W
108.	Des Moines, IA	41°35'N	93°35'W
109.	Dubuque, IA	42°31'N	90°41'W
110.	Sioux City, IA	42°30'N	96°28'W
111.	Waterloo, IA	42°30'N	92°20'W
112.	Concordia, KS	39°35'N	97°39'W
113.	Dodge City, KS	37°45'N	100°02'W
114.	Goodland, KS	39°20'N	101°43'W
115.	Topeka, KS	39°02'N	95°41'W
116.	Wichita, KS	37°43'N	97°20'W
117.	Covington, KY	39°04'N	84°30'W
118.	Lexington, KY	38°02'N	84°30'W
119.	Louisville, KY	38°13'N	85°48'W
120.	Alexandria, LA	31°19'N	92°29'W
121.	Baton Rouge, LA	30°30'N	91°10'W
122.	Lake Charles, LA	30°13'N	93°13'W
123.	New Orleans, LA	30°00'N	90°03'W
124.	Shreveport, LA	32°30'N	93°46'W
125.	Caribou, ME	46°52'N	68°01'W
126.	Portland, ME	43°41'N	70°18'W
127.	Baltimore, MD	39°18'N	76°38'W
128.	Blue Hill, MA	42°13'N	71°07'W
129.	Boston, MA	42°20'N	71°05'W
130.	Nantucket, MA	41°17'N	70°05'W
131.	Pittsfield, MA	42°27'N	73°15'W
132.	Worcester, MA	42°17'N	71°48'W
133.	Alpena, MI	45°04'N	83°27'W
134.	Detroit, MI	42°23'N	83°05'W

The United States of America (USA) (Continued)

	LOCATION	LATITUDE	LONGITUDE
135.	Detroit, MI	42°23'N	83°05'W
136.	Detroit, MI	42°23'N	83°05'W
137.	Flint, MI	43°03'N	83°40'W
138.	Grand Rapids, MI	42°57'N	86°40'W
139.	Houghton Lake, MI	47°06'N	88°34'W
140.	Lansing, MI	42°44'N	85°34'W
141.	Marquette, MI	46°33'N	87°23'W
142.	Muskegon, MI	43°13'N	86°15'W
143.	Sault Ste. Marie, MI	46°29'N	84°22'W
144.	Duluth, MI	46°45'N	92°10'W
145.	International Falls, MN	48°38'N	93°26'W
146.	Minneapolis, MN	45°00'N	93°15'W
147.	Rochester, MN	44°01'N	92°27'W
148.	St. Cloud, MN	45°34'N	94°10'W
149.	Jackson, MS	32°20'N	90°11'W
150.	Meridian, MS	32°21'N	88°42'W
151.	Vicksburg, MS	32°21'N	90°51'W
152.	Columbia, MO	38°58'N	92°20'W
153.	Columbia, MO	38°58'N	92°20'W
154.	Kansas City, MO	39°02'N	94°33'W
155.	Kansas City, MO	39°02'N	94°33'W
156.	St. Joseph, MO	39°45'N	94°51'W
157.	St. Louis, MO	38°40'N	90°15'W
158.	Springfield, MO	37°11'N	93°19'W
159.	Billings, MT	45°47'N	108°30'W
160.	Glasgow, MT	48°12'N	106°37'W
161.	Great Falls, MT	47°30'N	111°16'W
162.	Havre, MT	48°34'N	109°40'W
163.	Helena, MT	46°35'N	112°00'W
164.	Kalispell, MT	48°12'N	114°19'W
165.	Miles City, MT	46°24'N	105°48'W
166.	Missoula, MT	46°52'N	114°00'W
167.	Grand Island, NE	40°56'N	98°21'W
168.	Lincoln, NE	40°49'N	96°41'W
169.	Lincoln, NE	40°49'N	96°41'W

The United States of America (USA) (Continued)

	LOCATION	LATITUDE	LONGITUDE
170.	Norfolk, NE	42°01'N	97°25'W
171.	North Platte, NE	41°09'N	100°45'W
172.	Omaha, NE	41°15'N	96°00'W
173.	Scottsbluff, NE	41°52'N	103°40'W
174.	Valentine, NE	42°53'N	100°31'W
175.	Elko, NV	40°50'N	115°46'W
176.	Ely, NV	39°15'N	114°53'W
177.	Las Vegas, NV	36°10'N	115°10'W
178.	Reno, NV	39°32'N	119°49'W
179.	Winnemucca, NV	40°58'N	117°45'W
180.	Concord, NH	43°13'N	71°34'W
181.	Mt. Washington, NH	44°16'N	71°18'W
182.	Atlantic City, NJ	39°23'N	74°27'W
183.	Newark, NJ	40°44'N	74°11'W
184.	Trenton, NJ	40°15'N	74°43'W
185.	Albuquerque, NM	35°05'N	106°38'W
186.	Clayton, NM	36°27'N	103°12'W
187.	Raton, NM	36°54'N	104°27'W
188.	Roswell, NM	33°24'N	104°33'W
189.	Roswell, NM	33°24'N	104°33'W
190.	Silver City, NM	32°41'N	108°16'W
191.	Albany, NY	42°40'N	73°49'W
192.	Binghampton, NY	42°06'N	75°55'W
193.	Binghampton, NY	42°06'N	75°55'W
194.	Buffalo, NY	42°52'N	78°55'W
195.	New York, NY	40°40'N	73°50'W
196.	New York, NY	40°40'N	73°50'W
197.	New York, NY	40°40'N	73°50'W
198.	Rochester, NY	43°12'N	77°37'W
199.	Syracuse, NY	43°03'N	76°10'W
200.	Asheville, NC	35°35'N	82°35'W
201.	Cape Hatteras, NC	35°14'N	75°31'W
202.	Charlotte, NC	35°03'N	80°50'W
203.	Greensboro, NC	36°03'N	79°50'W
204.	Raleigh, NC	35°46'N	78°39'W

The United States of America (USA) (Continued)

	LOCATION	LATITUDE	LONGITUDE
205.	Wilmington, NC	34°14'N	77°55'W
206.	Bismarck, ND	46°50'N	100°48'W
207.	Fargo, ND	46°52'N	96°49'W
208.	Williston, ND	48°09'N	103°39'W
209.	Akron, OH	41°04'N	81°31'W
210.	Cincinnati, OH	39°10'N	84°30'W
211.	Cleveland, OH	41°30'N	81°41'W
212.	Columbus, OH	39°59'N	83°03'W
213.	Dayton, OH	39°45'N	84°10'W
214.	Mansfield, OH	40°46'N	82°31'W
215.	Toledo, OH	41°40'N	83°35'W
216.	Youngstown, OH	41°05'N	80°40'W
217.	Oklahoma City, OK	35°28'N	97°33'W
218.	Tulsa, OK	36°07'N	95°58'W
219.	Astoria, OR	46°12'N	123°50'W
220.	Burns, OR	43°36'N	119°03'W
221.	Eugene, OR	44°03'N	123°04'W
222.	Meacham, OR	45°31'N	118°26'W
223.	Medford, OR	42°20'N	122°52'W
224.	Pendleton, OR	45°40'N	118°46'W
225.	Portland, OR	45°32'N	122°40'W
226.	Salem, OR	44°57'N	123°01'W
227.	Sexton Summit, OR	42°36'N	123°30'W
228.	Allentown, PA	40°37'N	5°30'W
229.	Erie, PA	42°07'N	80°05'W
230.	Harrisburg, PA	40°17'N	76°54'W
231.	Philadelphia, PA	40°00'N	75°10'W
232.	Pittsburgh Airport, PA	40°20'N	79°55'W
233.	Pittsburgh, PA	40°26'N	80°00'W
234.	Reading, PA	40°20'N	75°55'W
235.	Scranton, PA	41°25'N	75°40'W
236.	Williamsport, PA	41°16'N	77°03'W
237.	Block Island, RI	41°11'N	71°34'W
238.	Providence, RI	41°50'N	71°25'W
239.	Charleston, SC	32°48'N	79°58'W

The United States of America (USA) (Continued)

	LOCATION	LATITUDE	LONGITUDE
240.	Columbia, SC	34°00'N	81°00'W
241.	Greenville/Spartanburg, SC	34°52'N	82°25'W
242.	Aberdeen, SD	45°28'N	98°30'W
243.	Huron, SD	44°22'N	98°12'W
244.	Rapid City, SD	44°06'N	103°14'W
245.	Sioux Falls, SD	43°34'N	96°42'W
246.	Bristol, TN	36°35'N	82°12'W
247.	Chattanooga, TN	35°02'N	85°18'W
248.	Knoxville, TN	36°00'N	83°57'W
249.	Memphis, TN	35°10'N	90°00'W
250.	Nashville, TN	36°10'N	86°50'W
251.	Oak Ridge, TN	36°02'N	84°12'W
252.	Abilene, TX	32°27'N	99°45'W
253.	Amarillo, TX	35°14'N	101°50'W
254.	Austin, TX	30°18'N	97°47'W
255.	Brownsville, TX	25°54'N	97°30'W
256.	Corpus Christi, TX	27°47'N	97°26'W
257.	Dallas/Ft. Worth, TX	32°47'N	97°05'W
258.	Dallas, TX	32°47'N	96°48'W
259.	Del Rio, TX	29°23'N	100°56'W
260.	El Paso, TX	31°45'N	106°30'W
261.	Galveston, TX	29°17'N	99°48'W
262.	Houston Intercon., TX	29°30'N	95°20'W
263.	Houston, TX	29°45'N	95°25'W
264.	Houston Hobby, TX	29°55'N	95°20'W
265.	Lubbock, TX	33°35'N	101°53'W
266.	Midland, TX	32°00'N	102°09'W
267.	Port Arthur, TX	27°50'N	97°05'W
268.	San Angelo, TX	31°28'N	100°28'W
269.	San Antonio, TX	29°25'N	98°30'W
270.	Victoria, TX	28°49'N	97°01'W
271.	Waco, TX	31°33'N	97°10'W
272.	Wichita Falls, TX	33°55'N	98°30'W
273.	Milford, UT	38°22'N	113°00'W
274.	Salt Lake City, UT	40°45'N	111°55'W

The United States of America (USA) (Continued)

	LOCATION	LATITUDE	LONGITUDE
275.	Wendover, UT	40°45'N	114°02'W
276.	Burlington, VT	44°28'N	73°14'W
277.	Lynchburg, VA	37°24'N	79°09'W
278.	Norfolk VA	36°54'N	76°18'W
279.	Richmond, VA	37°34'N	77°27'W
280.	Roanoke, VA	37°15'N	79°58'W
281.	Olympia, WA	47°03'N	122°53'W
282.	Quillayute, WA	47°57'N	124°33'W
283.	Seattle, WA	47°35'N	122°20'W
284.	Seattle/Tacoma, WA	47°16'N	122°30'W
285.	Spokane, WA	47°40'N	117°25'W
286.	Stampede Pass, WA	47°16'N	121°22'W
287.	Tatoosh Island, WA	48°23'N	124°44'W
288.	Walla Walla, WA	46°05'N	118°18'W
289.	Yakima, WA	46°37'N	120°30'W
290.	San Juan, PR	18°29'N	66°08'W
291.	Swan Island	17°24'N	83°56'W
292.	Beckeley, WV	37°46'N	81°12'W
293.	Charleston, WV	38°23'N	81°40'W
294.	Elkins, WV	38°56'N	79°53'W
295.	Huntington, WV	38°24'N	82°26'W
296.	Parkersburg, WV	39°17'N	81°33'W
297.	Green Bay, WI	44°32'N	88°00'W
298.	La Crosse, WI	43°48'N	91°04'W
299.	Madison, WI	43°04'N	89°22'W
300.	Milwaukee, WI	43°03'N	87°56'W
301.	Casper, WY	42°50'N	106°20'W
302.	Cheyenne, WY	41°08'N	104°50'W
303.	Lander, WY	42°49'N	108°44'W
304.	Sheridan, WY	44°48'N	106°57'W

SOUTHEAST ASIA

	LOCATION	LATITUDE	LONGITUDE
1.	Moulmein, Burma	16°26'N	97°39'E
2.	Tavoy, Burma	14°06'N	98°13'E
3.	Mergui, Burma	12°26'N	98°37'E
4.	Victoria Point, Burma	9°58'N	98°35'E
5.	Toungoo, Burma	18°55'N	96°28'E
6.	Sandoway, Burma	18°27'N	94°18'E
7.	Bassein, Burma	16°46'N	94°46'E
8.	Mingaladon, Burma	16°54'N	96°08'E
9.	Hmawbi, Burma	17°07'N	96°04'E
10.	Akyab, Burma	20°07'N	92°52'E
11.	Mandalay, Burma	21°56'N	96°05'E
12.	Meiktila, Burma	20°53'N	95°53'E
13.	Minbu, Burma	20°10'N	94°58'E
14.	Pyinmana, Burma	19°43'N	96°13'E
15.	Shanthe, Burma	20°58'N	95°55'E
16.	Lashio, Burma	22°58'N	97°45'E
17.	Heho, Burma	20°44'N	96°47'E
18.	Taunggyi, Burma	20°47'N	97°03'E
19.	Kengtung, Burma	21°18'N	99°37'E
20.	Amherst, Burma	16°05'N	97°34'E
21.	Diamond Island, Burma	15°51'N	94°19'E
22.	Mergui, Burma	12°26'N	98°36'E
23.	Rangoon, Burma	16°46'N	96°11'E
24.	Tavoy, Burma	14°07'N	94°18'E
25.	Phrae, Thailand	18°10'N	100°08'E
26.	Prachnap Kirikhan, Thailand	11°48'N	99°48'E
27.	Ban Don, Thailand	9°08'N	99°18'E
28.	Nakhon Si Tham., Thailand	8°25'N	99°58'E
29.	Phuket, Thailand	7°58'N	98°24'E
30.	Phuket/Hin Luk, Thailand	8°06'N	98°18'E
31.	Trang, Thailand	7°30'N	99°40'E
32.	Songkhla, Thailand	7°11'N	100°37'E
33.	Narathiwat, Thailand	6°26'N	101°50'E
34.	Pattani, Thailand	6°46'N	101°09'E
35.	Udorn, Thailand	17°23'N	102°47'E

Southeast Asia (Continued)

	LOCATION	LATITUDE	LONGITUDE
36.	Sakon Nakhon, Thailand	17°10'N	104°09'E
37.	Nakhon Phanom, Thailand	17°23'N	104°39'E
38.	Khon Kaen, Thailand	16°20'N	102°51'E
39.	Mukdahan, Thailand	16°33'N	104°44'E
40.	Chaiyaphum, Thailand	15°48'N	102°01'E
41.	Roi Et, Thailand	16°03'N	103°41'E
42.	Ubon, Thailand	15°14'N	104°52'E
43.	Surin, Thailand	14°53'N	103°29'E
44.	Ban Nong Hoi, Thailand	17°17'N	104°06'E
45.	Nong Khai, Thailand	17°15'N	102°44'E
46.	Nam Phong, Thailand	16°39'N	102°58'E
47.	Mae Hong Son, Thailand	19°16'N	97°56'E
48.	Muang Chiang Rai, Thailand	19°53'N	99°49'E
49.	Mae Sariang, Thailand	18°10'N	97°50'E
50.	Chiang Mai, Thailand	18°46'N	98°58'E
51.	Lampang, Thailand	18°17'N	99°31'E
52.	Ban Mae Sot, Thailand	16°41'N	98°32'E
53.	Uttaradit, Thailand	17°40'N	100°14'E
54.	Loei, Thailand	17°32'N	101°30'E
55.	Phitsanulok, Thailand	16°47'N	100°16'E
56.	Koke Kathiem, Thailand	14°53'N	100°40'E
57.	Kanchanaburi, Thailand	14°01'N	99°32'E
58.	Bangkok, Thailand	13°44'N	100°30'E
59.	Don Muang AFB, Thailand	13°54'N	100°36'E
60.	Aranyaprathet, Thailand	13°42'N	102°35'E
61.	Hua Hin, Thailand	12°34'N	99°48'E
62.	Ban Sattahip, Thailand	12°39'N	100°57'E
63.	Chanthaburi, Thailand	12°37'N	102°07'E
64.	Ban Ta Khli, Thailand	15°16'N	100°17'E
65.	U-Tapao, Thailand	12°41'N	101°01'E
66.	Sara Buri, Thailand	14°30'N	100°55'E
67.	Nakorn Rajasima, Thailand	14°58'N	102°07'E
68.	Udon Thani, Thailand	17°26'N	102°46'E
69.	Nakhon Sawan, Thailand	15°48'N	100°10'E
70.	Chumphon, Thailand	10°27'N	99°15'E

Southeast Asia (Continued)

	LOCATION	LATITUDE	LONGITUDE
71.	Songkhla, Thailand	7°11'N	100°37'E
72.	Battambang, Cambodia	13°06'N	103°12'E
73.	Siem Reap, Cambodia	13°25'N	103°49'E
74.	Krakor, Cambodia	12°31'N	104°11'E
75.	Stung Treng, Cambodia	13°31'N	105°58'E
76.	Kampot, Cambodia	10°37'N	104°13'E
77.	Svay Rieng, Cambodia	11°05'N	105°48'E
78.	Luang-Prabang, Laos	19°53'N	102°08'E
79.	Xieng Khouang, Laos	19°26'N	103°08'E
80.	Vientiane, Laos	17°58'N	102°34'E
81.	Savannakhet, Laos	16°33'N	104°45'E
82.	Seno, Laos	16°40'N	105°00'E
83.	Pakse, Laos	15°07'N	105°47'E
84.	Thakhek, Laos	17°24'N	104°49'E
85.	Lao Cai, Vietnam	22°30'N	103°57'E
86.	Hanoi, Vietnam	21°03'N	105°52'E
87.	Phu Lien, Vietnam	20°48'N	106°38'E
88.	Thai Nguyen, Vietnam	21°36'N	105°50'E
89.	Moncay, Vietnam	21°31'N	107°58'E
90.	Thanh Hoa, Vietnam	19°48'N	105°47'E
91.	Cao Bang, Vietnam	22°40'N	106°15'E
92.	Chapa, Vietnam	22°21'N	103°49'E
93.	Vinh, Vietnam	18°39'N	105°41'E
94.	Hatinh, Vietnam	18°41'N	105°54'E
95.	Donghoi, Vietnam	17°29'N	106°36'E
96.	Rach-Gia, Vietnam	10°00'N	105°05'E
97.	An Xuyen, Vietnam	9°10'N	105°10'E
98.	Con Son, Vietnam	8°42'N	106°35'E
99.	Bien Hoa, Vietnam	10°58'N	108°49'E
100.	Ho Chi Minh, Vietnam	10°49'N	106°39'E
101.	Vung Tau, Vietnam	10°22'N	107°05'E
102.	Vinh Long, Vietnam	10°15'N	105°57'E
103.	Can Tho, Vietnam	10°02'N	105°45'E
104.	Binh Thuy, Vietnam	10°05'N	105°43'E
105.	Soc Trong, Vietnam	9°34'N	105°57'E

Southeast Asia (Continued)

	LOCATION	LATITUDE	LONGITUDE
106.	Lai Khe, Vietnam	11°12'N	106°37'E
107.	Long Xuyen, Vietnam	10°19'N	105°28'E
108.	Phan Thiet, Vietnam	10°56'N	108°06'E
109.	Cam Ranh, Vietnam	12°00'N	109°14'E
110.	Pleiku Cu Hanh, Vietnam	14°00'N	108°01'E
111.	Pleiku, Vietnam	13°58'N	108°02'E
112.	An Khe, Vietnam	13°58'N	108°40'E
113.	Ban Me Thout Eas, Vietnam	12°39'N	108°07'E
114.	Dalat, Vietnam	11°44'N	108°22'E
115.	Hensel AAF, Vietnam	13°51'N	108°03'E
116.	Kontum, Vietnam	14°21'N	108°01'E
117.	Dong Ha, Vietnam	16°49'N	107°06'E
118.	Quang Tri, Vietnam	16°46'N	107°10'E
119.	Hue Phu Bai, Vietnam	16°23'N	107°42'E
120.	Da Nang, Vietnam	16°02'N	108°12'E
121.	Marble Mountain, Vietnam	16°02'N	108°15'E
122.	Quang Ngai, Vietnam	15°07'N	108°46'E
123.	Chu Lai, Vietnam	15°25'N	108°42'E
124.	Qui Nhon, Vietnam	13°45'N	109°13'E
125.	Tuy Hoa, Vietnam	13°03'N	109°20'E
126.	Nha Trang, Vietnam	12°13'N	109°11'E
127.	Phu Cat, Vietnam	13°57'N	104°03'E
128.	Duc Pho, Vietnam	14°49'N	108°58'E
129.	Camp Evans, Vietnam	16°33'N	107°23'E
130.	English, Vietnam	14°28'N	109°02'E
131.	Butterworth, Malaysia	5°27'N	100°23'E
132.	Alor Star, Malaysia	6°11'N	100°24'E
133.	Ipoh, Malaysia	4°34'N	101°05'E
134.	Kuala Lumpur, Malaysia	3°08'N	101°33'E
135.	Malacca, Malaysia	2°16'N	102°15'E
136.	Penang, Malaysia	5°17'N	100°16'E
137.	Kota Bharu, Malaysia	6°10'N	102°17'E
138.	Kuala Trengganu, Malaysia	5°24'N	103°06'E
139.	Kuantan, Malaysia	3°46'N	103°12'E
140.	Mersing, Malaysia	2°27'N	103°50'E

Southeast Asia (Continued)

	LOCATION	LATITUDE	LONGITUDE
141.	Temerloh, Malaysia	3°27'N	102°26'E
142.	Cameron Highlands, Malaysia	4°28'N	101°23'E
143.	Singapore, Singapore	1°20'N	103°50'E
144.	Kuching, Malaysia	1°32'N	110°20'E
145.	Padang, Indonesia	0°52'S	100°21'E
146.	Medan, Indonesia	3°33'N	98°40'E
147.	Pakanbaru, Indonesia	0°27'N	101°26'E
148.	Singkep, Indonesia	0°28'S	104°34'E
149.	Palembang, Indonesia	2°54'S	104°42'E
150.	Pangkalpinang, Indonesia	2°09'S	106°08'E
151.	Tandjungpandan, Indonesia	2°45'S	107°45'E
152.	Tangerang, Indonesia	6°17'S	106°34'E
153.	Djakarta, Indonesia	6°09'S	106°50'E
154.	Djakarta, Indonesia	6°16'S	106°53'E
155.	Bogor, Indonesia	6°32'S	106°45'E
156.	Kalidjati, Indonesia	6°31'S	107°39'E
157.	Semarang, Indonesia	6°58'S	110°22'E
158.	Madiun, Indonesia	7°36'S	111°25'E
159.	Surabaja, Indonesia	7°13'S	112°43'E
160.	Surabaja, Indonesia	7°22'S	112°47'E
161.	Bandung, Indonesia	6°58'S	107°34'E
162.	Bandung, Indonesia	6°45'S	107°34'E
163.	Surakarta, Indonesia	7°31'S	110°45'E
164.	Jogjakarta, Indonesia	7°47'S	110°25'E
165.	Wedi-Birit, Indonesia	7°45'S	110°36'E
166.	Tarakan, Indonesia	3°19'N	117°33'E
167.	Pontianak, Indonesia	0°08'S	109°24'E
168.	Pontianak, Indonesia	0°00'N	109°20'E
169.	Balikpapan, Indonesia	1°16'S	116°53'E
170.	Jefman, Indonesia	0°55'S	131°07'E
171.	Manokwari, Indonesia	0°53'S	134°03'E
172.	Biak, Indonesia	1°12'S	136°07'E
173.	Boruku, Indonesia	1°10'S	136°04'E
174.	Sentani, Indonesia	2°34'S	140°30'E
175.	Tanahmerah, Indonesia	6°05'S	140°19'E

Southeast Asia (Continued)

	LOCATION	LATITUDE	LONGITUDE
176.	Merauke, Indonesia	8°31'S	140°24'E
177.	Amahai, Indonesia	3°19'S	128°55'E
178.	Menado, Indonesia	1°32'N	124°55'E
179.	Makasser, Indonesia	5°03'S	119°33'E
180.	Bali, Indonesia	8°44'S	115°10'E
181.	Kupang, Indonesia	10°10'S	123°39'E
182.	Ambon, Indonesia	3°42'S	128°04'E
183.	Tawau, Sabah	4°15'N	117°53'E
184.	Sandakar, Sabah	5°54'N	118°03'E
185.	Labuan, Sabah	5°17'N	115°14'E
186.	Kinabalu, Sabah	5°56'N	116°03'E
187.	Seria, Brunei	4°38'N	114°22'E
188.	Brunei, Brunei	4°55'N	114°55'E
189.	Kuching, Sarawak	1°29'N	110°20'E
190.	Sibu, Sarawak	2°20'N	111°50'E
191.	Bintulu, Sarawak	3°12'N	113°02'E
192.	Miri, Sarawak	4°23'N	113°59'E
193.	Dili, Portuguese Timor	8°33'S	125°32'E
194.	Laoag, Philippines	18°11'N	120°31'E
195.	Dagupan, Philippines	16°03'N	120°20'E
196.	Basa, Philippines	14°59'N	120°29'E
197.	Clark AFB, Philippines	15°11'N	120°33'E
198.	Baguio, Philippines	16°25'N	120°35'E
199.	Loakan, Philippines	16°22'N	120°37'E
200.	San Fernando, Philippines	16°35'N	120°18'E
201.	Cubi Point, Philippines	14°47'N	120°16'E
202.	Manila, Philippines	14°30'N	121°01'E
203.	Sangley Point, Philippines	14°29'N	120°54'E
204.	Manila, Philippines	14°31'N	121°00'E
205.	Coron, Philippines	12°00'N	120°12'E
206.	Calayan, Philippines	19°16'N	121°28'E
207.	Busco, Philippines	20°27'N	121°58'E
208.	Aparri, Philippines	18°22'N	121°38'E
209.	Tuguegarao, Philippines	17°37'N	121°44'E
210.	Baler, Philippines	15°46'N	121°34'E

Southeast Asia (Continued)

	LOCATION	LATITUDE	LONGITUDE
211.	Casiguran, Philippines	16°17'N	122°07'E
212.	Daet, Philippines	14°07'N	122°57'E
213.	Legaspi, Philippines	13°08'N	123°44'E
214.	Masbate Bay, Philippines	12°22'N	123°37'E
215.	Borongan, Philippines	11°37'N	125°26'E
216.	Cebu, Philippines	10°19'N	123°54'E
217.	Mactan, Philippines	10°18'N	123°58'E
218.	Surigao, Philippines	9°48'N	125°30'E
219.	Cagayande Oro, Philippines	8°25'N	124°36'E
220.	Malaybalay, Philippines	8°09'N	125°05'E
221.	Francisco Bangoy, Philippines	7°07'N	125°39'E
222.	Davao, Philippines	7°07'N	125°38'E
223.	Hinatuan, Philippines	8°22'N	126°20'E
224.	Roxas, Philippines	11°35'N	122°45'E
225.	Iloilo, Philippines	10°42'N	122°32'E
226.	Bacolod, Philippines	10°38'N	122°55'E
227.	Dumaguete, Philippines	9°18'N	123°18'E
228.	Dipolog, Philippines	8°36'N	123°21'E
229.	Cotabato, Philippines	7°14'N	124°15'E
230.	Zamboanga, Philippines	6°55'N	122°03'E
231.	Puerto Princesa, Philippines	9°44'N	118°45'E
232.	Cuyo, Philippines	10°51'N	121°02'E
233.	Tolo Boy, Philippines	6°03'N	121°00'E
234.	Sanga Samoa, Philippines	5°02'N	119°44'E
235.	Echague, Philippines	16°42'N	121°42'E
236.	Cap-St.-Jacques, Vietnam	10°20'N	107°05'E
237.	Pasuran, Indonesia	7°38'S	112°55'E
238.	Amboina, Indonesia	3°42'S	128°10'E
239.	Koepang, Indonesia	10°10'S	123°34'E
240.	Pattle, Vietnam	16°33'N	111°37'E
241.	Phnom Penh, Cambodia	11°33'N	104°51'E
242.	Tacloban, Philippines	11°15'N	125°00'E
243.	Kota Kinabala, Malaysia	5°57'N	116°03'E

FORM **NTIA-29**
(4-80)

U.S. DEPARTMENT OF COMMERCE
NAT'L. TELECOMMUNICATIONS AND INFORMATION ADMINISTRATION

BIBLIOGRAPHIC DATA SHEET

	1. PUBLICATION NO.	2. Gov't Accession No.	3. Recipient's Accession No.
	NTIA Report 84-148		

4. TITLE AND SUBTITLE
Microwave Terrestrial Link Rain Attenuation Prediction Parameter Analysis

5. Publication Date
April 1984

6. Performing Organization Code
NTIA/ITS.S3

7. AUTHOR(S)
E. J. Dutton

9. Project/Task/Work Unit No.
9104503

8. PERFORMING ORGANIZATION NAME AND ADDRESS
U.S.Dept of Commerce, NTIA/ITS.S3
325 Broadway
Boulder, CO 80303

10. Contract/Grant No.

11. Sponsoring Organization Name and Address
USACEEIA
Ft. Huachuca, AZ

12. Type of Report and Period Covered

13.

14. SUPPLEMENTARY NOTES

15. ABSTRACT *(A 200-word or less factual summary of most significant information. If document includes a significant bibliography or literature survey, mention it here.)*

Because rain attenuation continues to be a problem for the operation of microwave links worldwide, this report examines the behavior and the prediction of rain rate and rain attenuation distributions on a worldwide basis. Particular emphasis is placed on seven areas of the world of special interest to the U. S. Army Communications Electronics and Engineering-Installation Agency (USACEEIA).

16. Key Words *(Alphabetical order, separated by semicolons)*

attenuation distributions; contour maps; microwave links; model-data comparisons; rain attenuation

17. AVAILABILITY STATEMENT

☒ UNLIMITED.

☐ FOR OFFICIAL DISTRIBUTION.

18. Security Class. *(This report)*
UNCLASSIFIED

20. Number of pages
176

19. Security Class. *(This page)*
UNCLASSIFIED

21. Price:

☆ U. S. GOVERNMENT PRINTING OFFICE: 1984—779-331/9326 REGION NO. 8